Identifying a Novel Role for Cytoplasmic Dynein in Microtubule Acetylation and Investigating the Multi-hit Hypothesis in Motor Neuron Disease

Matin Hemati Gourabi

Doctor of Philosophy in Neuroscience

University of Sussex

October 2020

Declaration

I hereby declare that the research contained in this thesis, unless otherwise formally indicated within the text, is the original work of the author. The thesis has not been and will not be submitted in whole or in part to this or any other university for award or any other degree, and does not incorporate any material already submitted for a degree.

Signature

Abstract

Spinal muscular atrophy with lower extremity predominance (SMA-LED) and amyotrophic lateral sclerosis (ALS) are childhood and adult-onset motor neuron diseases, respectively, that are characterised by loss of motor neurons. Although the underlying molecular mechanisms of these disorders are not fully understood, deficiencies in axonal transport, microtubule dynamics and protein quality control systems have been implicated in the pathogenesis. As such, this thesis investigates consequences of mutations in dynein cytoplasmic 1 heavy chain (*DYNC1H1*), encoding the heavy chain subunit of cytoplasmic dynein, on MT stability in cellular models of SMA-LED. In addition, it investigates how defective cytoplasmic dynein could make cells more prone to toxic protein aggregation.

Post-translational acetylation of α-tubulin modulates MT dynamics and altered MT dynamics has been linked to neurodegeneration. Analysing fibroblasts derived from an SMA-LED patient and a mouse model of SMA-LED known as Legs at odd angles (*Loa*), identified a reduced interaction between dynein and alpha-tubulin N-acetyltransferase 1 (ATAT1), the canonical enzyme for acetylation of MTs. The alteration in dynein-ATAT1 interaction suggests a regulatory role of dynein in MT acetylation, which when compromised could contribute to the pathology of SMA-LED.

Furthermore, dynein is involved in autophagic removal of misfolded protein aggregates and damaged organelles. There is a plethora of evidence suggesting decreased autophagic activity with ageing, which could contribute to the cytoplasmic accumulation of misfolded proteins and mislocalisation of TDP-43 as hallmarks of ALS. Here, I utilised cells derived from the *Loa* mouse model and manipulation of the autophagy associated kinase TANK-binding kinase 1 (TBK1) to reveal a significant increase in the levels of LC3II and p62, as autophagy markers, when TBK1 is genetically or pharmacologically inhibited in cells harbouring the *Loa* mutation. Importantly, analysis of *Loa* fibroblasts and hippocampal neurons after an exposure to sequential hits such as TBK1 or proteasome inhibitors led to significant increase in TDP-43 mislocalisation. Moreover, there was a delayed recovery in clearance of stress granules in *Loa* fibroblasts and neurons, which could mediate further

formation of protein aggregates, demonstrating the vulnerability of neurons harbouring defective dynein to ageing and cellular stress.

In conclusion, these data suggest regulation of microtubule acetylation through dynein-dependent recruitment of ATAT1 to the microtubule and a potential mechanism involved in the pathogenesis of SMA-LED. Moreover, these data support a multiple-hit hypothesis of neurodegeneration in which the dynein malfunction could establish the primary susceptibility which in combination with variations in another ALS-linked gene such as TBK1 or functional decline in the ubiquitin-proteasome system could exacerbate the formation of aggregates and mislocalisation of TDP-43 that are hallmarks of ALS. Therefore, these data provide further insight into the origin or progression of SMA-LED and ALS, opening the way to find more effective therapeutic targets of the disease.

List of Figures

Figures

Figures

Figures

List of Table

Table

Abbreviations

AD	Alzheimer's disease
AMPK	AMP-activated protein kinase
ALS	Amyotrophic lateral sclerosis
ALS2	*Alsin*
Arp1	Actin related protein 1
αTAT1	α-tubulin N-acetyltransferase 1
Atg	Autophagy related protein
BICD1/2	Bicaudal D 1/2
BAG3	Bcl2-associated athanogene 3
BUZ	Binder of ubiquitin zinc finger
C9orf72	Chromosome 9 open reading frame 72
CASA	Chaperon-assisted selective autophagy
CCT	Chaperonin containing T complex
CHIP	HSC70-interacting protein
CK2	Casein kinase 2
CMA	Chaperon-mediated autophagy
CMD	Congenital muscular dystrophy
CMT	Charcot-Marie-Tooth disease
CNS	Central nervous system

Abbreviations

CTF	C-terminal fragment
DCSMA	Dominant congenital spinal muscular atrophy
DCNT1	Dynactin
DENN	Differentially expressed in normal and neoplastic cells
DMB	Dynein motor-binding
DPR	Dipeptide-repeat
DYNC1H1	Dynein cytoplasmic 1 heavy chain 1
eMI	Endosomal microautophagy
ENU	N-ethyl-N-nitrosourea
ER	Endoplasmic reticulum
fALS	Familial ALS
FBD	Fetal brain disruption
FIP200	Focal adhesion kinase family interacting protein of 200kDa
FUS	Fused in sarcoma
G3BP	rasGAP SH3 domain binding protein 1
GEF	Guanine exchange factor
GRD	Glycine-rich domain

Abbreviations

HC	Dynein Heavy Chain
HD	Huntington's disease
HDAC6	Histone deacetylase 6
HMSN	Hereditary motor sensory neuropathy
hnRNP	Heterogeneous nuclear ribonucleoprotein
HSP40	Heat shock protein 40
hsc70	Heat shock cognate chaperone of 70 kDa
HSP	Hereditary spastic paraplegia
Hsp90	Heat shock protein 90
Htt	Huntingtin
IC	Dynein Intermediate Chain
KIR	Keap1-binding region
LC	Dynein Light Chain
LC3	Light chain 3
LIC	Dynein Light Intermediate Chain
LIR	LC3-interacting region
LIS1	Lissencencephaly
LMN	Lower motor neuron

Abbreviations

LRRK2	Leucine-rich repeat kinase 2
MAP	Microtubule-associated protein
MCD	Malformations of cortical development
MEF	Mouse Embryonic Fibroblast
MHAC	Microhydranencephaly
MN	Motor neuron
MND	Motor neuron disease
MT	Microtubule
MTOC	Microtubule-organizing centre
mTOR	Mammalian target of rapamycin
NBR1	Next to BRCA1 gene 1 protein
NDEL1	Nuclear distribution E-like
NDP52	Nuclear domain 10 protein 52
NES	Export motif
NLS	Nuclear localization signal
Nt	N-terminal degrons
PB1	Phox-and-Bem1
PBP	Progressive bulbar
PD	Parkinson disease

Abbreviations

PE	Phosphatidylethanolamine
PICALM	Phosphatidylinositol-binding clathrin assembly protein
PI3K	Phosphatidylinositol 3-phosphate kinase
PLA	Proximity ligation assay
PLS	Primary lateral sclerosis
PMA	Progressive muscular atrophy
PMN	Progressive motor neuropathy
PQC	Protein quality control
PS	Perry syndrome
PtdIns3P	Phosphatidylinositol 3-phosphate
PTM	Posttranslational modifications
RAN	Repeat Associated Non-ATG
RanBPM	Ran-binding protein M
RNP	Ribonucleoprotein
ROS	Reactive oxygen species
RRM	RNA recognition motifs
sALS	Sporadic ALS
Scr-shRNA	Scrambled RNA

Abbreviations

SDD	Scaffold dimerization domain
shRNA	Short hairpin RNA
siRNA	Short interfering RNA
SIRT	Sirtuins
SMA-LED	Spinal muscular atrophy with lower extremity predominance
SG	Stress granule
SOD1	Superoxide dismutase 1
Stx17	Syntaxin 17
TBA	Tubastatin
TBCE	Tubulin-binding cofactor E
TBK1	TANK-binding kinase
TDP-43	TAR-DNA binding protein-43
TIA1	T cell-restricted intracellular antigen-1
TUBA4A	Tubulin Alpha 4A
TUBA1A	Tubulin Alpha 1A
Ub	Ubiquitin
UBA	Ubiquitin-associated
UBL	Ubiquitin-like

Abbreviations

UBQLN	Ubiquilin
ULD	Ubiquitin-like domain
ULK1	Unc-51 like autophagy activating kinase
UMN	Upper motor neuron
USP14	Ubiquitin carboxyl-terminal hydrolase 14
UPS	Ubiquitin-proteasome system
VAMP3	Vesicle-associated membrane protein 3
VCP	Valosin containing protein
WIPI1	WD repeat domain phosphoinositide-interacting protein 1

Acknowledgements

First of all, I would like to express my sincere gratitude and appreciation to my supervisor, Professor Majid Hafezparast for providing the opportunity to complete my PhD in his lab and for the consistent support, valuable guidance, and advice he has provided throughout this research. His knowledge, expertise and patience have deeply inspired me and it was a great privilege to work under his guidance and supervision. Furthermore, I am thankful for the support and feedback that I have received from my co-supervisor, Dr Sarah King. She has always been willing to help in any way she could.

My appreciation also extends to my laboratory colleagues. I would like to thank Dr Fabio Simoes for being willing and enthusiastic to assist in any way he could throughout my entire PhD and for all his valuable comments and suggestions in completion of this study. I would like to thank Dr Greig Joilin for a great deal of support during my PhD and the comments and recommendations on this dissertation. I am also thankful to Eleni Christoforidou for helping me to conduct some experiments. I would also like to thank a past member of Hafezparast lab, Dr Muruj Barri for her support and guidance throughout my PhD.

I would like to extend my appreciation to Marion Brownridge for all the financial support she provided for my PhD.

I would like to say special thanks to my mum, Parvin, and my dad, Behrouz for all the unconditional support throughout life and my education. With a great deal of support they provided me, I have been able to pursue what I want to achieve in life and this PhD would not have been possible without their sacrifices and all their support. I would like to thank my brother, Mehran who has always been there for me and for all his positive energy and a huge amount of support he provided me. From the bottom of my heart, I would also like to say a big thank you to my husband, Hamed, for endless support and encouragement that he provided me during this PhD. I am extremely grateful for his feedback and advice in my academic endeavours.

Chapter 1: Introduction

1.1 The central nervous system

The central nervous system (CNS) consists of the brain and spinal cord. The CNS is mainly involved in the integration of sensory information and subsequent responses. In this system, the motor cortex, basal ganglia, cerebellum and some parts of the brainstem are implicated in the planning and initiation of movement. Importantly, a wide variety of neuronal cell types are created during the neuronal development in the vertebrate. This diversity is essential for the establishment of neuronal circuits. Therefore, neurodegeneration and loss of neuronal cells in the CNS underlie several neurological conditions. One of the CNS neuronal cell types is motor neurons (MN) which is involved in several developmental stages and signaling pathways.

1.1.1 Motor system

As aforementioned, the motor cortex, basal ganglia, cerebellum, and parts of the brainstem participate in planning and initiation of movement. Indeed, the precise timing and pattern of the movement are coordinated by MNs in the spinal cord (Kiehn, 2016). Corticospinal tract is the major and fastest descending tract and main pathway conducting motor impulses from the motor cortex to the spinal cord. Moreover, there are multiple indirect pathways, including corticobulbospinal pathways and tracts from secondary cortical motor cortices (Dum & Strick, 1991) (**Figure 1.1**). Upon damage to the corticospinal tract, the indirect pathways become more dominant (Schwerin et al., 2008).

Figure 1.1

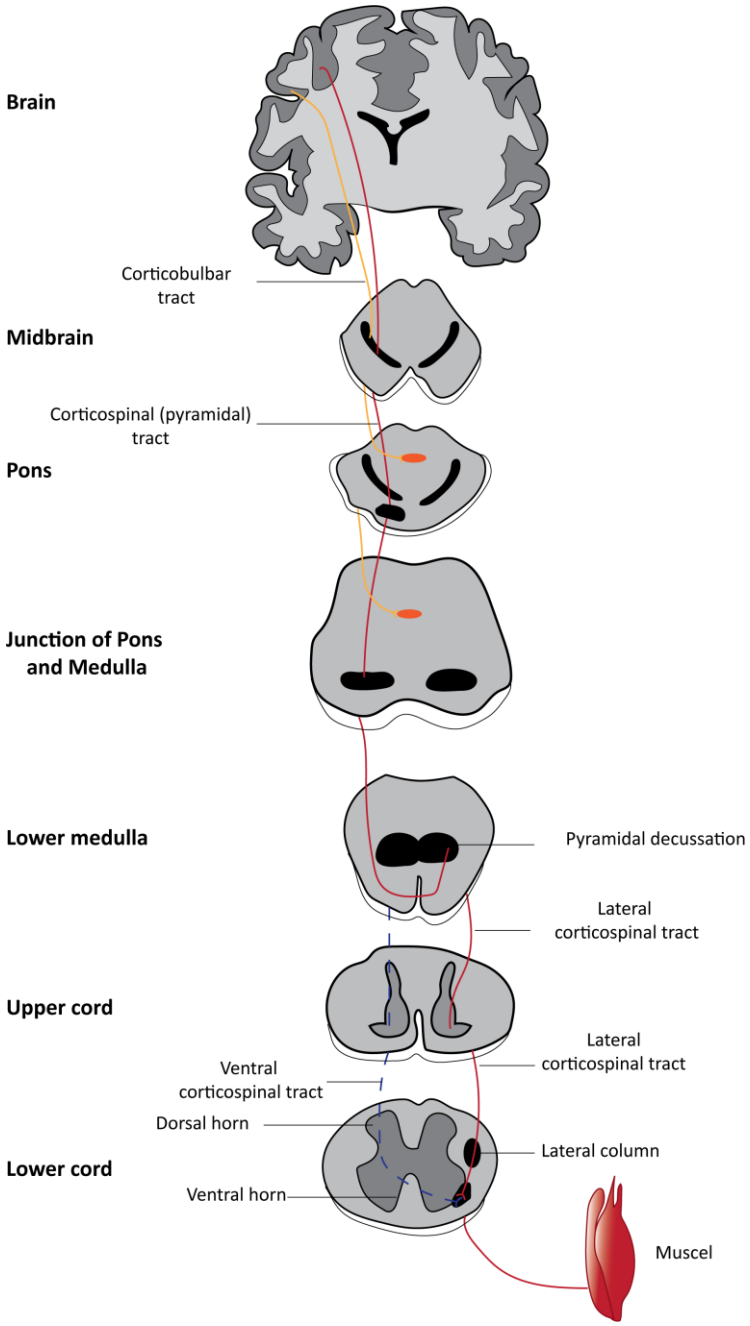

Figure 1.1 Schematic representation of the corticospinal tract. The lateral corticospinal tract (red), ventral corticospinal tract (blue), and corticobulbar (orange) are shown. Adopted from (Ragagnin, Shadfar, Vidal, Jamali, & Atkin, 2019).

1.1.2 Motor neuron

MNs are heterogeneous throughout the CNS and present diverse morphologies and arrangement innervating hundreds of fibres within one muscle controlling a range of ownstream targets. MNs are divided into the upper motor neuron (UMN) and the lower motor neuron (LMN). The UMNs of the corticospinal and corticobulbar tracts originate in motor cortex, premotor cortex and supplementary motor area. The axons projected from these neurons descend subcortical region and enter the cerebral peduncle in the midbrain. To innervate the LMNs, UMNs of corticobulbar tract exit the tract. At the caudal region of the medulla, most of spinal UMNs form the lateral corticospinal tract and the remaining UMNs form the ventral corticospinal tract at the target level of spinal cord (**Figure 1.1**). Some UMNs are innervating distal extremities that descend via lateral corticospinal tract to form direct synapses with alpha-MNs (Purves et al., 2004).

LMNs have been divided into three subtypes based on the region they innervate including, branchial, visceral, and somatic. Moreover, somatic LMNs have been classified into three groups: alpha, beta, and gamma (Stifani, 2014).

It has been reported that specific MNs subpopulations are more vulnerable than others. Among the UMN and LMN, corticospinal MNs, innervating voluntary muscles, degenerate more readily than specific subgroups of lower MNs including oculomotor neurons and Onuf's nuclei MN, which are resistant to degeneration. The clinical symptoms of degeneration of UMN include spasticity, uncontrolled movement, and paralysis (Stifani, 2014). The differences between UMN and LMN are summarized in **Table 1.1**.

Table 1.1 Comparisons of UMNs and LMNs

	UMNs	LMNs
Location of cell body	Cortex	Brainstem and spinal cord
Neurotransmitter	Glutamate	Acetylcholine
Synaptic target	Within the CNS (Lower motor neurons)	Outside the CNS (Muscles)
Symptoms upon lesion	Spasticity	Paralysis

Table 1.1 Comparisons of UMNs and LMNs. Table showing principal differences between UMNs and LMNs. It summarizes differences in location of cell body, neurotransmitter, synaptic target, and symptoms upon lesion.

Consequently, due to the distinctive and irreplaceable function of MNs, their loss or degeneration leads to progressive muscular atrophy, spinal muscular atrophy (SMA), primary lateral sclerosis (PLS), and amyotrophic lateral sclerosis (ALS).

1.2 Motor neuron diseases

Motor neuron diseases (MND) belong to the group of disorders that are defined by the presence of MN degeneration. The worldwide all-age prevalence of MNDs is 4.5 per 100,000 people. While, motor neuron diseases have low prevalence and incidence, but they cause severe disability with a high fatality rate. Importantly, incidence of MNDs has geographical heterogeneity, which is not explained by any risk factor. MNDs are categorised according to underlying genetics, aetiological pathology, and clinical presentation but classification based on the specific type of MNs affected (UMN, LMN or both) is more common. Moreover, MNDs in accordance to the speed of MN loss are classified into the slow or fast progressive, which at later stages, lead to the deficits of

neuronal functions including memory, movement, and cognition, see **Table 1.2**. The two MNDs including amyotrophic lateral sclerosis (ALS) (see section 1.2.2), and spinal muscular atrophy, lower extremity predominance (SMA-LED) (see section 1.2.1), representing the adult-onset and childhood forms of MND respectively, will be the focus of this thesis.

Table 1.2 Summary of three main types of MND

Motor neuron disease	Disease	Symptom	Onset	Ref
UMN	**Hereditary spastic paraplegia (HSP)**	Muscle weakness and spasticity	Variable (Childhood to age 70)	(Giudice, Lombardi, Santorelli, Kawarai, & Orlacchio, 2014)
	Primary lateral sclerosis (PLS)	Stiffness and slow movement	Age of 20	(Gordon et al., 2006)
LMN	**Progressive muscular atrophy (PMA)**	Muscle weakness, muscle cramps	Adulthood	(Bogucki, Pigo'nska, Szadkowska, & Gajos, 2016)
	Charcot-Marie-Tooth (CMT) disease	Muscle weakness, decreased reflexes, vibratory sensory loss	variable (First to second decade of life)	(Hoyle, Isfort, Roggenbuck, & Arnold, 2015)
	Monomelic amyotrophy (MMA) or Hirayama disease		Early twenties	(Verschueren, 2017)
	Multifocal motor neuropathy	Weakness of	Age of 50	(Lawson & Arnold,

	(MMN)	upper limbs		2014)
	Spinal muscular atrophy (SMA)	Weakness of lower limbs	Variable	(Liewluck & Saperstein, 2015)
	Spinal muscular atrophy, lower extremity predominance (SMA-LED)	Muscle weakness, in some cases, compounded with cognitive impairment	Congenital or early childhood onset	(Harms et al., 2010)
	Spinobublar muscular atrophy (SBMA) or Kennedy's disease	Weakness of leg, cramps and tremor	Variable (age of 30-50 years)	(Verschueren, 2017)
	Distal hereditary motor neuropathies (dHMN)	Weakness of the distal limb	Variable	(Verschueren, 2017)
	Progressive bulbar palsy (PBP)	Bulbar muscles with less prominent limb weakness	Age 50 years	(Zhang, Chen, Tang, Zhang, & Fan, 2017)
UMN and LMN	**Amyotrophic lateral sclerosis (ALS)**	Muscle weakness, muscle atrophy, respiratory muscle decline	Around age 60 (rare juvenile cases)	(Swinnen & Robberecht, 2014)

Table 1.2 Table summarizes three main types of MND based on the type of affected neurons. The symptoms and diseases onset are also summarized. UMN = upper motor neuron, LMN = lower motor neuron.

1.2.1 SMA-LED

Spinal muscular atrophy with lower extremity predominance (SMA-LED) is a congenital or early childhood onset MND with incidence rate of 1 in 10,000 live births and has been reported for decades (Fleury & Hageman, 1985; Mercuri et al., 2004). In SMA-LED patient, the proximal muscles of lower limbs are affected predominantly (Harms et al., 2010). Moreover, with identification of further patients, the clinical phenotype of SMA-LED has expanded to MN degeneration, congenital or early childhood onset with little or no progression, and in some cases with intellectual disability (Harms et al., 2010; Niu, Wang, Shi, & Jin, 2015).

1.2.1.1 Genetics of SMA-LED

Mutations in motor protein dynein cytoplasmic 1, heavy chain 1 (*DYNC1H1*) (OMIM #158600), and motor adaptor bicaudal D homolog 2 (*BICD2*) (OMIM #615290) with a frequency of approximately 2 % in European population have been identified in many cases of SMA-LED (Deng, Klein, et al., 2010; Oates et al., 2013; Peeters et al., 2013). Initially, three missense mutations (I584L, K671E, and Y970C) in the tail domain of *DYNC1H1* were recognised as causative (Harms et al., 2012) followed by identification of an additional tail domain mutation (H306R) in a pedigree with Charcot-Marie-Tooth type 2, with the same mutation also found in some SMA-LED cases (Tsurusaki et al., 2012; Weedon et al., 2011; Willemsen et al., 2012).

Two DYNC1H1 mutations, DYNC1H1^{R339G} homozygous and DYNC1H1^{D338N} heterozygous identified in SMA-LED patients (Scoto et al., 2015), are discussed further in this thesis. The locations of these two mutations in dynein heavy chain are shown in figure 1.2 A.

1.2.1.1.1 DYNC1H1^{R399G}

Scoto et al. reported the tail domain p.R399G *DYNC1H1* mutation (see location on Figure 1.2) (Scoto et al., 2015). In that family, the lower limb denervation, muscle atrophy, and lower limb weakness were reported in heterozygous father who had a positive family history for cognitive impairment. In heterozygous mother, only positive family history for the neurodevelopmental delay was reported. The heterozygous father was able to walk independently and the symptoms started in adulthood. The homozygous offspring exhibited a severe phenotype. The onset was at birth and the child showed arthrogryposis in both lower and upper limbs and talipes and axial hypotonia. The homozygous offspring never achieved independent ambulation but was able to sit independently and stand with support.

Moreover, with an examination at age 9.5, distal lower limb muscle atrophy and proximal weakness were reported. In addition, performing cognitive test, mental retardation and attention deficit hyperactivity disorder (ADHD) was confirmed. The fibroblasts derived from this patient at age 9.5 were used in our study.

1.2.1.1.2 DYNC1H1^{D338N}

Scoto et al. also reported the p.D338N *DYNC1H1* de novo heterozygous mutation (see location on Figure 1.2) (Scoto et al., 2015). The patient displayed symptoms such as talipes and arthrogryposis at birth. Moreover, examination at age 3 represented that patient was able to sit independently. Additionally, contractures at hips, knees were reported in the patient as well as adducted thumbs. Muscle atrophy in upper limbs and lower limbs and muscle weakness in bulbar muscles were reported. The cognitive test was not performed but the speech delay was reported. The fibroblasts derived from this patient at age 3 were used in our study.

1.2.1.2 Motor proteins

As mentioned above, the relevance of motor protein function for motor neuron patients has been appeared. Indeed, alterations of motor protein function cause a broad spectrum of neurological phenotypes. There are three superfamilies of cytoskeletal molecular motors, including myosin, kinesin and dynein that are involved in cellular transport (Hirokawa & Takemura, 2005)**.** This thesis will elaborate on dynein, although myosin and kinesin will be discussed briefly.

1.2.1.2.1 Myosin

Myosin superfamily is a large and diverse family and members are grouped into many classes. Myosins contain actin-and ATP-binding sites and moves along actin filaments to drive the short-range transport that usually occurs beneath the plasma membrane. The energy for the motility of myosin is generated by hydrolysing ATP. In areas of the cells adjacent to plasma membrane with defined actin orientation such as cell periphery, myosin V is involved in transport of the cargo toward the cell membrane and myosin VI is involved in the opposite direction transport toward the centre. Moreover, interaction of cargo activates the myosin by conformational changes (Yao et al., 2015). In addition to the role of myosin in the transport of vesicles, organelles and ribonucleoproteins (RNPs), myosin is also involved in a variety of activities in living cells such as actin organisation, intracellular trafficking, cell division, and cell signaling (Titus, 2018).

Consequently, disruption of myosin function has been demonstrated to cause the accumulation of vesicles in the cell periphery and blockage of several endocytic processes (Aschenbrenner, Naccache, & Hasson, 2004). Deficiency of myosin has also been described in several disorders, including hypertrophic cardiomyopathy (β-cardiac myosin), Usher syndrome (myosin VIIa), and cancer. Loss of organelle transport affected by myosin Va has also been found in Griscelli syndrome and Elejalde disease (Titus, 2018).

1.2.1.2.2 Kinesin

Kinesin superfamily proteins with more than 45 members are MT-based motor proteins and organised into 15 families (Hirokawa & Tanaka, 2015). Members of kinesin-1,-2, -3, and -4 mediate intracellular transport, and the remaining regulates the processes such as mitosis and cytoskeletal remodelling (Silverman et al., 2010).

In kinesin heavy chain, there is a microtubule-binding region connecting kinesin to the microtubule (MT). Kinesin moves along the MT to transfer the organelles and cargoes toward the cell periphery. Consequently, missense mutation in N-terminal motor domain of kinesin-1 affecting its MT-binding region causes deficiency in mitochondrial transport in a patient with hereditary spastic paraplegia, an axonal degeneration disorder (Mandal & Drerup, 2019). Moreover, kinesin-based transport has been identified as a crucial mechanism for adhesion structures such as focal adhesions (Stehbens & Wittmann, 2012). Importantly, kinesin mutations have been implicated in pathology of ALS (Brenner et al., 2018).

1.2.1.2.3 Cytoplasmic dynein 1

Dynein family is another cytoskeletal motor protein families. Dyneins are MT-associated motor proteins and based on structure and function are classified into two groups; axonemal and cytoplasmic dyneins (Roberts, Kon, Knight, Sutoh, & Burgess, 2013). The axonemal dynein mediates ciliary and flagellar beating (Summers & Gibbons, 1971). In contrast, cytoplasmic dyneins are responsible for minus-end intracellular transport (Ishikawa & Marshall, 2011; Roberts, 2018). Cytoplasmic dynein-1 is more abundant in all MT-containing cells and cytoplasmic dynein-2 is found within and around the base of cilia and flagella, involved in retrograde intraflagellar transport. In this study, cytoplasmic dynein-1, henceforth referred to as dynein, its structure and function (see section 1.2.1.2.3.2) will be discussed further.

Dynein is a protein complex consisting of multiple polypeptide subunits and mainly responsible for the minus-end directed transport and involved in cell division and neurodevelopment (Carter, 2013; Roberts et al., 2013; Trokter, Mücke, & Surrey, 2012; Zhang et al., 2017). Dynein is also involved in retrograde transport of late endosomal cargoes and deficiency in dynein function causes the dispersion of late endocytic organelles (Harada et al., 1998).

Dynein functions as a protein complex formed around a homodimer of heavy chains (HC) (DYNC1H1), the force-generating subunits. HC contains 4,634 amino acid residues and homodimer of two heavy chains (> 500 kDa each) form the core of dynein, which contain elements required for motility (**Figure 1.2 A**) (**Figure 1.3 B**). The motor domain of HC at its C-terminus belongs to the AAA+ superfamily and includes a ring of six AAA+ ATPase modules, and a 15nm stalk domain which is responsible for MT-binding and generating movement along the MT (Carter, 2013; Roberts et al., 2013; Vallee, McKenney, & Ori-McKenney, 2012).

Figure 1.2

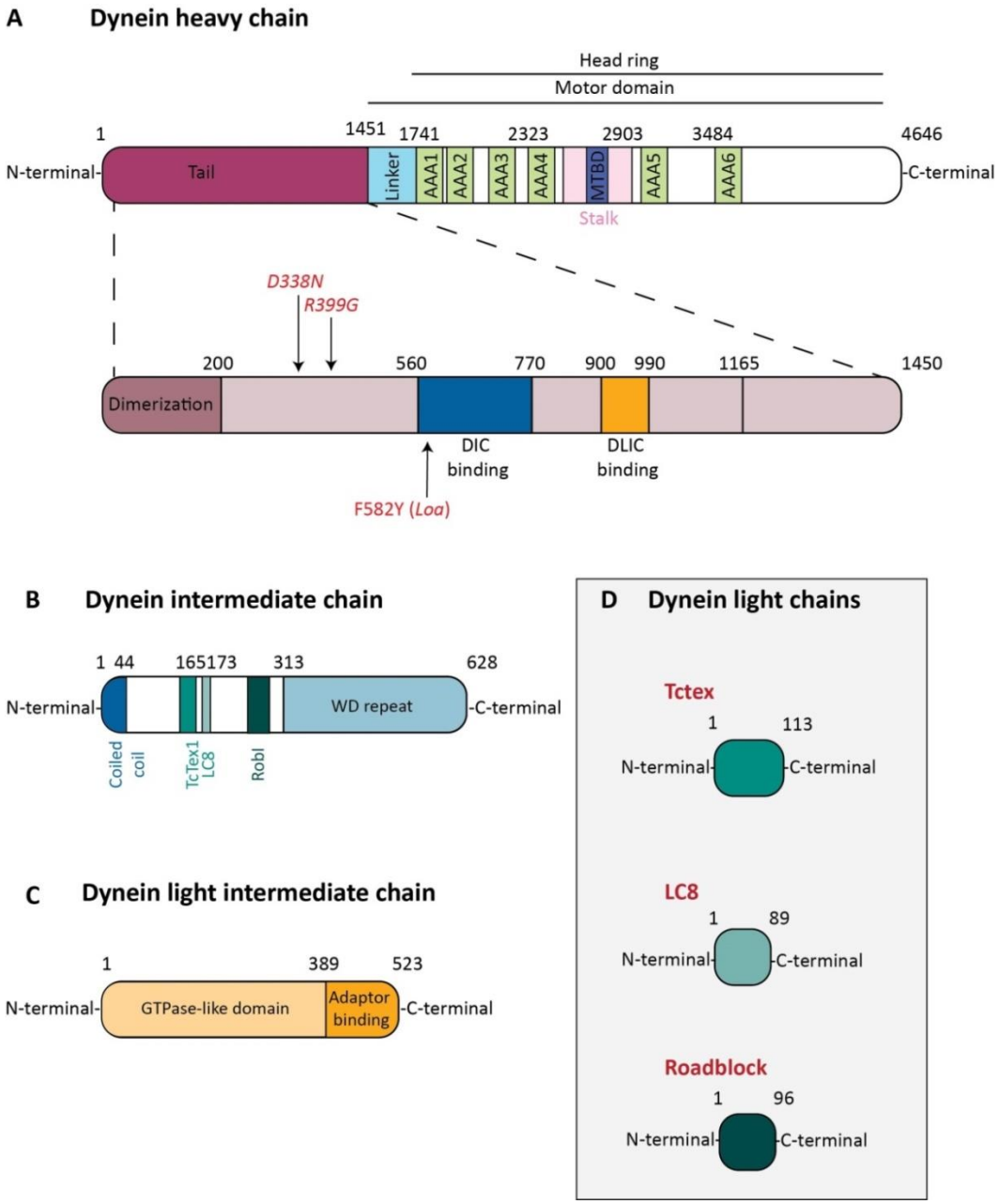

Figure 1.2 Schematic representation of functional domain of dynein. (**A**) The domain structure of human dynein heavy chain. The scheme presents the homodimerisation region and likner. Positions of DYNC1H1 of human and mouse mutations (indicated in red) mentioned in this study. (**B**) The domain structure of dynein intermediate chain (IC) domain. The light chain binding sites are indicated. (**C**) The domain structure of human dynein light intermediate chain (LIC). (**D**) The domain structures of three light chains (Tctex, LC8, and Roadblock 1) are shown. Adopted from (Hoang et al., 2017) with added information.

Figure 1.3

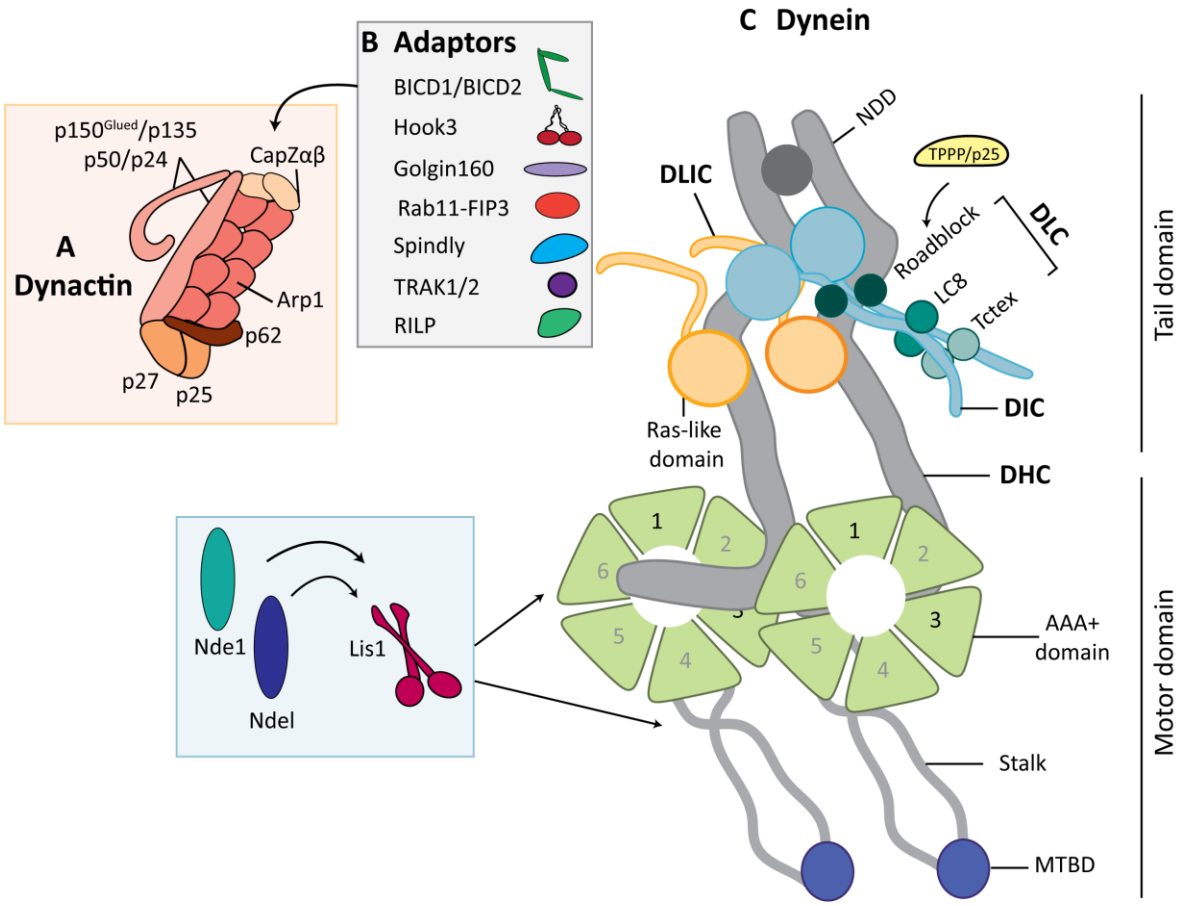

Figure 1.3 The cytoplasmic dynein 1 complex and its regulators. (**A**) Structure of dynactin. Dynactin is one of regulators of cytoplasmic dynein 1 and contains a filament of eight copies of the actin related Arp1, the large subunit p150glued, and 14 additional subunits. Some of dynein cargo-adaptors are indicated that regulate the interactions with different cargoes. (**B**) Cargo adaptors. Some of cargo adaptors are shown, which link different cargoes to the dynein for transport. (**C**) The cytoplasmic dynein 1 molecule is a complex of two dynein heavy chains (C), two intermediate chains (IC), two light intermediate chains (LIC), and three light chains (LC). The two DHCs are connected by an N-terminal dimerization domain (NDD). The C-terminal motor domain comprises a ring of six AAA+ ATPase modules (numbered 1-6) and a stalk that contains the MT binding domain (MTBD) at the end of a long coiled-coil stalk. The N-terminal tail domain interacts with smaller non-catalytic subunits, and is involved in dimerization and cargo interaction. The dynactin complex and Lis1/Ndel/Nde1 complex are important factors in the both regulation of cargo interaction and motor function. Adopted from (Hoang et al., 2017).

The tail domain has been identified to serve as a platform to link with adaptors like dynactin and dynein cargoes (Urnavicius et al., 2018). Residues 1-200 in the N-terminal tail domain of HC have been demonstrated to be responsible for dimerization (**Figure 1.2 A**). Following this region, each tail forms a rod containing binding site for an intermediate chain (IC) (IC1 encoded by *DYNC1I1* and IC2 encoded by *DYNC1I2*) and a light intermediate chains (LIC) (LIC1 encoded by *DYNC1LI1* and LIC2 encoded by *DYNC1LI2*) (Williams et al., 2007). The binding region for IC is estimated between residues 560 and 770 (Steffen, Hodgkinson, & Wiche, 1996). The LIC binding region is identified between residues 900 and 990 (**Figure 1.2 A**) (Tynan, Gee, & Vallee, 2000).

Moreover, at the N-terminus of two ICs, there is an extended region for the binding of light chain dimers, which maintains the ICs together and keeps the HCs parallel to each other (Stuchell-Brereton et al., 2011). Between the two isoforms of IC, IC2 has been recognised to be crucial for association of dynein with the Golgi apparatus for Golgi positioning (Palmer, Hughes, & Stephens, 2009; Roberts et al., 2013). Furthermore, it has been reported that IC2 interacts with proteins such as cytosolic chaperonin containing T complex protein 1 (CCT) which is critical for its folding (Özdemir, Machida, Imataka, & Catling, 2016). Besides, IC via binding to snapin coordinates late endocytic transport, and deletion of *snapin* impedes the retrograde transport of late endosomes (Cai et al., 2010).

Three classes of light chains (LC) consist of LL1/2 (LC81/2), LT1/3 (Tctex1 and Tctex1L), and Roadblock-1/2 bind to each IC (King, 2000; Pfister et al., 2006) (**Figure 1.2 D**). IC contains a WD40 repeat domain, and the Roadblock interacts with the region immediately preceding WD40 repeat domain, whereas Tctex and LC8 bind to the extended N-terminal domain (Susalka et al., 2002).

LC8 is highly conserved and ubiquitously expressed homodimer proteins consisting of 89 amino acid residues (Rapali et al., 2011) (**Figure 1.2 D**) (**Figure 1.3 C**). LC8 interacts with tubulin polymerisation-promoting protein (TPPP/p25) contributing to the dynamic of MT (Oláh et al., 2019). Moreover, LC3 binds directly to α or β-tubulin enhancing the MT dynamic and stability, with loss of LC8 resulting in apoptosis and mitotic block (Asthana,

Kuchibhatla, Jana, Ray, & Panda, 2012). Additionally, Roadblock-type 1 regulates the subcellular localisation of cargoes and transport of lysosomes and signaling endosomes (Terenzio et al., 2020).

LICs through binding to HC participate in different cellular functions such as ER-Golgi trafficking, neurogenesis, neuronal migration, and brain development (Brown, Hunt, & Stephens, 2014; Gonçalves, Dantas, & Vallee, 2019; Palmer et al., 2009). Moreover, the mutation in the gene encoding LIC1 helix causes impaired dynein-driven positioning of lysosomes (Lee et al., 2018). LIC1 has been found to interact with adaptor proteins such as FIP3, RILP, BICD2, hook proteins, and Spindly and attaches to dynein heavy chain with a Ras-like domain (Gama et al., 2017; Scherer, Yi, & Vallee, 2014; Schroeder, Ostrem, Hertz, & Vale, 2014; Schroeder & Vale, 2016).

Importantly, the C-terminal of HC motor domain comprises a pseudohexameric ring with six non-identical AAA domains (AAA1-AAA6) which form a ring (Schmidt, Gleave, & Carter, 2012) (**Figure 1.2 A) (Figure 1.3 C**). Motor domain also contains three appendages including the stalk, buttress/strut and the linker (Bhabha, Johnson, Schroeder, & Vale, 2016). The tip of the stalk is an MT-binding domain (MTBD) (between residues 3039-3291) which is small globular polypeptide region protruding from between AAA4 and AAA5 (Burgess, Walker, Sakakibara, Knight, & Oiwa, 2003).

Among the AAA+ sites, AAA1-AAA4 are capable of binding to adenosine triphosphate (ATP) but AAA1, AAA3 and AAA4 are capable of hydrolysis. AAA5 and AAA6 lack the motifs for ATP binding and hydrolysis and are thought to modulate the conformational changes in AAA+ ring (Gee, Heuser, & Vallee, 1997). Mutations in different AAA+ sites result in the reduction of motor velocity and deficiencies in linker swing, while mutations in AAA3 results in a strong attachment to MT which only can be detached by force (DeWitt, Cypranowska, Cleary, Belyy, & Yildiz, 2015).

The next section will focus on the regulation of dynein functions.

1.2.1.2.3.1 Regulators of cytoplasmic dynein 1

Dynein is regulated spatially and temporally to perform different activities. Dynein's function relies on several regulators as well as cargo adaptors modulating its activation and functions. The main regulators of dynein consist of dynactin, Lissencephaly-1 (Lis1), Ndel, and Ndel1 (Cianfrocco, DeSantis, Leschziner, & Reck-Peterson, 2015; Roberts et al., 2013; Vallee et al., 2012) (**Figure 1.3**).

Dynactin is a multisubunit protein complex and consists of more than 20 subunits. Dynactin is mainly built around a filament of actin-related protein 1 (Arp1), and the largest subunit $p150^{Glued}$ sits on top (Schroer, 2004) (**Figure 1.3 A**). Dynactin interacts with N-terminus of IC through its dynein-binding site in $p150^{Glued}$, although a stable interaction depends on the presence of cargo adaptors such as Bicaudal D2 (BICD2) and Hook3 (Schlager, Hoang, Urnavicius, Bullock, & Carter, 2014) (**Figure 1.3 B**). The dynactin-BICD2 complex interacts with the motor domain of dynein and activates dynein by induction of asymmetry in the dimer of dynein tails (Torisawa et al., 2014). Moreover, this interaction promotes the binding of dynein to MT, a crucial step for processive movement, by orienting the dynein dimer to an optimal conformation and reorienting of motor domains in a parallel manner, which is conducive for processive motility (Jha & Surrey, 2015; King & Schroer, 2000; Urnavicius et al., 2015, 2015). In addition, interaction between dynactin with a cargo adaptor such as BICD2, Hook3, Spindly, or Rab11-FIP3 enhances its processivity *in vitro* (McKenney, Huynh, Tanenbaum, Bhabha, & Vale, 2014; Schlager, Hoang, et al., 2014).

Furthermore, dynein-dynactin complex promotes efficient binding of the cargo to this complex versus kinesin-1 and stimulates the movement of cargo toward the MT minus end (Elshenawy et al., 2019). However, interaction between dynein and dynactin might get lost when dynein and dynactin become engaged with its cargo-associated adaptor (Chowdhury, Ketcham, Schroer, & Lander, 2015; Ketcham & Schroer, 2018). It has also been reported that disruption of dynein-dynactin interaction causes Golgi fragmentation

and impairs the ER-Golgi transport (Lord, Ferro-Novick, & Miller, 2013) (**see section 1.2.1.2.3.2.3**).

Lis1, another conserved dynein-regulatory factor, is an essential effector binding dynein at two sites in the motor domain. The binding of Lis1 is required for several dynein functions such as axonal transport, vesicular transport, neuronal migration, and mitosis (Htet et al., 2020; Moughamian, Osborn, Lazarus, Maday, & Holzbaur, 2013; Yi et al., 2011) (**Figure 1.3**). Lis1 binds to dynein motor domain based on the nucleotide state of motor domain and modulates the MT-binding state of dynein and promotes the formation of an activated dynein-dynactin complex consisting of two dynein dimers (DeSantis et al., 2017). Lis1 enhances the stepping rate of dynein-dynactin complex, elevating force production for an efficient competition versus kinesin (Elshenawy et al., 2020). Although it has been shown that sustained binding of Lis1 is not necessary for the fast velocity (Htet et al., 2020). It has also been found that after assembly of the complex, Lis1 detaches from motile dynein-dynactin complex (Elshenawy et al., 2020).

Nde1 and Ndel1 also appear to promote the interaction of dynein and Lis1, which is essential for dynein functions (Torisawa et al., 2011). Ndel1 is involved in the organisation of cytoskeleton, and the depletion of Ndel leads to the axonal enlargement (Kuijpers et al., 2016). Moreover, aberrant activation of Lis1/Ndl/dynein complex by cyclin-dependent kinase 5 (CDK5) affects the release of dynein from MT and inhibits the motility of dynein (Klinman & Holzbaur, 2015).

Although dynein's partners such as dynactin and Lis1/Nde1/Ndel complex regulate dynein processivity and cargo interaction, but also there have been a group of adaptor proteins including BICD1, BICD2, Hook3, Rab11-FIP3, RILP, TRAK1 and 2, Spindly and Golgin160 that control dynein's function (Jha & Surrey, 2015; McKenney et al., 2014, 2014)**.** It has been shown that binding of adaptors and dynactin to dynein by induction of conformational changes in the motor domains, promotes the separation of motor heads and thus triggers directional motility regulating the speed and processivity of dynein (Schlager, Serra-Marques, et al., 2014; Urnavicius et al., 2015, 2015). Interestingly, kinesin-1 also regulates

the transport of dynein to the axonal terminal, which is necessary for neuronal function (Twelvetrees et al., 2016).

Apart from the extrinsic factors regulating dynein's function, it has been shown that human dynein-1 and dynein-2 are autoregulated through intracomplex interactions. The autoinhibited conformation of dynein-1 and dynein-2 decreases velocity, ATPase activity, and MT-binding rate. Moreover, the autoinhibition of dynein-1 affects its interaction with dynactin and BICD2 (Toropova, Mladenov, & Roberts, 2017; K. Zhang et al., 2017). It has been shown that Lis1 is also involved in the regulation of autoinhibited conformation of dynein, which ensures its localisation and activity (Marzo, Griswold, & Markus, 2020).

1.2.1.2.3.2 Functions of cytoplasmic dynein 1

Dynein performs a wide variety of cellular function and mediates the trafficking of several proteins and membrane-bound vesicles initiating cascades vital for cellular homeostasis and survival. Dynein is also involved in trafficking of organelles and regulates organelle positioning. The focus of the following sections will be on the role of dynein in cellular pathways relevant to this research.

1.2.1.2.3.2.1 Intracellular trafficking and axonal transport

Various intracellular cargoes such as vesicles and organelles bind to dynein to move along the MT to reach the appropriate region (Hancock, 2014). The regulation of the trafficking system ensures proper sorting of cellular components and subsequent degradation of substrates. Consequently, deficiencies in cellular trafficking system such as endo-lysosomal pathway including, autophagy (**see section 1.2.1.2.3.2.2**) , endocytic trafficking and lysosomal degradation lead to imbalance membrane trafficking and insufficient

clearance of protein aggregates (**see section 1.2.2.3.1.3.3.4**) (Wang, Telpoukhovskaia, Bahr, Chen, & Gan, 2018).

Neurons use axonal transport to shuttle proteins, organelles and a variety of membrane bound vesicles between soma and synapses (Hirokawa, Niwa, & Tanaka, 2010). For the retrograde axonal transport, dynein is recruited to the plus-end of MT at the distal part of axon for presynaptic activities and initiation of retrograde transport (Moughamian & Holzbaur, 2012; Nirschl, Magiera, Lazarus, Janke, & Holzbaur, 2016). Transport of dynein is also critical for maintenance of homeostasis at the tip of axon (Stokin et al., 2005). Moreover, mutations in transport-related genes cause neurodegenerative phenotype in mice and human (Hafezparast et al., 2003; Puls et al., 2003). Deficits in axonal transport have been associated with many neurodegenerative conditions and have been considered as a causative step of axon and synapse loss (De Vos, Grierson, Ackerley, & Miller, 2008). Furthermore, slowing of axonal transport has been identified as an initial step in the pathogenesis of neurodegenerative diseases such as Huntington's disease and ALS (Perlson, Maday, Fu, Moughamian, & Holzbaur, 2010). Additionally, abnormalities in transport of organelles have been reported in ALS cases and animal models of ALS (Bilsland et al., 2010; Breuer & Atkinson, 1988). Indeed, the studies have shown that ageing causes a reduction in the retromer, a complex involved in retrograde transport of cargo from endosome to the trans-Golgi, which is under the regulation of dynein. In addition, concomitant disruption of dynein activity leads to the dysregulation of retromer, resulting in a further deficiency in retrograde transport (Kimura et al., 2016). Function of dynein in axonal transport is regulated through different factors such as glycogen synthase kinase 3 beta (GSK3β) (Gibbs, Greensmith, & Schiavo, 2015). It has been shown that GSK3β-dependent phosphorylation of IC-1 and IC-2 inhibits the retrograde transport of acidic organelles. Consequently, phosphorylation of IC-1 reduces dynein interaction with Lis1 and Ndel1 which enhances dynein force (Gao et al., 2015; McKenney, Vershinin, Kunwar, Vallee, & Gross, 2010). In addition, interaction between dynein and dynactin is necessary for axonal transport and disruption of the dynein-dynactin complex results in MN loss and muscle denervation (LaMonte et al., 2002). BICD1 and BICD2 also facilitate

recruitment of dynein-dynactin to Rab6-positive Golgi during axonal transport (Matanis et al., 2002). Interesting, binding of various activating adaptor, regulates binding affinity of dynein to different cargoes for axonal transport. As an instance, Hook1 activates dynein for retrograde transport of signaling endosomes but it is not required for transport of autophagosomes or mitochondria (Olenick, Dominguez, & Holzbaur, 2019).

1.2.1.2.3.2.2 Autophagy

Autophagy is the main degradation pathway to remove aggregated proteins and defective organelles and dynein plays a key role in this process particularly in neurons (see section 1.2.2.3.1.3). In neurons, autophagosomes are generated in the distal part of the axon through recruitment of JNK-interacting protein 1 (JIP1) bind to dynein-dynactin complex for the initiation of their retrograde movement (Fu, Nirschl, & Holzbaur, 2014; Ikenaka et al., 2013; Maday, Wallace, & Holzbaur, 2012). JIP1 also binds to dynactin directly, which is required for sustained transport of autophagosome along the axon (Fu et al., 2014). In addition, for efficient transport of membrane-bound cargoes such as autophagosome, interaction between dynein complex with regulatory factors such as huntingtin-associated protein-1 (HAP1) is necessary (Wong & Holzbaur, 2014). Dynein also interacts with snapin, which facilitates movement of autophagosome toward the cell soma for degradation (Cheng, Zhou, Lin, Cai, & Sheng, 2015). Indeed, dynein contributes to the efficient fusion of the autophagosome with the lysosome (Kimura, Noda, & Yoshimori, 2008).

Consequently, decreased levels of dynactin-1 affecting dynein's function results in the accumulation of autophagosomes leading to loss of MNs (Ikenaka et al., 2013). In support of this notion, blocking the interaction of dynein-dynactin through the expression of the dominant-negative dynein inhibitor CC1 attenuates the movement of autophagosome (Maday et al., 2012). Study of dynein mutations in fly and mouse models has also shown impaired autophagic clearance of PolyQ-htt, increased number of autophagosomes and

the levels of LC3II causing a reduction in clearance of aggregated proteins (Ravikumar et al., 2005).

Collectively, impaired proteostasis has been considered as a consequence of dynein dysfunction in autophagy, which leads to the protein accumulation, subsequent neuronal vulnerability and neurodegeneration (Boland et al., 2008).

1.2.1.2.3.2.3 Positioning and integrity of Golgi apparatus

Dynein function is central in organelle positioning. It has been shown that dynein generates pulling force along the MT for positioning of organelles (Shekhar, Wu, Dickinson, & Lele, 2013). Importantly, dynein plays an important role in positioning of Golgi apparatus. Golgi apparatus has a crucial role in maintenance of cellular homeostasis (Jaarsma & Hoogenraad, 2015; Millarte & Farhan, 2012). The Golgi ribbons are highly dynamic and formed of membrane-bound cisternae laterally connected. The proper cisternal-stacking morphology of Golgi is essential for its function in posttranslational modification (PTM), maturation, and transport of proteins (Klumperman, 2011). Therefore, organisation of Golgi stack is maintained by a set of proteins consist of Golgi matrix proteins (including GRASP55/65, GM130, Golgin45, Golgin84 and Golgin160), MT and MT-associated proteins, proteins of transport machinery, and signaling proteins (Martinez-Alonso, Tomás, & Martinez-Menárguez, 2013; Puthenveedu, Bachert, Puri, Lanni, & Linstedt, 2006).

Importantly, dynein interacts with different dynein-interacting proteins on the Golgi membrane. However, among these dynein-interacting proteins, only Golgin160 is necessary for recruitment of dynein. Golgin160 localises on the *cis*-Golgi and through its CC7 domain, interacts with IC (Yadav, Puthenveedu, & Linstedt, 2012; Yadav et al., 2012) (**Figure 1.4**).

Figure 1.4

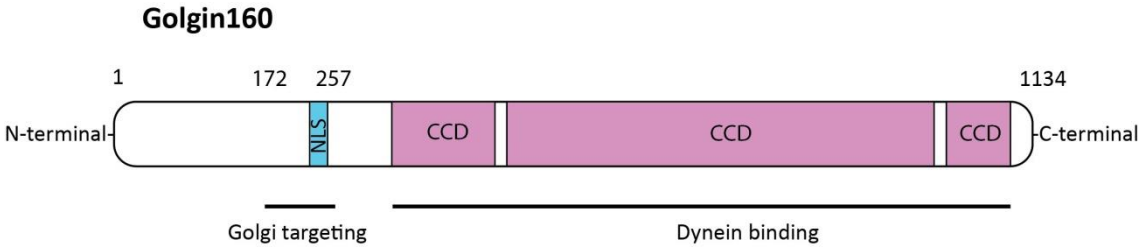

Figure 1.4 Schematic representation of functional domain of Golgin160. The potential coiled-coil domain, nuclear localising signal (NLS) and Golgi targeting region are shown. Adopted from (Gillingham & Munro, 2003).

The recruitment of dynein through Golgin160 is essential not only for the positioning of the Golgi apparatus but also retrograde movement involved in centripetal motility of Golgi membrane (Yadav et al., 2012).

Moreover, Golgin160 via its N- terminus domain links to Arf 1 (small GTPase) on Golgi membranes controlling the localisation and association of Golgin160 with dynein complex interaction (Gilbert, Sztul, & Machamer, 2018). Consequently, this interaction regulates the integrity of Golgi, peri-centrosomal position, and ER-Golgi trafficking (Altan-Bonnet, Sougrat, & Lippincott-Schwartz, 2004; Nakamura, Wei, & Seemann, 2012; Yadav, Puri, & Linstedt, 2009). Structural modifications and reduction in Golgi matrix proteins alter Golgi morphology, have been considered as the early pathological symptoms appearing in neurodegenerative diseases before the appearance of other pathological features (Williams, Hicks, Machamer, & Pessin, 2006; Xiang et al., 2013). As an example, it has been observed that Golgi fragmentation occurs before formation of somatodendritic SOD1 inclusions (van Dis et al., 2014).

Dysfunctions of dynein and endosomal abnormalities have been identified to induce Golgi fragmentation (van Dis et al., 2014). It has been shown that the knockout of *Dync1h1* in

mice or dynein inhibition by Ciliobrevin D treatment results in Golgi fragmentation (Sainath & Gallo, 2015). Golgi fragmentation has been detected in MNs of ALS patients (see section 1.2.1) and SMA-LED (see section 1.2.2) patients with a mutation in *bicaudal D homolog 2* (*BICD2*) (Martinez-Carrera & Wirth, 2015; Mourelatos, Gonatas, Stieber, Gurney, & Dal Canto, 1996; Neveling et al., 2013; She, Pan, Tan, & Yang, 2017; Sundaramoorthy, Sultana, & Atkin, 2015).

1.2.1.2.3.3 Mutations of dynein

Disruption of dynein function in MNs results in ALS-like feature (Teuling et al., 2008). Indeed, mutations in *DYNC1H1* have been identified in several neurodevelopmental and neurodegenerative diseases including striatal atrophy, neuronal migration defects, and SMA (Franker & Hoogenraad, 2013; Harms et al., 2010; Willemsen et al., 2012). In addition, mutation of *Tubulin Alpha 1 A* (*TUBA1A*) (R402) also affects the dynein motor activity, which leads to defected migration of cortical neurons in developing mouse brain (Aiken, Moore, & Bates, 2019).

Importantly, the investigation of disease-related dynein mutations leads to understanding the complexity of the dynein structure and its function. Moreover, mouse genetics model has contributed to the further understanding of the functions of cytoplasmic dynein.

In the following sections, human *DYNC1H1* mutations and three mouse lines carrying dynein mutation will be discussed further.

1.2.1.2.3.3.1 Human *DYNC1H1* mutations

Mutations in dynein contribute to several developmental neuropathies and MNDs. The human *DYNC1H1* mutations affect different cellular functions, and they are associated with a variety of nervous system deficiencies, such as SMA, motor-sensory neuropathies, Charcot-Marie-Tooth disease (CMT), and malformations of cortical development (MCD) including lissencephaly, pachygyria and polymicrogyria (Peeters et al., 2013). More than 30 heterozygous missense mutations have been found in patients diagnosed with SMA-LED and MCD. It is noteworthy that disease-associated mutations have a dominant-negative or dominant gain-of-function effect (**Table 1.3**) (Hoang, Schlager, Carter, & Bullock, 2017).

It has been shown that tail domain mutations of *DYNC1H1* (K671E, I584L) in SMA-LED disease result in late-onset mitochondria pathology by affecting the morphology and function of mitochondria (Eschbach et al., 2013). Furthermore, SMA-related mutations in the tail domain of dynein (R264L, R598) increase the binding of dynein to the BICD2 causing abnormalities in the Golgi apparatus (Neveling et al., 2013; Scoto et al., 2015). Also, the combination of mutations in tail and motor domains results in the impaired Golgi membrane trafficking in DYNC1H1 patients (Fiorillo et al., 2014). Additionally, most of dynein heavy chain mutations affect the dynein complex motility but not binding of dynein to its cargo adaptors (Hoang et al., 2017). Moreover, dynein by stabilising MT promotes axonal growth and modulates injury-induced Schwann cell remodelling during peripheral nerve regeneration (Priest, Navarro, Bremer, & Granato, 2019). Aforementioned, two mutations in the tail domain of HC (R399G and D338N) (see section 1.2.1.1.1 and 1.2.1.1.2) have been recognised in congenital SMA-LED. These substitution mutations occurred in the HC homodimerisation domain cause lower limb weakness and muscle atrophy with unknown pathogenesis (Schiavo, Greensmith, Hafezparast, & Fisher, 2013).

Table 1.3 Summary of mutations in human *DYNC1H1*

Mutations in human *DYNC1H1*			
Gene	**Mutation in protein**	**Location**	**Disease**
DYNC1H1	H306R	Tail domain	SMA-LED
	I584L	Tail domain	SMA-LED
	K671E	Tail domain	SMA-LED
	Y970C	Tail domain	SMA-LED
	R399G	Tail domain	SMA-LED
	D338N	Tail domain	SMA-LED
	M581L	Tail domain	SMA-LED
	V612M	Tail domain	SMA-LED
	V673C	Tail domain	SMA-LED
	H306R	Tail domain	SMA-LED
	W673C	Tail domain	SMA-LED
	E603V	Tail domain	SMA-LED
	R264L	Tail domain	SMA-LED/MCD
	I584L	Tail domain	SMA-LED
	R1603T	Motor domain	SMA-LED
	E2616K	Motor domain	SMA-LED
	R598C	Tail domain	SMA-LED/HMSN
	K129I	Tail domain	SMA-LED/MCD

Δ659-662	Tail domain	MCD
E1518K	Motor domain	MCD
R1567Q	Motor domain	MCD
R1962C	Motor domain	MCD
R2720K	Motor domain	MCD
K3241T	Motor domain	MCD
K3336N	Motor domain	MCD
R3344Q	Motor domain	MCD
R3384Q	Motor domain	MCD
H3822P	Motor domain	MCD
K3336N	Stalk	MCD
H3822P	Motor domain	SMA-LED/MCD
R3384Q	Stalk	MCD
R3344Q	Stalk	MCD
K3241T	Stalk	MCD
R3344Q	Stalk	MCD
V236I	Tail domain	CMT
V2734M	Motor domain	CMD

Table 1.3 Summary of mutations in human *DYNC1H1*. Table summarizes locations and the type of disease associated with mutation. The mutations studied in this thesis are highlighted in red.

1.2.1.2.3.3.2 Mouse models of *Dync1h1* mutations

The *legs at odd angles* (*Loa*) mouse was generated by mutagenesis experiments with treating mice with *N-ethyl-N-nitrosourea* (ENU) mutagen (Oliver & Davies, 2012). This line was identified by the twisting of the body and hind limbs clenching when suspended by the tail (Hafezparast et al., 2003). Homozygous *Dync1h1*^{Loa} mice die by day one after birth (Hafezparast et al., 2003).

Dync1h1^{Loa} mice carry a point mutation from phenylalanine to tyrosine (F580Y) within the tail domain of dynein heavy chain (Hafezparast et al., 2003) (**Figure 1.2 A**). This residue lies within the binding site for IC and homodimerisation region (Habura, Tikhonenko, Chisholm, & Koonce, 1999; Tynan et al., 2000). This mutation has been shown to impact the binding affinity of the HC to the other components of the dynein complex. The alteration in binding affinity has also been shown to cause severe motor and sensory neuron loss (Deng et al., 2010). This mutation also alters dynein run length, which leads to deficiencies of cortical lamination and migration (Ori-McKenney & Vallee, 2011). Moreover, this mutation causes motor neuropathy due to the reduction in dynein processivity and retrograde transport. Subsequent analysis showed the age-dependent progressive muscle atrophy and reduced locomotor ability in heterozygous *Loa* mice (Hafezparast et al., 2003). The altered retrograde axonal transport in *Loa* mutation has been considered as a contributing factor to neurodevelopmental phenotype in these mice. Delayed Golgi ribbon reassembly after nocodazole washout has also been observed in mouse embryonic fibroblasts from *Loa* homozygous mice (Hafezparast et al., 2003). This mutation also enhances the binding affinity of the HC with the IC leading to the impaired interaction of dynein complex with dynactin subunits (p150/p135) (W. Deng et al., 2010; Ori-McKenney, Xu, Gross, & Vallee, 2010).

Similar to the *Loa* mouse model, the Cramping-1 (*Cra1*) model was generated using ENU induced mutagenesis (Hafezparast et al., 2003). *Cra1* mice harbour dominantly inherited missense point mutation at the opposite end of the homodimerisation domain (Y1055C),

which neurological phenotype overlaps that of *Loa*. Similar to homozygous *Loa* mice, homozygous *cra1* mice die by day one after birth but the heterozygous mice have a normal life span (Hafezparast et al., 2003). Like as *Loa* mice, the heterozygous mice exhibit the grasping reflex. The *Cra* mutation has not been appeared to alter the basic function of dynein such as mitosis but impact the retrograde transport and results in loss of 80 % of the embryonic spinal anterior horn cells (Hafezparast et al., 2003). Both *Loa* and *Cra1* heterozygous mice can be considered as models to study developmental or degenerative processes (Dupuis et al., 2009; Ilieva et al., 2008).

The Sprawling (*Swl*) mice carry mutation consists of a three-amino-acid residue deletion (Chen et al., 2007). The deletion of region corresponding to residues 1040-1043 in tail domain of cytoplasmic dynein heavy chain results in substitution of four amino acids residues to a single resides. This mutation results in a dominant phenotype and the homozygotes of *Swl* die at the late implantation stage but the heterozygous mice exhibit a normal life span (Scaravilli & Duchen, 1980). Similar to other mouse models, the heterozygous mice display a hind limb grasping. The impaired retrograde transport has been reported in *Swl* heterozygous mice. Importantly, none of *Loa*, *Cra1* or *Swl* impacts the homodimerization of the HC within the N-terminal 200 residues (Zhao et al., 2016).

1.2.1.3 Contribution of impaired cytoskeleton to the degeneration of motor neurons

The cytoskeleton is a critical component of all eukaryotic cells. The combination of protein polymers and a collection of associated factors form a dynamic network of filamentous arrays, which regulates a variety of functions. Moreover, cytoskeletal elements provide a platform for the motor proteins function involved in intracellular transport and cell motility (see section 1.2.1.2) (Tuszynski, Brown, & Sept, 2003).

In neurons, the cytoskeleton is associated with branching patterns, organelle positioning, and the polarity. In particular, with long axons, MNs are highly dependent on cellular

transport, which is facilitated through the cytoskeleton. Importantly, many of the cytoskeleton abnormalities have been identified as a contributing factor to ageing and neurodegeneration (Mattson & Magnus, 2006). Three types of cytoskeletal structures consist of microfilaments, intermediate filament, and MT. This thesis will elaborate on MT, PTMs of MT, and its implications in neurodegeneration (see section 1.2.1.3.3).

1.2.1.3.1 Microfilament

Actin is highly conserved protein and forms the polymeric filaments (F-actin). The assembly of an actin filament is vital for forming the subcellular compartments and cellular functions (Kruppa, Kendrick-Jones, & Buss, 2016). There are 6 isoforms of actin having distinct biological role (Vedula & Kashina, 2018). For instance, it has been shown that actin is involved in the formation of autophagosome precursors (Kast & Dominguez, 2015). Furthermore, it has been demonstrated that actin is enriched in growth cones and the dynamics of actin is critical for the morphology of growth cones (Dent & Gertler, 2003). Moreover, it has been demonstrated that the tau, the MT-associated protein, induces the accumulation and over stabilisation of filamentous actin in a mouse model of Alzheimer's disease (Fulga et al., 2007).

1.2.1.3.2 Intermediate filament

The intermediate filament proteins are grouped into six different types based on the sequence similarity and the cell type specific expression. Importantly, neurons express several types of intermediate filaments based on the developmental stage or their position in the nervous system. As an example, adult neurons synthesize nestin and α;-internexin while precursor cells express vimentin. The intermediate filaments in neurons contribute to the dynamics of axonal cytoskeleton, axonal outgrowth and guidance (Nixon & Shea, 1992). Thus, the perturbation of the organisation and structure of these filaments

is associated with neurodegenerative disease (Perrot, Berges, Bocquet, & Eyer, 2008). For example, abnormal accumulations of intermediate filaments in neurons have been observed in ALS and mutations in peripherin, a component of the intermediate filaments, have been reported in sporadic cases of ALS (sALS) (Gros-Louis et al., 2004; Perrot & Eyer, 2009).

1.2.1.3.3 Microtubule

MTs have been recognised as core components of the cytoskeleton in eukaryotic cells and are critical for different cellular functions such as cell division, shaping, and intracellular transport. The regulation of organelle positioning is also dependant on MT (Janke & Magiera, 2020; Subramanian & Kapoor, 2012). The critical function of MTs has been demonstrated within neurons. MTs are involved in intracellular transport of organelles, RNA granules and proteins along the axon and therefore are vital for the maintenance of neuronal circuitry (Baas, Rao, Matamoros, & Leo, 2016). MTs are stiff tubes, about 25 nm in diameter and are made from polar polymers of αβ-tubulin heterodimers (**Figure 1.5**). MTs have special dynamic properties. At any point in time in a population of MTs, subsets of MTs are growing while others are shrinking quickly. The combination of growth, shrinkage and rapid transitions between two is known as dynamic instability. The dynamic instability of MT allows the cell to rapidly reorganise the cytoskeleton when necessary. The dynamicity and stability of MTs are focus of the next section (see section 1.2.1.3.3.1 Microtubule stability). Moreover, heterodimer of α- and β-tubulin undergoes multiple PTMs which are not uniformly distributed along MTs. PTMs are discussed in at section 1.2.1.3.3.3 (**Figure 1.6**).

Figure 1.5

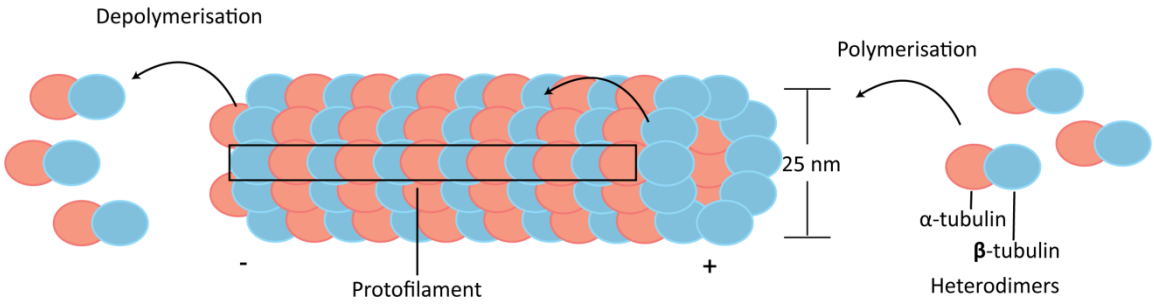

Figure 1.6 Schematic representation of MT structure. MTs are stiff tubes, about 25 nm in diameter and formed of α- and β-tubulin heterodimers. MTs have polar structure and polarity arises from the head to tail arrangement of α- and β-tubulin dimers in a protofilament.

1.2.1.3.3.1 Microtubule stability

MTs are highly dynamic structures, and they fluctuate between polymerisation and the depolymerisation phase, which is known as dynamic instability. An intact MT structure is necessary for successful completion of many cellular functions, such as mitosis, positioning of organelles, and assembling of cilia. Moreover, in differentiated and non-dividing cells, such as neurons, the polarity of MT bundles is needed for polarised growth of axon (Bornens, 2008; Pongrakhananon et al., 2018; Stiess & Bradke, 2011). In axons, MTs are uniformly arrayed with their plus-end positioned distal towards the axon terminal, whereas in dendrites, MT polarity is mixed based on position within the dendritic arbor, neuronal type and organism. It has been shown that most of axonal MTs are more stable than MTs of dendrites; however, a fraction of dynamic MT in axons undergoes phases of growing and shrinking (Howard & Hyman, 2003). Additionally, it has been found that tubulin mutations changing MT dynamic disturb all different stages of

neuronal development including neurogenesis, neuronal migration, and neuronal differentiation (Francis et al., 2006; Guerrini, Dobyns, & Barkovich, 2008).

Due to various functions of MT, the dynamic state of MT is controlled by the intrinsic GTPase activity of tubulin, MT-associated proteins (MAP) and motor proteins, as well as MT PTMs (see section 1.2.1.3.3.3 Microtubule post-translational modification) (Akhmanova & Steinmetz, 2015; Janke & Bulinski, 2011; Janke & Montagnac, 2017).

MAPs such as MT plus-end-tracking proteins through binding to the MT ends control dynamic of MT and its connections with other structures (Akhmanova & Steinmetz, 2015). As an instance, MAP4 interacts with 90-kDa heat shock protein (Hsp90) to regulate MT acetylation and the depletion of Hsp90 leads to MT instability (Wu, Ding, Zheng, & Liao, 2019). Furthermore, dynein alters the MT dynamics, which reciprocally affects the mobility of dynein and its cargo. Additionally, dynein via end-on configuration and holding on a shrinking MT plus end reduces MT depolymerisation (Laan et al., 2012). This end-on pulling is also important for spindle positing (Redemann et al., 2010). Kinesin-4 and kinesin-8 also accumulate at MT ends and members of the kinesin-4 family suppress MT growth at the cell cortex regulating organisation of MT arrays at the cell edge (van der Vaart et al., 2013). Moreover, kinesin-4 motor is involved in controlling the length of axonemal MT (He et al., 2014). The dynamicity of MTs is also regulated through their PTMs (see section 1.4.2.3.3 for further details) (Song & Brady, 2015). Importantly, MT abnormalities are implicated in neurodegenerative disorders such as Alzheimer's disease, Parkinson disease, and ALS (Brunden, Lee, Smith III, Trojanowski, & Ballatore, 2017). The importance of regulation of MT dynamics in ALS is discussed further in the next section.

1.2.1.3.3.2 Microtubule neuronal function and its implication in ALS

In ALS, impairment of neuronal MT results in the changes in physical length of the axon in MNs or alteration in axonal transport. Therefore, it is becoming more apparent that MTs are critical components of ALS (Clark, Yeaman, Blizzard, Chuckowree, & Dickson, 2016).

Moreover, the impairment of axonal transport system, a proposed mechanism for the progression of ALS, highlights the significance of the cytoskeleton, particularly MT (Clark et al., 2016). The polarised MTs within the axon facilitate the transport of organelles necessary for appropriate axon branching and extension and consequently, changes in the MT properties affect the distances travelled by cargoes. Additionally, the abundance of the MT polymers is associated with the cargo pause time and provides the stop points for effective cargo offloading along the axon (Yogev, Cooper, Fetter, Horowitz, & Shen, 2016).

Alterations in MT dynamic in ALS results in accumulation of abnormal mitochondria, misfolded proteins, and reduction of vesicle and mRNA transport. Additionally, changes in MT dynamic have been considered as an initial driving force in both familial cases of ALS (fALS) and sALS (Fanara et al., 2007). Importantly, mutations in Tubulin Alpha 4a (TUBA4A), a component of MTs, including R320C/H, W407X, R215C, and A383T have been identified in ALS patients. These TUBA4 mutations alter the MT stability and repolymerisation capability and cause the spinal onset ALS, with UMN and LMN loss (Smith et al., 2014).

1.2.1.3.3.3 Microtubule post-translational modifications

MTs are subjected to PTMs, and these modifications are essential for the organisation, processivity of motor proteins (see section 1.2.1.2) on MT, MTs dynamics, and their interaction with other cellular components (Sainath & Gallo, 2015; Sirajuddin, Rice, &

Vale, 2014). Some of these PTMs, such as phosphorylation, acetylation, methylation, palmitoylation, ubiquitylation and polyamination, are not specific to MT. However, other modifications, including glutamylation, tyrosination, and polyglutamylation, are more frequent on MTs (Janke & Magiera, 2020) (**Figure 1.6**). The C-terminal domain of α-tubulin has been considered as a hot spot for these modifications, while less modification occurs on the C-termini of β-tubulin (Song & Brady, 2015). The PTMs of MTs have been found in all cell types, and they are even more diverse in neurons, labelling MT subpopulations specialised for specific functions (Janke & Kneussel, 2010). In the following section, some of the PTMs of MTs with the particular focus on acetylation and deacetylation will be discussed.

Figure 1.6

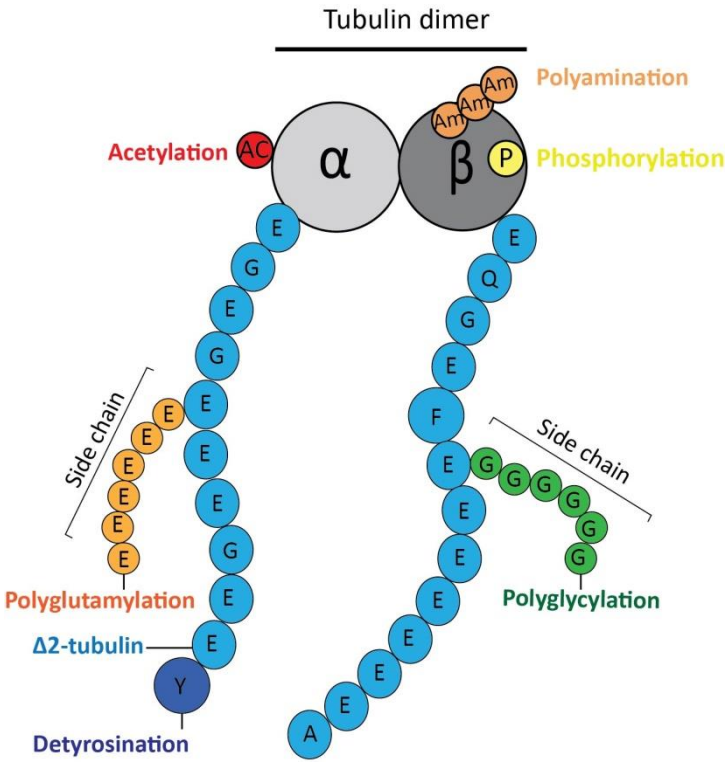

Figure 1.6 Posttranslational modifications of tubulin dimer. Microtubules (MTs) are made of α-tubulin and β-tubulin dimers. The posttranslational modifications are detected on various regions of the tubulin dimer. The α-tubulin acetylation is found at the luminal surface of MT. Polyamination and phosphorylation are present in the globular, folded part of β-tubulin and influence stability of the MT. Detyrosination and Δ2-tubulin are found within the carboxy-terminal tails of α-tubulin, and polyglutamylation and polyglycylation are recognised within the carboxy-terminal tails of both α-tubulin and β-tubulin, which regulate interactions between MTs and associated proteins. Adopted from (Janke & Bulinski, 2011).

1.2.1.3.3.3.1 Tyrosination and detyrosination

Most of α-tubulin contains the terminal tyrosine, and this tyrosine is removed by cytosolic carboxypeptidase. The removal of tyrosin residues occurs in polymerised α-tubulin. In neuronal cells, both tyrosinated and detyrosinated tubulins are distributed along the axonal MTs. However, detyrosinated tubulins are enriched in the proximal segment of axons, and the tyrosinated tubulins are abundant in the distal region of axons (Geuens et al., 1986; Nieuwenhuis et al., 2017). Additionally, tyrosination at the MTs plus-end is important for the formation and organisation of a functional growth cone and regulates a gradient distribution of the components of growth cone required for the growth cone pathfinding during development (Marcos et al., 2009).

Moreover, tyrosination of MT is important for directed signaling and regulation of motor proteins. Tyrosinated tubulins enriched in the somatodendritic compartment prevent binding of kinesin-1 to the MT. Therefore, an increased level of detyrosination abolishes target tracking of kinesin-1 (Konishi & Setou, 2009). Detyrosination reduces active disassembly of MTs and leads to inhibition of activity of neuronal depolymerising motors of kinesin-13 family resulting in MT stabilisation (Peris et al., 2009). Additionally, C-terminal tyrosination of α-tubulin determines the initiation of dynein-driven motility and regulates the motility of dynein-dynactin complex and its adaptor BICD2 on MT (McKenney, Huynh, Vale, & Sirajuddin, 2016).

1.2.1.3.3.3.2 Δ2-tubulin

Δ2-tubulin is a further modification of detyrosination where the terminal glutamate is removed, and then tubulins cannot be tyrosinated (Janke & Kneussel, 2010) (**Figure 1.6**). Both detyrosinated and Δ2-tubulin have been found accumulated in long-lived MTs and are enriched in neurons (Paturle-Lafanechère et al., 1994). Moreover, the increase in

glutamylation on Δ2-tubulin is reported in both acute and slow-developing neurodegeneration (Vu, Akatsu, Hashizume, Setou, & Ikegami, 2017).

1.2.1.3.3.3.3 Polyglutamylation and polyglycylation

Polyglutamylation and polyglycylation are other types of PTMs, where the glutamate or glycine is added to glutamate side chains on C-terminal domains of both α-tubulin and β-tubulin (Mukai et al., 2009) (**Figure 1.6**). The reverse enzyme, deglutamylase, is also involved in the regulation of glutamylation, which has the same affinity for both soluble and polymerised tubulin (Audebert et al., 1993). MT polyglutamylation influences the charges on the carboxy-terminal tails of tubulins. Additionally, polyglutamylation through interactions with MAPs stabilises the MT and regulates electrostatic MT-MAP interactions, which consequently controls the processivity of kinesin and dynein on MTs (Bodakuntla, Jijumon, Villablanca, Gonzalez-Billault, & Janke, 2019; Bonnet et al., 2001, 2001, 2001; Sirajuddin et al., 2014). Glutamylation has been found in many cell types, and high level of glutamylation has been reported on the centrioles during cell division. Besides, it has been reported that the balanced level of MT polyglutamylation is critical in neurons, and hyperglutamylation is associated with neurodegeneration. Furthermore, polyglutamylation regulates the interaction of dynein and MT (Kubo, Yanagisawa, Yagi, Hirono, & Kamiya, 2010). It has also been shown that polyglutamylation is vital for axonal transport, and its dysregulation leads to neurodegeneration (Janke & Magiera, 2020).

1.2.1.3.3.3.4 Polyamination

Polyamination has been described by the addition of amines to glutamine residues of tubulin and recognised as an irreversible PTM. Both α-tubulin and β-tubulin are subjected to this PTM, but mostly it occurs in β-tubulin. The polyamination is mediated via

transglutaminases. The enzyme transglutaminase is involved in tubulin polyamination and polyaminates both free tubulin and polymerised MTs (Song & Brady, 2015). Furthermore, the polyamination sites are located either next to the GTP-binding pocket of β-tubulin, or at the boundary of the α-tubulin-β-tubulin dimer. Polyamination is specific to neuronal MT, and it has not been detected in non-neuronal cells. Polyamination contributes to MT stability in neurons, and it is critical for neuronal development and maturations (Song et al., 2013).

1.2.1.3.3.3.5 Acetylation

In neuronal cells, it has been reported that acetylated MTs are enriched in axons. Acetylation of α-tubulin on the amino group of Lys40 is a marker of stable, long-lived MT (LeDizet & Piperno, 1986; Perdiz, Mackeh, Poüs, & Baillet, 2011). However, there is an on-going debate as acetylation represents stability or it is a modification that takes place on those MTs that survive long enough to go through this modification. It is important to note that currently, the general agreement is with the latter. Importantly, two studies have reported that acetylation protects the MTs from mechanical breakage during ageing by increasing flexibility and resilience against the mechanical stresses (Portran, Schaedel, Xu, Théry, & Nachury, 2017; Xu et al., 2017). This is supported by Eshun-wilson et al.'s study in which they showed that acetylation of Lys40, positioned in an unstructured loop of α-tubulin, decreases the interprotofilament interaction and facilitates protofilament sliding thus enhancing MT flexibility (Eshun-Wilson et al., 2019). Moreover, the acetylation of β-tubulin's Lys25 is carried through the acetyltransferase San (Chu et al., 2011). Nevertheless, the acetylation of α-tubulin has been recognised as an important factor for different cellular and developmental processes such as regulation of MT architecture, morphological transition and migration of cortical neurons (Cueva, Hsin, Huang, & Goodman, 2012; Dompierre et al., 2007; Li et al., 2012; MISSING:reed2006microtubule, 2021).

Moreover, the acetylation of MT is necessary for efficient intracellular trafficking by impacting recruitment and motility of motor proteins (Bhuwania, Castro-Castro, & Linder, 2014; Godena et al., 2014). As an example, Kinesin-1 binds to the acetylated MT with higher affinity and acetylation enhances the motility of kinesin-1 on MT (Cai, McEwen, Martens, Meyhofer, & Verhey, 2009; MISSING:reed2006microtubule, 2021). Similarly, dynein (see section 1.2.1.2.3) binds more effectively to the acetylated MT *in vitro* (Dompierre et al., 2007). Increasing MT acetylation also contributes to efficient axonal transport of cargoes (such as mitochondria) in hippocampal neurons (Chen, Owens, Makarenkova, & Edelman, 2010). Additionally, MT acetylation by moderating the MT dynamics control developmental processes such as axon over branching and pathfinding and loss of MT dynamics results in excessive axonal branching (Wei et al., 2017).

In living cells, different types of proteins have been identified to balance the MT acetylation. Leucine-rich repeat kinase 2 (LRRK2) is one of those proteins that binds to MT, and its mutation alters tubulin acetylation level leading to transport deficiency in Parkinson's disease (Godena et al., 2014).

Moreover, several enzymes have been identified contributing to acetylation of Lys40 such as arrest-defective-1 (ARD1)-N-acetyltransferase 1 (NAT1) complex, histone acetyltransferase GCN5, elongator complex protein 3 (ELP3), and α-tubulin N-acetyltransferase 1 (α-TAT1)/MEC17. Among these enzymes, the α-TAT1 has been recognised as the main enzyme for the acetylation of α-tubulin in *Tetrahymena, C. elegances*, and mice, which function is the focus of next section (Akella et al., 2010; Kalebic, Sorrentino, et al., 2013; Kim, Li, Gorbani, You, & Yang, 2013; Shida, Cueva, Xu, Goodman, & Nachury, 2010).

1.2.1.3.3.3.5.1 Function of α-tubulin N-acetyltransferase 1 (α-TAT1)

As mentioned in the previous section, acetylation of α-tubulin is mainly driven by α-TAT1 which plays important roles in subcellular specialisation of subsets of MT and regulates development of dentate gyrus, mouse forebrain (G.-W. Kim et al., 2013). α-TAT1 also mediates hyperacetylation of MTs during stress responses (G.-W. Kim et al., 2013; Li et al., 2019) and normal sperm flagellar function (Kalebic, Sorrentino, et al., 2013).

In turn, α-TAT1 function is regulated through another kinase TGF-β-activated kinase 1 (TAK1), which phosphorylates α-TAT1 at Ser237 to increase its catalytic activity (Shah et al., 2018). Additionally, a group of proteins in vertebrate termed CAMSAP1-CAMSAP3 via interfering with α-TAT1 function decreases MT acetylation (Pongrakhananon et al., 2018). α-TAT1 also acetylates itself in an autoregulatory mechanism which is necessary for the effective modification of tubulin (Kalebic, Martinez, et al., 2013).

Mouse α-TAT1 consists of five isoforms and human α-TAT1 contains seven isoforms (see **Table 1.4**). The α-TAT1 core consists of a six-stranded β-sheet surrounded by five α-helicases (Szyk et al., 2014). The catalytic activity of α-TAT1 is within residues 2-336 in the N-terminal domain of the protein with the minimal functional catalytic region containing residues 2-193. The C-terminal region is not involved in catalytic activity (Friedmann, Aguilar, Fan, Nachury, & Marmorstein, 2012) (**Figure 1.7**).

Table 1.4 Isoforms of mouse and human of α-TAT1

A

Mouse α-TAT1				
Isoform	**Identifier**	**Length**	**Mass (KDa)**	**Sequence**
Isoform 1	Q8K341-1	421	47	Canonical
Isoform 2	Q8K341-2	398	44	195-218: RPPTSSLRATRHSRAAVADPIPAA → P
Isoform 3	Q8K341-3	353	39	324-353: GTPWGLVAQSCHYSRHGGFNTSFLGTGNQE → SHT HTTTVSLDAWYFHRQPRTEAGGTGSGG 354-421: Missing
Isoform 4	Q8K341-4	333	37	323-333: RGTPWGLVAQS → SSLPRSDESRY 334-421: Missing
Isoform 5	Q8K341-5	310	35	195-218: RPPTSSLRATRHSRAAVADPIPAA → P 323-333: RGTPWGLVAQS → SSLPRSDESRY 334-421: Missing

B

Human α-TAT1				
Isoform	**Identifier**	**Length**	**Mass (KDa)**	**Sequence**
Isoform 1	Q5SQI0-1	421	46	Canonical
Isoform	Q5SQI0-2	409	45	1-12: Missing

2				13-36: ERITVLDQHLRPPARRPGTTTPAR → MWLTWPFCFL TITLREEGVCHLES
Isoform 3	Q5SQI0-3	398	44	195-218: RPPAPSLRATRHSRAAAVDPTPAA → P
Isoform 4	Q5SQI0-4	333	37	323-333: RGTPPGLVAQS → SSLPRSEESRY 334-421: Missing
Isoform 5	Q5SQI0-5	323	36	324-421: Missing
Isoform 6	Q5SQI0-6	310	35	195-218: RPPAPSLRATRHSRAAAVDPTPAA → P 323-333: RGTPPGLVAQS → SSLPRSEESRY 334-421: Missing
Isoform 7	Q5SQI0-7	300	33	195-218: RPPAPSLRATRHSRAAAVDPTPAA → P 324-421: Missing

Table 1.4 Isoforms of mouse and human of α-TAT1 (**A**) Table A represents the isoforms of mouse α-TAT1, length, mass and similarity of sequences. (**B**) Table B represents isoforms of human α-TAT1, length, mass and similarity of sequences. The identifiers are unique numbers defined by UniProt database.

Figure 1.7

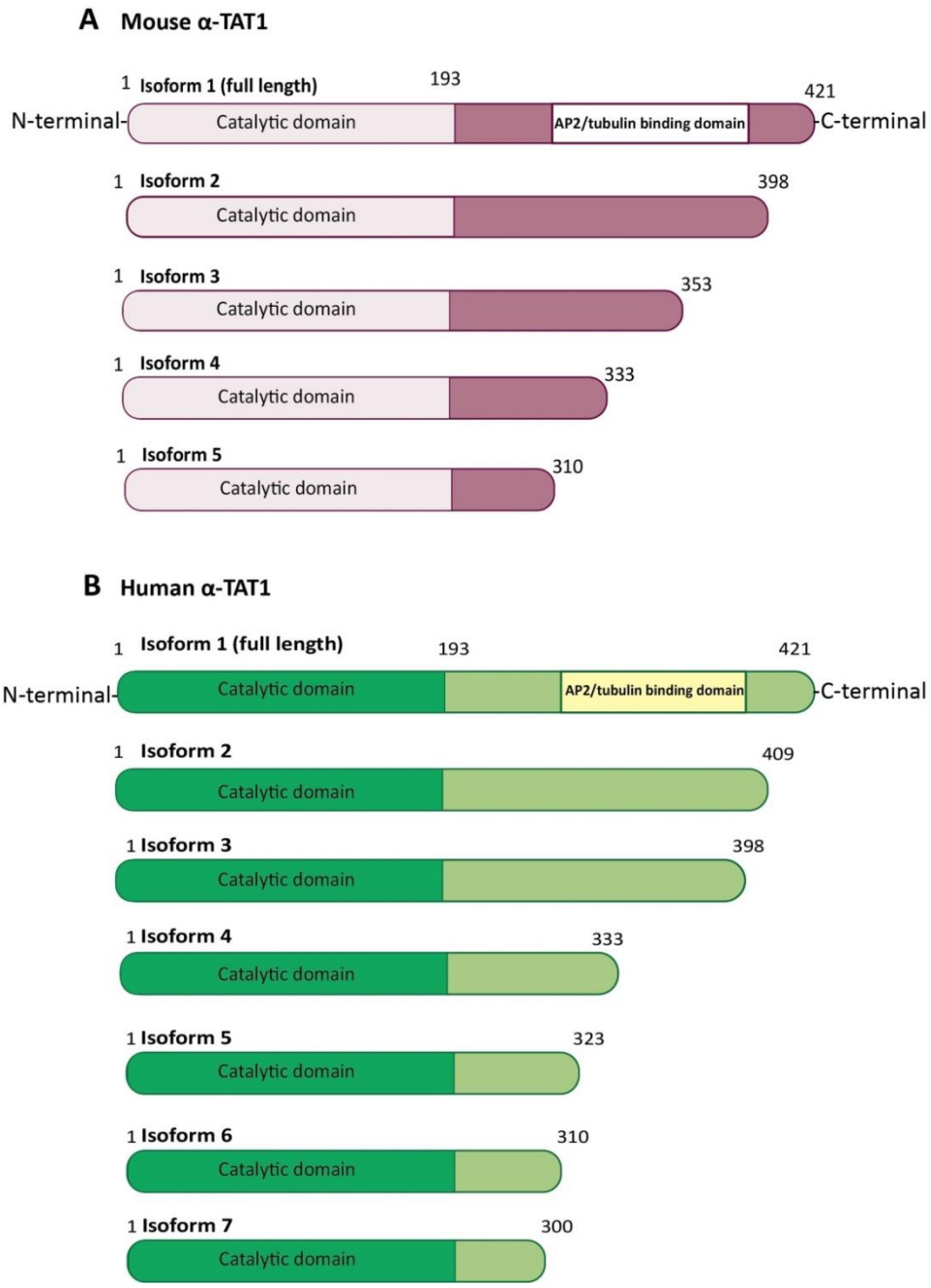

Figure 1.7 Schematic representation of α-TAT1 isoforms. (**A**) Schematic representation of different isoforms of mouse α-TAT1. (**B**) Schematic representation of different isoforms of human α-TAT1. The catalytic and AP2/tubulin binding domains are shown. The numbers represent number of amino

Acetylation is the only PTM that occurs in the lumen of MT. α-TAT1 enters the MT lumen to reach the acetylation site through the irregularities and lateral imperfection (Howes, Alushin, Shida, Nachury, & Nogales, 2014; Shida et al., 2010; Soppina, Herbstman, Skiniotis, & Verhey, 2012; Xu et al., 2017) and then diffuse passively to spread the acetylation longitudinally (Coombes et al., 2016; Ly et al., 2016) (**Figure 1.8**). In addition, α-TAT1 interacts with outside of the MT via the tubulin C-termini, which facilitates α-TAT1 entrance to the luminal site of action if MT go through the lateral opening between protofilaments (Howes et al., 2014). Once α-TAT1 enters the MT lumen, the mobility of α-TAT1 is regulated by its affinity for acetylation sites, where α-TAT1 rebinds from highly concentrated α-tubulin acetylation sites (Coombes et al., 2016; Ly et al., 2016).

Figure 1.8

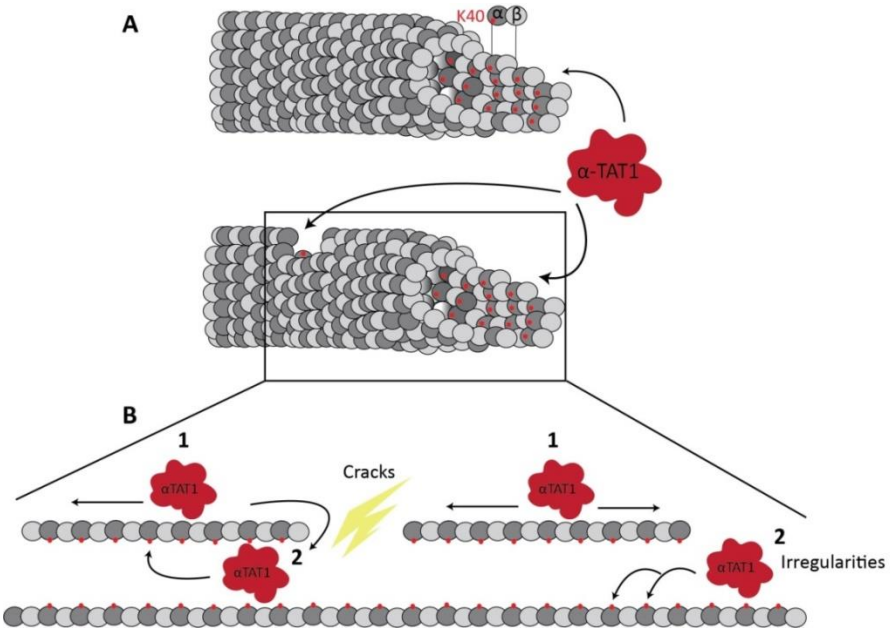

Figure 1.8 Modes of K40 acetylation by α-TAT1. (**A**) Schematic representation of different entry sites of α-TAT1 into the lumen of MT. The integrity of MT determines the availability of these sites. (**B**) The proposed model for α-TAT1 access to the lumen involving a first step during which α-TAT1 scans the outer surface of MT (**1**) in order to find accessible K40 modification sites at MT ends or at cracks in the MT lattice. Once in the lumen, α-TAT1 modifies available K40 sites (**2**). Adopted from (Janke & Montagnac, 2017).

1.2.1.3.3.3.6 Deacetylation

Deacetylation identified for the first time in the modifications of histones to silence gene transcription, but now deacetylation is recognised as a common PTM in multiple subcellular compartments. There have been two groups of protein deacetylases in eukaryotic cells, eleven subtypes of classical histone deacetylases (HDAC1-11) and seven subtypes of sirtuins (SIRTs). HDACs are also classified into two classes; class I HDACs and class II HDACs. Class I HDACs are mainly localised in the nucleus, whereas class II HDACs are shuttled between the cytoplasm and the nucleus (Fischle, Kiermer, Dequiedt, & Verdin, 2001). Among the mammalian HDACs, HDAC6, a well-characterised cytoplasmic class IIb deacetylase, deacetylases several substrates such as heat shock proteins and cortactin (Verdel et al., 2000).

HDAC6 with 1215 amino acid residues is the largest member of the HDAC family. HDAC6 contains two functional deacetylase domains (DD1 and DD2) (**Figure 1.9**). Deacetylase domains counteract with negatively-charged MT surface through the ionic interactions, which are independent of the catalytic domain (Ustinova et al., 2020; Valenzuela-Fernandez, Cabrero, Serrador, & Sánchez-Madrid, 2008).

Figure 1.9

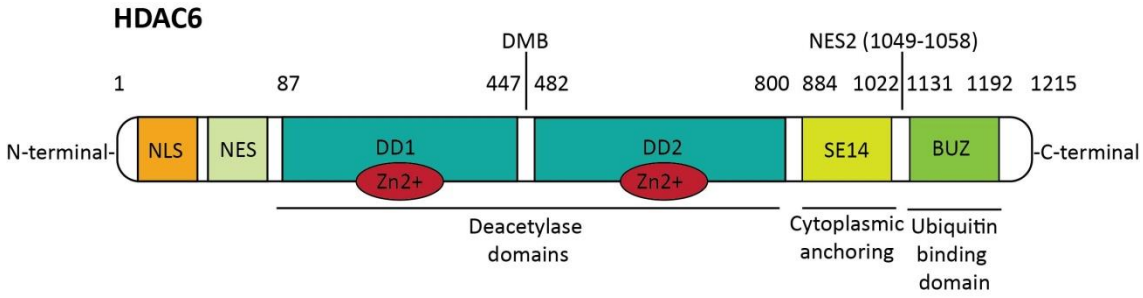

Figure 1.9 Schematic representation of functional domains of HDAC6. HDAC6 contains nuclear localisation signal (NLS), nuclear export signal (NES1 and NES2), two tandem catalytic domains (DD1 and DD2) containing zinc as cofactor, the dynein motor binding (DMB), Ser-Glu-containing tetrapeptide (SE14), and the zinc finger ubiquitin-binding domain (BUZ). Adopted from (Y. Li et al., 2013).

HDAC6 is predominantly localised in the cytoplasm and the nuclear export signals (NES) and the Ser-Glu-containing tetrapeptide (SE14) motif regulate its subcellular localisation. Although it has been shown that by activation of the nuclear localisation signal (NLS), upon arresting cell cycle, HDAC6 transfers to the nucleus (Bertos et al., 2004; Verdel et al., 2000). HDAC6 through its C-terminal binder of ubiquitin zinc finger (BUZ) domain binds to polyubiquitinated proteins (Ouyang et al., 2012). Moreover, binding of BUZ domain with ubiquitin-like interferon-stimulated gene 15 promotes the autophagic clearance of aggregated proteins (Nakashima, Nguyen, Goins, & Chiocca, 2015). Additionally, HDAC6 through its dynein motor-binding (DMB) region interacts with dynein-dynactin complex for the retrograde transport of polyubiquitinated proteins along the MTs (Kawaguchi et al., 2003).

1.2.1.3.3.3.6.1 Function of histone deacetylase (HDAC6)

HDAC6 as a main α-tubulin deacetylase controls the stability of MT pool and MT-mediated processes via both deacetylase-dependent and –independent mechanisms (Hubbert et al., 2002; Matsuyama et al., 2002; Yang, Zhang, Zhang, Zhang, & Xu, 2013). Once tubulin dimers are released from MTs, they will be rapidly deacetylated (Perdiz et al., 2011) (**Figure 1.10 i**). HDAC6 is also recruited to MT for the autophagic degradation of misfolded proteins and stress granules (SG). HDAC6 is also involved in several biological processes, such as cell migration, cell spreading, and viral infection (Kawaguchi et al., 2003; Yan, 2014).

Importantly, function of HDAC6 is regulated through other proteins. It has been shown that interaction of HADC6 with TPPP/p25, an MT-associated protein, affects its deacetylase activity and results in the hyperacetylation of MT (THokési et al., 2010). In addition, binding of Cep70, the centrosomal protein, to HDAC6 inhibits the deacetylase activity of HDAC6 and promotes the tubulin acetylation and MT stability (Shi et al., 2015).

Figure 1.10

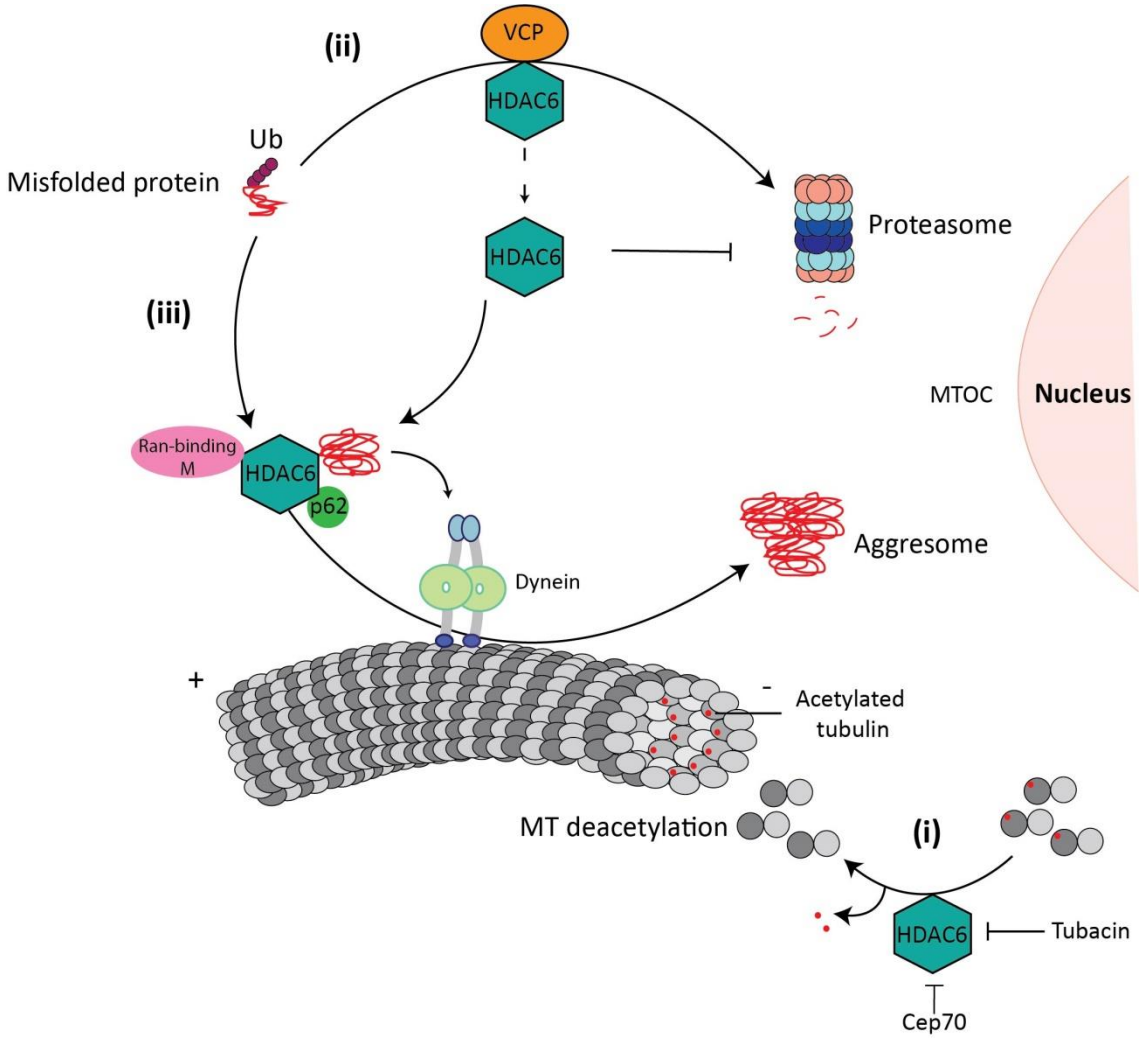

Figure 1.10 Schematic representation of HDAC6 cellular function. HDAC6 regulates several functions. (**i**) HDAC6 deacetylase α-tubulin. (**ii**) The balance between HDAC6 and its partner, VCP determines the fate of polyubiquitinated proteins. (**iii**) P62 interacts with HDAC6 and regulates its function. HDAC6 through interaction with dynein facilitates transport of aggregated protein to MTOC to form aggresome.

Moreover, HDAC6 regulates basal autophagy and targets damaged mitochondria and protein aggregates for autophagy-lysosome degradation (Lee et al., 2010). Indeed, HDAC6 is a linker between autophagy and ubiquitin proteasome system (UPS), which upon proteasome inhibition, HDAC6 activates the autophagy pathway as a compensatory mechanism (Pandey et al., 2007).

Furthermore, HDAC6 is an essential factor for aggresome formation and upon proteasome inhibition; the valosin-containing protein (VCP) through biding to HDAC6 induces the formation of aggresomes (Boyault et al., 2006, 2007) (**Figure 1.10 ii**). The Ran-binding protein M (RanBPM) also interacts with HDAC6 and regulates the function of HDAC6 in aggresome formation (Salemi, Almawi, Lefebvre, & Schild-Poulter, 2014) (**Figure 1.10 iii**). In addition, co-localisation of p62 with HDAC6 controls its activity and absence of p62 leads to hyperactivity of HDAC6 (Yan et al., 2013).

HDAC6 function is also critical during development, and inhibition of HDAC6 by Tubastatin A results in the overproduction of reactive oxygen species (ROS) and increases the DNA damage in mouse embryos (Wang, Ling, Ai, & Bai, 2019). Additionally, mice lacking HDAC6 show deficiencies in the immune system and bone homeostasis (G.-W. Kim et al., 2013). Importantly, HDAC6 has been identified as a promising therapeutic target for several diseases including neurological disease. Blocking HDAC6 activity inhibits the accumulation of insoluble hyperphosphorylated tau and alleviates pathogenic features of tau-driven neurological disorders (Falkenberg & Johnstone, 2014; Selenica et al., 2014). Moreover, it has also been reported that inhibition of HDAC6 in CMT2A peripheral neuropathy results in restoring the level of α-tubulin acetylation especially in distal parts of the nerves and improves the motor function in mice (Picci et al., 2020). Inhibition of HDAC6 also results in upregulation of key members of chaperon-mediated autophagy and reduces expression of alpha-synuclein in a rat model of Parkinson's disease. Consequently, inhibition of HDAC6 protects the dopaminergic neurons against alpha-synuclein and reduces astrogliosis (Francelle, Outeiro, & Rappold, 2020).

It has also been shown that genetic deletion of HDAC6 significantly decelerates disease progression in the mutant $SOD1^{G93A}$ mouse model of ALS and attenuates MN degeneration (Dompierre et al., 2007; Taes et al., 2013). In addition, inhibition of HDAC6 in cells expressing mutant FUS has been shown to rescue the defects of axonal transport (Guo et al., 2017). Furthermore, inhibition of HDAC6 has been considered as a strategy to alleviate the vulnerability of striatal neurons in Huntington's disease through activation of autophagic flux and removal of defected mitochondria (Guedes-Dias et al., 2015).

1.2.2 Amyotrophic lateral sclerosis

As mentioned previously, in this thesis, I also investigated mechanisms contributing to the ALS. ALS (OMIM: 105400) is an incurable adult-onset neurodegenerative disease with relentlessly progressive degeneration of UMN and LMN, leading paralysis and failure of respiratory muscles and death at the late stage of disease (Taylor, Brown Jr, & Cleveland, 2016). The precise worldwide incidence rates are difficult to ascertain based on the continents and ethnicities. However, ALS in the European population has an incidence of 2.2 per 100,000 people per year, similar to the US population. The lower incidence has been measured in East Asia to be 0.89 per 100,000 people per year, and in South Africa to be 0.79 per 100,000 per year (Logroscino & Piccininni, 2019). The estimated lifetime risk of developing ALS is ~ 1 in 472 in women, and 1 in 350 in men and incidence peaks at age 75-79 for both sexes (Al-Chalabi & Hardiman, 2013). Age of onset is variable but in most cases, it begins at ~ 50-60 years of age (Swinnen & Robberecht, 2014). ALS before the age of 40 years is rare; however, rises exponentially with age (Alonso, Logroscino, Jick, & Hernán, 2009).

Of note, ALS has been considered as a heterogeneous disorder with clinicopathological variability. The location of symptom onset, the time of disease onset, rate of disease progression, and the levels of cognitive impairment vary between patients (Takeda, Kitagawa, & Arai, 2020). The clinical diagnosis of ALS is based on the history and physical

examination showing progressive dysfunction of UMNs and LMNs (Ajroud-Driss & Siddique, 2015).

In addition to clinical variations, there is a noticeable variation in disease aetiology. Approximately 10 % of cases are recognised as fALS with having a family member diagnosed with ALS, and 90 % of cases are known as sALS, with no family member diagnosed with the disease. ALS is also suggested to manifest through a multi-step process incorporating additive effects from genetic vulnerability and environmental insults (Al-Chalabi & Hardiman, 2013). A considerable amount of efforts have been put to identify the environmental factors causing ALS, but they remain unknown. However, in most ALS patients, the genetic contribution is an important factor even in sALS cases (Simpson & Al-Chalabi, 2006).

Furthermore, ageing has been known as a leading risk factor for many late-onset neurodegenerative diseases, particularly in ALS (Johnson, 2015). Some *in vitro* studies have reported that the combination of cellular senescence and environmental factors enhances the risk of neurodegenerative diseases (Goldman, 2014). Ageing can be described as failures in repair systems, which results in defective cellular and molecular processes leading to ageing phenotype (Kirkwood & Melov, 2011). The hallmarks of ageing consist of altered cellular communication, genomic instability, defective nutrient sensing, and loss of proteostasis (López-Otin, Blasco, Partridge, Serrano, & Kroemer, 2013). Moreover, the presence of protein aggregates due to the failure of protein quality control (PQC) system (see section 1.2.2.3.1) is a hallmark of ageing as well as neurodegenerative diseases such as ALS.

1.2.2.1 Familial ALS (fALS)

ALS cases are considered as fALS if at least one first- or second-degree relative is diagnosed to have ALS (Byrne, Elamin, Bede, & Hardiman, 2012). In the absence of family history, presence of some factors such as atypical rapid or slow disease progression, early

age of onset, and dementia alert to a familial aetiology (Ajroud-Driss & Siddique, 2015). Most forms of fALS show an autosomal dominant pattern of inheritance, although, in some cases of sALS, the mode of inheritance is autosomal recessive or X-linked dominant (Andersen & Al-Chalabi, 2011). Of all fALS, 60-70 % are categorised by mutations in known genes (Renton, Chiò, & Traynor, 2014).

The first reported ALS-associated gene is Cu/Zn superoxide dismutase1 (*SOD1*) gene, mutations in which are responsible for 20 % of familial cases (Rosen et al., 1993). More than 160 pathogenic variants of SOD1 have been identified (Andersen & Al-Chalabi, 2011). The native SOD1 protein catalyses the reduction of superoxide to hydrogen peroxide and oxygen. Subsequently, hydrogen peroxidase is catalysed by both catalase and peroxiredoxin and is converted to water (Rakhit & Chakrabartty, 2006). A consequence of mutations in SOD1 is the accumulation of ubiquitinated inclusions in MNs and astrocytes (Andersen, 2006).

With the progress of next-generation sequencing techniques, the number of ALS-associated genes has increased and these genes have been found in 70 % of fALS cases and 10 % of sALS cases (Renton et al., 2014) (**Figure 1.11**).

Figure 1.11

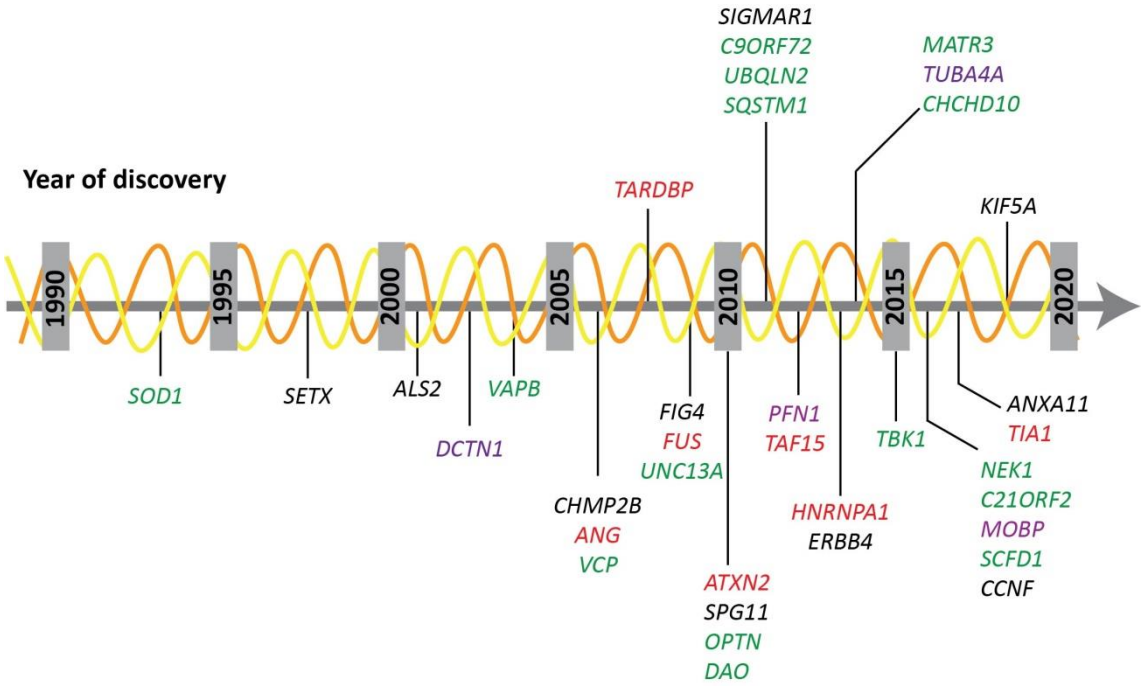

Figure 1.11 The ALS-associated genes. The chronological representation of the discovery of the ALS-gene mutations. Each of these genes has been reported in more than one family, or in multiple, unrelated cases of sALS. Genes implicated in protein homeostasis are shown in green. Genes involved in altered RNA-binding proteins are shown in red. Genes involved in cytoskeletal dynamics are shown in purple.

Table 1.5 outlines genes implicated in the ALS and their contribution to the fALS and sALS. This thesis will elaborate on *Sequestosome*, *TBK1*, *C9orf72*, *TARDBP*, and *FUS* to their relevance in this research.

Table 1.5 Monogenic causes of ALS and their frequencies

Gene	Protein	Chromosomal locus	Inheritance	Prevalence fALS/sALS (in percentage)
C9orf72	Unknown	9p21.2	AD, DN	40/10
SOD1	Superoxide dismutase 1	21q22.1	AD, AR, DN	12/1.5
FUS	Fused in sarcoma	16p11.2	AD, DN	4/1
TARDBP/TDP43	TAR DNA binding protein 43	1p36.22	AD	4/<1
CCNF	Cyclin F	16p13.3	AD	NA/NA
NEK1	NIMA related kinase 1	4q33	AD	NA/NA
TBK1	TANK binding kinase 1	12q14.2	AD, DN	NA/NA
VCP	Valosin containing protein	9p13.3	AD, DN	1/1
SQSTM1	Sequestosome 1	5q35.3	AD	1/<1
MATR3	Matrin 3	5q31.2	AD	<1/<1
CHCHD10	Coiled-coil-helix-coiled-coil-helix domain containing 10	22q11.23	AD	<1/<1
PFN1	Profilin 1	17p13.3	AD	<1/<1
TUBB4A	Tubulin alpha 4a	2q35	AD	1/<1
UBQLN2	Ubiquilin 2	Xp11.21	XL	<1/<1

OPTN	Optineurin	10p13	AD	<1/<1
KIF5A	Kinesin family member 5A	12q13.3	AD	NA/NA
HNRNPA1	Heterogeneous nuclear ribonucleoprotein A1	12q13.13	AD, DN	<1/<1
HNRNPA2B1	Heterogeneous nuclear ribonucleoprotein A2/B1	7p15.2	AD	<1/<1
CHMP2B	Charged multivesicular body protein 2B	3p11.2	AD	<1/<1
SETX	Senataxin	9q34.13	AD	<1/<1
SPG11	Spastic paraplegia 11	15q21.1	AR	<1/<1
ALS2	Alsin	2q33.1	AR	12/1.5
ALS3	Unknown	18q21	AD	NA/NA
ALS7	Unknown	20p13	AD/AR	NA/NA
VAPB	VAMP (Vesicle-associated membrane protein) associated protein B and C	20q13.33	AD	<1/<1
ANG	Angiogenin	14q11.1	AD	<1/<1
FIG4	FIGURE 4 phosphoinositide 5-	6q21	AD/AR	<1/<1

	phosphatase			
ATXN2	Ataxin 2	12q24.1	AD	<1/<1
SIGMAR1	Sigma nonopioid intracellular receptor 1	9p13.3	AR	<1/<1
ERBB4	Erb-b2 receptor tyrosine kinase 4	2q33.3-q34	AD	NA/NA
UNC13A	Unc-13 homolog A (*C.elegans*)	19p13.22	NA	NA/NA
DAO	D-amino-acid oxidase	12q24	AD	<1/<1
DCTN1	Dynactin subunit 1	2p13	AD	<1/<1
NEFH	Neurofilament, heavy polypeptide	22q12.2	AD	<1/<1
PRPH	Peripherin	12q13.12	AD	<1/<1
TAF15	TATA-box binding protein associated factor 15	17q12	AR/AD	<1/<1
SPAST	Spastin	2p24-p21	AD	<1/<1
ELP3	Elongator acetyltransferase complex subunit 3	8p21.1	Allelic	<1/<1
LMNB1	Lamin B1	5q23.2	NA	NA/NA
GLE1	GLE1 RNA export mediator	9q34.11	AD	<1/<1

SS18L1	Calcium-responsive transactivator	20q13.33	AD	<1/<1
GRN	Granulin precursor	17q21.31	AD	<1/<1
EWSR1	EWS RNA binding protein 1	22q12.2	AD	<1/<1

Table 1.5 Monogenic causes of ALS and their frequencies. Table summarizes ALS-associated genes, their chromosomal locus, inheritance and prevalence. AD = autosomal dominant, AR = autosomal recessive, DN = *de novo*, XL = X-linked, NA = not available.

The most common gene linked to fALS is *C9orf72*, which accounts for 25 % of fALS cases (Taylor et al., 2016). The frequency data of other recently identified gene are sparse, and most of these genes are inherited in an autosomal-dominant manner with age-dependent penetrance (Volk, Weishaupt, Andersen, Ludolph, & Kubisch, 2018). The products of ALS-linked genes are categorised into three main biological processes: protein-quality control (*UBQLN1*, *VCP*, *OPTN*, *TBK1*, *C9orf72*, *VAPB*), RNA metabolism and processing (*FUS*, *TARDBP*, *HNRNPA1*, *MATR3*), and cytoskeletal dynamics (*PFN1*, *KIF5A*, *TUBA4A*, *DCTN1*). Moreover, the percentage of genetic contribution to ALS is varied depending on the geographic and population variations. Nevertheless, the point mutations in *SOD1*, *TARDBP, FUS* or abnormal expansion of *C9orf72* account for more than 50 % of fALS (Taylor et al., 2016).

1.2.2.2 Sporadic ALS (sALS)

The patients with no evident family history of ALS are classified as sALS and they comprise 90-95 % of all ALS cases (Zarei et al., 2015). It has been demonstrated that missense mutations in SOD1 cause 1-2 % of sALS cases (Gamez et al., 2006; Taylor et al., 2016) and the intronic expansion of *C9orf72* is responsible for 10 % of sALS cases (Cooper-Knock et al., 2012; Taylor et al., 2016).

Importantly, it is hypothesised that interactions between genetic susceptibility and environment cause sALS (Ajroud-Driss & Siddique, 2015). Additionally, the gene variants have been identified in the pathogenicity of sALS as well as fALS cases. It has been demonstrated that genetic variants synergise the susceptibility, even if the variants are not causative for ALS. Moreover, oligogenic basis has been proposed for the disease, in which at least two pathogenic ALS gene variants are incorporated to initiate the disease. In other words, patients might carry one known ALS-linked gene variant, which in association with potentially unrecognised pathogenic variants causing the neurodegeneration (Mejzini et al., 2019).

1.2.2.3 ALS pathology

Distinct biological pathways have been found contributing to ALS pathology, however, two pathological processes considered to be central in ALS: 1. Conformational changes, impaired trafficking of critical proteins, and accumulation of ubiquitinated protein; and 2. Perturbations of processing of RNA and RNA-binding proteins such as FUS and TDP-43 (Peters, Ghasemi, & Brown, 2015).

Deficiencies in distinct pathways of protein quality control system contributing to protein accumulation are summarized in **Table 1.6**.

Table 1.6 Proteostasis imbalance

Disruption of proteostasis	Impairment of the autophagy	Impairment of CMA and the UPS	Impairment in other modes of n protein clearance
ALS			
Misfolded and aggregated TDP-43, SOD1 and FUS inclusions in the brain, spinal cord, and motor neurons; inclusions may contain ubiquitin and ubiquitin ligases	↓Autophagy, but if cellular stress is severe, autophagy activation may be detrimental ↓Autophagosome maturation (*C9ORF72*) ↓Cargo loading (*SQSTM1*, *UBQLN2*, *OPTN*, and *TBK1*) ↓Autophagosome retrograde transport (DCTN and C9ORF72) ↓Lysosomal function (CHMP2B and GRN)	↓CMA clearance of TDP-43 Aggregated proteins block the proteasome ↓HSP70and HSP40 ↓Provision of SOD1 and VCP for UPS degradation	↓Glymphatic flow may impede efflux of neurotoxic proteins
Frontotemporal dementia			

Misfolded and aggregated form of tau, TDP-43 and FUS P62 and ubiquitin found in inclusions	Autophagosome accumulation ↓Cargo loading into autophagosome by p62 ↓Axonal autophagosome transport ↓Endosomal trafficking	↓CMA and UPS clearance Poly(GA) aggregates caused by *C9ORF72* mutations P62 dysfunction	↓Glymphatic flow

Table 1.6 Proteostasis imbalance. Table summarises impairments in autophagy, CMA and UPS system, impacting clearance of neurotoxic protein associated with ALS and frontotemporal dementia.

1.2.2.3.1 Protein quality control systems

In the cellular system, maintenance of protein balance through the timely degradation of misfolded proteins is crucial for cell survival. Within neurons and other cell types, intracellular clearance of misfolded and toxic proteins is predominantly dependant on two main protein degradation systems, including the UPS and autophagy proteolysis. However, there are other molecular mechanisms, including chaperones and heat shock proteins, which assist cellular homeostasis. In the following section, different types of mechanisms involved in the elimination of either misfolded proteins or protein aggregations which also contribute to the pathology of ALS will be discussed.

1.2.2.3.1.1 Chaperons and heat shock proteins

Misfolded proteins are implicated in pathology of neurodegenerative diseases such as ALS. Molecular chaperones such as heat shock proteins, which are expressed inducibly in the nervous system, mediate either correct folding or removal of misfolded proteins. Chaperons recognise exposed hydrophobic surfaces on misfolded proteins. However, if chaperons fail the recognition of misfolded proteins, then chaperons promote the degradation of misfolded proteins through UPS or autophagy (Kim, Hipp, Bracher, Hayer-Hartl, & Hartl, 2013).

As an instance, Hsp70 recognises the soluble misfolded proteins and targets them toward the UPS. Moreover, it has been shown that Hsp40 functions as co-chaperon for Hsp70 to refold the soluble misfolded proteins (Evans, Wisén, & Gestwicki, 2006). The chaperone Hsp70 also distinguishes the misfolded protein contains KFERQ motifs and facilitates their degradation through chaperon-mediated autophagy (CMA) (see section 1.2.2.3.1.3.2) (Kaushik & Cuervo, 2012). The subsets of misfolded proteins that resist these two degradation mechanisms are directed to autophagy-lysosome pathway (see section 1.2.2.3.1.3).

1.2.2.3.1.2 Ubiquitin-proteasome system

The UPS is mainly involved in the degradation of soluble and monomeric proteins through recruitment of Hsp70 and the sequential actions of three classes of ubiquitin ligase (E1, E2 and E3) (Gong, Radulovic, Figueiredo-Pereira, & Cardozo, 2016). Moreover, UPS is involved in the degradation of mitochondrial proteins that build up upon dysregulation of mitochondrial import or sorting (Wrobel et al., 2015).

For the ubiquitin-proteasome degradation, at the first step, ubiquitin (Ub), 76-amino-acid polypeptide conjugates to the targeted protein (Hershko & Ciechanover, 1998). Then, ubiquitin is activated through the ATP-dependent formation of a high energy thioester bond between the active site of the ubiquitin-activating enzyme (E1) and the carboxyl terminus of ubiquitin. At the next step, ubiquitin is transferred to ubiquitin conjugases (E2), and secondly, ubiquitin ligase (E3) conjugates to lysine or N-terminal amino group residues within the substrate. Finally, ubiquitin chains through ubiquitin ligase, which recognises specific motifs and links to the targeted protein. Additional ubiquitin molecules are conjugated onto the first, forming a polyubiquitinated protein (Adams, 2003) (**Figure 1.12**).

Figure 1.12

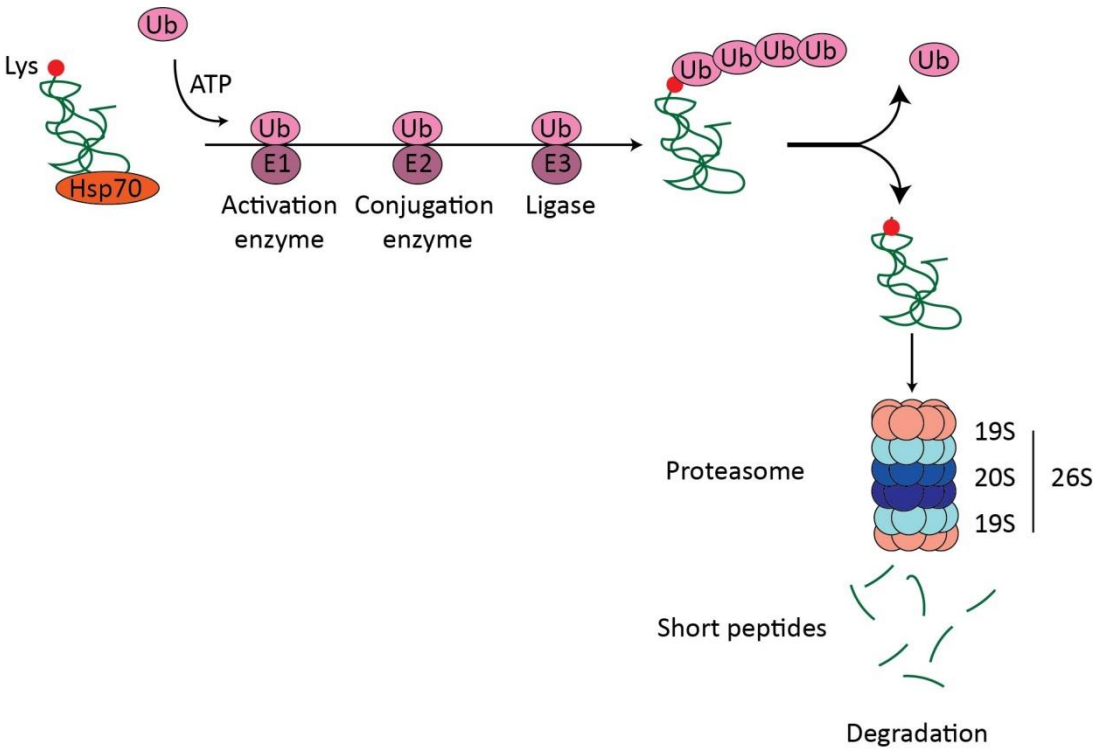

Figure 1.12 Ubiquitin-proteasome pathway. The sequential actions of three enzymes are required for targeting of protein substrates by ubiquitin. Ubiquitin is activated by a specific activating enzyme (E1) to form an ubiquitin-E1-thiolester. Activated ubiquitin is transferred to a carrier protein or "conjugase", E2. Ubiquitin is then transferred by a ligase (E3) and linked by an isopeptide bond to a lysine residue on the substrate protein. After linkage of ubiquitin to the substrate and formation of polyubiquitin chain, ubiquitylated substrate processed to short peptide fragments by the 26S proteasome. Adopted from (Taylor, Hardy, & Fischbeck, 2002).

Consequently, the ubiquitylated substrates are recognised by the 19S particle of the UPS. After binding to the RPN subunits of the 19S ring, ubiquitin motifs are eliminated by three enzymes, including ubiquitin carboxyl-terminal hydrolase 14 (USP14), ubiquitin C-terminal hydrolase UCH37, and the 26S proteasome regulatory subunit RPN11. After removal of ubiquitin chains, proteins are unfolded via the 26S proteasome AAA-ATPase subunits, including RPT1, RPT2, RPT3, RPT4, RPT5 and RPT6 subunits of the 19S component. At the final stage, the substrates entre to the central β-subunit of the 20S, which possesses peptidase activity leading to degradation of the protein (Boland et al., 2018).

It has been reported that protein aggregates and mutant forms of some proteins such as tau block the proteasome and also high production of misfolded proteins result in overwhelmed UPS, which lead to activation of autophagy (see section 1.2.2.3.1.3) as a compensatory mechanism (Ciechanover & Kwon, 2015; Lamark & Johansen, 2010).

Of note, the UPS and autophagy-lysosome are mechanistically linked. Proteasome inhibition induces the autophagy and increases the expression of ATG genes to promote the formation of autophagosome (Han et al., 2011). Moreover, degradation of some misfolded proteins such as mutated α-synuclein is mediated through different degradation pathways, including UPS, autophagy and CMA (Cuervo, Stefanis, Fredenburg, Lansbury, & Sulzer, 2004).

1.2.2.3.1.3 Autophagy

Autophagy is an evolutionarily conserved lysosomal degradation pathway that occurs at the basal level to perform homeostatic functions necessary for protein and organelle turnover. Autophagy is upregulated under several conditions such as cellular injuries and nutrient starvation (Levine & Kroemer, 2008). Autophagy retains the cell homeostasis through the removal of protein aggregates and defected or non-functional organelles via

lysosome degradation. Moreover, autophagy is the main degradation pathway in neurons based on their post-mitotic nature, their polarised shape, and synaptic activities. Neuronal autophagy regulates several pathways, including neuronal differentiation, neuronal survival, brain metabolism, and quality control of cytosolic components (Lee, Hwang, & Lee, 2013). Autophagy initiation is spatially limited in subcellular compartments during neuron development (Crawley et al., 2019). Consequently, autophagy dysfunction affects cellular homeostasis and leads to the accumulation of insoluble ubiquitin-positive inclusions and axonal pathology (Vicencio et al., 2020). Reciprocally, disease-associated proteins such as mutant huntingtin protein also impact autophagic degradation by increasing the number of autophagosomes (Kegel et al., 2000).

Based on the mechanisms that deliver cargos to the lysosome, three main types of autophagy are recognised: microautophagy (see section 1.2.2.3.1.3.1), chaperon-mediated autophagy (CMA) (see section 1.2.2.3.1.3.2), and macroautophagy (see section 1.2.2.3.1.3.3).

1.2.2.3.1.3.1 Microautophagy

Microautophagy is a form of autophagy that occurs directly on the lysosome or vacuole in the yeast cell. The maintenance of organellar size, membrane homeostasis, removal of proteins and organelles are the major functions of microautophagy. In microautophagy, cytosolic cargo is internalised into small vesicles through invagination of the lysosomal or vacuolar membrane, and then cargo is degraded in the lumen of lysosome or vacuole (Li, Li, & Bao, 2012; Sakai, Koller, Rangell, Keller, & Subramani, 1998) (**Figure 1.13 ii**).

Figure 1.13

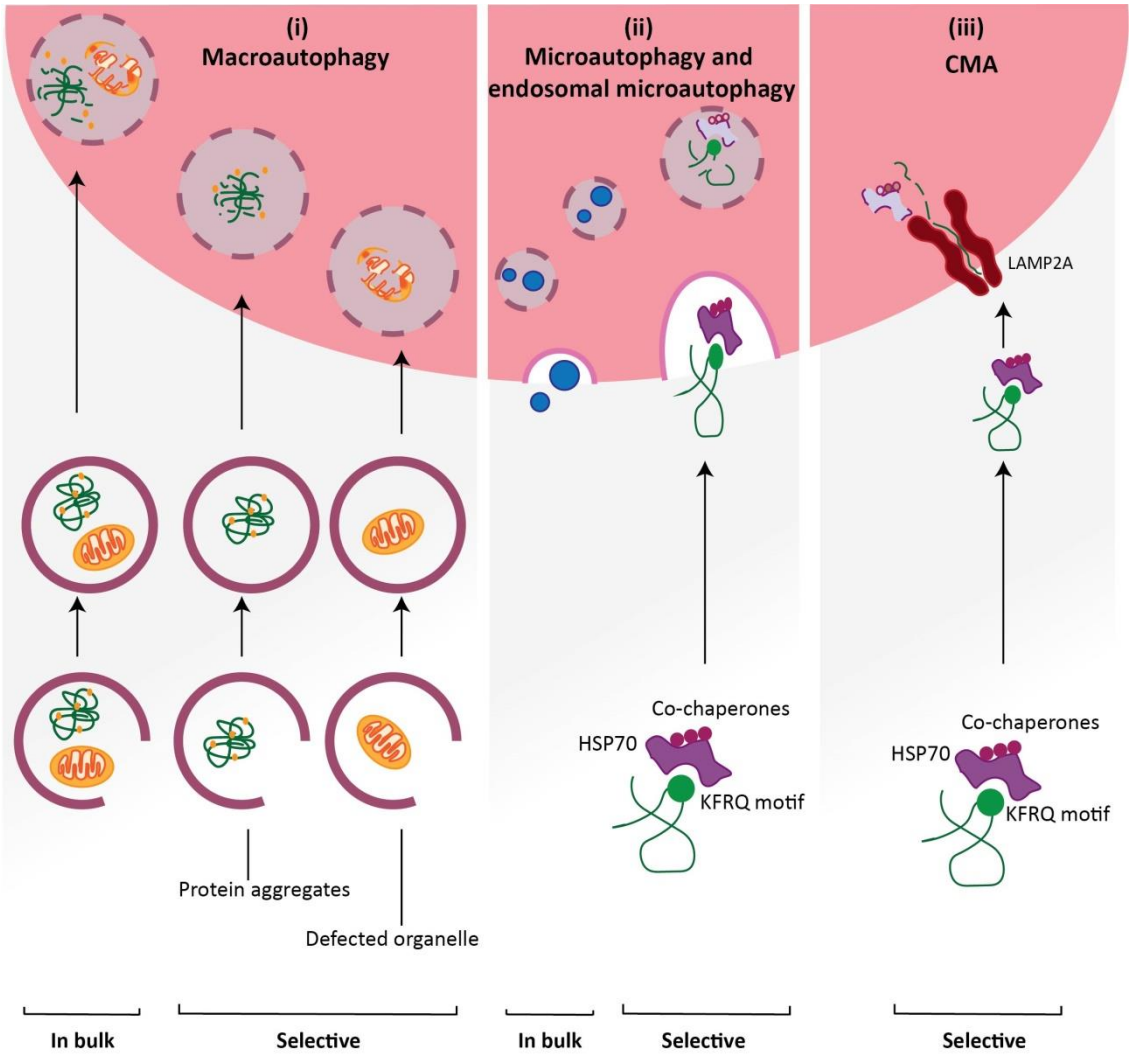

Figure 1.13 Different types of autophagy. (**i**) Macroautophagy through delimiting membrane sequesters cytosolic cargoes. The membrane seals and forms the autophagosome, and then autophagosomes moves toward the lysosome for degradation. Fusion of autophagosome and lysosome lead to degradation of trapped cargoes. (**ii**) Microautophagy is mediated through the invagination of the lysosomal membrane via targeting of proteins through Hsc70 and co-chaperons. (**iii**) In chaperon mediated autophagy (CMA), proteins containing KFERG-like motif are delivered to the lysosome via Hsc70 and co-chaperons. Adopted from (Kaushik & Cuervo, 2018).

Microautophagy is studied mainly in yeast cells, which typically have a large degradation lysosome (Wen-You & Noboru, 2020). In mammalian, microautophagy termed as endosomal microautophagy (eMI), which occurs on endosomes in which endosomes take up substrate either randomly or selectively.

In this system, endosomes recognise KFERQ-like motifs on the substrate and with the assistance of Hsc70, the substrates deliver to the endosomes (Sahu et al., 2011). Afterwards, the Hsc70 binds to the phosphatidylserine at the endosome membrane and deforms the membrane through oligomerisation (Uytterhoeven et al., 2015). Then, the membrane invagination in eMI is completed by endosomal sorting complex required for transport (ESCRT) protein. Subsequently, the substrates within the endosome break down in lysosome's lumen (Sahu et al., 2011). It is noteworthy that Hsc70 is at the centre of protein triage among three types of autophagy in mammals.

Additionally, a cross-talk between eMI and macroautophagy has been found in *Drosophila*, suggesting the similar upstream pathway regulated both eMI and macroautophagy (Mukherjee, Patel, Koga, Cuervo, & Jenny, 2016). It has also been reported that in macroautophagy-deficient cells, rapamycin activates the microautophagy significantly (Sato et al., 2019).

Importantly, microautophagy has been involved in the regulation of macroautophagy through degradation of autophagy receptors, such as p62, NBR1, NDP2, TAX1BP1, and NCOA4 during first hours of starvation. The degradation of autophagy adaptors stops initiation of macroautophagy (Mejlvang et al., 2018).

1.2.2.3.1.3.2 Chaperon-mediated autophagy

Like macroautophagy, CMA is essential for amino acid recycling during periods of reduced nutrient availability. In this pathway, proteins are transferred into the lysosomal lumen for degradation without enclosure by any membrane structure, and degradation of protein is independent of their ubiquitination (Lamark & Johansen, 2010) (**Figure 1.13 iii**). In this type of autophagy, Hsp90 and other co-chaperone HspA8/Hsc70 recognise the CMA-specific pentapeptide motif KFERQ of cytosolic proteins and guide proteins toward lysosome membrane protein receptor (LAMP2A). It has been estimated that about 40 % of proteins in the mammals contain motif KFERQ and PTMs of this motif also regulate CMA targeting of proteins by the conformational switch that exposes or masks the motif (Kaushik & Cuervo, 2018). Furthermore, the level of LAMP2A is determinant of the rate of CMA. Also, co-chaperones such as carboxyl terminus of Hsc70-interacting protein (CHIP), Hsp40, and Hsp70 modulate proteins targeting to the lysosome (Ferreira et al., 2013). After binding to LAMP2A, the proteins unfold and enter the lumen of lysosome for degradation (Li, Yang, & Mao, 2011).

Degradation of specific cellular proteins through CMA regulates multiple cellular functions such as glucose and lipid metabolism, cellular reprogramming, and cellular response to stress (Kaushik & Cuervo, 2018). This degradation system is not able to degrade protein aggregates and only mediates degradation of misfolded or partially folded proteins elevating the cellular resistance against the proteotoxicity (Anguiano et al., 2013; Cuervo et al., 2004). CMA is vital in neurons during brain injury and toxic protein aggregation (Chen & Klionsky, 2011). Under normal condition, both macroautophagy and CMA function at the basal level, but during the cellular stress, they are activated to maintain cellular homeostasis and interact directly to coordinate the protein degradation. Consequently, blockage of CMA results in an increased level of Beclin1 and activation of macroautophagy (Massey, Follenzi, Kiffin, Zhang, & Cuervo, 2008).

In turn, failure in macroautophagy leads to activation of CMA; however, CMA is not capable of compensation of macroautophagy-mediated degradation of defected organelles (Wu et al., 2015). In general, although macroautophagy and CMA can reimburse for some of each other's function, they are not redundant, and their loss of function remains apparent even with upregulation of other pathways (Kaushik & Cuervo, 2018). The pathogenic variants of several CMA substrates are implicated in neurodegenerative diseases including Parkinson disease, Alzheimer's disease, frontotemporal lobar degeneration and ALS**.** Moreover, some of the neurodegenerative-related proteins including α-synuclein, PARK7, leucine-rich repeat serine/threonine-protein kinase2, and TDP-43 have been recognised as CMA substrates. Reciprocally, aggregation of these proteins such as TDP-43 disrupts CMA and UPS degradations (Ciechanover & Kwon, 2015; Kaushik & Cuervo, 2018).

Furthermore, rates of CMA decrease with age in human and rodents. Decreased level of LAMP2A and changes in stability and dynamics of the receptors in the lysosomal compartment have also been reported as some possible reasons for the decreased rate of CMA with age (Kiffin et al., 2007).

1.2.2.3.1.3.3 Macroautophagy

Macroautophagy is the most predominant and far better characterised than the other two forms of autophagy, and it is mediated through autophagy-related proteins necessary for the efficient formation, maturation and degradation of autophagosomes through fusion with the lysosome. In this process, cytoplasm components are sequestered within double-membrane structures termed autophagosomes, which subsequently undergo maturation steps before degradation through fusion with lysosomes.

In addition to canonical autophagy, there are several types of noncanonical autophagy (Nishida et al., 2009). ATG5-independent alternative macroautophagy is one of those

pathways. In this type of autophagy, the membrane is driven from the *trans*-Golgi and only ULk1 and PI3k are involved in this type of autophagy (Torii et al., 2020). The process of macroautophagy has been divided into different steps including initiation, maturation and degradation

1.2.2.3.1.3.3.1 Initiation step

The first step of macroautophagy is the formation of the autophagosome. The formation of autophagosomes is a hallmark of the autophagy process. In the initial step, vesicles arise from a variety of membrane sources including endoplasmic reticulum (ER), the Golgi and mitochondria coalescence form small flattened membrane sac named phagophore. Several autophagy-related (ATG) proteins are conjugated to the phagophore to form the autophagosome (Mizushima, Yoshimori, & Ohsumi, 2011) (**Figure 1.14 i**).

Figure 1.14

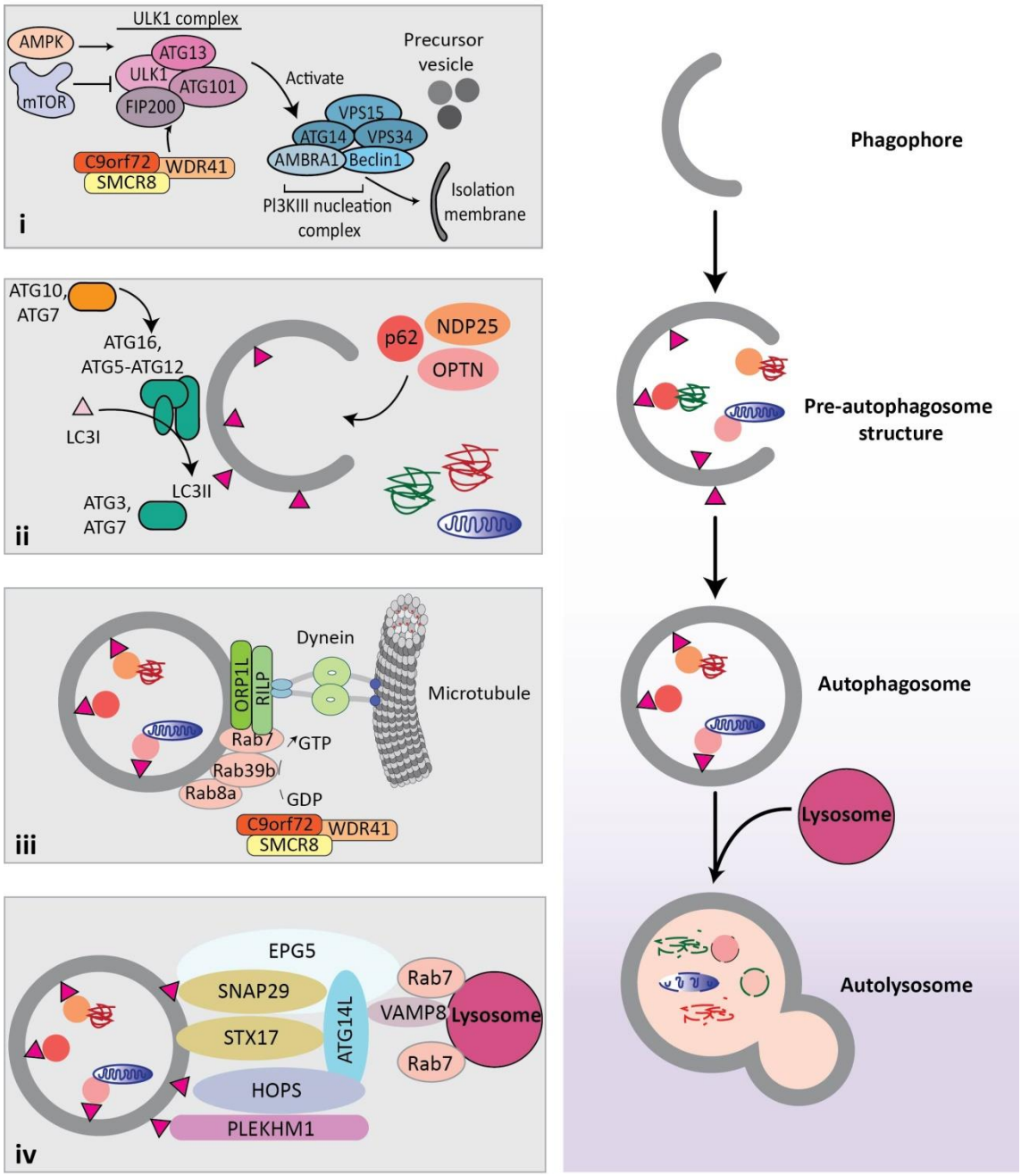

Figure 1.14 Different phases of macroautophagy. Macroautophagy consists of (**i**) phagophore nucleation, (**ii**) autophagosome maturation, (**iii**) transport of autophagosome toward lysosome and (**iv**) autophagosome-lysosome fusion and degradation.

Furthermore, soluble N-ethylmaleimide-sensitive factor attachment protein receptor (SNARE) is involved in the homotypic fusion of phagophore precursors to increase its size (Moreau, Ravikumar, Renna, Puri, & Rubinsztein, 2011). Additionally, the phagophore membrane consists of the multipass transmembrane ATG9 protein, which enlarges and form a cup-shaped double membrane that surrounds the portion of cytoplasm and through the acquisition of lipids complement the process of the autophagosome formation (Puri, Renna, Bento, Moreau, & Rubinsztein, 2013).

The complex of ATG5-ATG12-ATG16L1 resulted from catalytic activities of ATG7 and ATG10 is necessary for the formation of the autophagosome. For the development of phagophore, recruitment of MT-associated protein1 light chain 3 (LC3) to the membrane is necessary. Then, LC3 is cleaved by ATG4B to form the LC3I, which subsequently binds to phosphatidylethanolamine to form LC3II (Fujita et al., 2008; Kabeya et al., 2000) (**Figure 1.14 ii**). The process of LC3 lipidation is mainly associated with the autophagy, but also it is reported that LC3 attaches to the endolysosomal membrane and conjugates to the plasma membrane during viral infection (Beale et al., 2014; Jacquin et al., 2017). As phagophore extends, the complex of ATG5-ATG12-ATG16L1 dissociates whereas the LC3II presents both inside and outside of autophagosome remains linked to the membrane even after lysosomal fusion; thus, LC3II has been considered as a marker of autophagy (Ravikumar et al., 2010). Conjugations of ATGs to the autophagic membranes are controlled by further post-translational modification such as phosphorylation of LC3 by Kinase A, which affects its function in autophagy negatively (Cherra III et al., 2010). In contrast, phosphorylation of LC3C and GABARAPL2 by TBK1 increases the efficiency of cargo engulfment and inhibits ATG4-mediated delipidation and premature elimination of nascent autophagosome (Herhaus et al., 2020). Furthermore, it is revealed that MT-associated protein 1A and 1B (MAP1A/B) interact with LC3 and regulate its recruitment to the MT controling both biogenesis and degradation of autophagosome (Xie et al., 2011). Moreover, post-translational modifications and MT dynamics are necessary for the regulation of autophagy. Upon starvation, the increased level of MT acetylation promotes the

consequent formation of autophagosome and autophagic degradation (Geeraert et al., 2010).

The function of LC3 is further discussed in section 1.3.2.3.1.3.4.1. Importantly, the complex of ATG8/LC3/GABARAP family facilitates binding of autophagy receptors (**Figure 1.14 ii**). Autophagy receptors have been considered as important partners of selective autophagy, including p62, next to BRCA1 gene1 protein (NBR1), nuclear domain 10 protein 52 (NDP52) and optineurin, which bind to autophagic cargoes selectively through ubiquitin-binding domains and bind to LC3 family member via their LC3-interacting region motif. In addition, there are several autophagy receptors such as BNIP3L and ATG30 involved in the degradation of organelles, including mitochondria and peroxisomes (Menzies, Fleming, & Rubinsztein, 2015).

Furthermore, regulation of initiation phase is mediated via a protein complex consists of Unc-51 like autophagy activating kinase (ULK1 or UKL2), ATG13, ATG101 and focal adhesion kinase family interacting protein of 200kDa (FIP200). This complex functions as a sensor for upstream regulatory pathways, including the mTOR complex 1, adenosine monophosphate (AMP)-activated protein kinase (AMPK) and p53 pathways. In nutrient-rich conditions, mammalian target of rapamycin (mTOR) binds to the ULK1-ATG13-FIP200 complex and by phosphorylation of ULK1 and ATG13 inhibits initiation of the autophagosome. Upon cellular stress or starvation, inhibition of mTOR leads to dephosphorylation of ULK1 kinase complex, which subsequently induces the phosphorylation of beclin1 and AMBRA in PIK3C3 complex. Consequently, this complex enhances the activity of the VPS34 complex which triggers the autophagosome nucleation (Molino, Zemirli, Codogno, & Morel, 2017; Russell et al., 2013). It has been shown that inhibition of ULK1 prevents the autophagy initiation and attenuates the axonal degeneration caused by injury-activated autophagy (Vahsen et al., 2020). Moreover, PIK3C3 complex facilitates the formation of phosphatidylinositol 3-phosphate (PtdIns3P), which is lipid components of autophagosome membrane, and it is required for binding of WD repeat domain phosphoinositide-interacting protein 1 (WIPI1) and WIPI2 to the

membrane of autophagosome (Ravikumar et al., 2010). After formation of the phagophore, the structure enlarges, and sequestration of cytosolic cargoes starts.

1.2.2.3.1.3.3.2 Maturation and degradation step

After the expansion of the phagophore, the autophagosome undergoes maturation. During maturation, the ATGs gradually release from the membrane and proteins required for delivery of autophagosomes and autophagosome-lysosome fusion conjugate to the autophagosome membrane (Dikic & Elazar, 2018). In this process, autophagosomes formed in random regions of cytoplasm or formed at the distal part of axons move along the MT toward the perinuclear region where lysosomes are abundant and during this process fuse with several vesicles from the endosomal pathway to form amphisomes, which eventually fuse with lysosome and form autolysosome (Wong & Holzbaur, 2014) (**Figure 1.14 iii**). Importantly, ATG complex involved in lipid conjugation of LC3 regulates the stability of axonal MT and changes in the expression level of ATG5 or ATG16L lead to impaired MT dynamics. Based on the importance of MT dynamics, it has been suggested that alterations in autophagy machinery not only promotes the degradation of the inclusions but also affect the MT dynamics and axonal integrity (Negrete-Hurtado et al., 2020). Additionally, polyamines such as spermine and spermidine which are inducers of autophagy degradation, through binding to MT protein Tubb6 and increasing MT acetylation, facilitate retrograde transport of autophagosome from the cell periphery to prenuclear region (Phadwal et al., 2018). Indeed, the different subsets of MT regulate different stages of autophagy pathways and providing barriers to avoiding fusion of the pre-mature autophagosome with lysosomes (Fass, Shvets, Degani, Hirschberg, & Elazar, 2006).

Trafficking of autophagosome toward pre-nuclear region is driven by dynein (Xu et al., 2014). Moreover, the age-related attenuation of IC binding has been reported that affects binding affinity of dynein to dynactin, as well as cargoes (Kimura, Imamura, Ono, & Terao,

2007). Perturbation of dynein-dynactin function leads to impaired clearance of protein aggregates and axonal degeneration (Hafezparast et al., 2003; LaMonte et al., 2002). Knockdown of dynein also prompts increased level of LC3II, p62 expression and results in accumulation of autophagic vacuoles. The impairment in dynein-dependent transport also suppresses autophagosome-lysosome fusion (Li et al., 2013).

At the final step, the efficient fusion of autophagosome-lysosome is mediated by a member of the SNARE protein family including STX17-SNAP29-VAMP7/AMP8 or STX7-SNAp29-YKT6 (Lawrence & Zoncu, 2019; Menzies et al., 2015; Saleeb, Kavanagh, Dun, Dalgarno, & Duncan, 2019) (**Figure 1.14, iv**).

STX17 binds directly to the LC3 on the fully formed autophagosome, which prevents the fusion of lysosomes with phagophores (Kumar et al., 2018). Moreover, for autophagosome-lysosome fusion, the HOPS complex, PLEKHM1, and EPG5 interact with proteins on both the autophagosomal membrane and lysosomal membrane. Then, PLEKHM1 and EPG5 bind to LC3 on autophagosome membrane and lysosomal small GTPases such as $RAB7^{GTP}$ (McEwan et al., 2015; Wang et al., 2016).

Afterwards, degradation of the inner autophagosomal membrane starts with release of acidic hydrolases (Wen-You & Noboru, 2020). Lysosomes contain more than 60 lysosomal hydrolases to digest the sequestered materials. Efficient degradation of autophagy substrate occurs if the acidic lysosomal pH is maintained correctly (Mizushima, Levine, Cuervo, & Klionsky, 2008). Poor lysosomal acidification is recognised in neurodegenerative disease such as Parkinson disease and Alzheimer's disease attributed to impaired autophagy unrelated to autophagy proteins (Colacurcio & Nixon, 2016).

The inner autophagosomal membrane and sequestered components are then degraded in these lytic organelles consist of many hydrolases including lipases, proteases, nucleases, and glycosylases. Degradation within autolysosomes begins with breaking up the inner autophagosome membrane, but the outer autophagosome membrane is resistant to degradation (Wen-You & Noboru, 2020). After degradation, the residues are transported

back to the cytoplasm and consumed for different cellular purposes (Kawano-Kawada, Kakinuma, & Sekito, 2018; Mizushima, 2009; Nakatogawa, 2020).

The number of lysosomes is also another factor that affects the degradation of autophagosomes. Furthermore, a sufficient number of lysosomes must be available for fusion with autophagosome, and under certain conditions, through the lysosomal reformation, they can regenerate new lysosome to maintain a pool of lysosome in the cell (Sardiello et al., 2009).

1.2.2.3.1.3.3.3 Marker of autophagy

To investigate autophagy pathway, there are two types of well-studied markers, including p62 and LC3. P62 has also been recognised as a marker of aggregates which will be discussed in section (1.3.2.3.1.3.5.1.1). The next section will be focused on LC3.

1.2.2.3.1.3.3.3.1 LC3

As mentioned above, the conjugation of LC3 to the autophagosome membrane is a vital process for autophagy initiation. After induction of autophagy, phosphatidylethanolamine (PE) is conjugated to small ubiquitin-like LC3 proteins (autophagy modifiers) to form LC3II, which anchor to the growing phagophore membrane. This conjugation is mediated by the lipidation cascade enzymes (ATG3, ATG5, ATG7, ATG12, and ARG16L1), which enables cargo selection and autophagosome formation (Nakatogawa, 2013). In humans, autophagy-modifier proteins have been classified into two subfamilies: (i) LC3A, LC3B, LC3C, and (ii) GABRAP, GAPRAP-L1, and GABRAP-L2/GATE-16. The LC3 subgroup is mainly involved in the elongation of the phagophore membrane, whereas the GABRAP subfamily mediates autophagosome sealing and autophagosome-lysosome fusion at later stages (Cemma, Grinstein, & Brumell, 2016). LC3 protein undergoes two processing steps, (i) the conversion of pro-LC3 to active LC3 (LC3I) through an initial proteolytic cleavage of the peptide bond and (ii) delipidation of LC3II through cleavage of the amide bond to provide

a free cytosolic pool of LC3 (Zhang, Li, Ouyang, Liu, & Cheng, 2016). Membrane-conjugated LC3/GABARAP proteins act as scaffolds to recruit various proteins to the phagophore. The LC3 binding proteins consist of a short hydrophobic LC3-interacting region (LIR) which first identified in p62. The LIR motif contains the WxxL sequence, N-terminally preceded by negatively charged residues in which the aromatic residue is the most crucial determinant. The conserved hydrophobic residues of the core LIR motif anchor into hydrophobic pockets centred in the Ub-like domain, while adjacent acidic residues form electrostatic interactions with the N-terminal arm of the ATG8 homologues. Moreover, the core LIR motif changes into an extended β-conformation, which lead to the formation of an intermolecular parallel β-sheet with the β2 strand of the ATG8 homologues (Alemu et al., 2012).

1.2.2.3.1.3.3.4 Dysregulation of autophagy in neurodegenerative disease

Altered activity of proteolytic system and presence of intracellular protein aggregates are characteristic of many late-onset neurodegenerative diseases such as Parkinson disease, Huntington's disease, and ALS (Ramesh & Pandey, 2017; Wang, Abraham, Gao, & Yang, 2016). The clearance of aggregated proteins is vital in neurons as aggregates within neurons cause toxic effects and oxidative stress. Macroautophagy as discussed previously has a crucial role in either normal or pathological condition and removes defected organelles and misfolded/toxic protein inclusions.

More importantly, genetic variants associated with neurodegenerative diseases have been revealed to modulate different aspects of the autophagic pathway, including regulation of initiation (via Beclin 1 interaction), sequestration of the components into autophagosomes, trafficking of autophagosomes to lysosomes, and the degradation capacity of lysosomes (He & Klionsky, 2009).

1.2.2.3.1.3.3.4.1 Deficiency of autophagy in ALS

Accumulation of protein aggregates is a hallmark of ALS. The ubiquitinated proteins found in ALS cases have been classified into the Lewy body-like hyaline inclusions or skein-like inclusions (Blokhuis, Groen, Koppers, van den Berg, & Pasterkamp, 2013). In ALS, the protein inclusions have been found in the spinal cord and other brain regions, including frontal and temporal cortices (Al-Chalabi et al., 2012). Consequently, formation of aggregation disturbs proteasome activity, chaperon protein function and damages organelles such as Golgi and mitochondria (Mammucari & Rizzuto, 2010; Tummala et al., 2005).

Importantly, it has been shown that mutation of *Alsin* (*ALS2*), the activator of Rab5, affects the autophagic removal of aggregate-prone proteins. Besides, missense mutations of *ALS2* result in mislocalisation of proteins and decreased fusion of autophagosome to endosome (Otomo, Kunita, Suzuki-Utsunomiya, Ikeda, & Hadano, 2011). Additionally, the human *dynactin subunit 1* gene (*DCTN1*), encoding the vital component of the MT-based motor complex, is among the ALS-linked genes. Missense mutations of *DCTN1* have been recognised as a genetic risk factor for ALS (Huang et al., 2012; Münch et al., 2004).

Importantly, several autophagic components are encoded by ALS-linked genes. Autophagy adaptors including p62 and optineurin, TBK1, a kinase involved in phosphorylation of autophagic adaptors are among ALS-linked gene. In addition, C9ORF72, major genetic factor in ALS, modulates endosomal trafficking in association with RABGEFs and knockdown of *C9ORF72* leads to an increased level of LC3II (see section 1.2.2.3.1.3.3.4.1.3) (Farg et al., 2014). Indeed, mutations in *C9ORF72* are concomitant to disruption of the autophagosome-lysosome network, including intervention with dynactin-dynein coordinated transport along the axons of MNs (Nassif, Woehlbier, & Manque, 2017).

Moreover, mutation in genes that affect the fusion of autophagosome and lysosomes are recognised in ALS. Mutation in the *CHAMP2B* gene encoding a protein of endosomal sorting complex required for transport of autophagosome has been identified in ALS and

FTD (Skibinski et al., 2005). The VCP is another ALS-linked protein involved in autophagic removal of SGs and C9ORF72, which also modulate autophagy initiation and autophagic flux (Evans & Holzbaur, 2019). The focus of the following section will be on ALS-genes involved in protein quality control systems particularly autophagy-lysosome pathway.

1.2.2.3.1.3.3.4.1.1 SQSTM1/p62

P62 is a scaffold protein and belongs to a subfamily of pattern recognition receptors termed sequestosome-like receptors and is involved in diverse signaling pathways, including amino acid sensing, oxidative stress, DNA damage response, and autophagy (Deretic, 2012; Linares et al., 2015). P62 consists of six functional motifs and several domains which are related to its function in autophagy (**Figure 1.15**).

Figure 1.15

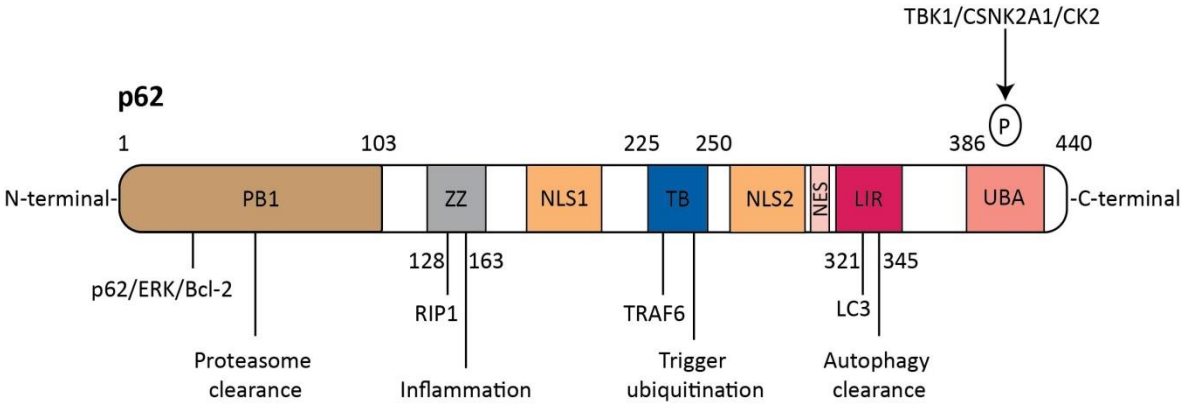

Figure 1.15 Schematic representation of the functional domain of p62. N-terminal Phox and Bem1 domain (PB1) interacts with Rpt1, a subunit of 26S subunit, involved in proteasome degradation. The zinc finger (ZZ) domain binds to RIP1 kinase which in involved in inflammation. Nuclear localisation signals 1/2 (NLS1/2) are involved in nucleo-cytoplasmic shuttling of p62. The TRAF6-binding domain (TB) interacts with TRAF6 proteins to trigger protein ubiquitination. LC3-interacting region (LIR) interacts with LC3 and is involved in autophagy clearance. The C-terminal ubiquitin-associated domain (UBA) is involved in degradation of ubiquitinated proteins. Adopted from (Sánchez-Martin & Komatsu, 2018).

The N-terminal Phox-and-Bem1 domain (PB1) allows self-oligomerisation of p62 and strengthens p62 binding to the Atg/LC3 autophagic membrane (Bjorkoy et al., 2005). The PB1-mediated oligomerisation is also crucial for cargo collection and delivery of cargo to autophagosome (Ciuffa et al., 2015). The central ZZ-type zinc finger domain is important for autophagy and p62 aggregation and recognises the N-terminal arginine-residue, a degradation signal in proteins (Zhang et al., 2018). The nuclear export motif (NES), nuclear localisation signal (NLS), and LIR domains are involved in binding of Atg/LC3/GABARAP family members and the C-terminal ubiquitin-associated (UBA) domain, which links p62 to ubiquitinated proteins.

Furthermore, p62 is subject to several posttranslational modifications. Ubiquitylation of p62 is necessary for activation of its autophagy function through affecting the dimerization of the C-terminal UBA domain. Also, the ubiquitylation, particularly on K420, switch on p62 recognition of poly-Ub chains and regulate the autophagy process (Peng et al., 2017). Additionally, acetylation of p62 via acetyltransferase TIP60 is necessary for regulation of p62 and increases the sequestration and removal of ubiquitylated proteins (You et al., 2019). Importantly, phosphorylation of p62 is necessary for its binding to K48-linked polyubiquitin chains and increases the autophagosomal engulfment of ubiquitinated proteins (Matsumoto, Shimogori, Hattori, & Nukina, 2015).

Moreover, multiple kinases, including casein kinase 2 (CK2) and TBK1 are responsible for phosphorylation of p62 at Ser403 which enhances its affinity for ubiquitinated cargo (Matsumoto, Wada, Okuno, Kurosawa, & Nukina, 2011). Besides, the autophagy kinase ULK1 phosphorylates Ser407 leading to destabilization of p62 UBA dimer, which consequently promotes the phosphorylation of Ser403 and increases autophagy degradation (Lim et al., 2015).

1.2.2.3.1.3.3.4.1.1.1 Functions of SQSTM1/p62

P62 shuttles between the nucleus and cytoplasm and through binding with ubiquitinated cargoes facilitates nuclear and cytoplasmic protein quality control.

P62 is an autophagy adaptor and also it is degraded through the autophagy. Inhibition of autophagy results in the formation of p62 aggregates in mice, *Drosophila*, and *C.elegance* (Nezis et al., 2008; Tian et al., 2010). In contrast, induction of p62 expression assists the proteostasis in an autophagy-dependent manner, which leads to extended longevity in *C.elegance* (Kumsta et al., 2019).

Furthermore, p62 has been found in ubiquitin-positive aggregates in neurodegenerative disease, including Huntington's disease, Alzheimer's disease, and ALS (Rui et al., 2015). Additionally, in some ALS cases, p62 co-localises with TDP-43 (see section 1.2.2.3.2.1.1) and FUS (see section 1.2.2.3.2.1.2) in ubiquitinated inclusions in MNs in spinal cord of sALS patients (Deng, Zhai, et al., 2010).

P62 has been reported to have a dual role in degradation of proteins via proteasome system and autophagy-lysosome pathway (Bjørkøy, Lamark, & Johansen, 2006; Seibenhener et al., 2004) (**Figure 1.16**).

Figure 1.16

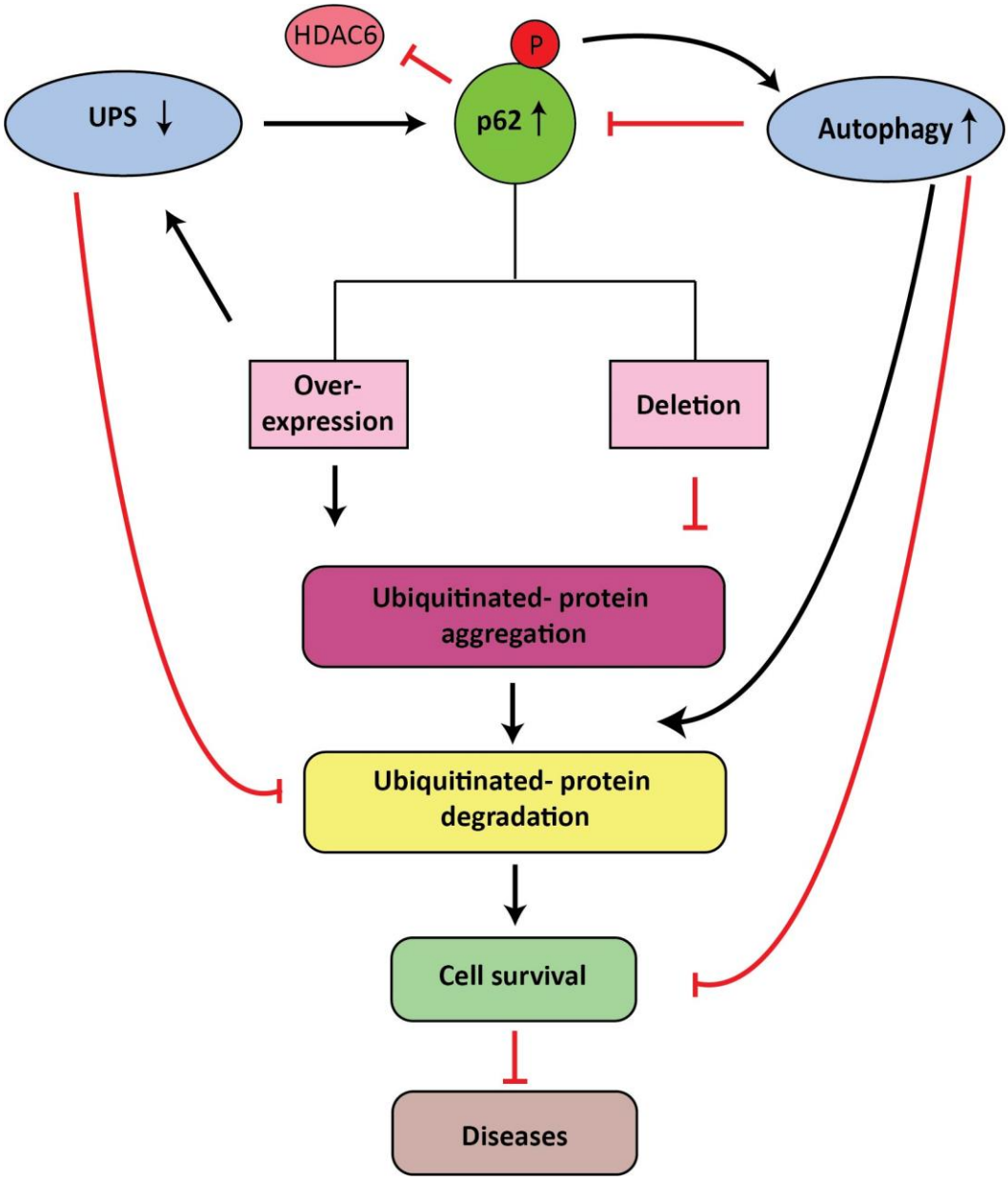

Figure 1.16 The interactions of p62 with UPS and autophagy. UPS inhibition leads to upregulation and phosphorylation of p62 on Ser405 and Ser409, promoting degradation of ubiquitinated cargoes through autophagy. Upregulation of p62 inhibits the HDAC6. HDAC6 plays important role in aggresome formation and autophagosome-lysosome fusion. The ratio of p62 to HDAC6 maintains the homeostasis of autophagic process. Moreover, autophagy impairment affecting p62 level compromises the function of UPS. P62 overexpression enhances the protein aggregation and promotes the cell survival. Adapted from (Liu et al., 2016).

Upon inhibition of proteasome system, proteotoxic stress induces phosphorylation of p62 on Ser405 which subsequently promote the autophagic degradation of ubiquitinated protein targeted by p62. Furthermore, it has been reported that accumulation of protein aggregates such as polyQ-expanded proteins promotes the ULK1-dependent phosphorylation of p62 which triggers the autophagic removal of protein aggregates (Lim et al., 2015).

In addition to the role of p62 in UPS and autophagy, p62 contributes to the N-end rule pathway. P62 is an N-recognin of N-end rule pathway and interacts with N-degrons via the ZZ domain (Cha-Molstad et al., 2017). Binding of p62 to N-degron results in the delivery of cargoes to the phagophore for the autophagic degradation (Cha-Molstad et al., 2018).

1.2.2.3.1.3.3.4.1.1.2 Mutation of *SQSTM1/p62* gene

P62 mutation is linked to the neurodegenerative phenotype, and it is associated with neurodegenerative disorders including ALS and FTD (Gal et al., 2009; Teyssou et al., 2013). Multiple mutations in p62/SQSTM1 have been identified in both fALS and sALS, leading to loss of function of p62 in autophagy. There are several mutations recognised in the UBA domain of SQSTM1, such as P394L and G413S which result in reduced affinity of p62 for binding to polyubiquitin chains and causes loss of basal autophagy (Fecto et al., 2011). Furthermore, it has been shown that G427R mutant causes reduction in inclusion body formation and under oxidative stress increases number of TDP-43 positive SGs (Deng et al., 2020).

Moreover, mutations in the LIR domain such as the L341V found in sALS compromised its binding to LC3, which affect ubiquitinated cargo delivery and incorporation of ubiquitinated substrates to autophagosomes (Chen et al., 2014; Goode et al., 2016).

1.2.2.3.1.3.3.4.1.2 TANK binding kinase 1 (TBK1)

TBK1 is a protein kinase, which is ubiquitously expressed and shows the diffuse staining in the cytoplasm. TBK1 is expressed at moderate levels in all tissues, but in neuronal cells of the cerebral cortex, hippocampus and lateral ventricle, it is expressed at higher level (Uhlén et al., 2015). TBK1 consists of a serine/threonine kinase domain, a ubiquitin-like domain (ULD) and two coiled-coil domains (CCD1 and CCD2) (**Figure 1.17**).

Figure 1.17

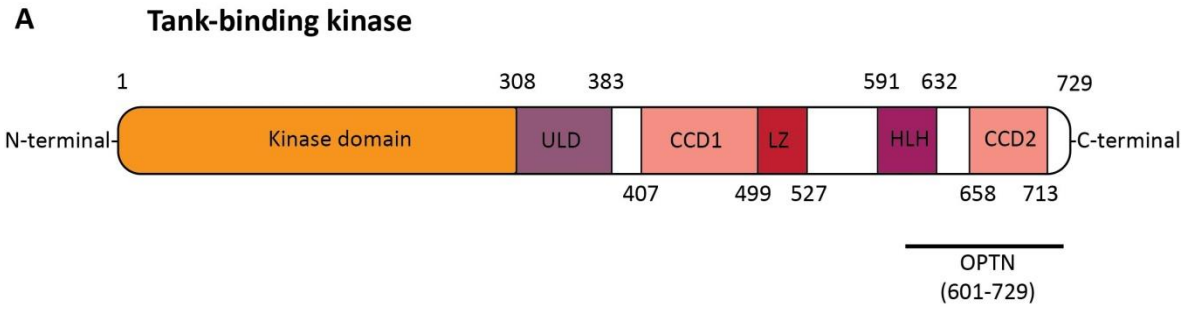

Figure 1.17 Schematic representation of functional domain of TBK1. TBK1 consists of kinase domain, ubiquitin-like domain (ULD), coiled-coil domain 1 (CCD1), leucine zipper domain (LZ), helix-loop-helix motif (HLH), coiled-coil domain 2 (CCD2). Adopted from (Yu et al., 2012).

In the kinase domain, there is an active loop (Leu164-Gly199), including Ser172, which phosphorylation activates TBK1. Moreover, poly-ubiquitination of Lys30 and Lys401 is required for the TBK1 activation. Subsequently, phosphorylation of Ser172 through conformational changes allows substrate binding (Tu et al., 2013).

ULD is involved in the activity of the kinase domain, and deletion of ULD attenuates kinase activity (Ikeda et al., 2007). ULD via three residues, Leu316, Ile353 and Val382, forms a hydrophobic patch mediating protein-protein interaction. This hydrophobic patch also

mediates interactions between the ULD and CCD1 and mutation affecting the region around the hydrophobic patch prevents activation of downstream pathway of TBK1 (Li et al., 2012).

CCD1 is recognised as a scaffold dimerization domain (SDD) that mediates homodimerization. Furthermore, CCD2 domain binds to the adaptor proteins, such as NAP1, TANK, and Sintbad regulating the downstream pathways of TBK1. Binding of TANK to the TBK1 regulates its function in inflammation and binding of Sintbad and NAP1 control TBK1 function in autophagy (Goncalves et al., 2011).

1.2.2.3.1.3.3.4.1.2.1 Functions of TBK1

TBK1 is involved in inflammation and autophagy. TBK1 initiates immune response, modulates production of IFNα and IFNβ, and induces the transcription of interferon-inducible genes (Nakashima et al., 2015). In this thesis, focus will be on the role of TBK1 in autophagy.

TBK1 plays a critical role in autophagy by phosphorylation of the autophagy receptors such as p62, OPTN, and NDP52, and interacts with these receptors through the CCD2 domain (Le Ber et al., 2015; Oakes, Davies, & Collins, 2017) (**Figure 1.18**).

Figure 1.18

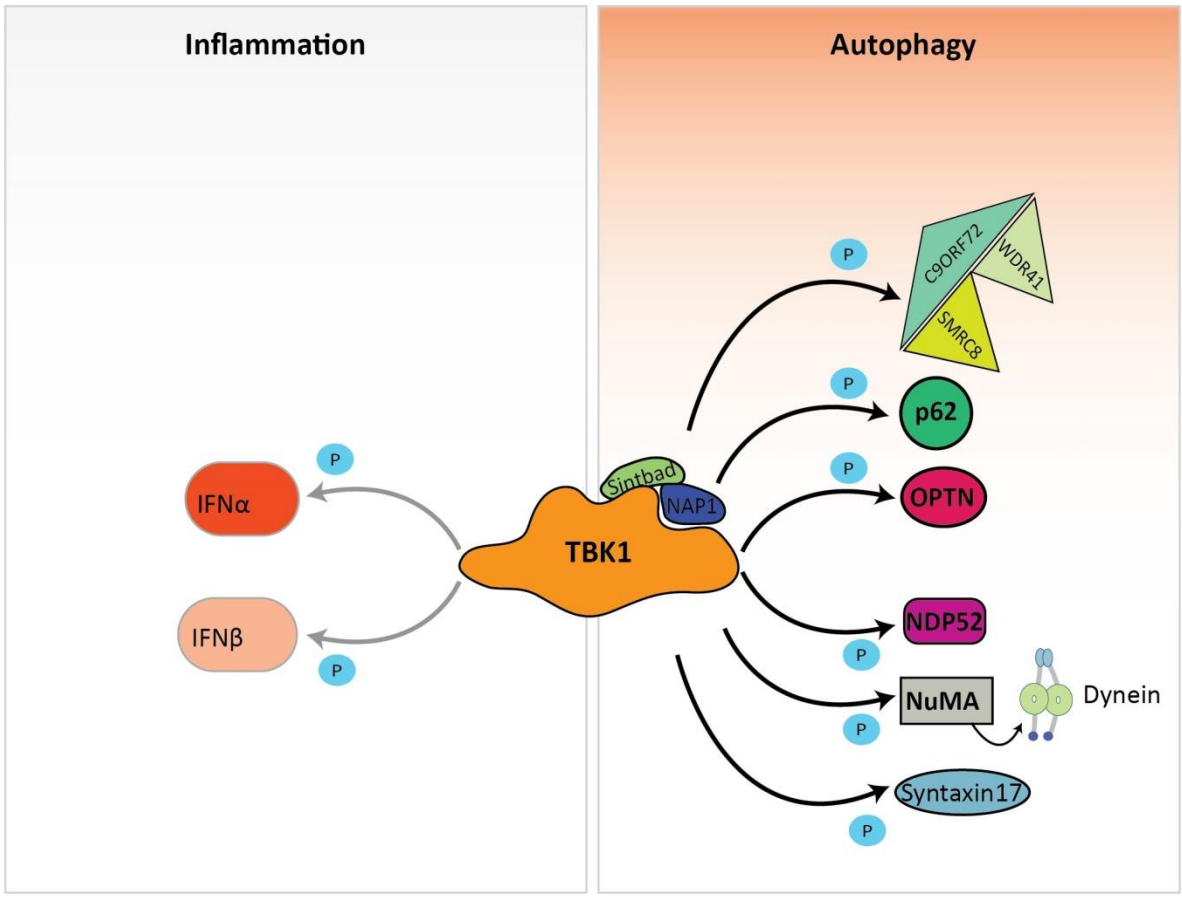

Figure 1.18 Schematic representation of cellular function of TBK1. TBK1 phosphorylates various substrates implicated in autophagy and inflammation.

TBK1-dependent phosphorylation of autophagy receptors such as OPTN enhances its affinity to LC3 and ubiquitin (Heo, Ordureau, Paulo, Rinehart, & Harper, 2015). It has been demonstrated that loss of TBK1 interaction with its adaptor proteins such as p62 and OPTN leads to inefficient removal of protein aggregates via autophagy degradation. Therefore, in the TBK1-associated neurodegeneration, haploinsufficiency has been suggested as the most likely pathogenetic mechanism (Freischmidt et al., 2015).

Moreover, TBK1 phosphorylates STX17, which is critical for the initiation of autophagy through controlling FIP200-ATG13 complex (see section 1.2.2.3.1.3.3.1) (Kumar et al., 2019). TBK1 is also associated with phosphorylation of NuMA, a phosphoprotein which is associated with dynein. Additionally, a study showed that inhibition or knockdown of TBK1 alters the levels of cytoplasmic dynein (Pillai et al., 2014). TBK1 co-localises with LC3 and Rab8b, which are involved in autophagosome maturation (Pilli et al., 2012). TBK1 also mediates autophagosome maturations through phosphorylation of Smith-Magenis Syndrome Chromosome Region, Candidate 8 (SMCR8) in C9ORF72 complex that acts as GDP/GTP exchange factor for Rab7 (Van Mossevelde et al., 2016).

Furthermore, TBK1 is a crucial factor for efficient mitophagy. TBK1 via phosphorylation of OPTN and the efficient requirement of OPTN regulates mitophagy. It has been reported that loss of functional TBK1 causes accumulation of defective mitochondria which in turn impairs axonal transport (Lazarou et al., 2015; Li et al., 2016).
TBK1 mutation will be the focus of the next section.

1.2.2.3.1.3.3.4.1.2.1 Mutation of *TBK1* gene

Initially, genetic alterations in *TBK1* were identified in diseases with neuroinflammatory components (Ritch et al., 2014). Later mutations in TBK1 recognised in ALS, FTD and ALS-FTD in which loss of functions mutations result in 50 % loss of TBK1 protein (Freischmidt et al., 2015; Pottier et al., 2015). The occurrence of TBK1 mutations in patients with FTD-ALS comorbidity (10.8 %) is more frequent than in those with ALS alone (0.5 %) (Le Ber et al., 2015). More than 90 TBK1 mutations have been identified in patients with ALS, ALS-FTD or FTD. Eighty-eight of these mutations were recognised in ALS patient. More than 40 mutations cause either a frameshift or a premature stop leading to truncated products (Freischmidt et al., 2015; Oakes et al., 2017).

Those mutations resulting in protein truncation and loss of the CCD2 domain alter kinase activity and the phosphorylation of substrates (Freischmidt et al., 2015). Moreover,

mutations within the ULD disrupt the TBK1 recruitment to ubiquitinated proteins and organelles. Mutations in the CCD1 region also affect the dimerization of TBK1 followed by changes in TBK1 activity and mutations in CCD2 domain impede binding of TBK1 adaptors (Goncalves et al., 2011; Tu et al., 2013).

Moreover, TBK1 mutations impact activation of autophagy receptors affecting autophagic removal (Pottier et al., 2015). As an instance, $TBK1^{E696K}$ blocks efficient autophagosome formation via disruption of interaction between TBK1 and autophagy adaptor OPTN (Moore & Holzbaur, 2016). Additionally, Brenner et al. showed that heterozygous *Tbk1* deletion causes the increased level of p62, OPTN and LC3II in the primary MNs. However, the level of TDP-43 is not affected by *Tbk1* haploinsufficiency (Brenner et al., 2019).

Altogether, studies of TBK1 mutation elucidation different function of TBK1 in neurodegenerative disease, particularly in ALS, provided a better inside into the importance of functional TBK1 in the distinct mechanism.

1.2.2.3.1.3.3.4.1.3 C9orf72

C9ORF72 is a highly conserved protein localises to different intracellular membranes, such as lysosome in mammalian cells (Farg et al., 2014). The *C9orf72* gene consists of 11 exons with three main alternatively spliced transcript variants producing two protein isoforms (**Figure 1.19**). In C9ORF72, the only protein domain identified is the differentially expressed in normal and neoplastic cells (DENN) protein module. The DENN protein module is an interactive platform, which is found in several classes of proteins of the membrane trafficking machinery such as guanine exchange factor (GEF) that activates Rab proteins (small-GTPases). Rab proteins are necessary for a wide range of vesicular trafficking events. C9ORF72 interacts with Rab1, Rab5, Rab7, and Rab11 in neuronal cell lines and with Rab7 and Rab11 in human spinal cord MNs (Farg et al., 2014).

Figure 1.19

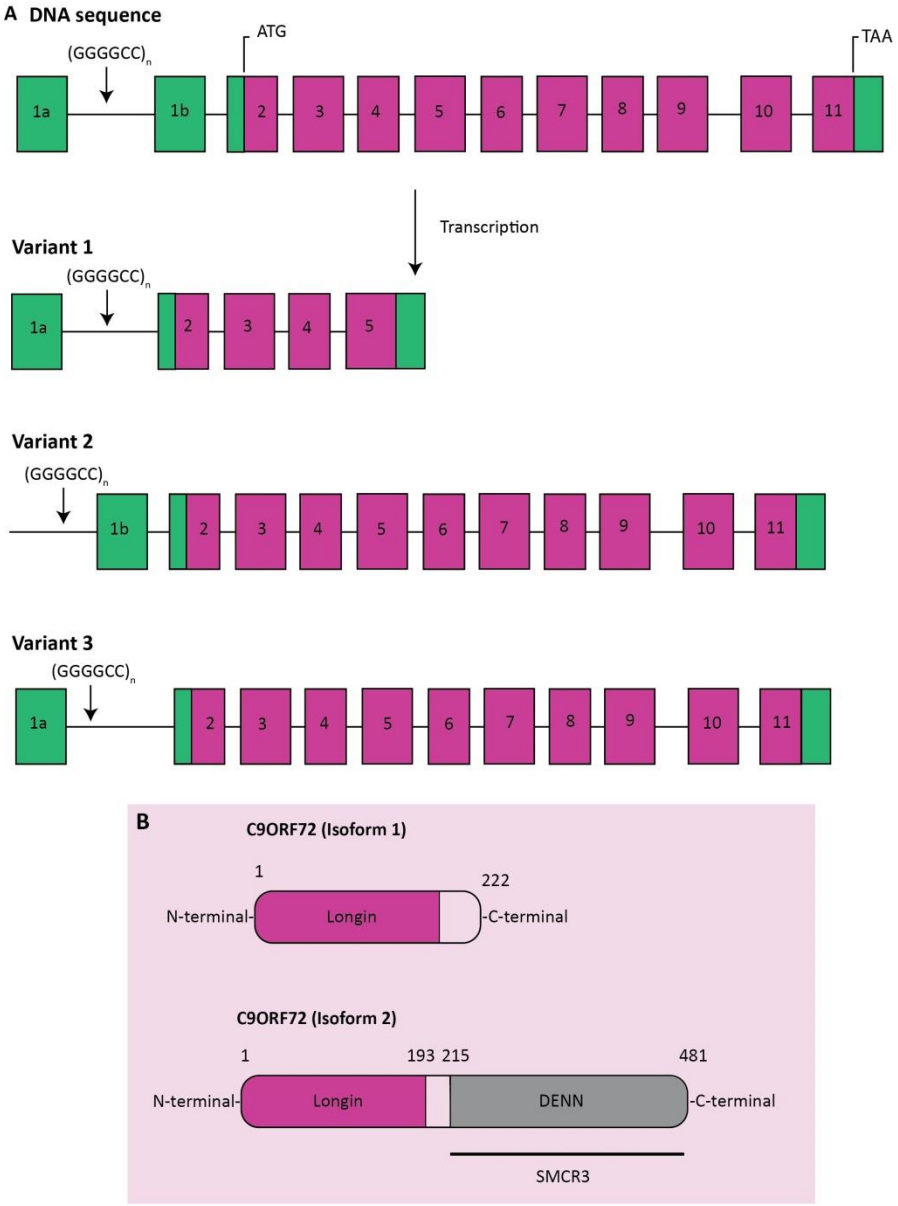

Figure 1.19 Schematic representation of C9ORF72 transcript variants and protein. (**A**) The *C9orf72* gene consists of 11 exons, has three main alternatively spliced transcripts variants and produces two protein isoforms. In this figure, coding exons are indicated in pink and non-coding exons in green. The (GGGGCC) repeat expansion is located in the first intron of variants 1 and 3 and within the promoter region of variant 2. (**B**) Variant 1 encodes C9ORF72-s (short), a 222 amino acid protein of 24 kDa, and variants 2 and 3 encodes C9ORF72-L (long), a 481-amino acid of 54 kDa. Adopted from (Balendra & Isaacs, 2018).

1.2.2.3.1.3.3.4.1.3.1 Functions of C9ORF72

C9ORF72 co-localises with Rab proteins in neuronal cell lines, and knockdown of C9ORF72 increases the level of LC3II, autophagosome marker (Farg et al., 2014). Moreover, C9ORF72 functions in a complex with the WDR41 and SMCR8 proteins to produce GEF activity for Rab8a and Rab39b (Sellier et al., 2016) (**Figure 1.20**).

Figure 1.20

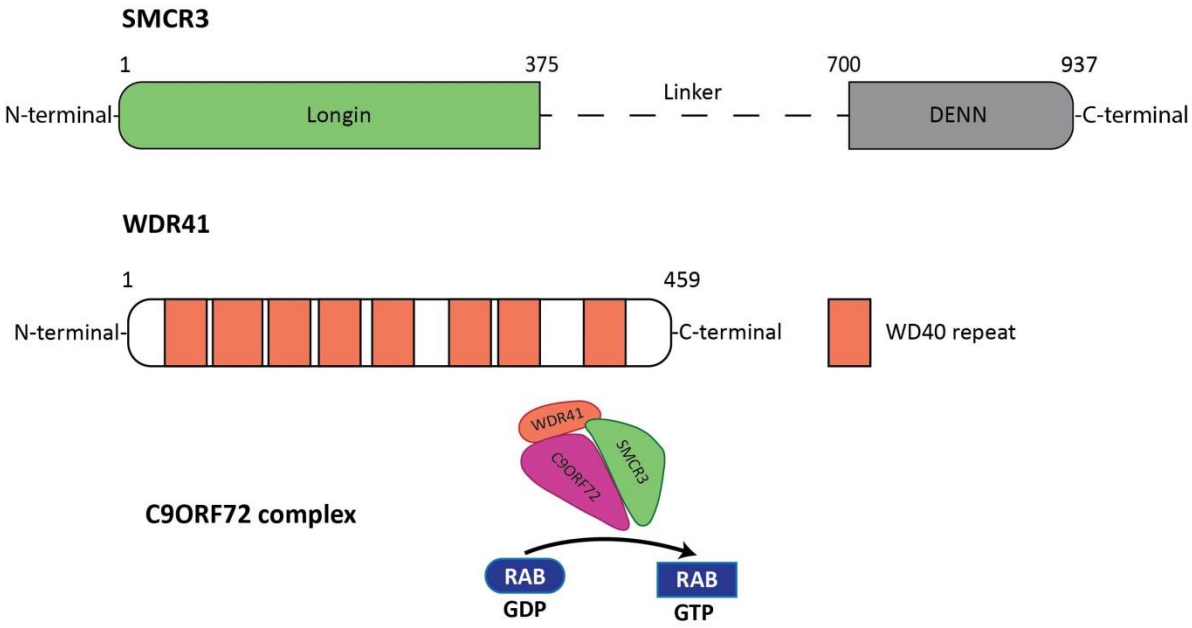

Figure 1.20 C9ORF72 complex. The protein structure of SMR3 and WDR41 are shown and representation of SMCR3, WDR41 and C9ORF72 complex are shown.

SMRC8 contains a DENN module, and it is essential for the stability of C9ORF72 complex. In addition, knockdown of SMCR8 causes a significant reduction in C9ORF72 protein levels (Amick, Roczniak-Ferguson, & Ferguson, 2016; Behrends, Sowa, Gygi, & Harper, 2010; Behrends et al., 2010; Sullivan et al., 2016). Subsequently, interaction between SMCR8 and C9ORF72 activates the FIP200/ULK1 complex leading to the initiation of

autophagosome formation (see section 1.2.2.3.1.3.3.1). Moreover, reduced macroautophagy initiation and accumulation of p62 and TDP-43 have been reported in MEFs lacking C9ORF72 (Sellier et al., 2016).

Phosphorylation of SMCR8 by TBK1, which triggers the GEF activity of complex, is also necessary for binding of Rab39b to C9ORF72. The complex of C9ORF72-SMCR8 functions as GDP/GTP exchange factor for Rab8a and Rab39b through which control the autophagic flux (Sellier et al., 2016).

WDR41 (WD repeat domain 41) is a 52 kDa protein containing a protein-protein interaction domain consisting of six WD40 repeats WDR41 which interacts with autophagy adaptors such as p62 and OPTN (Sellier et al., 2016) (**Figure 1.20**). WDR41 is also necessary for recruitment of the C9ORF72 to lysosome (Amick, Tharkeshwar, Amaya, & Ferguson, 2018). Additionally, WDR41 is associated with Golgi membrane and enriched at the cis-Golgi (Sullivan et al., 2016).

C9ORF72 also interacts with endosomes and regulates the vesicle trafficking and lysosomal biogenesis in the MNs. It has been found that a reduced level of C9ORF72 results in a reduced number of lysosomes. Importantly, accumulation of Ataxin-2 Q30x synergizes the effect of C9ORF72 depletion suggesting the double-hit mechanism in the pathology of ALS (Sellier et al., 2016). Importantly, C9ORF72 localises in SGs and interacts with p62. The incorporation of C9ORF72 into the SGs is critical for arginine methylation of SGs and recruitment of p62 to SGs (Chitiprolu et al., 2018). C9ORF72 also regulates neuronal receptors. It has demonstrated that the low level of C9ORF72 increases levels of NMDA and AMPA receptors on neuritis and dendritic spines (Shi et al., 2018). The effects of C9ORF72 repeat expansion will be discussed in the next section.

1.2.2.3.1.3.3.4.1.3.2 Repeat expansion of *C9orf72* gene

Repeat expansions (GGGGCC) in the non-coding region of the *C9orf72* gene are the most common genetic cause of ALS (Renton et al., 2011). The *C9orf72* gene contains 5-10 intronic hexanucleotide GGGGCC repeat expansion, whereas, in C9ALS/FTD patient, hundreds to thousands of hexanucleotide repetitions $(G4C2)_n$ have been found. These non-coding DNA repeat extensions are demonstrated to cause epigenetic transcriptional silencing of the *C9orf72* gene by histone trimethylation in lysine resides (Belzil et al., 2013). Moreover, G-rich sequences present in both non-coding DNA and RNA result in propensity to form stable G-quadruplex secondary structures, which prevent transcription and trigger abnormal interactions with diverse proteins (Fratta et al., 2012). These mechanisms lead to a decreased level of mRNA and protein of C9ORF72 near to 50 % in C9ALS/FTD patients (Nassif et al., 2017).

Two mechanisms contributing to the pathogenesis of C9orf72 repeat expansion, including the gain of toxicity through dipeptide repeats (DPR) protein and reduction in the function of the C9ORF72 protein have been suggested (**Figure 1.21**).

Figure 1.21

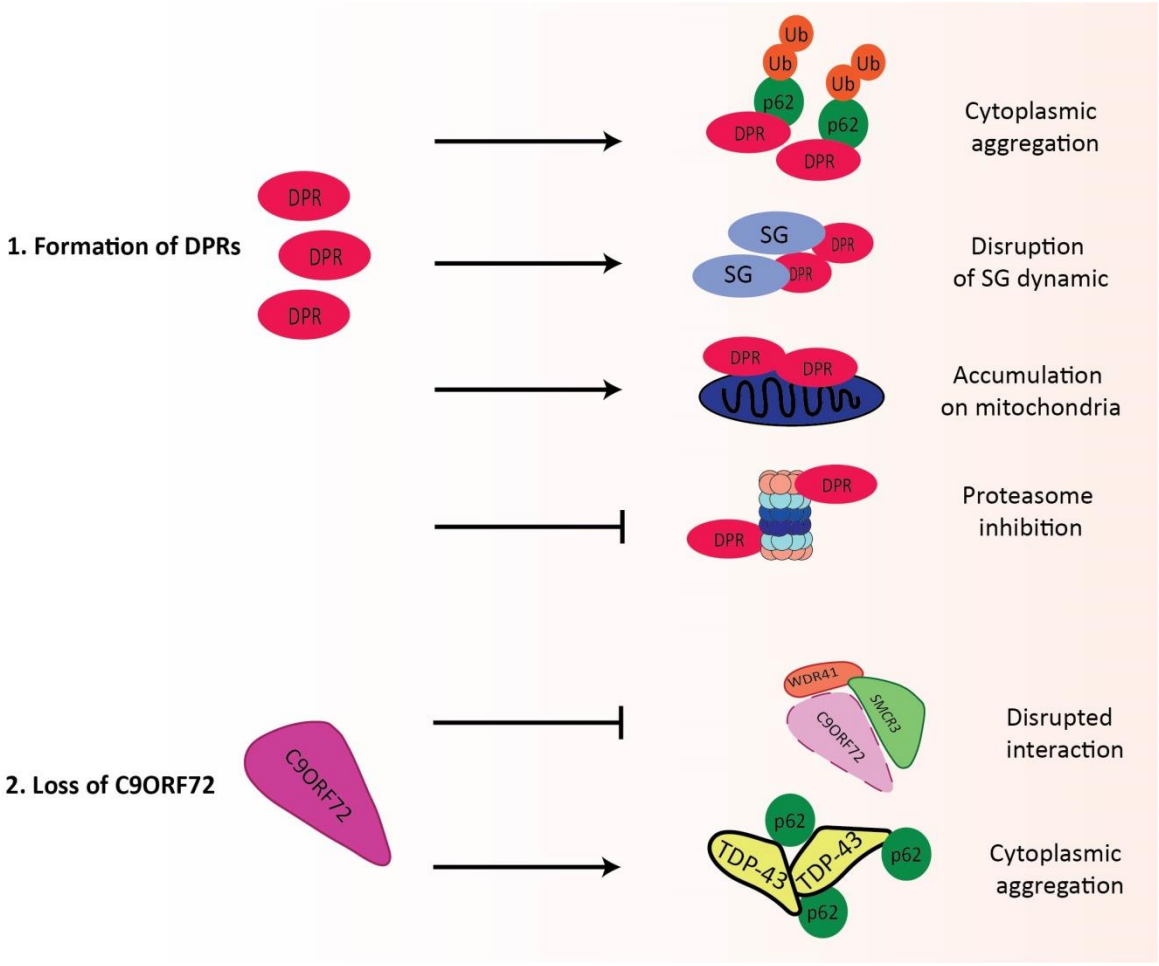

Figure 1.20 Pathological mechanisms of *C9ORF72* repeat expansion. 1. Dipeptide repeats (DPRs) are present in cytosolic protein inclusions and co-localises with p62 and ubiquitinated proteins. The DPRs also bind and contribute to mitochondria dysfunction. Additionally, DRPs bind to proteasome and inhibits proteasome degradative pathway. Moreover, DRPs localises within stress granules (SG) and result in disruption of SG dynamic. 2. Diminished level of C9ORF72 leads to disturbance in interaction of C9ORF72 with SMCR3 and WDR41. It also leads to the formation of cytoplasmic aggregates.

C9ORF72 repeat expansions through an abnormal Repeat Associated Non-ATG (RAN) translation form five toxic DPRs (poly (GA), poly (GR), poly (GP), poly (PA) and poly (PR)) (Mori, Weng, et al., 2013). The DRPs cause aggregation-prone unfolded conformations and form cytoplasmic protein inclusions in the neurons of hippocampus, cerebellum, and cortex of C9ALS/FTD patients (Mori, Weng, et al., 2013). Additionally, DPRs bind to the 26S proteasome subunit and disturb the activity of the proteasome degradation pathway compromising neuronal proteostasis (Guo et al., 2018; Gupta et al., 2017).

Moreover, the recruitment of p62 into the aggregates of DPR proteins has been reported in postmortem tissues from C9ALS patients (Ash et al., 2013). It has also been shown that DPR inclusions containing more than one DPR are p62-positive but TDP-43 negative (Mann et al., 2013). Some of DRP proteins (poly (GR) and poly (PR)) interact with lox-complexity domains of ALS-associated RNA-binding proteins such as TDP-43 and FUS, which alter their phase separation and affect the assembly and dynamics of SGs (Balendra & Isaacs, 2018; Mori, Arzberger, et al., 2013). In *Drosophila* models of C9ALS/FTD, the accumulations of DPRs has been shown to result in the cytoplasmic mislocalisation of TDP-43, which in turn through nuclear depletion of karyopherin-α, a nuclear protein, lead to further TDP-43 mislocalisation (see section 1.2.2.3.2.1.1) contributing to the C9ALS pathology (Solomon et al., 2018).

The second mechanism involved in the pathology of C9ALS is the decreased level of C9ORF72 mRNA and protein (Belzil et al., 2013). The repeat expansion through inhibition of transcription suppresses the production of C9ORF72 protein (DeJesus-Hernandez et al., 2011). It has been reported that reduced level of endogenous C9ORF72 in mice expressing 66 GGGGCC repeats, leads to the early premature death. Furthermore, inactivation of endogenous C9ORF72 results in exacerbation of cognitive deficits, neuronal loss in the hippocampus, glial activation and accumulation of DPR proteins resulting from autophagy deficiency (Zhu et al., 2020). Additionally, loss of cerebellar Purkinje cell and cortical neurons, as well as astrogliosis, has been reported in the mouse brain expressing the repeat expansions of *C9orf72* (Chew et al., 2015).

Furthermore, knockdown of *C9orf72* in the human cell and primary neurons inhibits autophagy initiation leading to cytoplasmic aggregation of TDP-43 and p62 (Webster et al., 2016). However, a reduced level of C9ORF72 in mice is not sufficient to cause neuronal death and neurodegeneration, but it is related to age-dependent abnormalities outside of the nervous system (O'rourke et al., 2016; Sullivan et al., 2016). Importantly, it has been shown that reduced level of C9ORF72 accompanied by an additional protein stressor, such as Ataxin2 a risk factor for ALS, results in MNs toxicity and the motor dysfunction in zebrafish (Sellier et al., 2016).

1.2.2.3.2 Stress granules

RNA granules belong to the family of macromolecular aggregates that form in response to different environmental stresses. These granules have been classified based on their constituents and functions in different processes. The well-studied groups of RNA granules are germ granules, p-bodies, and SGs. Germ granules have been found in germ cells, which control fertility, while p-bodies are involved in mRNA storage and RNA decay. In this study, the focus will be on the SGs.

SGs are dynamic and transient structures to save energy expenditure in response to certain types of stress such as ER stress, hypoxia, arsenite, heat shock, and viral infection. Formation of SGs promotes cell survival through suppressing translation and sequestering apoptosis regulatory factors. Importantly, lack of proper SG formation contributes to the neurodegeneration (Shukla & Parker, 2016).

SGs are composed of translational factors, RNA-binding proteins, and ribosome subunits (Elbaum-Garfinkle et al., 2015; Han et al., 2012; Molliex et al., 2015). Size of SG is dependent on the type of stress and the exposure time but generally size of SGs varies between 0.1 μm^2 and 4 μm^2 (Anderson & Kedersha, 2008, 2009; Buchan & Parker, 2009; Panas, Ivanov, & Anderson, 2016).

SG assembly is a multi-step process which is under control of nucleocytoplasmic trafficking, cytoskeletal structure, and mRNA translation (Protter & Parker, 2016).

The first step starts with accumulation of nucleating proteins such as G3BP1, TIA-1 and fragile X mental retardation proteins and dissociation of translational factors, which form cytoplasmic foci (Bounedjah et al., 2014) (**Figure 1.22 i**).

Figure 1.22

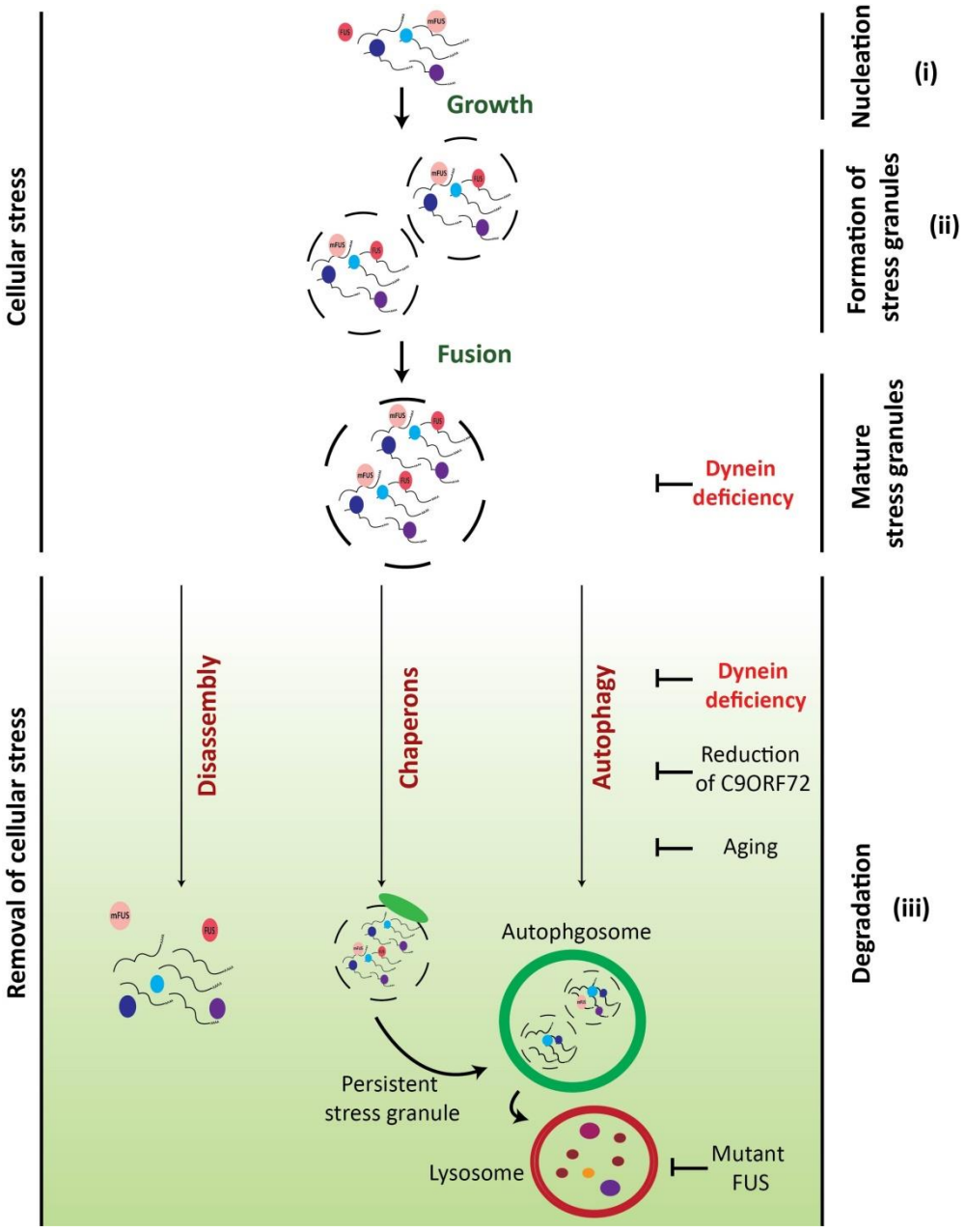

Figure 1.22 Stress granule formation and its cellular fate. (**i**) Under cellular stress, the granule compartments composed of untranslating mRNAs and RNA-binding proteins form. (**ii**) Stress granules (SGs) fuse and shape mature SGs. (**iii**) Upon removal of stress, the SGs disassemble and released mRNAs which follow translation. Chaperons are also involved in removal of proteins trapped in the SGs. Autophagy is involved in removal of core complex of SG and its inhibition disrupts the clearance of SGs.

Following granule nucleation, addition of RNA-binding proteins such as FUS and TDP-43 with prion-like domain increases the SGs integrity (Arimoto-Matsuzaki, Saito, & Takekawa, 2016; Mahboubi & Stochaj, 2017). TDP-43 and FUS are key elements in dynamicity of SGs (see sections 1.2.2.3.2.1.1 and 1.2.2.3.2.1.2) (Alami et al., 2014; Khalfallah et al., 2018; Wang, Wu, & Shen, 2008). The mechanism of involvement of TDP-43 and FUS in dynamicity of SG will be discussed in following sections. Moreover, the low complexity region in these proteins is involved in the liquid-liquid phase separation (LLPSS) ensuring a dynamic structure (Molliex et al., 2015). At the last step, with heterotypic association of different SG components, the mature SGs form (Panas et al., 2016) (**Figure 1.22 ii**).

Importantly, cytoskeletal machinery; particularly MTs and MT-associated motor proteins such as dynein and kinesin are necessary for assembly of SGs. Localisation of dynein in SGs is critical for SG assembly and HC and IC are part of SG core complex (Jain et al., 2016). Furthermore, dynein increases the integrity of the TIA-1 complexes and knockdown of dynein results in the reduced number of SG-positive cells (Loschi, Leishman, Berardone, & Boccaccio, 2009). It has also been shown that disruption of dynein function by overexpression of p50 or knockdown of HC or LC-2 impairs SG formation (Kwon, Zhang, & Matthias, 2007; Tsai, Tsui, & Wei, 2009). Not only dynein but also its adaptor proteins, including dynactin subunit 1 and BICD1 participate in the assembly of SG (Loschi et al., 2009).

Moreover, dynein in conjugation with HDAC6 regulating the level of MT acetylation controls SGs assembly (Kwon et al., 2007). MT network is also required for growth of SG and inhibition of MT results in smaller SG with failure in the formation of mature SG (Ivanov, Chudinova, & Nadezhdina, 2003). Additionally, chronic stress enhances the level of HDAC6, followed by a decreased level of acetylation (Silva et al., 2019). Consequently, reduced level of acetylation results in the consolidation and enlargement of the SGs (Chernov et al., 2009; Pandey et al., 2007).

Aforementioned, SGs are dynamic structures, and upon stress removal, the RNAs are first titrated out and follow the translation. Then, the outer proteins are removed by UPS, and

at the end, the core complex of SG disassembles into the smaller core structure (Wheeler, Matheny, Jain, Abrisch, & Parker, 2016) (**Figure 1.22 iii**). Importantly, autophagy (Monahan, Shewmaker, & Pandey, 2016) and chaperone-mediated protein degradation (Ganassi et al., 2016) mediate the SG disassembly, mechanisms that have been shown to become less efficient as neurons age (Calderwood, Murshid, & Prince, 2009; Nixon & Yang, 2012). It has also been reported that disease-associated mutation of TIA1 results in accumulation of non-dynamic SGs and delayed disassembly (Mackenzie et al., 2017). Moreover, ALS-mutant TDP-43 causes alteration in the protein solubility and an early TDP-43 association with granules resulting in formation of large granules (Dewey et al., 2011).

1.2.2.3.2.1 Dynamics of stress granules

Disassembly of SG is a multi-step process. SGs consist of a solid core, which is surrounded by a dynamic shell exchanging the proteins and RNA with the cytoplasm. The first step in disassembly of SGs starts with the production of small cores that degrades through chaperons, followed by proteasome degradation to remove the scaffolds proteins (Wheeler et al., 2016).

Protein chaperones such as Hsp70 accumulates in SG and mediates disassembly of SG in mammals and inhibition of Hsp70 decreases clearance of SG after removal of stressor (Walters, Muhlrad, Garcia, & Parker, 2015). Furthermore, other mechanisms such as 5’ to 3’ digestion of mRNA molecules contribute to the clearance of SGs (Sheth & Parker, 2003). Upon inhibition of these degradative systems or resistance SGs to protease, cells through activation of autophagy pathway control clearance of SGs (Buchan, Kolaitis, Taylor, & Parker, 2013) (**Figure 1.22, iii**). It has been shown stimulation of autophagy diminishes the accumulation of SG-related proteins and inhibition of the autophagy-lysosome pathway impedes the degradation of SGs (Seguin et al., 2014; Silva et al., 2019). Additionally, autophagy adaptors such as p62 and UBQLN2 localise into SGs promoting the degradation

of SGs through the autophagy pathway and dynein-dependant movement of autophagosome toward lysosome is necessary for efficient disassembly of SGs (Dao et al., 2018; Tsai et al., 2009; Zheng et al., 2020). Conjugation of p62 with SGs is required for arginine methylation of proteins such as FUS. Indeed, C9ORF72, through association with p62 regulates autophagic degradation of SG. Consequently, repeat expansion of C9ORF72 affects the conjugation of p62 to SGs and results in accumulation of SG (Chitiprolu et al., 2018).

Moreover, VCP/Cdc48 (the yeast homologue of VCP) is involved in SG degradation through autophagy and mutations in *VCP* result in a reduction of autophagy-related clearance of SGs (Buchan et al., 2013, 2013; Ju et al., 2009). Consequently, deficiency in the removal of SGs or persistent SGs triggers the formation of stable aggregates and contributes to neurodegeneration and cell death (Li, King, Shorter, & Gitler, 2013).

1.2.2.3.2.1.1 TDP-43

TAR-DNA binding protein-43 (TDP-43) is a 43 kDa RNA/DNA-binding protein, recognised initially as a transcriptional repressor of HIV1 TAR-DNA, related to a spectrum of neurological disease, namely TDP-43 proteinopathy (Berning & Walker, 2019).

TDP-43 is highly conserved and belongs to the heterogeneous nuclear ribonucleoprotein (hnRNP) family and contains 414 amino acids. It comprises of an N-terminal domain (NTD) with a nuclear localisation signal (NLS) promoting self-oligomerisation, two RNA recognition motifs (RRM1) at amino acid 106-176 and RRM2 at amino acid (191-262) through which binds to RNA targets, and the glycine-rich domain (GRD) which links the TDP-43 to the protein targets (Da Cruz & Cleveland, 2011). The GRD domain also consists of a prion-like domain, which is responsible for TDP-43 aggregation (Budini et al., 2012). The nuclear localisation signal (NLS) and NES are signal sequences that regulate the nucleocytoplasmic shuttling of TDP-43 (**Figure 1.23**).

Figure 1.23

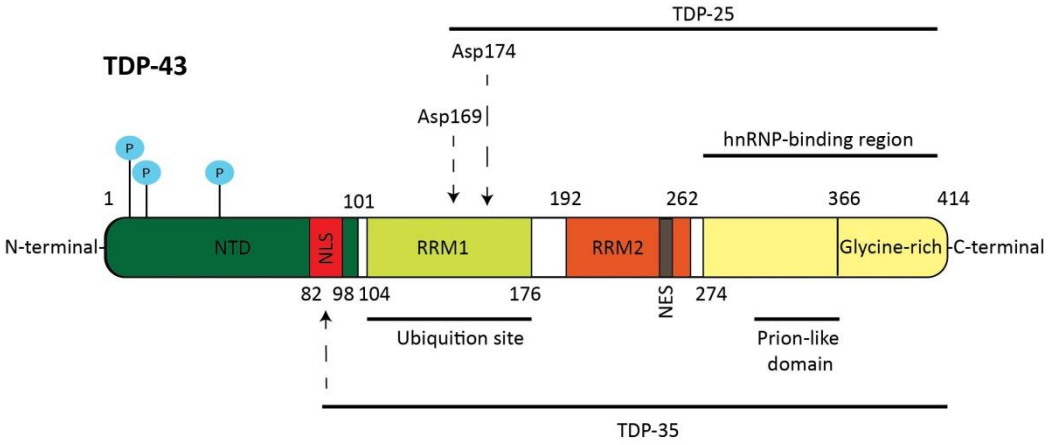

Figure 1.23 Schematic representation of functional domain of TDP-43. TDP-43 contains an N-terminal domain (NTD) including nuclear localisation signal (NLS), two tandem RNA recognition motifs (RRM1 and RRM2) including nuclear export signal (NES) and a C-terminal glycine-rich region. The cleavage sites for C-terminal fragments of TDP-35 and TDP-25 are indicated. The phosphorylation sites at 8 tyrosine, 14 threonine, and 41 serine are represented. Adopted from (Prasad et al., 2019).

TDP-43 is localised predominantly in the nucleus, and it regulates the RNA processing, but it also shuttles to the cytoplasm. The nuclear TDP-43 is involved in multiple processes, including transcriptional regulation, splicing, miRNA biogenesis, and RNA metabolisms. Cytoplasmic TDP-43 is involved in distinct processes including mRNA stability, mRNA translation and as an RNA-binding protein; it is part of RNA granules.

Moreover, TDP-43, under stress conditions, localises in the cytoplasm to regulate mRNA stability, translation and controls nucleocytoplasmic transport. Cytoplasmic mislocalisation of TDP-43 results in depletion of nuclear TDP-43 leading to the loss of its nuclear functions (Russo et al., 2017). Importantly, TDP-43 is important for SG maturation and TDP-43 depletion impairs SG coalescence. Reduced level of TDP-43 also accelerates SG disassembly (Khalfallah et al., 2018). TDP-43 cytoplasmic mislocalisation is not only limited to ALS patients with *TARDBP* mutations but also in other ALS cases, TDP-43

mislocalisation has been observed with an exception for a familial form of ALS caused by SOD1 mutation (Igaz et al., 2008; Tan et al., 2007).

Under pathological conditions, TDP-43 forms aggregates containing both full-length and wild-type TDP-43 in the vast majority of sALS and fALS patients (Ayala et al., 2008; Ederle & Dormann, 2017). It is noteworthy that TDP-43 is not prone to aggregation unless it is overexpressed or purified (Hergesheimer et al., 2019). Besides, TDP-43 has been recognised as a major component of the pathological inclusion found in more than 90 % of all ALS cases in comparison to FUS, which is detected in only 2 % of ALS cases (Ling, Polymenidou, & Cleveland, 2013).

1.2.2.3.2.1.2 Cellular function and regulation of TDP-43

TDP-43 regulates RNA processing pathways, including alternative splicing, transcriptional repression, RNA stability, and miRNA biogenesis. Therefore, a wide range of RNA transcripts, including pre-mRNA, long intronic sequences and microRNA are targets of TDP-43 (Narayanan et al., 2013) (**Figure 1.24 i and ii**). TDP-43 via a negative feedback loop regulates its own transcription to maintain consistent protein levels (Mercado, Ayala, Romano, Buratti, & Baralle, 2005). The regulation of TDP-43 level is vital to cell survival as both depletion and overexpression of TDP-43 are toxic (Herzog, Deshpande, Shapiro, Rodal, & Paradis, 2017; Voigt et al., 2010; Wu et al., 2010).

Figure 1.24

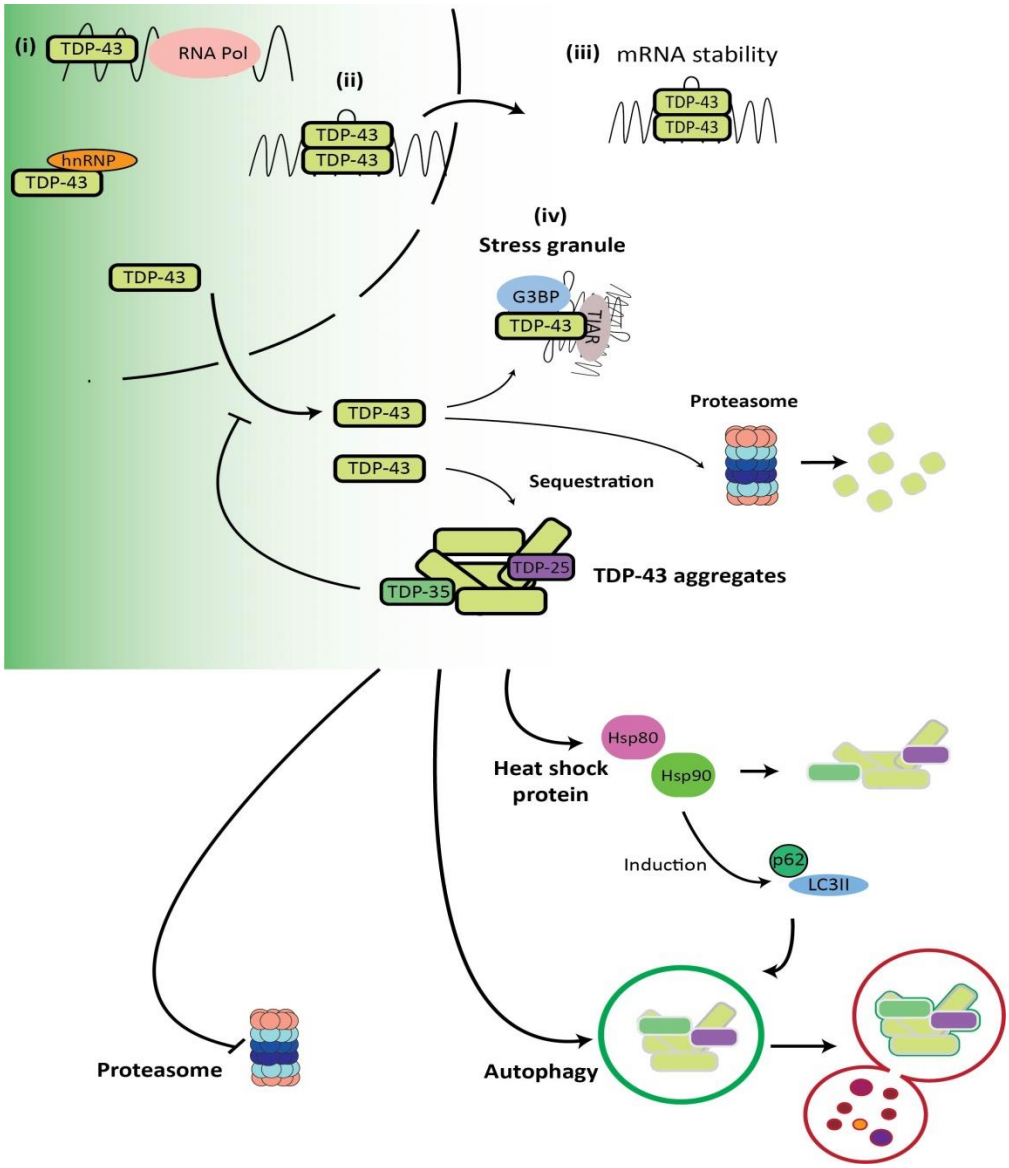

Figure 1.24 Physiological function and regulation of TDP-43. In physiological conditions, TDP-43 shuttles between the nucleus and the cytoplasm. TDP-43 regulates many processes that affect the cellular fate of different RNAs. The processes include (**i**) RNA transcription, (**ii**) RNA stabilisation, (**iii**) Stabilisation of mRNA, (**iv**) Stress granule localisation. Under normal condition, the proteasome degrade misfolded proteins and maintain the balance of cytoplasmic TDP-43. In a pathological condition, cytoplasmic TDP-43 forms aggregates. TDP-43 aggregates cannot' be degraded through proteasome and are toxic for the cells and lead to degeneration. The cytoplasmic TDP-43 aggregates result in TDP-43 loss of function, which promotes cellular stress. The mechanisms regulating TDP-43 include heat shock proteins, proteasome system, and autophagy.

Additionally, C-terminal glycine-rich domain of TDP-43 promotes its interaction with other proteins such as hnRNPs, proteins regulating RNA splicing and mRNA translation (Freibaum, Chitta, High, & Taylor, 2010).

Importantly, TDP-43 is necessary for optimal SG dynamic in primary neurons and glia exposed to oxidative stress (Khalfallah et al., 2018). TDP-43 localises into the SGs and recruitment of TDP-43 to SG modulates the SG response by controlling expression of key proteins of SGs such as G3BP and TIA-1 (Aulas & Vande Velde, 2015; McDonald et al., 2011). In addition, the C-terminal domain of TDP-43 also mediates the liquid-liquid phase separation, which is necessary for the formation of SGs (**Figure 1.24 iv**) (Li et al., 2018).

UPS and autophagy pathway coordinate degradation of both wild-type and aggregated TDP-43 (Huang et al., 2014). However, wild-type TDP-43 is mainly degraded by the UPS, while aggregated forms of TDP-43 degrade by autophagy (Scotter et al., 2014). It has been reported that inhibition of UPS leads to increased levels of ubiquitinated TDP-43 (Walker et al., 2015). Knockdown of proteasome subunit also promotes the formation of TDP-43 aggregates. These findings are supported by another study by Cascella et al. that showed the involvement of UPS in degradation of the monomeric form of TDP-43 before formation of TDP-43 aggregates (Cascella et al., 2017).

Furthermore, co-localisation of TDP-43 with LC3 and p62, the autophagy markers, supports the hypothesis that physiological rate of autophagy is necessary to prevent the accumulation of TDP-43 aggregates (King, Maekawa, Bodi, Troakes, & Al-Sarraj, 2011). In addition, co-localisation of VCP, OPTN, p62 with TDP-43 has been reported in spinal MNs of sALS patient (Ayaki et al., 2014). TDP-43 in turn regulates the autophagy and lack of TDP-43 results in a decreased level of ATG7 and LC3II accompanied by accumulation of p62 (Bose, Huang, & Shen, 2011). TDP-43 also stabilises mRNA of dynactin 1 and downregulation of TDP-43 decreases the level of dynactin, which consequently impairs the fusion of autophagosome-lysosome (Xia et al., 2015).

Heat shock proteins are also involved in regulation of the cytoplasmic level of TDP-43. Overexpression of heat shock proteins such as HspB8 induces degradation of TDP-43 and increases the level of p62 and LC3II, which suggest the pro-autophagic role of HspB8 (Crippa et al., 2010). Furthermore, downregulation of Hsp90 promotes autophagic degradation of TDP-43, which may represent the regulation of autophagy by heat shock proteins (Jinwal et al., 2012). Hsp40 and Hsp70 chaperones also promote degradation of the misfolded TDP-43 through proteasome pathway (Maurel et al., 2018). In addition to chaperons, proteins such as PABPN1 through maintaining the solubility and localisation of TDP-43 in the nucleus promote degradation of misfolded TDP-43 via proteasome system (Chou et al., 2015).

Collectively, both the proteasome system and autophagy are necessary for the regulation of TDP-43 and based on the importance of both systems in controlling the level of TDP-43 could consider valuable therapeutic targets.

1.2.2.3.2.1.3 Posttranslational modifications of TDP-43

In addition to the different level of regulation, it has been demonstrated that TDP-43 undergoes several PTMs that affect its structure, localisation, general functions, and its aggregative propensity. These modifications also contribute to the pathogenesis of TDP-43 proteinopathies. The PTMs include phosphorylation, ubiquitination, acetylation, and cleavage. Phosphorylation and ubiquitination are two pathologically significant PTMs in TDP-43. However, other PTMs such as acetylation and cysteine oxidation have been identified in ALS patients.

The insoluble and aberrantly phosphorylated form of TDP-43 has been reported in ALS cases, which also showed pronounced ubiquitination (Neumann et al., 2006). The phosphorylation of TDP-43 increases cytoplasmic mislocalisation and aggregation of TDP-43. So far, several potential phosphorylation sites including 8 tyrosine, 15 threonine, and 41 serine and residues have been found in TDP-43 (Neumann et al., 2009).

Importantly, multiple ubiquitination sites have been identified near the RRM1 domain. Ubiquitination facilitates the cytoplasmic accumulation of TDP-43 into inclusions and adding polyubiquitin chains to TDP-43 mark TDP-43 for different degradation pathways. The K-36-linked polyubiquitin chains mark TDP-43 for degradation through UPS, and K-63-linked polyubiquitin chains mark TDP-43 for autophagic degradation (Scotter et al., 2014). Moreover, the 20 lysine residues in the TDP-43 have been recognised as a potential site for the acetylation. Residues such as K-145 and K-192 are also prone to acetylation. Acetylation alters both function and localisation of TDP-43 via enhancing its ability to interact with nucleic acids (French et al., 2019). Furthermore, TDP-43 acetylation affects its RNA binding, impair mitochondrial functions, and induce accumulation of the insoluble and hyperphosphorylated TDP-43 aggregates in the neuronal cell (Cohen et al., 2015).

Importantly, TDP-43 C-terminal fragments (CTFs) are neuropathological signature of ALS, marked by specific phosphorylation and ubiquitination. The 25-kDa C-terminal fragment (CTF-25) has been frequently found in the cytoplasmic aggregation of TDP-43 whereas CTF-35 is rarely observed (Berning & Walker, 2019; Hasegawa et al., 2008). Further investigations in brain autopsies of FTLD patients have been revealed three cleavage sites including Arg208, Asp219 and Asp247 in the N-terminal of CTFs, which form different sizes of CTFs (Rohn, 2008).

1.2.2.3.2.1.4 Mutation of *TARDBP* gene

Several ALS-linked mutations in the *TARDBP* gene have been identified. More than 50 ALS-associated dominant missense mutations in the *TARDBP* gene have been reported in both fALS and sALS (Gendron, Rademakers, & Petrucelli, 2013). The mutations occur in different regions across the gene. However, the majority of the ALS-associated mutations appear in the exon 6 of the gene encoding C-terminal glycine-rich region except for the D169G point mutation that resides in RNA recognition motif1 (Sreedharan et al., 2008).

TDP-43 mutations affect a variety of TDP-43 features including enhanced propensity to aggregate, increased cytoplasmic mislocalisation, modified protein stability, protease resistance and altered binding affinity to other proteins (Prasad, Bharathi, Sivalingam, Girdhar, & Patel, 2019). Mutations such as G294V, A315T, M337V, A382T, and G376D, enhance the cytoplasmic mislocalisation of TDP-43 (Prasad et al., 2019). Furthermore, A90V mutation in the NLS leads to sequestration of endogenous TDP-43 into insoluble cytoplasmic aggregates (Winton, Van Deerlin, et al., 2008).

Additionally, some of the mutations have been found affecting the function of TDP-43 in the dynamics of SG. TDP-43 with the G348C mutation forms significantly larger SGs and the mutant TDP-43 incorporates into the SGs earlier than the wild-type TDP-43 (Liu-Yesucevitz et al., 2014).

1.2.2.3.2.1.2 FUS

FUS is an RNA-binding protein encoded by the *FUS*/*TLS* (*fused in sarcoma*/*translocation in liposarcoma*) gene, and it is mainly localised in the nucleus, but low level of FUS also accumulates in the cytoplasm (Andersson et al., 2008). FUS/TLS, a heterogeneous ribonuclear protein, is composed of 526 amino acid residues and belongs to the FET/TET family (**Figure 1.25**).

Figure 1.25

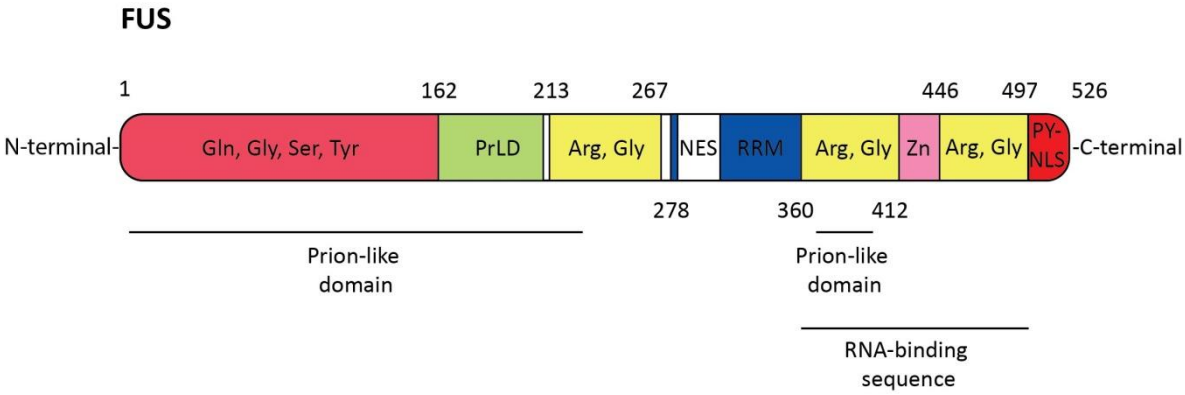

Figure 1.25 Schematic representation of functional domain of FUS. FUS is a member of TET family and contains Glutamine/Glycine/Serine/Tyrosine rich domain (Gln, Gly, Ser, Tyr), Prion-like domain (PrLD), arginine/Glycine rich domain (Arg, Gly), nuclear export signal (NES), RNA recognition motif (RRM), Zinc finger domain (Zn), and Atypical nuclear localisation signal (PY-NLS). Prion-like domains and RN1-binding sequences are shown. Adopted from (Aulas & Vande Velde, 2015) with added information.

In this family, proteins consist of an N-terminal transcription activation domain SYGQ-rich region, a C2/C2 zinc finger (ZnF) motif, and one or more arginine-glycine-glycine (RGG)-repeat sequence. The SYGQ domain is essential for FUS aggregation in yeast, and mutations in tyrosine residues in this domain inhibit the incorporation of cytoplasmic FUS into SGs (Kato et al., 2012). FUS consists of zing finger motif, nuclear localisation signal (NLS), and conserved proline and tyrosine residues (PY-NLS) located in C-terminal of protein (Iko et al., 2004). The RGG-ZnF-RGG domain has been suggested as the major RNA-binding sequence. This predominantly nuclear protein also has a low-complexity prion-like domain, which is important for its ability to phase-separate and its recruitment into RNA granules (St George-Hyslop et al., 2018). The prion-like domains are also involved in misfolding of FUS protein, but this domain is not sufficient for FUS aggregation and toxicity by itself, and both N-terminal and C-terminal part of protein are required for FUS aggregation (Sun et al., 2011).

1.2.2.3.2.1.2.1 Cellular function of FUS

FUS in the nucleus forms a stable complex with many members of the hnRNP family. FUS is involved in multiple steps of RNA-localisation and RNA processing, including regulation of transcription, splicing, and miRNA processing. Moreover, FUS has been discovered contributing to other processes, such as the maintenance of genome integrity (Ratti & Buratti, 2016). It has been reported that loss-of-function of FUS in *Drosophila* leads to reduced viability, impaired locomotive behaviour, neuromuscular junction disruption, and MN degeneration (Sasayama et al., 2012).

Upon cellular stress, FUS starts to move into the cytoplasm and become part of SG; although, it is not essential for the formation of SG (Patel et al., 2015). Moreover, it has been shown that FUS is more prone to localise in the SG compartment rather than TDP-43. Recruitment of FUS into the SGs prevents the formation of aggregates, whereas disruption of RNA recognition motif results in aberrant phase separation and seeds the formation of aggregates (Marrone et al., 2019; Shelkovnikova, Robinson, Connor-Robson, & Buchman, 2013) (**Figure 1.26**). Furthermore, FUS facilitates recruitment of mRNA into SGs which is a reversible process. However, subsequent chronic stress results in formation of irreversible pathological aggregates (Shelkovnikova, Robinson, Southcombe, Ninkina, & Buchman, 2014).

Figure 1.26

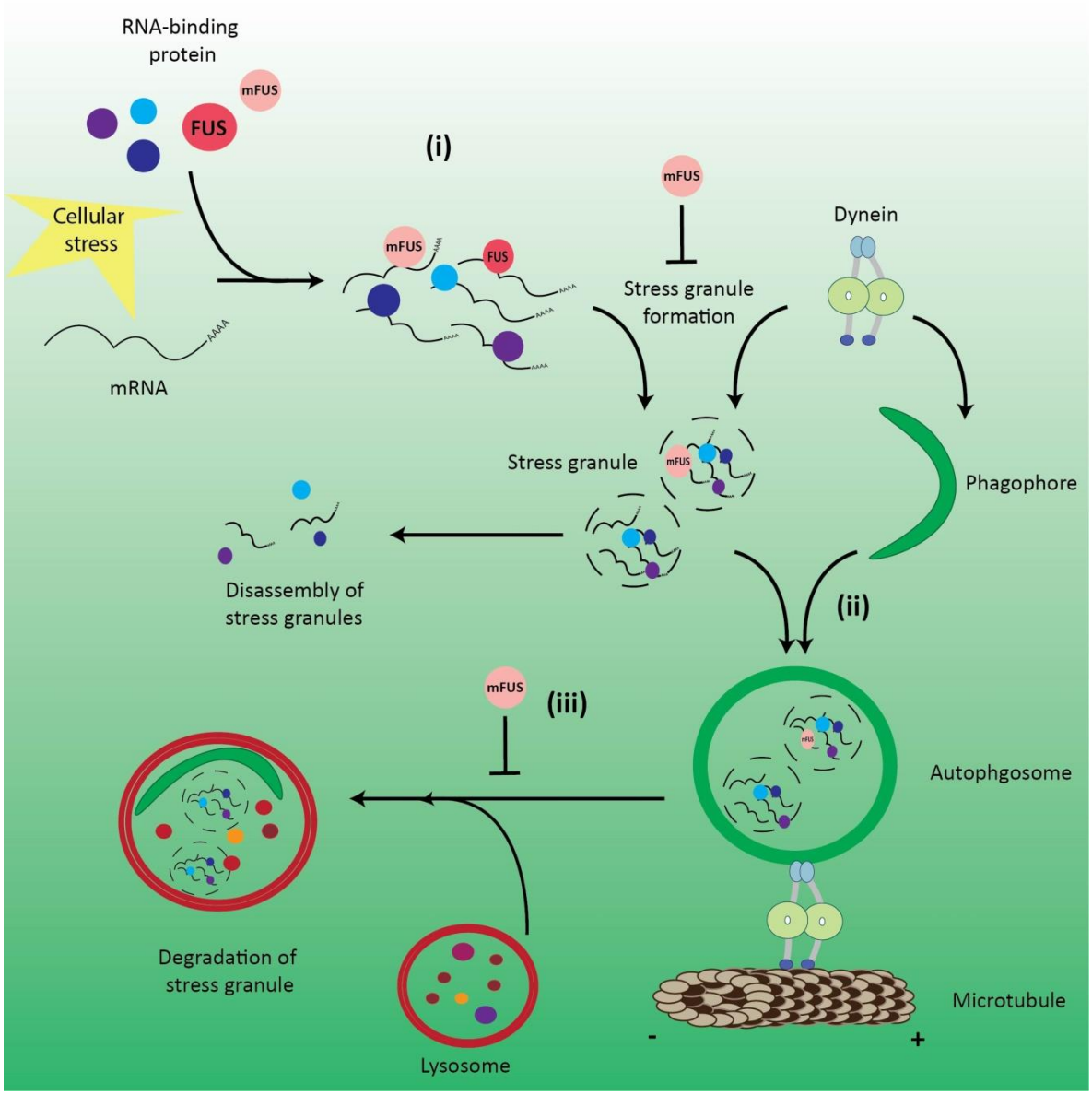

Figure 1.26 Schematic representation of FUS physiological function. (**i**) FUS as an RNA binding protein localises in stress granules (SGs) and also facilitates recruitment of mRNA into SGs. (**ii**) Autophagy pathway is involved in removal of persistence SGs. (**iii**) Mutant FUS (mFUS) impairs autophagic degradation of SGs.

The formation of FUS-positive inclusion in the cytoplasm reduces staining of nuclear FUS, but it is less frequent in comparison to a decreased level of nuclear TDP-43 (Tateishi et al., 2010; Vance et al., 2009). Moreover, the mislocalisation of FUS and FUS-positive inclusions in neurons and glial cells of the spinal cord are histopathological hallmarks of FUS-ALS, and it has been reported that FUS-ALS is mainly a lower MN disease (King et al., 2015; Kwiatkowski et al., 2009).

Consequently, FUS proteins trapped in SGs, which are not released even after removal of stressors co-localises with LC3, a marker of autophagosomes, and this subset of cytoplasmic inclusions are also immunoreactive for p62 (**Figure 1.26 ii**) (Daigle et al., 2016; Ling et al., 2013). Additionally, activation of autophagy diminishes cytoplasmic FUS while autophagy reduction increases the number of FUS-positive SGs (Marrone et al., 2019; Ryu et al., 2014). Furthermore, it has been reported that mutant FUS disturbs autophagosome-lysosome fusion via affecting Rab1 function and overexpression of Rab1 rescues the autophagy in mutant FUS-expressing cell (Soo et al., 2015).

It is noteworthy to mention that PTMs such as methylation regulates the FUS-localisation and it has been reported that genetic inhibition of arginine methylation of FUS reimposes nuclear import of ALS-associated FUS mutants (Dormann et al., 2012).

1.2.2.3.2.1.2.1 Mutation of *FUS* gene and ALS pathology

The mutations in RNA-binding proteins disturb the SGs dynamics and lead to cellular toxicity (Vance et al., 2013). After the identification of TDP-43 mutations and its implications in ALS, mutations in the *FUS* gene have been discovered in fALS and sALS cases (Kwiatkowski et al., 2009). ALS-linked mutations in *FUS* have been described having heterogeneity effects with varying severity, ages of onset and progression. As an example, the P525L mutation has been reported to cause juvenile ALS, whereas R521C and R518K mutations have been found in late-onset disease (Deng, Gao, & Jankovic, 2014). Over 50 mutations in the *FUS* gene have been found in fALS and sALS cases. These mutations

account for about 4 % of fALS and 1 % of sALS patients. The vast majority of mutations have been heterozygous with autosomal dominant inheritance (Vance et al., 2009). Most of the mutations located in the glycine-rich regions and extreme region of C-terminal lead to FUS cytoplasmic accumulation (Lagier-Tourenne, Polymenidou, & Cleveland, 2010). However, FUS truncating mutations cause more aggressive phenotype than missense mutations (Waibel et al., 2013).

It has been shown that wild-type FUS localises in less than 10 % of SGs, although localisation of FUS into SG compartment increases when FUS is mutated (Lenzi et al., 2015). Expression of mutant FUS (mFUS) in MNs has been reported to result in the formation of dense FUS-positive SGs increasing susceptibility of MNs to cellular stress (Higelin et al., 2016).

FUS mutations have been shown to impact the autophagy pathway and recruitment of ATG9 and LC3II to the early autophagosome. MFUS also affects the autophagy flux through disruption of autophagosome-lysosome fusion (**Figure 1.26 iii**) (Soo et al., 2015). Importantly, the study of a mouse model of FUS has shown that mFUS causes neurodegeneration in the absence of cytoplasmic pathology and even significant mislocalisation, which suggest that nuclear gain of toxic function by mFUS as a disease mechanism (Devoy et al., 2017). Therefore, accumulation of cytoplasmic insoluble FUS aggregates and simultaneous depletion of nuclear FUS may provoke neurodegeneration through a gain of toxic function, a loss of function, or both.

1.3 Research aims

The focus of this thesis is elucidating the cellular and molecular mechanism, which underpins the degeneration of MNs in SMA-LED, a congenital or early childhood disease, and ALS, an adult-onset neurodegenerative disease. In SMA-LED, mutations in *DYNC1H1* encoding the heavy chain (HC) subunit of cytoplasmic dynein and *BICD2* encoding an adaptor of dynein have been recognised to be the main genetic causes of the disease (Harms et al., 2012; Neveling et al., 2013; Oates et al., 2013; Scoto et al., 2015). In Hafezparast lab, reduced MT acetylation and Golgi fragmentation were reported in patient fibroblasts with *DYNC1H1* mutations.

MT acetylation promotes motor protein binding and modulates motor-protein trafficking (MISSING:reed2006microtubule, 2021) and also through increasing flexibility assists MT lattice to cope with mechanical stress (Xu et al., 2017). In turn, dynein controls the extension of MT into the growth cone by regulating MT plus ends (Lazarus, Moughamian, Tokito, & Holzbaur, 2013).

HDAC6 and α-TAT1 have been identified as the main regulators of α-tubulin deacetylation and acetylation, respectively (Sadoul & Khochbin, 2016). The aim was to determine how mutations in HC of dynein contribute to reduced MT acetylation and also to further investigate the effects of *DYNC1H1* mutations on the interaction between dynein and Golgin160, a dynein cargo adaptor for Golgi membrane. Golgi fragmentation has been reported as an early event that occurs before the aggregation of mutant proteins (Gosavi, Lee, Lee, Patel, & Lee, 2002). To achieve this, Loa^{Hom} MEFs and patient fibroblasts including p.R339G and p.D338N were used to investigate the role of dynein in regulation of MT acetylation and also to study interaction between dynein and Golgin160.

In ALS, mislocalisation of protein and cytoplasmic accumulation of insoluble protein aggregates are key pathological hallmarks (Ramesh & Pandey, 2017). Of importance, TDP-43 mislocalisation and aggregation have been implicated in ALS, as the principal component of the ubiquitin positive inclusions (Suk & Rousseaux, 2020). Moreover,

SQSTM/p62 is another ALS associated protein, which is also found in inclusions in ALS and mutations in *SQSTM/p62* gene are also linked with ALS (Gal, Ström, Kilty, Zhang, & Zhu, 2007; Teyssou et al., 2013). Moreover, p62 is an autophagy adaptor whose TBK1-dependent phosphorylation is vital for efficient sequestration of ubiquitinated proteins into the autophagosome (Deng et al., 2020). Furthermore, *TBK1* is an ALS associated gene and its mutations have been linked with ALS (Freischmidt et al., 2015). Of note, removal of protein aggregates mainly relies on autophagy pathway. Importantly, dynein mediates the transport of autophagosomes and their fusion with the lysosome is necessary for efficient degradation of protein aggregates. Additionally, variations in *DYNC1H1* have been identified in both sALS cases and healthy control, suggesting that variations and subsequent alterations in dynein function might render cells more susceptible to genetic and environmental insults leading to neurodegeneration.

Moreover, dynein regulates the formation of SGs and lack of functional dynein disturbs the formation of SGs and inhibition of dynein activity causes a complete abolishment in SG formation (Tsai et al., 2009). In addition, dynein modulates the disassembly and clearance of SGs (Chernov et al., 2009). As of the importance of dynein in SGs formation and degradation, it was sought to investigate regulatory role of dynein in dynamic of SGs.

My hypothesis was dynein modulates MT acetylation and formation of protein aggregates contributing to neuronal degeneration in motor neuron diseases. My objectives were to investigate consequences of mutations in cytoplasmic dynein 1 heavy chain 1 on MT acetylation and whether dynein dysfunction makes cell more prone to form toxic protein aggregation. To address the objectives, the aims were to test interaction of dynein with HDAC6 and α-TAT1 and to test a two-hit hypothesis in *Loa* mice to further elucidate effects of dynein dysfunction accompanied by deficiencies in the protein quality control system on the protein aggregation and cytoplasmic mislocalisation of TDP-43. This was performed in *Loa* homozygous mice where *Dync1h1* is mutated and also various treatments were used to recapitulate deficiencies in protein quality control system.

Chapter 2: Methods

2.1 Genotyping

2.1.1 DNA preparation

The tissue was obtained from an ear punch, which is approximately 0.2-0.3 cm^2. For the genotyping of mouse embryonic fibroblast (MEF), the fibroblasts grown in a T25 flask (Corning, Cat: 430639) were trypsinized (Life Technologies, Cat: 10462502), and then cells were centrifuged at 390 x g for 5 minutes, and the cell pellet was washed with Dulbecco's phosphate-buffered saline (DPBS). Then, the tissue sample or cell pellet were lysed by adding 200 µL of lysis buffer (100 mM Tris-HCl at pH 8.0, 5 mM EDTA, 0.2 % SDS, and 200 mM NaCl) and 2 µL of Proteinase K (20 mg/mL) (NEB, Cat: P8107S) and followed by incubation in 55 °C water bath overnight. Subsequently, the samples were centrifuged at 16,000 x g for 15 minutes, and the supernatant containing the DNA was decanted into another tube, and a 1:20 dilution of DNA sample was prepared. Then, 1 µL of diluted DNA was used for each Polymerase Chain Reaction (PCR) reaction.

2.1.2 Genotyping *Loa* Mice

After preparation of tissue from mice or fibroblast (section 2.1.1), the genotyping was performed using PCR, followed by a restriction digest. The PCR reaction was made of HotStarTaq Master Mix (Qiagen, Cat: 203443), primers, diluted DNA sample, and with the volume made up to 10 µL with double distilled water (see **Table2.1**). The primers described in **Table2.2** were used to amplify the region including c.1739T>A mutation using

PCR program described in **Table2.3**. As mutation generated another restriction site for *RsaI* (GT^{V} AC) in the PCR product, the 989 bp PCR product was incubated with the 5 U of *RsaI* (NEB, Cat: R0167S) at 37 °C for 2 hours followed by loading samples onto the 2 % agarose gel, which run for 30 minutes at 90 V (small tank) or 120 V (large tank). In the presence of the mutation, the restriction enzyme would cut at the primary restriction site and the second restriction site generating fragments of 252 bp, 135 bp, bp and 603 bp. In the absence of mutation, two fragments would be generated, including a 387 bp and a 602 bp fragment (**Figure 2.1**).

Table 2.1 PCR reaction

PCR reaction	Volume
HotStarTaq	5 µL
Forward primer (10 mM)	1 µL
Reverse primer (10 mM)	1 µL
Diluted DNA sample	1 µL
Distilled water	2 µL

Table 2.1 PCR reaction Table shows components and volumes needed for each PCR reaction.

Table 2.2 Sequences of primers

Primer	Sequence (5′-3′)
Forward primer	AAGCACCTGAACCCCAAGAC
Reverse primer	GTAGGACTCCCACACCAACG

Table2.2 Sequences of primers. Table shows sequences of primers used for the genotyping of the *Loa* mice.

Table 2.3 PCR program for *Loa* genotyping

Number of cycles	Temperature	Time
1	95 °C	15 minutes
35	95 °C	30 seconds
	64 °C	30 seconds
	72 °C	1 minute
1	72 °C	10 minutes

Table2.3 PCR program for *Loa* genotyping. Table shows PCR program for *Loa* genotyping including number of cycles, temperature, and time.

Figure 2.1

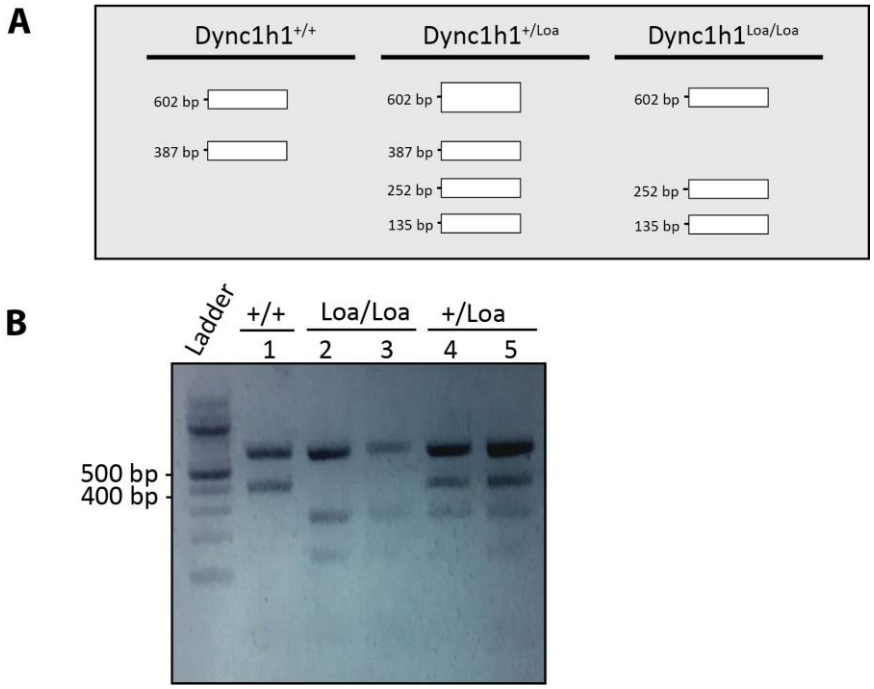

Figure 2.1 (**A**) Schematic representation of the band pattern for Dync1h1^{Loa} genotyping. (**B**) An image showing results of genotyping for DYNC1H1$^{+/+}$ (lane 1) and DYNC1H1$^{+/Loa}$ (lane 4 and 5), DYNC1H1$^{Loa/Loa}$ (lane2 and 3) fibroblasts including 100 bp ladder. The PCR products were run on a 2% agarose gel for 20 minutes.

2.1.3 Genotyping DYNC1H1^{D338N} fibroblast

The DNA samples were prepared, as described in section 2.1.1. To determine the presence of c.1012G > A mutation, the primers described in Table 2.4 were used for the multiplex PCR. Two reactions were set up for each sample, which each reaction contained three primers. The two outer primers produce a 537 bp fragment. The inner primers, inner wild-type forward annealing to the wild-type allele and an inner mutant forward primer annealing to the mutant allele, would produce a 413 bp fragment (**Figure 2.2**). The PCR reaction was set up as detailed in **Table 2.1** and PCR program was used as described in **Table 2.5**. The expected pattern of the results of the genotype is represented in Figure 2.2.

Table 2.4 Sequences of primers

Primer	Sequence (5′-3′)
Outer forward primer	GCAACATCAAAATGTTCC
Outer reverse primer	CGATGTCTCTCAACAATACC
Inner wild-type forward	GACTACAATCCTCTGATGAAAG
Inner mutant forward	GACTACAATCCTCTGATGAAAA

Table 2.4 Sequences of primers. Table shows sequences of primers used for the genotyping of the DYNC1H1^{D338N} fibroblasts. The last 3' end base pair targeting mutation is underlined.

Table 2.5 PCR program for DYNC1H1^{D338N} **genotyping**

Number of cycles	Temperature	Time
1	95 °C	15 minutes
35	94 °C	30 seconds
	60.5 °C	30 seconds
	72 °C	1 minute
1	72 °C	10 minutes

Table 2.5 PCR program for DYNC1H1^{D338N} **genotyping.** Table shows for PCR program for DYNC1H1^{D338N} genotyping including number of cycles, temperature, and time.

Figure 2.2

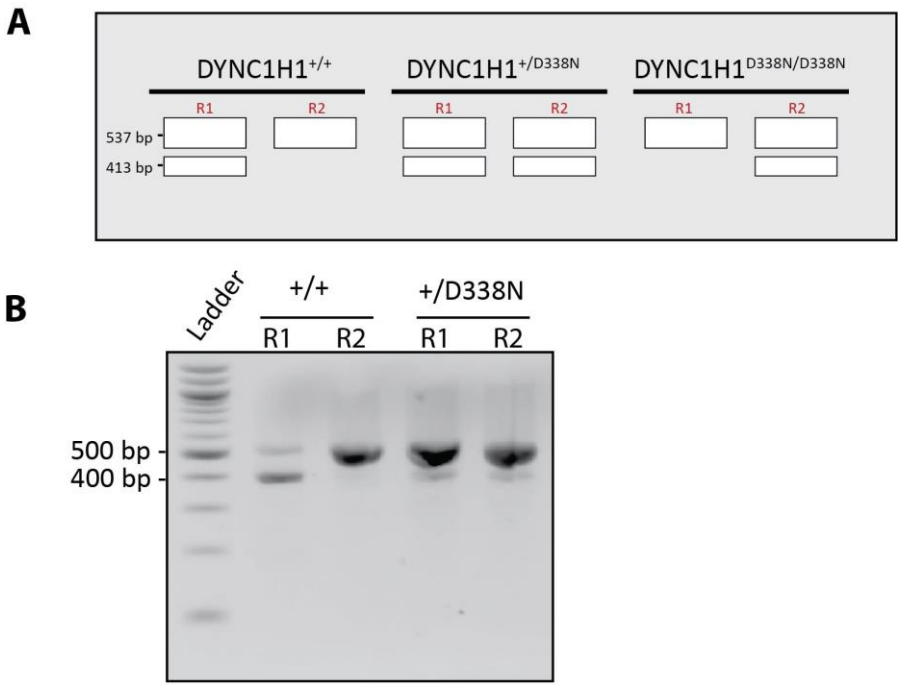

Figure 2.2 (**A**) Schematic representation of the band pattern for DYNC1H1^{D338N} genotyping. (**B**) An image showing results of genotyping for DYNC1H1$^{+/+}$ and DYNC1H1$^{+/D338N}$ fibroblasts. The PCR products were run on a 2% agarose gel for 20 minutes. R1: reaction 1, R2: reaction 2, and 100 bp ladder.

2.2 Dissection and tissue culture

2.2.1 Isolation of mouse embryonic fibroblasts

The pregnant female mouse was sacrificed at day 13 by cervical dislocation. The uterine horns were dissected out and briefly rinsed in 70 % ethanol and placed into the dish containing DPBS. Afterwards, each embryo was separated from the placenta, and surrounding membranes and then brain, spinal cord, and dark red organs were cut away. The remaining tissue was washed with DPBS to remove as much blood as possible and transferred to a 35 mm plate (Fisher, Cat: 10810765). By adding 1 mL DPBS, the tissue was minced until the tissue was homogenous. Subsequently, the cell suspension was

transferred to a 15 mL falcon tube and incubated with 2 mL of trypsin-EDTA with gentle shaking at 37 °C for 15 minutes. During the incubation, 100 U of DNase was added to avoid high viscosity, and then, two volumes of fresh media (see **Table2.6**) were added and let the remaining pieces of tissue to settle down at the bottom of the tube. The supernatant was centrifuged at 200 x g for 5 minutes. The pellet was resuspended in pre-warmed medium, and one embryo equivalent was plated into the 100 mm plate (Corning, Cat: 10075371) and incubated at 37 °C. It is noteworthy that there is a difference in rate of growth between wild-type and *Loa* fibroblasts and there is increased growth rate in *Loa* fibroblasts.

Table 2.6 Component of medium for MEFs and NIH3T3 cells

Culture reagent	The volume needed for 0.5 L of complete medium	Concentration
DMEM (Gibco, cat: 21969035)	440 mL	-
Bovine growth serum (GE Healthcare Hyclone SH30541.03)	50 mL	10 %
L-Glutamine (100X) (Gibco, Cat: 11500626)	5 mL	1 %
Penicillin/Streptomycin (Gibco, Cat: 11528876)	5 mL	1 %

Table 2.6 Table shows the components of cell culture medium for mouse embryonic fibroblast (MEF) and NIH3T3 cell line. The volume needed for making 0.5 L of complete medium and the final concentrations are shown.

2.2.4 Culture media

Table 2.7 describes the culture medium used for Neuro2A cell line.

Table 2.7 Components of medium for Neuro2A cells

Culture reagent	The volume needed for 0.5 L of complete media	Concentration
DMEM (Gibco, Cat: 21969035)	440 mL	-
Foetal Bovine Serum (FBS) (Gibco, Cat: 10270106)	50 mL	10 %
L-Glutamine (100X) (Gibco, Cat: 11500626)	5 mL	1 %
Penicillin/Streptomycin (Gibco, Cat: 11528876)	5 mL	1 %

Table 2.7 Table shows the concentrations and components of cell culture medium for Neuro2A cell line. The volume needed for making 0.5 L of complete medium and the final concentrations are shown.

2.2.2 Primary culture of embryonic mouse spinal motor neurons

Prior to isolation of MNs, under the laminar hood, the sterilized 13 mm coverslips were placed in each well of 24-well plate and coated with 3 µg/mL of Poly-L-Ornithine (Sigma-Aldrich, Cat: P4957) and incubated at room temperature overnight protected from light. After that, the coverslips were coated with 1.1 mg/mL laminin (Sigma-Aldrich, Cat: L2020)

and incubated for at least 2 hours in the 37 °C 5 % CO_2 incubator. For the dissection of the spinal cord, the pregnant female mouse was sacrificed at E12.5-E13 day using intraperitoneal injection as a primary method and cervical dislocation as a secondary method. The female mouse was placed with the anterior side up, and lower abdomen was opened laterally, and embryos were separated from uterus and placed in the dish containing HBSS with 2 % Penicillin/Streptomycin. Each embryo was decapitated using fine-tip forceps at the intracranial notch just below the base of the skull. The embryo was placed on its ventral side down in the dish and using fine-tip forceps, the skin overlying the spinal cord was removed. The cord was separated using the tip of the forceps inserted in the medial opening of the cord, and the cord was left up. Once spinal cord was isolated, meninges were removed in one movement starting from the rostral side. Subsequently, the spinal cord was laid down on dorsal side up, and the dorsal horn was removed using a blade. Then, the dissected cord was kept in a 15 mL falcon tube containing the 1 mL HBSS (Gibco, Cat: 10617394) and 10 µL of Trypsin 2.5 % w/v in PBS was added into the tube and incubated at 37 °C 5 % incubator for 10 minutes. Afterwards, using P1000 pipette, the tissue was taken up with as little of the HBSS as possible and placed in the tube containing 800 µL of L15 media (Gibco, Cat: 11570396), 100 µL of BSA (4 % w/v in L15) and 100 µL of DNase (1 mg/mL in L15) (Sigma-Aldrich, Cat: DN25). The tissue was triturated four times gently and let it sit for 2 minutes to allow undissociated tissue to sink, and then the supernatant containing MNs was transferred to another 15 mL falcon tube. After that, 1 mL BSA (4 % w/v in L15) was added gently to the tube by placing the tip of the P1000 at the bottom of the tube to ensure having two separate layers. The tube was spin down at 380 x g for 5 minutes, and then the supernatant was removed. The pellet was resuspended in neurobasal medium (see **Table 2.8**), the laminin was removed from the wells, and the neurons were plated on coated coverslips.

Table 2.8 Components of culture medium for motor neuron

Culture reagent	The volume needed for 50 mL of motor neuron medium	Concentration
Neurobasal medium (Gibco, Cat: 10888-022)	47.8 mL	-
B-27 supplement (50X) (Gibco, Cat: 17504-044)	1 mL	2 %
Horse serum (Sigma, Cat: H1270)	1 mL	2 %
Glutamax (100X) (Gibco, Cat: 11574466)	0.5 mL	1 %
Penicillin/Streptomycin (Gibco, Cat: 11528876)	0.5 mL	1 %
β-mercaptoethanol (50mM) (Gibco, Cat: 11528926)	25 µL	0.05 %
CTNF (10 µg/mL) (Gibco, Cat: 10583395)	2.5 µL	0.005 %
GDNF (10 µg/mL) (Gibco, Cat: 10679963)	0.5 µL	0.001 %
BDNF (10 µg/mL) (Invitrogen, Cat: 10477253)	0.5 µL	0.001 %

Table2.8 Table shows the components of culture medium for motor neuron. The volume needed for making 5 mL of motor neuron medium and the final concentrations are shown.

2.2.3 Primary culture of postnatal mouse hippocampal neurons

Before isolation of hippocampal neuron, The 16 mm coverslips were plated in 12-well plate, and then the 12-well plate was coated with 50 mg/mL Poly-D-lysine and incubated at 37 °C 5 % CO_2 incubator for 3 hours. Subsequently, Poly-D-lysine was aspirated, and 10mg/mL of laminin was added to the wells and incubated overnight at 37 °C 5 % CO_2 incubator. Before starting the dissection, the maintenance medium (see **Table 2.9**) was added to the wells and kept under a laminar hood. To culture primary hippocampal neurons, the p0-p2 newborn mouse was sacrificed by cervical dislocation, and the mouse was decapitated, and the head was placed on the sterilized paper towel. The skin was removed and using a set of fine scissors; the skull was cut from the neck to the snout end. Using a tick curved forceps brain was scooped out of the skull and placed in the dish containing dissection medium (see **Table 2.10**). The hemispheres were separated, and the hemisphere was turned so that the medial side faces upwards. The thalamus, using thin curved forceps, was removed to expose the hippocampus, and then the remaining meninges were removed and the hippocampus dissected out. The two hippocampi were transferred to an eppendorf tube containing the dissection medium

Under the laminar flow hood, 90 % of dissection medium was removed from the tube, and 1 mL of dissection medium was added to the tube, and this step was repeated twice. Afterwards, 1 mL of pre-incubated plating medium (see **Table 2.11**) was added to the tube and remove, and this step was performed twice. Then, 0.5 mL of pre-incubated plating medium was added to the tube, and the tissue was triturated with a P1000 pipet. The content of the tube was transferred to a 15 mL falcon tube and 3 mL of pre-incubated plating medium was added to the tube and mixed by pipetting. The 0.5 mL of cell suspension was added per well and incubated at 37 °C 5 % CO_2 incubator for 3 hours. Subsequently, 1.5 mL of pre-incubated maintenance medium was added per well and incubated at 37 °C 5 % CO_2 incubator.

Table 2.9 Components of maintenance medium for hippocampal neuron

Culture reagent	The volume needed for making 100 mL maintenance medium	Concentration
Neurobasal medium (Gibco, Cat: 10888-022)	96 mL	-
B-27 supplement (50X) (Gibco, Cat: 17504-044)	2 mL	2 %
L-Glutamine (100X) (Gibco, Cat: 11500626)	1 mL	1 %
Penicillin/Streptomycin (Gibco, Cat: 11528876)	1 mL	1 %

Table 2.9 Table shows the components of maintenance medium for hippocampal neuron culture. The volume needed for making 100 mL of maintenance medium and the final concentrations are shown.

Table 2.10 Components of dissection medium for hippocampal neuron

Culture reagent	The volume needed for making 100 mL dissection medium	Concentration
HBSS (Gibco, Cat: 10617394)	97.9 mL	-
HEPES 1 M (Gibco, Cat: 11574456)	1 mL	1 %
Glucose 20 %	0.1 mL	0.1 %

Sodium Pyruvate 11 mg/mL (Gibco, Cat: 11360070)	1 mL	1 %

Table 2.10 Table shows the components dissection medium for hippocampal neuron culture. The volume needed for making 100 mL of dissection medium and the final concentrations are shown.

Table 2.11 Components of plating medium for hippocampal neuron

Culture reagent	The volume needed for making 50 mL plating medium	Concentration
Basal Medium Earle (BME) (Gibco, Cat: 41010026)	43.275 mL	-
FBS (Heat inactivated) (Gibco, Cat: 10270106)	5 mL	10 %
Sodium pyruvate (Gibco, Cat: 11360070)	0.5 mL	1 %
L-Glutamine (100X) (Gibco, Cat: 11500626)	0.5 mL	1 %
Penicillin/Streptomycin (Gibco, Cat: 11528876)	0.5 mL	1 %
Glucose 20 %	0.225 mL	

Table 2.11 Table shows the components plating medium for hippocampal neuron culture. The volume needed for making 5 mL of plating medium and the final concentrations are shown.

2.3 Preparation of plasmid and cloning

2.3.1 Transformation of DH5-α E.coli

Chemically competent DH5-α E.coli (ThermoFisher, Cat: 18265017) were used for the propagation of plasmids. The tubes containing 50 µL of competent cells were thawed on ice and once thawed 2 µL of plasmid DNA was added to the cell and incubated on ice for 30 minutes with occasional agitation. The competent cells were heat-shocked in a water bath at 42 °C for 40 seconds and then were incubated on ice for 2 minutes. 200 µL of lysogeny broth (LB) was added to the bacteria/DNA mixture which followed by incubation at 37 °C for 1 hour in a shaker at 220 rpm. The mixture then was plated onto LB agar plates containing appropriate selection antibiotic (see **Table 2.12** for concentration). The plates were incubated overnight at 37 °C.

Table 2.12 List of antibiotics used for selection of transformed cells

Antibiotic	High copy plasmid	Low copy plasmid
Ampicillin	50 µg/mL	20 µg/mL
Kanamycin	40 µg/mL	10 µg/mL

Table 2.12 List of antibiotics used for selection of transformed cells. Table shows antibiotics and their concentrations used for selection of transformed cells in the overnight culture for plasmid purification and transformed cells.

2.3.2 Plasmid purification

2.3.2.1 Miniprep

Minipreps were performed using the NEB Spin Miniprep kit (NEB, Cat: T1010) as per the manufacturer's instructions. For the purification of 0.4-0.5 µg of plasmid DNA, 5 mL of LB containing the selective antibiotic (See **Table 2.12** for concentrations) was inoculated with transformed DH5-α E.coli with the relevant plasmid. The 5 mL of culture was incubated overnight x at 37 °C on a shaker at 200 rpm. The next day, the overnight-culture was transferred to the eppendorf tube and centrifuged at 16000 x g for 1 minute at room temperature. The supernatant was removed and the pellet was resuspended in 200 µL of Plasmid Resuspension buffer (containing RNAse) which followed by lysis and neutralization steps according to the manufacturer's instructions. The resulting solution was centrifuged at 16,000 x g for 5 minutes to pellet down the cell lysis. After being centrifuged, the supernatant was transferred to an NEB spin column which was then centrifuged for 1 minute at 16,000 x g and flow-through discarded. After subsequent series of washes, the 30 µL of double distilled water was added to the centre of membrane of the spin column. After 1 minute, the final step was performed by centrifugation at 16,000 x g for 1 minute. The flow-through containing the purified plasmid was collected in a new eppendorf tube and resuspended in 30 µL of double distilled water and then the DNA concentration was measured using NanoDrop 2000 spectrophotometer.

2.3.2.2 Maxiprep

Maxipreps were performed using the PureLink HiPure Plasmid Maxiprep Kit (Invitrogen, Cat: K2100-06) according to manufacturer's instructions with some adjustments in centrifugation speeds and times. For the purification of 2-5 µg of plasmid DNA, based on

the copy number of plasmid, 100-200 mL of LB containing the selective antibiotic was inoculated with transformed DH5-α E.coli with the relevant plasmid and incubated overnight at 37 °C on a shaker at 200 rpm. The overnight culture was transferred to falcon tube and centrifuged at 3760 x g for 15 minutes. Meanwhile, the HiPure Maxi column was equilibrated as per the manufacturer's instructions. After centrifugation, the supernatant was discarded and the pellet was resuspended in Resuspension buffer which followed by lysis and neutralization steps according to the manufacturer's instructions. After pelleting the cell lysis, the supernatant was loaded onto the equilibrated HiPure Maxi column and then 10.5 mL of isopropanol was added to the elute and was mixed before centrifugation at 3760 X g for 2 hours at 4 °C. The supernatant was removed and then pellet was washed in 5 mL freshly made 70 % ethanol and centrifuged at 3760 x g for 20 minutes at 4 °C. The pellet was air dried for 7 minutes and resuspended in 200-500 µL of double distilled water and then the DNA concentration was measured using NanoDrop 2000 spectrophotometer.

2.3.3 Sub-cloning of ATAT1 construct

To sub-clone ATAT1 cDNA to a V5-tagged plasmid, the NEB Gibson assembly cloning kit (NEB, Cat: E2611) was used according to manufacturer's instructions. Briefly, at the first step, a set of primers were designed using NEBuilder assembly tool to amplify DNA insert with 15-20 bp overlapping ends. The mixture of PCR product, the linear V5-tagged plasmid (restriction enzyme digest), and Gibson assembly master mix were incubated at 50 °C for 1 hour. At the final step, the assembled DNA was transformed into competent cells for propagation

2.4 Transfection

2.4.1 Transfection of cells with Lipofectamine 3000

Transfections with lipofection were performed using Lipofectamine 3000 (ThermoFisher Scientific, Cat: 15282465) according to the manufacturer's instructions. Briefly, cells were seeded on either a 24 or 6-well plate (see **Table 2.13** for reagent volume) to be 70-80 % confluent at the time of transfection. Prior to lipofection, the complete medium was replaced with Opti-MEM medium (ThermoFisher Scientific, Cat: 31985062). To prepare the reagents for lipofection, the plasmid DNA was diluted in Opti-MEM medium and mixed with P3000 reagent in a 1:2 ratio. The Lipofectamine 3000 reagent was also diluted in Opti-MEM medium separately. Then, diluted DNA and diluted Lipofectamine 3000 reagent were mixed and incubated for 20 minutes at room temperature. Subsequently, the DNA-Lipofectamine 3000 reagent complexes were added to each well dropwise and incubated at 37 °C for 24-48 hours.

Table 2.13 Lipofectamine 3000	Lipofectamine 3000	
	24-well	**6-well**
Volume of Opti-MEM medium to dilute DNA	25 µL	125 µL
Volume of P3000 reagent	2 µL	10 µL
Volume of Opti-MEM medium to dilute Lipofectamine 3000 reagent	25 µL	125 µL
Volume of Lipofectamine 3000 reagent	0.75	3.75
Volume added to cells	50 µL	250 µL

Table 2.13 Lipofectamine 3000. Table shows volumes of media and reagents used for transfection of cells using Lipofectamine 3000.

2.4.2 Transfection of cells with Nucleofection

Nucleofection of primary MEFs was performed using the Nucleofector 2b device (Cat: AAB-1001) according to the manufacturer's instructions. Briefly, the MEF were grown in the large flask. On the day of transfection, cells were detached by adding the trypsin and then 2 X 10^6 cells were counted and centrifuged to pellet down. The cells were resuspended in transfection solution containing 80 µL of Nucleofactor reagent, 20 µL supplements, and before nucleofection, 5 µg of DNA was added to the cells and mixed thoroughly. Afterwards, the cells were transferred to the cuvette ensuring that no bubbles are present in the cuvette and then placed in the machine and electroporated with A-023 program. After electroporation, the pre-warmed media was added to the cells and cells

were counted and certain number of cells was plated either on coverslips in 24-well plate or 100 mm dish. Cells were fixed or lysed after 24 hours and 48 hours.

2.5 Biochemistry

2.5.1 Cell lysis preparation

2.5.1.1 Cell homogenisation for SDS-PAGE

The 0.3 X 10^6 and 1 X 10^6 cells were plated in 6-well plate or 100 mm dish respectively, to get 90-100 % confluency for western blot analysis. After 24 hours, cells underwent any required drug treatment or the growth medium was removed, and the cell monolayer was washed with DPBS twice, and excess DPBS was aspirated. For homogenisation, an adequate volume of RIPA lysis buffer (see **Table2.14**) (100 µL to each well of 6-well plate and 200 µL to 100 mm dish) was added and swayed to distribute lysis buffer evenly. Cells were scraped using a cell scraper (Fisher, Cat: 11597692) and then were collected to a 1.5 mL eppendorf tube. The lysate was incubated on ice for 10 minutes and centrifuged at 1000 x g for 5 minutes at 4 °C. The supernatant was collected (avoiding the pellet) into a new eppendorf tube and stored at -80 °C.

Table 2.14 Component of RIPA lysis buffer

Stock	Volume for 1 mL	Concentration
RIPA lysis buffer (Sigma-Aldrich Cat: 20-188)	100 µL	10 %
Protease inhibitor (50X) (Roche, Cat:11836170001)	20 µL	2 %
Phosphatase inhibitor 2 (Sigma-Aldrich Cat: P5726)	10 µL	1 %
Phosphatase inhibitor 3 (Sigma-Aldrich Cat: P0044)	10 µL	1 %
Distilled water	680 µL	-

Table 2.14 Component of RIPA lysis buffer. Table shows components of lysis buffer for cell homogenization for SDS-PAGE including volumes needed to make 1 mL lysis buffer and final concentrations.

2.5.1.2 Cell homogenisation for immunoprecipitation

The 0.3 X 10^6 cells were plated in 35 mm plate to get 90-100 % confluency. The following day, cells in two 35 mm plates were transfected with PCDNAC3-V5 ATAT1. After 24 hours, the growth medium was removed, and the cell monolayer was washed with DPBS twice, and excess DPBS was aspirated. To lyse the cell, 100 µL of lysis Buffer with inhibitors (see **Table 2.15 and 2.16**) was added to each 35 mm plate and swirled to distribute lysis buffer evenly. Cells were scraped using a cell scraper and collected to an eppendorf tube. The lysate was incubated on ice for 30 minutes and centrifuged at 13,000 x g for 15 minutes at 4 °C. The supernatant was collected (avoiding the pellet) into a new eppendorf tube and stored at -80 °C or added to pre-washed Sepharose beads.

Table 2.15 Components of lysis buffer

Stock	Volume for 20 mL
HEPES 1 M, pH=7.2	200 µL
KCl 1 M	1 mL
0.5 % Triton X-100	100 µL
EDTA 0.5 M	40 µL
Distilled water	18.66 mL

Table 2.15 Components of lysis buffer. Table shows components of lysis buffer for cell homogenization for immunoprecipitation including volumes needed to make 20 mL lysis buffer.

Table 2.16 Components of lysis buffer for immunoprecipitation

Stock	Volume for 1mL
Lysis buffer	978 µL
Protease inhibitor (50X) (Roche, Cat:11836170001)	20 µL
DDT 1 M	2 µL

Table 2.16 Components of lysis buffer for immunoprecipitation. Table shows final components of lysis buffer for cell homogenization for immunoprecipitation including volumes needed to make 1 mL lysis buffer.

2.5.2 Measuring protein concentration

The protein concentration of cell lysate prior to loading on SDS-PAGE gels was determined using a bicinchoninic acid assay (BCA) (ThermoFisher Scientific, Cat: 23227). The assayed

was performed following the manufacturer's protocol but scaled down to a total column of 200 µL, and 1 µL of the sample was measured on a NanoDrop 2000 spectrophotometer.

2.5.3 Immunoprecipitation

To perform the immunoprecipitation (IP), the bottle of protein A sepharose beads (Life Technologies, Cat: 101041) was shaken to ensure all beads were mixed. 75 µL of beads were added to a narrow conical bottom and washed with cold DBPS three times. Each wash was consisted of adding 1 mL ice-cold DPBS, incubation on a rotator at 4 °C for 10 minutes and centrifugation at 2000 x g for 2 minutes at 4 °C. Afterwards, the beads were blocked with DPBS containing 3 % bovine serum albumin (BSA) (Sigma-Aldrich, Cat: A9706) on the rotator at 4 °C for 1 hour or overnight. The next day, the beads were centrifuged and blocking solution was discarded and beads were washed three times with ice-cold DPBS and blocked beads was incubated either with 2.5 µg of primary antibody (Rabbit anti ATAT1, Abcam, Cat: ab58742) against the protein of interest or IgG Mouse (as a control) (Merk Millipore, Cat: PP54) for 2 hours at 4 °C on the rotator. Simultaneously, to clear homogenate, supernatant from cell lysis was incubated with beads for 1 hour on the rotator at 4 °C. The clearance of cell lysis was followed by centrifugation for 2 minutes at 2000 x g, and then the cleared homogenate was collected. Afterwards, beads conjugated to the antibody and those conjugated to the IgG control underwent three washes with DPBS to ensure complete removal of unbound antibody or IgG. Subsequently, antibody and IgG-conjugated beads were incubated with 100 µL of cleared homogenate overnight at 4 °C with constant agitation. Following day, beads were centrifuged at 4 °C at 2000 x g for 2 minutes, and the supernatant was collected as an unbound fraction. The beads were washed with ice-cold DPBS 6 times and one time with distilled water as previously described. At the end, to break the interaction of beads and protein-linked antibody, 1X SDS was added to the beads and boiled for 5 minutes at 95 °C. Then, the samples were centrifuged at 16000 x g for 5 minutes, and the supernatant was collected and stored at -80 °C until analysed using SDS-PAGE and immunoblotting.

2.5.4 SDS-PAGE (Protein electrophoresis)

The sodium dodecyl sulphate-polyacrylamide gel electrophoresis (SDS-PAGE) was used for evaluation of specific protein expression. The 12 % Bis-Tris NuPAGE precast protein gel (Invitrogen Cat: 12070166) with 1 X NuPAGE MOPS SDS running buffer was used to resolve the proteins based on the molecular weight of the protein of interest (see **Table 2.17**). For protein electrophoresis, 20 µg of protein for each cell lysate or the maximum allowed for by the lowest concentrated sample was loaded into the wells. SeeBlue Plus2 Pre-stained protein standard (ThermoFisher, Cat: LC5925) was used and samples were electrophoresed for 90 minutes at 140 V to ensure the complete-separation of different size of proteins.

Table 2.17 List of protein targets for immunoblotting

Protein	Size (kDa)	Gel percentage	Protein concentration
TBK1	80	12 %	20 µg of MEF lysate/ Neuor2A lysate
P62	62	12 %	20 µg of MEF lysate/ Neuor2A lysate
TDP-43	43	12 %	20 µg of MEF lysate
LC3I/LC3II	16,18	12 %	20 µg of MEF lysate/ Neuor2A lysate
ATAT1	47	12 %	20 µg of MEF lysate/ human fibroblast lysate
Acetylated α-tubulin	50	12 %	20 µg of MEF lysate/ human fibroblast lysate

Tubulin	50	12 %	20 µg of MEF lysate/ human fibroblast lysate

Table 2.17 List of protein targets for immunoblotting. Table shows protein targets for immunoblotting. Table represents the size of protein, the percentage of gel used in SDS-PAGE, and the amount of protein loaded.

2.5.5 Immunoblotting and analysis

For the visualization of protein levels, after separation of protein by electrophoresis, proteins were transferred to the nitrocellulose or PVDF membrane (Amersham, Cat: 10600021) for the immunoblotting. All membranes with protein side facing up were blocked in 5 % skimmed milk in PBS-T (PBS and 0.05 % Tween-20 (Sigma, P9416)) and incubated overnight at 4 °C on the rocker with constant agitation. Afterwards, the membranes rinsed with PBS-T twice. Primary antibodies at the desired concentration (recommended by the manufacturer) (see **Table 2.18**) were diluted in 0.1 % sodium azide-PBS-T and applied to the membrane. The membranes were incubated at 4 °C on the rocker for 1 hour or overnight (see Table for the dilution factor and incubation time). Before incubation of the membrane with secondary antibodies, membranes were washed with PBS-T once for 15 minutes and three times for 5 minutes to ensure removal of excess of primary antibodies. The secondary antibodies conjugated with AP (see **Table 2.18**) were diluted in PBS-T and membranes were incubated for 1 hour at room temperature on the rocker. The membranes were subjected to further washes with PBS-T for 15 minutes once and three times for 5 minutes. At the final step, the substrate of alkaline phosphate (AP) was applied onto the protein covered the face of the membrane continuously over 1 minute. The membranes were placed in between transparency sheets and were placed in a cassette to protect from light. The membranes were scanned by Chemiluminescence Imaging Systems (F.chemiBis 3.2 M) and quantified using the Image J.

Note that for the florescent secondary antibodies, membranes were washed as described previously and were scanned by Odessy FC imaging system. The values of raw intensity were obtained using Image Studio Lite Ver 5.2.

Table 2.18 List of primary and secondary antibodies used for immunoblotting

Protein	Membrane	Blocking	Primary antibody	Dilution	Incubation time	Secondary antibody
Tubulin	Nitrocellulose	5 % Milk in PBS-T	Rabbit Anti tubulin (Abcam, Cat: ab18251)	1:2000 in PBS-T	Overnight at 4 °C	IRDye 680RD Donkey anti-Rabbit IgG (H + L) (LI-COR, 925-32212)
Acetylated tubulin	Nitrocellulose	5 % Milk in PBS-T	Mouse Anti-AC tubulin (Sigma-Aldrich, Cat: T7451)	1:2000 in PBS-T	Overnight at 4 °C	IRDye800CW Donkey anti-Mouse IgG (H + L) (LI-COR, 925-68073)
ATAT1	PVDF	5 % Milk in PBS-T	Rabbit Anti-C9orf134/TAT antibody (Abcam, Cat: ab58742)	1:500 in PBS-T	Overnight at 4 °C	Goat anti-rabbit IgG (whole molecule) AP (Sigma, A3812)
β-actin	PVDF	5 % Milk in PBS-T	Mouse Anti β-actin (Sigma-Aldrich, Cat: A5316)	1:5000 in PBS-T	Overnight at 4 °C	Goat anti-mouse IgG (whole molecule) AP

						(Sigma, A3562)
LC3	PVDF	5 % Milk in PBS-T	Rabbit Anti-LC3 (MBL, PM036)	1:500 in 5 % milk in PBS-T	Overnight at 4 °C	Goat anti-rabbit IgG (whole molecule) AP (Sigma, A3812)
P62	PVDF	5 % Milk in PBS-T	Mouse Anti-SQSTM1/p62 (Abcam, Cat: ab56416)	1:2000 in PBS-T	Overnight at 4 °C	Goat anti-mouse IgG (whole molecule) AP (Sigma, A3562)
TBK1	PVDF	5 % Milk in PBS-T	Rabbit monoclonal TBK1/NAK (Abcam, Cat: ab40676)	1:5000 in PBS-T	Overnight at 4 °C	Goat anti-rabbit IgG (whole molecule) AP (Sigma, A3812)
V5	PVDF	5 % Milk in PBS-T	Mouse anti-V5 (ThermoFisher Scientific, Cat: R960-25)	1:5000 in PBS-T	Overnight at 4 °C	Goat anti-mouse IgG (whole molecule) AP (Sigma, A3562)
Dynein IC	PVDF	5 % Milk in PBS-T	Mouse anti-Dynein intermediate chain 1 antibody 74.1 (Abcam,	1:1000 in PBS-T	Overnight at 4 °C	Goat anti-mouse IgG (whole molecule) AP

			Cat: ab23905)			(Sigma, A3562)
TDP-43	PVDF	5 % Milk in PBS-T	Rabbit Anti TDP-43 antibody (Protein Tech group, Cat: 10782-2-AP)	1:1500 in PBS-T	Overnight at 4 °C	Goat anti-rabbit IgG (whole molecule) AP (Sigma, A3812)
Cofilin	PVDF	5 % Milk in PBS-T	Rabbit Anti Cofilin (Abcam, Cat: ab11062)	1:10000 in PBS-T	Overnight at 4 °C	Goat anti-rabbit IgG (whole molecule) AP (Sigma, A3812)

Table 2.18 List of primary and secondary antibodies used for immunoblotting. Table shows primary antibodies, type of membrane, type of blocking solution, antibody dilution, incubation time, and secondary antibodies used for immunoblotting.

2.5.6 Immunocytochemistry

2.5.6.1 Formaldehyde fixation

Under the laminar hood, autoclaved 13 mm round glass coverslips (Fisher Scientific, cat: 12392128) were placed in 24-well or 6-well plate. To obtain 60-70 % cell confluency, 25,000 and 40,000 MEFs were seeded in 24-well plate and 6-well plate, respectively. For hippocampal culture, coated coverslips (see section 2.2.3) were placed in 12-well plate. Afterwards, each well containing coated coverslips were washed with 1 mL of distilled water twice followed by washing with maintenance medium. Then, hippocampal neurons

(from two hemispheres) were plated in a 12-well plate. For the culture of MEFs, after 24 hours, and for hippocampal culture, after four days (4 DIV) growth medium was removed. Cells grown on coverslips were washed with pre-warmed DPBS and were fixed with 4 % formaldehyde (ThermoFisher, Cat: 28906) for 7 minutes at room temperature for proximity ligation assay (PLA) and 5 minutes for Immunocytochemistry. After fixation, cells were washed with DPBS three times and kept in the fridge covered with 1 mL DPBS.

2.5.6.2 Immunostaining

The fixed cells were permeabilized with PBS containing 0.2 % Triton X-100 for 2 minutes on the rocker at room temperature to ensure maximum penetration of antibodies into the cells. All the reagents were used at 0.2 mL/13 mm coverslips. Subsequently, the permeabilizing solution was removed, and cells were blocked with 5 % BSA-DPBS for 30 minutes on the rocker to block unspecific binding of antibodies. The staining process was followed by adding the desired concentration of primary antibodies diluted in 1 % BSA-DPBS to the cells (see **Table 2.19**) overnight in a humidified box to avoid drying out (the humidified box was prepared with putting a wet paper towel in a box).

Table 2.19 List of primary antibodies used for immunocytochemistry

Protein	Primary Antibody	Dilution	Incubation time
FUS	Rabbit polyclonal anti-FUS (Protein Tech group, Cat: 11570-1-AP)	1:100	Overnight
TDP-43	Rabbit anti TDP-43 antibody (Protein Tech group, Cat: 10782-2-AP)	1:200	Overnight
P62	Mouse Anti-SQSTM1/p62 (Abcam, Cat: ab56416)	1:200	Overnight

Table 2.19 List of primary antibodies used for immunocytochemistry. Table shows primary antibodies, antibody dilution, and incubation time for immunocytochemistry.

Next day, cells were washed with PBSTS (1 mL PBS containing 0.1 % Tween, and 0.02 % SDS) for 5 minutes on the rocker. The desired concentrations of fluorescent secondary antibody solution were prepared in 1 % BSA in PBSTS (see **Table 2.20**) with the light switched off, and cells were incubated with secondary antibody in a dark box for 1 hour on the rocker at room temperature. Subsequently, cells were washed three times in PBSTS for 5 minutes.

Table 2.20 List of secondary antibodies used for immunocytochemistry

Secondary Antibody	Dilution	Incubation time
Goat Anti-rabbit Alexa fluor 546 conjugate (ThermoFisher Scientific, Cat: A11035)	1:200	1 hour
Goat Anti-Mouse Alexa fluor 488 conjugate (ThermoFisher Scientific, Cat: A11029)	1:200	1 hour

Table 2.20 List of secondary antibodies used for immunocytochemistry. Table shows secondary antibodies, antibody dilution, and incubation time for immunocytochemistry.

To prepare the slide, a droplet of ProLong Gold Antifade Mountant with DAPI, (Invitrogen, Cat: 11549306) was placed on the glass slides. Coverslips were removed with a tip-curved tool (or forceps) from the wells and coverslips were placed on slides with the cell side facing toward mounting media with minimum air bubbles. To seal, the edges of coverslips were sealed with quick-dry nail varnish, and before microscopy, slides were kept at 4 °C.

2.5.7 Proximity ligation assay (PLA)

To perform PLA, coverslips with fixed cells on top were stuck to glass slides using quick-dry nail varnish. Subsequently, using Immedge pen (hydrophobic pen), the reaction area was delimited. The cells were permeabilized with 0.2 % Triton X-100 in PBS for 5 minutes on the rocker. Then, 5 % BSA-DPBS solution was prepared and one drop (40 µL) of blocking solution was added to the top of each coverslip and incubated for 1 hour in humidity box at 37 °C in the 5 % CO_2 incubator. Afterwards, blocking solution was removed and coverslips were incubated with desired concentration of primary antibodies overnight at 4 °C (see **Table 2.21**).

Table 2.21 List of primary antibodies used for proximity ligation assay

Protein	Primary Antibody	Dilution	Incubation time
Dynein IC	Mouse Anti-Dynein intermediate chain 1 antibody [74.1] (Abcam, Cat: ab23905)	1:200	Overnight
Golgin160	Rabbit Anti GOLGA3 antibody (Novus, Cat: NBP1-91952)	1:200	Overnight
ATAT1	Rabbit Anti-C9orf134/TAT (ATAT1) antibody (Abcam, Cat: ab58742)	1:200	Overnight

Table 2.21 List of primary antibodies used for proximity ligation assay. Table shows primary antibodies, antibody dilution, and incubation time for proximity ligation assay.

Next day, the primary antibodies were removed, and coverslips were washed with 1X wash buffer A twice for 5 minutes on the rocker. Subsequently, plus and minus PLA probes were diluted in 1 % BSA-DPBS and cells were incubated with probes for 1 hour at 37 °C in

humidity box in the 5 % CO_2 incubator. At the next step, 5X ligation buffer was diluted at a 1:5 dilution in high purity water and Ligase was diluted at a 1:40 dilution in 1X ligation buffer. Wash buffer was taped off and the ligation solution was added and incubated for 1 hour at 37 °C in the 5 % CO_2 incubator. For the amplification step, cells were washed with 1X wash buffer A two times for 5 minutes on the rocker. Then, 5X amplification buffer was diluted at a 1:5 in high purity water and polymerase was added in the dark to diluted amplification buffer at a 1:80 dilution. Wash buffer was removed and amplification solution was applied and incubated for 100 minutes at 37 °C in the 5 % CO_2 incubator. For the final washes, cells were washed in 1X wash buffer B twice for 10 minutes and in 0.01X wash buffer B for 1 min at room temperature. A droplet of Duolink PLA mounting medium to mount another coverslip on the cells and then the coverslips were sealed with quick-dry nail varnish. All slides were kept in the freezer for up to 6 months.

2.5.8 Fluorescence *in situ* hybridization

To perform *in situ* hybridization, fixed cells were permeabilized with 0.1 % Triton X-100 in 2X saline sodium citrate (SSC) for 15 minutes at room temperature on the rocker (25 OSC/min). All the reagents were used at 0.2 mL/13 mm coverslips. Afterwards, cells were washed for 5 minutes with 1 M Tris, pH 8 at room temperature and then cells were blocked with blocking solution containing 0.0005 % BSA and 10 mg/mL yeast RNA diluted in 2X SSC at 37 °C in the 5 % CO_2 incubator. Subsequently, cells were washed with 1 M Tris, pH 8 for 5 minutes. For hybridization step, cells were incubated with hybridization buffer containing 1.3 ng Cy3 labelled oligo (dT) probe, 0.005 % BSA, 1 mg/mL yeast RNA, 10 % dextran sulfate, and 25 % formamide diluted in 2X SSC for 1 hour in a humidified box at 37 °C in the 5 % CO_2 incubator. At the final step, cells were washed with 4X SSC twice for 5 minutes and one time with 2X SSC for 5 minutes and mounted with ProLong Gold Antifade Mountant with DAPI. The coverslips were sealed with quick-dry nail varnish, and before microscopy, slides were kept at 4 °C.

2.6 Cell assays

2.6.1 Serum-deprivation starvation

To activate the autophagy, for each genotype (wild-type and *Loa* homozygous), 1 X 10^6 MEFs were seeded on 100 mm dishes and incubated overnight. Subsequently, the complete medium was removed and washed with DPBS twice. Then, MEFs were incubated with serum-free medium for 2 hours. After the starvation, the cells were lysed as described in section 2.5.1.1.

2.6.2 Treating MEFs with Ciliobrevin D, BX795, MG132 and Tubastatin

For each genotype (wild-type and Loa homozygous) 40,000 MEFs for immunostaining on autoclaved coverslips on 6-well plates and 300,000 MEFs for immunoblotting were seeded on 6-well plates (VWR, Cat: 734-1599) and incubated overnight. Then, the cells were incubated with complete growth medium (see **Table 2.22**) containing the required drug (see Table 2. for drug concentration and incubation time) or equivalent volume of the vehicle control. After the treatment, the cells were lysed as described in section 2.5.1.1 or fixed with 4 % formaldehyde.

Table 2.22 List of drugs used in this study

Drug	Concentration	Vehicle	Incubation time

	used	control	
Ciliobrevin D (Merk Millipore, Cat: 250401)	50, 60 and 100 µM	DMSO	6 hours
BX795 (Invivogen, Cat: tlrl-bx7)	5 and 10 µM	DMSO	6 hours
MG132 (Sigma-Aldrich, Cat: C2211)	10 µM	DMSO	6 hours
Tubastatin (Sigma-Aldrich, Cat: SML0065)	20 µM	DMSO	4 hours

Table 2.22 List of drugs. Table represents the working concentration, vehicle control and incubation time for drugs used in this study.

2.6.3 Arsenite treatment and recovery after washout

For each genotype (wild-type and Loa homozygous) 40,000 MEFs for immunostaining were seeded on autoclaved coverslips on 6 well plates and incubated overnight. Then, the cells were incubated with complete growth medium (see **Table 2.6**) containing the 1 mM sodium arsenite (Sigma-Aldrich, Cat: S7400) for 1 hour. After the treatment, the cells were washed with DPBS twice and recovered with complete growth medium for the specified time points and then fixed with 4 % formaldehyde.

2.7 Microscopy

2.7.1 Imaging and quantification

Images were collected using 63 X oil objective lenses on a Leica TSC SP8 confocal microscope (Leica Microsystems) equipped with Las X software (Leica) for acquisition. A Z-stack of 11 slices at a step size of 0.2 µm was used. The stack was max projected and used for further quantification as described in Section 2.7.1.1, 2.7.1.2, and 2.7.1.3.

2.7.1.1 Quantification of p62 puncta

A minimum of 70-100 cells was counted per treatments and per genotype. The green channel of RGB images was extracted and fixed-level binary thresholding was applied to all images. The p62 puncta were analysed for number and for size (ranging from 0.2 to 15 μm^2) using the "Analyse Particles" function of the Image J. Then, the number of p62 granules in the cell was normalized to the cell area.

2.7.1.2 Quantification of stress granules

Stress granules were quantified using Image J, as previously published (Khalfallah et al., 2018). To assess SG kinetics at different time points, SGs were identified by oligo (dT), and cells were scored as positive when they had at least two foci. A minimum of 70-100 cells was counted per time point, per condition per experiment. For SG number and size, the automatic recognition of Image J (function: Analyse particles) was used with setting the parameters for the size of SGs (ranging from 0.2 to 15 μm^2).

2.7.1.3 Quantification of localization of TDP-43

To measure fluorescence intensity of TDP-43 in Image J (All images were acquired with the same settings), the area of the cell and nucleus were selected using a drawing tool and using the set “management function”, “area integrated intensity” and “mean grey value” were measured. These values also were measured for the background. Subsequently, the corrected total cell fluorescence (CTCF) was calculated using the following formula:

CTCF= (Raw intensity – (Area of selected cell X Average of raw intensity of background readings))/Area of selected cells

At the final step, to measure the intensity of cytoplasmic TDP-43, the CTCF of nucleus was subtracted from CTCF of whole cells.

2.8 Statistical analysis

Statistical analysis was performed using GraphPad Prism. First, the outliers were removed from data obtained from more than three repeats, using ROUT method with the Q value set at the 1 %. Then, data was tested with the Shapiro-Wilk test to determine if the values were normally distributed. Then all data were tested using unpaired t-test (One sample t-test). For data with more than two levels within a single independent variable, a one way ANOVA with Tukey’s multiple comparison test was performed. The two-way ANOVA was performed where there were two independent variables. For the analysis of data with multiple time points across two genotypes, multiple t-tests were performed and Holm-Sidak correction for multiple comparisons was used to adjust the P values to mitigate type 1 errors. For all statistical tests a confidence level of 95 % was used, therefore p values of < 0.05 were deemed significant.

Chapter 3: Investigation of regulatory role of dynein in decreased level of microtubule acetylation in Loa^{Hom} MEFs

3.1 Introduction

SMA-LED is a congenital or early onset MND, which primarily targets the proximal muscles of the lower limbs. The aetiology is unknown but autosomal dominant missense mutations in *DYNC1H1* and *BICD2* are known genetic causes of SMA-LED (Harms et al., 2012; Neveling et al., 2013; Oates et al., 2013; Scoto et al., 2015), which are implicated in the pathogenesis of SMA-LED.

Dynein is a retrograde motor protein, which is involved in transport of a verity of cargoes including endosomes, organelles, cytoskeletal filaments, and autophagosomes toward the minus-end of MT. Moreover, dynein serves a vital function in axonal transport to maintain cellular homeostasis and protein balance (Schiavo et al., 2013). Importantly, PTMs of MTs have been reported to modulate axonal transport (Song & Brady, 2015). Particularly, MT acetylation contributing to MT stability modulates intracellular transport (Li & Yang, 2015). Moreover, it has been shown that increased level of MT acetylation enhances recruitments of dynein and kinesin onto the MT and their mobility (Dompierre et al., 2007). HDAC6 and α-TAT1 have been identified as the main regulators of α-tubulin deacetylation and acetylation, respectively (Sadoul & Khochbin, 2016). Moreover, an *in vitro* experiment suggested that α-TAT1 enters lumen of MTs through extremities to promote the acetylation of α-tubulin (Howes et al., 2014). Additionally, the existence of α-TAT1 at the cytosolic side of motile vesicles has been reported (Even et al., 2019). However, recruitments of α-TAT1 on MTs and potential role of motor proteins in recruitments of α-TAT1 remains to be elucidated.

Furthermore, dynein contributes to the integrity of Golgi apparatus and inhibition of dynein function disperses Golgi ribbon and results in fragmentation of Golgi (Palmer et al., 2009; Yadav & Linstedt, 2011). In addition, dynein through its IC subunit interacts with Golgin160, which mediates recruitment of dynein on to the Golgi (Yadav et al., 2012). Indeed, delayed reassembly of Golgi complex following nocodazole washout has been observed in the *Loa* mouse model of SMA-LED and also in patient fibroblasts harbouring the SMA-LED *DYNC1H1* mutation (Fiorillo et al., 2014; Hafezparast et al., 2003).

A research work conducted in Hafezparast lab showed the Golgi fragmentation in patient fibroblasts harbouring p.R399G DYNC1H1 substitution which was compounded with the decreased level of acetylation. Moreover, reduction in level of acetylation was reported in $D338N^{Het}$ fibroblasts but Golgi fragmentation was not found. These data suggest that decreased level of MT acetylation may be a common feature of SMA-LED and also fragmented phenotype of Golgi in one of disease-associated mutation may show the importance of Golgi pathology in SMA-LED.

The work presented here aimed to establish how dynein can contribute to the MT acetylation and to investigate potential consequences of dynein mutation on acetylation of MT. Therefore, levels of acetylated tubulin were measured and interaction between dynein and HDAC6 was investigated using PLA. Furthermore, PLA was performed to check the interaction of dynein with α-TAT1. IP was conducted for further investigation of dynein and α-TAT1 interaction. It was hypothesised that dynein mutation causes changes in HDAC6 or α-TAT1 function, which consequently impacts the levels of acetylation in MTs. Moreover, it was postulated that dynein mutation affects the interaction of dynein with Golgin160 resulting in fragmented Golgi phenotype.

3.2 Results

3.2.1 Altered level of α-tubulin acetylation in Loa^{Hom} MEFs and D338N^{Het} human fibroblasts

Previously, in Hafezparast lab, decreased level of acetylated α-tubulin was reported in Loa^{Hom} MEFs, D338N^{Het} and R399G^{Hom} human fibroblasts. In those experiments, to estimate the level of acetylated (AC) α-tubulin, the values of total tubulin and AC α-tubulin were obtained from two western blots. Consequently, the values of normalised AC α-tubulin were compared to the value of normalised total α-tubulin, which might have caused the variations. Here, these experiments were conducted to determine the level of AC α-tubulin using an anti-acetylated tubulin antibody and a fluorescent secondary antibody, which enabled us to quantify the acetylation level by normalising the western blot signal of AC α-tubulin to the amount of total α-tubulin on the same lane (**Figure 3.1 A**).

Moreover, the analysis of results of western blot confirmed the previous results showing the significant reduction in level of AC α-tubulin in D338N^{Het} human fibroblasts (**Figure 3.1 B, lane 2**) as shown by a one sample t-test ($P < 0.0008$, N = 6) (**Figure 3.1 C**). However, statistical analysis demonstrated no changes in the level of AC α-tubulin in R399G^{Hom} human fibroblasts compared to the wild-type human fibroblasts, which contradicted the previous result ($P = 0.3833$) (**Figure 3.1 B, lane 3**). Therefore, increasing the accuracy of western blot measurements by utilising fluorescent antibodies indicated that mutations in the heavy chain of *DYNC1H1* affect the level AC α-tubulin differentially.

Furthermore, to confirm the role of dynein in the regulation of the level of AC α-tubulin, the wild-type human fibroblasts were treated with Ciliobrevin D, a dynein ATPase inhibitor (CilD, 50 μM) for 2 and 4 hours (**Figure 3.1 D**). The analysis of levels of AC α-tubulin demonstrated a significant reduction in the level of AC α-tubulin in fibroblasts treated with CilD ($P = 0.0014$) (**Figure 3.1 E**). Tukey's multiple comparison test showed a significant

reduction in the level of AC α-tubulin in wild-type fibroblasts treated with CilD for 2 hours (*P* = 0.0123), a more significant reduction in the level of AC α-tubulin in fibroblasts treated for 4 hours (*P* = 0.0013).

Altogether, this set of data showed a significant reduction in the level of AC α-tubulin in Loa^{Hom} MEFs and $D338N^{Het}$ human fibroblasts suggesting a dynein-dependent regulation of α-tubulin acetylation. The role of dynein in the regulation of MT acetylation was also confirmed through inhibition of dynein in wild-type human fibroblasts, which demonstrated a decreased level of α-tubulin acetylation. However, $R399G^{Hom}$ human fibroblasts showed no alteration in the level of AC α-tubulin.

Figure 3.1

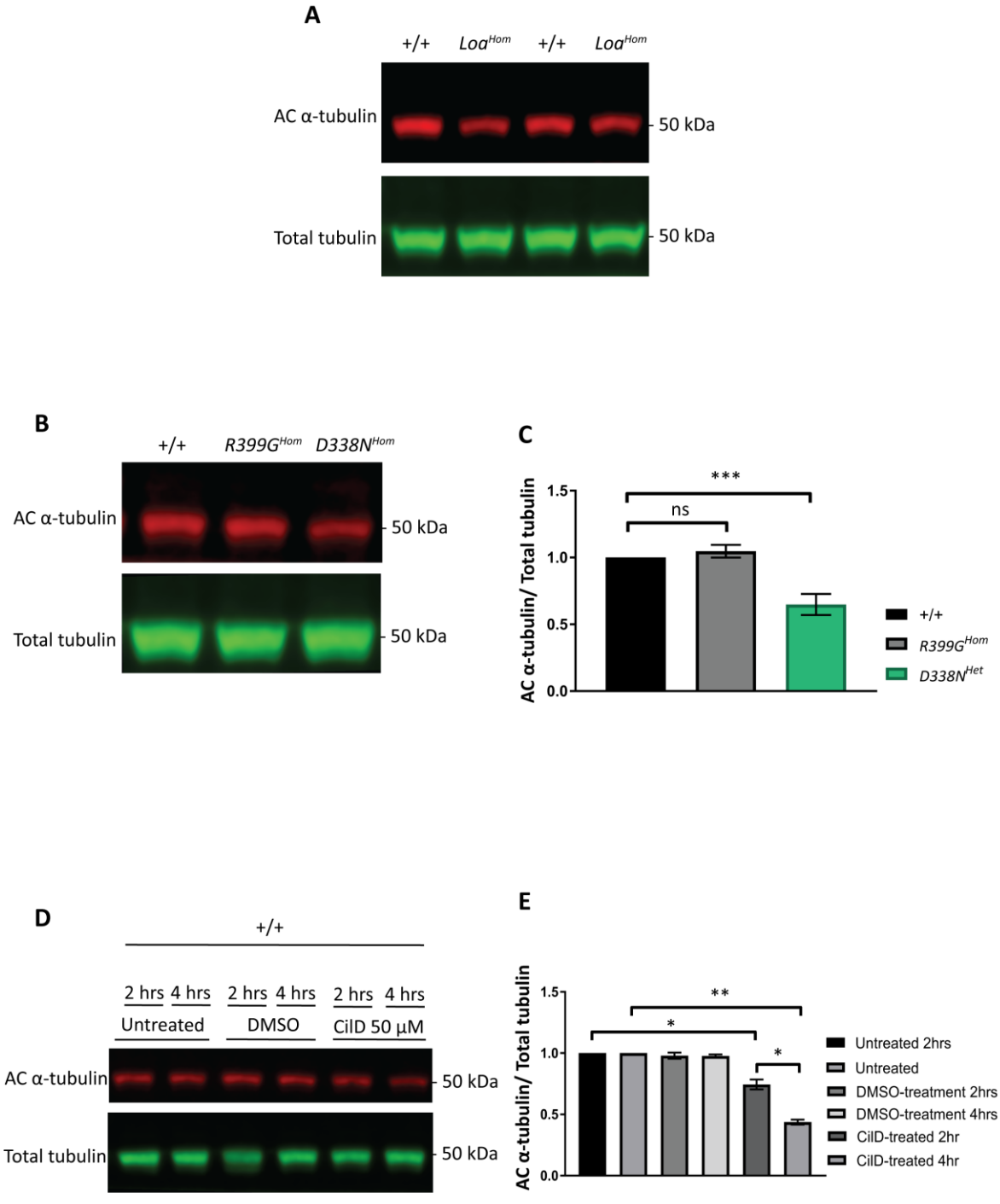
A
+/+
Loa^Hom
+/+
Loa^Hom
AC α-tubulin
50 kDa
Total tubulin
50 kDa
B
+/+
R399G^Hom
D338N^Hom
AC α-tubulin
50 kDa
Total tubulin
50 kDa
C
AC α-tubulin/ Total tubulin
1.5
1.0
0.5
0.0
***
ns
+/+
R399G^Hom
D338N^Het
D
+/+
2 hrs
4 hrs
2 hrs
4 hrs
2 hrs
4 hrs
Untreated
DMSO
CilD 50 µM
AC α-tubulin
50 kDa
Total tubulin
50 kDa
E
AC α-tubulin/ Total tubulin
1.5
1.0
0.5
0.0
**
*
*
Untreated 2hrs
Untreated
DMSO-treatment 2hrs
DMSO-treatment 4hrs
CilD-treated 2hr
CilD-treated 4hr

Figure 3.1 Altered level of α- tubulin acetylation in Loa^{Hom} **MEFs and** $D338N^{Het}$ **fibroblasts**. (**A**) Western blot analysis of cell lysate of wild-type and Loa^{Hom} MEFs using anti acetylated α-tubulin (AC α-tubulin) and anti α-tubulin antibodies. α-tubulin was used as a loading control. (**B**) Level of AC α- tubulin in wild-type, $R339G^{Hom}$ and $D338N^{Het}$ fibroblasts. (**C**) Data is presented as the mean ± SEM; where N = 3 and N = 6, technical repeats for $R339G^{Hom}$ and $D338N^{Het}$ human fibroblasts respectively. Statistic was performed with a one sample t-test, $R339G^{Hom}$ human fibroblasts (*P* = 0.3833) and $D338N^{Het}$ human fibroblasts (*** *P* = 0.0008). (**D**) Level of AC α- tubulin in wild-type fibroblasts untreated or treated with dynein inhibitor (CilD, 50 μM) for 2 and 4 hours. (**E**) Data is presented as the mean ± SEM; where N = 3 biological repeats. A one way ANOVA showed a significant difference in level of AC α- tubulin between untreated and treated wild-type fibroblasts (** *P* = 0.0014). Tukey's multiple comparison test showed a significant reduction in this measurement in wild-type MEFs treated with CilD for 2 hours (* *P* = 0.0123) and 4 hours (** *P* = 0.0013) compared to untreated MEFs.

3.2.2 Proximity ligation assay reveals a novel interaction between dynein intermediate chain and GFP-α-ATAT1 in wild-type MEFs

Alpha-TAT1 and HDAC6 regulate MT acetylation and deacetylation, respectively. The acetylation of lysine 40 (K40) of α-tubulin is catalysed by α-TAT1, whereas HDAC6 removes the acetyl group from tubulin.

Given that level of acetylation is decreased in Loa^{Hom} MEFs and $D338N^{Het}$ human fibroblasts and based on the regulatory role of α-TAT1 on MT dynamics, the aim was to determine how *DYNC1H1* mutations alter the level of AC α-tubulin and whether DIC is associated with recruitment of α-TAT1 on MT. To test these, wild-type MEFs were transfected with GFP-α-TAT1 (Isoform 1) and then by performing proximity ligation assay (PLA) between DIC and GFP, the interaction between DIC and GFP-α-TAT1 (Iso1) was checked. To include all negative controls to detect potential unspecific signal, the assay was performed by removing one of the primary antibodies. Negative controls of PLA are presented with DIC antibody only, α-TAT1 antibody only or without primary antibodies. Thus, one of the secondary probes will have no primary antibody to link, and subsequently, no PLA signal will be generated. The cells transfected with empty plasmid were also processed in parallel with other negative controls (**Figure 3.2**). Robust PLA signals were observed in cells transfected with GFP-α-TAT1 and treated with both primary antibodies, indicating close proximity between DIC and GFP-α-TAT, whereas, the negative controls demonstrated very few PLA puncta.

Figure 3.2

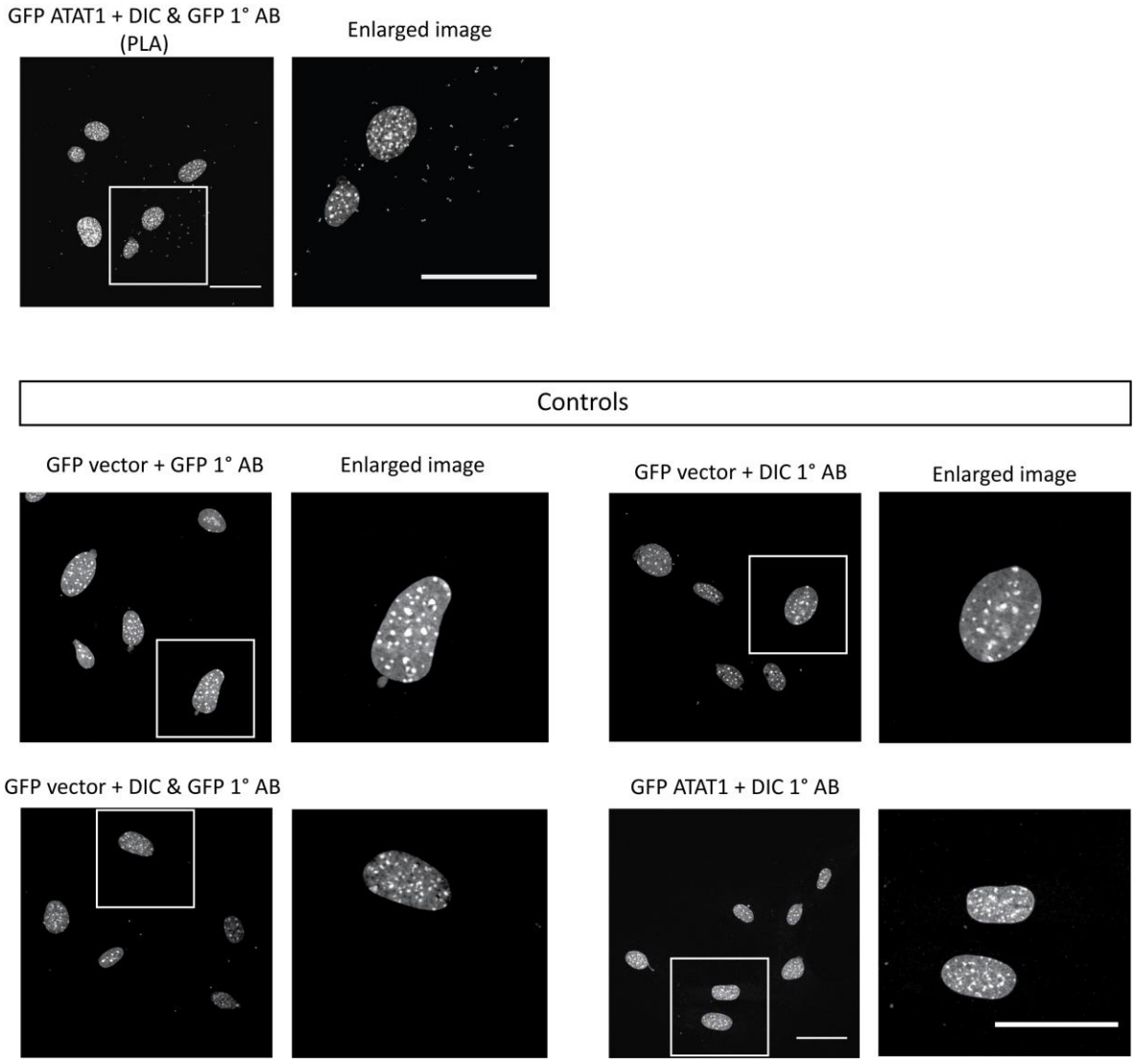
GFP ATAT1 + DIC & GFP 1° AB (PLA)
Enlarged image
Controls
GFP vector + GFP 1° AB
Enlarged image
GFP vector + DIC 1° AB
Enlarged image
GFP vector + DIC & GFP 1° AB
GFP ATAT1 + DIC 1° AB

Figure 3.2 Interaction between dynein intermediate chain and GFP-α-TAT1. Wild-type MEFs were transfected with GFP-α-TAT1. PLA was performed using the anti-DIC and anti-GFP antibodies. The nuclei were stained with DAPI. The representative images of PLA are shown as maximum projections of Z-stacks of confocal images and white dots represent PLA signals. Negative controls of PLA are presented with DIC antibody only, α-TAT1 antibody only or without primary antibodies. The empty GFP plasmid was also used as negative control. The enlarged images are from the boxed areas of the merged micrographs for better view of PLA signals. Scale bar, 50 μm.

3.2.3 Interaction of α-TAT1 and DIC in MEFs and human fibroblasts

The above data showed an interaction between DIC and GFP- α-TAT1 in wild-type MEFs transfected with GFP- α-TAT1. To confirm a protein-protein interaction between the endogenous DIC and α-TAT1 and also examine this interaction in mutant dynein MEFs, PLA was carried out on both wild-type and Loa^{Hom} MEFs. Distribution of the PLA puncta was throughout the cell (**Figure 3.3 B**).

Subsequently, to examine the interaction between the DIC and α-TAT1 in $D338N^{Het}$ fibroblasts, PLA was performed in both wild-type and $D338N^{Het}$ fibroblasts (**Figure 3.3 C**). As expected, very few dots were produced in control experiments using one of the primary antibodies or none of primary antibodies.

Collectively, these results for the first time showed that there is an interaction between DIC and α-TAT1 in MEFs and human fibroblasts.

Figure 3.3

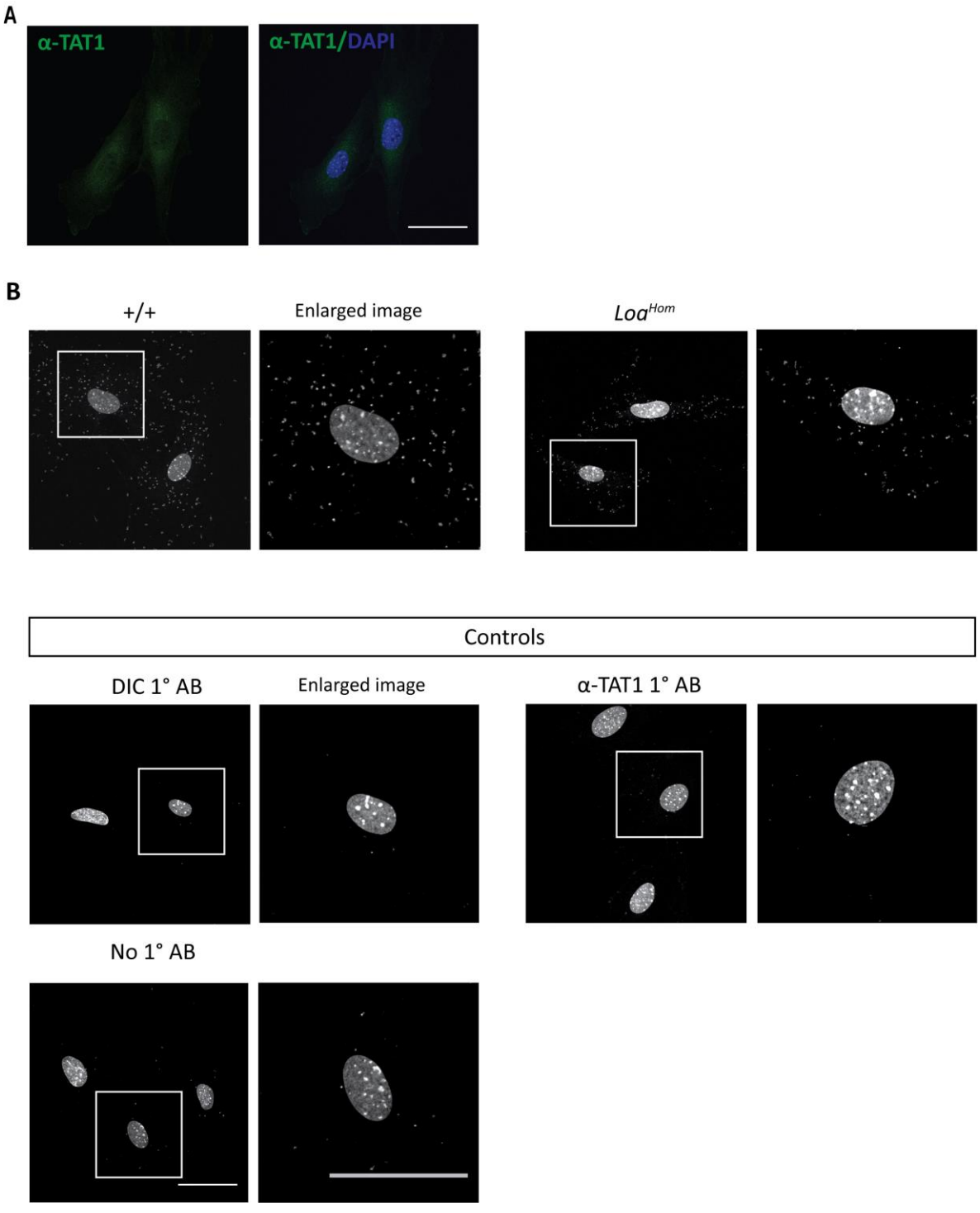
A
α-TAT1
α-TAT1/DAPI
B
+/+
Enlarged image
Loa^Hom
Controls
DIC 1° AB
Enlarged image
α-TAT1 1° AB
No 1° AB

Figure 3.3 continued

C

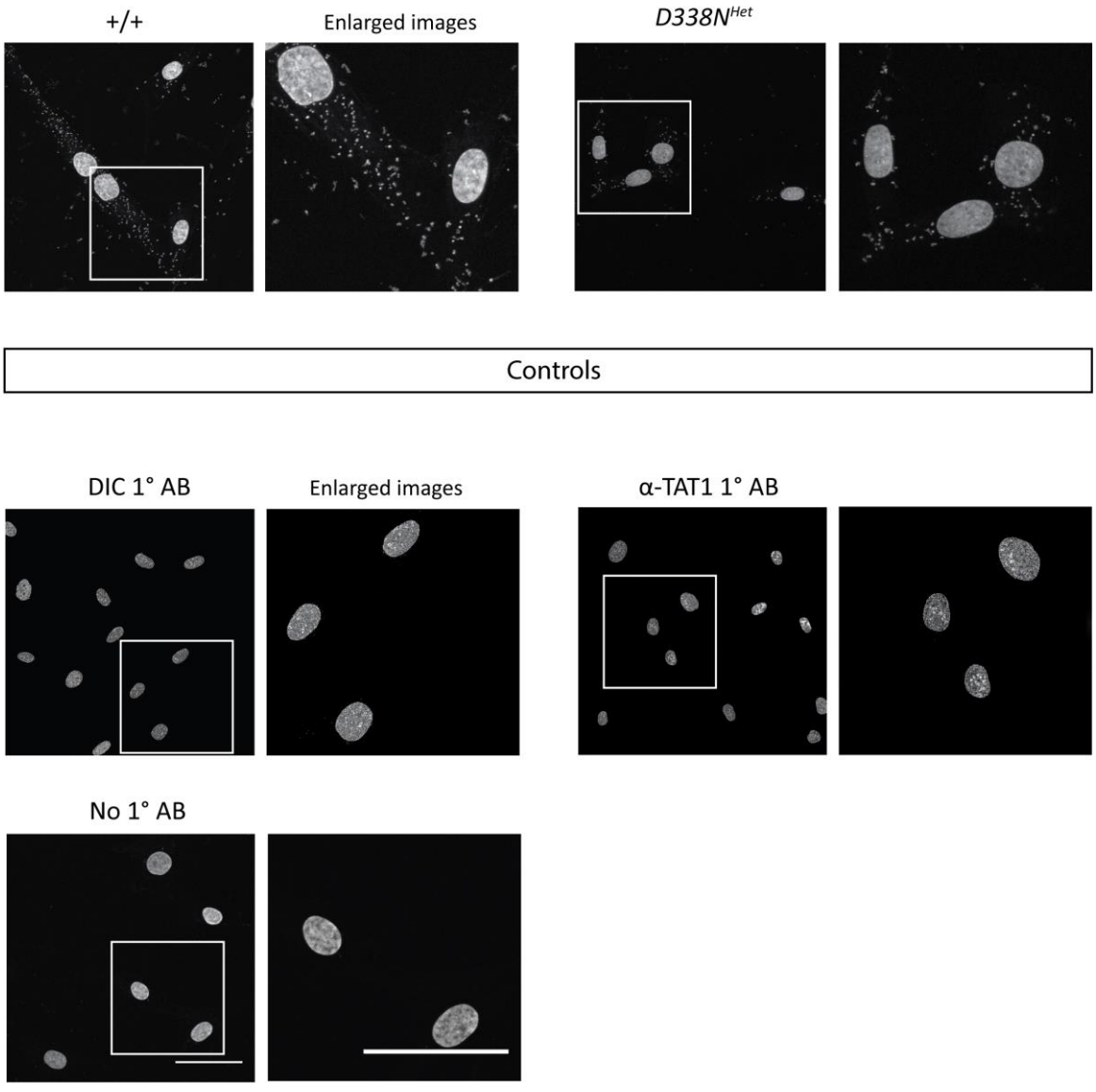

Figure 3.3 Decreased interaction between DIC and α-TAT1 in mutant fibroblasts. (**A**) Wild-type MEFs were immunostained using anti-α-TAT1 antibody. The nuclei were stained with DAPI. Scale bar, 50 μm. **(B**) Wild-type and Loa^{Hom} MEFs were fixed, and PLA was performed using mouse anti-DIC and rabbit anti-α-TAT1 antibodies. The nuclei were stained with DAPI. The representative images of PLA are shown as maximum projections of Z-stacks of confocal images and white dots represent PLA signal. Negative controls of PLA are presented with DIC antibody only, α-TAT1 antibody only or without primary antibodies. The enlarged images are from the boxed areas of the merged micrographs for better view of PLA signals. Scale bar, 50 μm. (**C**) Wild-type and $D338N^{Het}$ fibroblasts were fixed, and PLA was performed using mouse anti-DIC and rabbit anti-α-TAT1 antibodies. The nuclei were stained with DAPI. Representative images of PLA are shown as maximum projections of Z-stacks of confocal images. Negative controls of PLA are presented with DIC antibody only, α-TAT1 antibody only or without primary antibodies. The enlarged images are shown for better view of PLA signals. Scale bar, 50 μm.

3.2.4 Short interfering RNA against α-TAT1 attenuates interaction of DIC and α-TAT1 in wild-type MEFs

To reaffirm the α-TAT1-DIC interaction, short interfering RNA (siRNA) was used against α-TAT1 to knockdown α-TAT1 in wild-type MEFs. Wild-type MEFs were transfected either with a pool of α-TAT1-siRNA or scrambled RNA (ScrRNA) and incubated for 48 hours, followed by PLA analysis. The PLA signals showed that knockdown of α-TAT1 caused reduction in PLA dots in cells transfected with α-TAT1-siRNA compared to the cells transfected with ScrRNA and non-transfected cells (**Figure 3.4 A**).

Moreover, to confirm the knockdown of α-TAT1 by siRNA, western blot analysis with anti-α-TAT1 and β-actin antibodies was carried out. These data showed that treatment of wild-type fibroblasts with α-TAT1 siRNA resulted in a decrease of α-TAT1 (lane 3) compared to the MEFs transfected with ScrRNA and non-transfected MEFs (**Figure 3.4 B**).

Figure 3.4

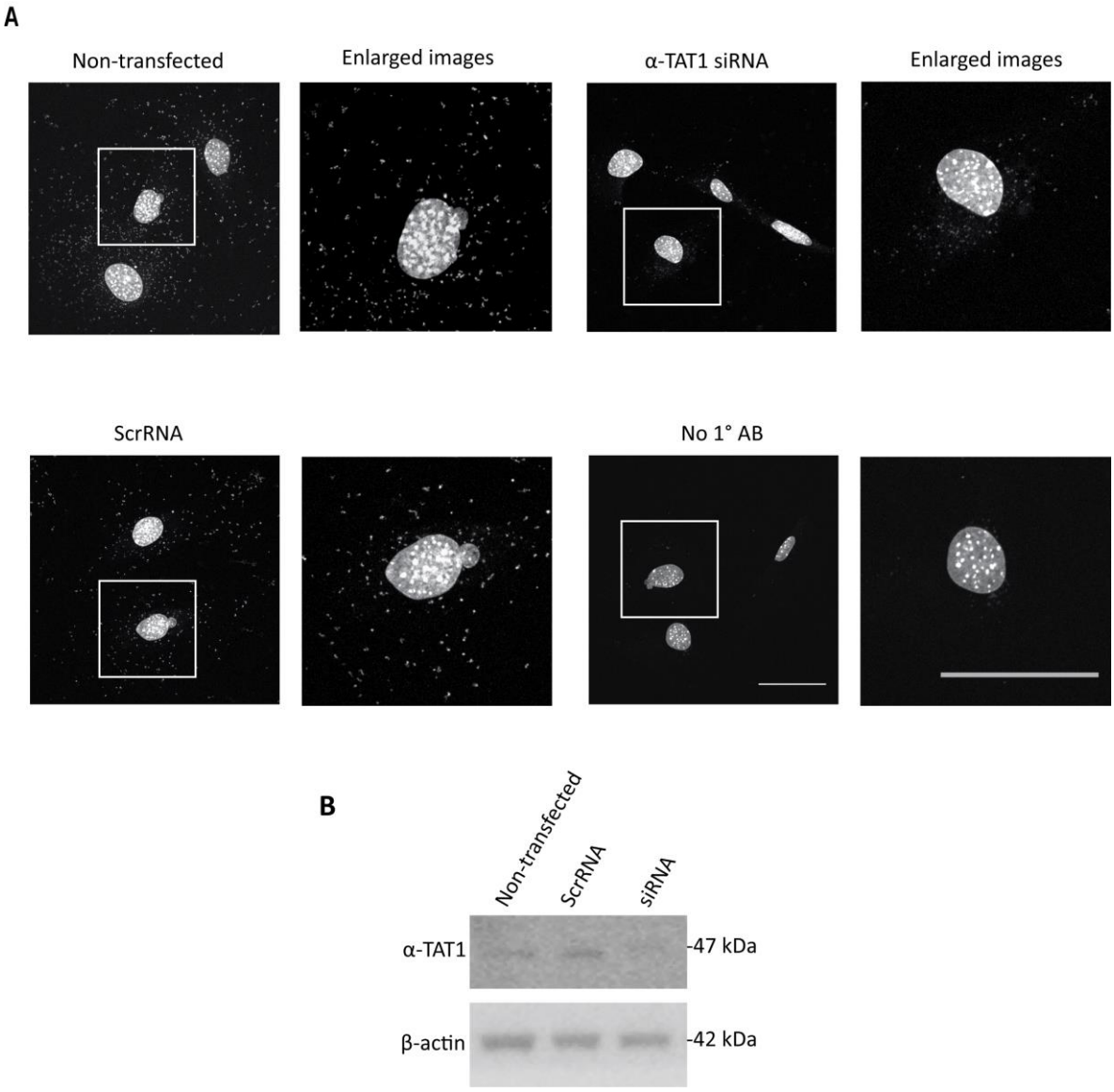
A
Non-transfected
Enlarged images
α-TAT1 siRNA
Enlarged images
ScrRNA
No 1° AB
B
Non-transfected
ScrRNA
siRNA
α-TAT1
-47 kDa
β-actin
-42 kDa

Figure 3.4 Knockdown of α-TAT1 attenuated the PLA signal. (**A**) Wild-type MEFs were knocked down by small-interfering RNA (siRNA) targeting α-TAT1. Non-targeting siRNA (ScrRNA) and non-transfected cells were used as a knockdown control. PLA was performed using mouse anti-DIC and rabbit anti-α-TAT1 antibodies. The nuclei were stained with DAPI. The representative images are shown as maximum projections of Z-stacks of confocal images and white dots represent PLA signal. Negative control of PLA is presented without primary antibodies. The enlarged images are from the boxed areas of the merged micrographs for the better view of PLA signals. Scale bar, 50 μm. (**B**) Western blot analysis shows reduction of α-TAT1 level using siRNA-α-TAT1. β-actin was used as a loading control.

3.6 The PLA demonstrates an interaction between α-TAT1 and DIC in neuronal cells

After showing the interaction of α-TAT1 with DIC in MEFs and human fibroblasts, it was sought to explore the presence of this interaction in MN cultures. The primary MNs on DIV7 were fixed, and then *in situ* PLA was conducted using the primary antibody of α-TAT1 and DIC to visualise the interaction. PLA signals were detected in wild-type MNs, confirming the presence of α-TAT1-DIC interaction in neuronal cells (**Figure 3.5**). Furthermore, the PLA signal was located mostly in the soma rather than in neurites and the negative controls showed no PLA signals.

Figure 3.5

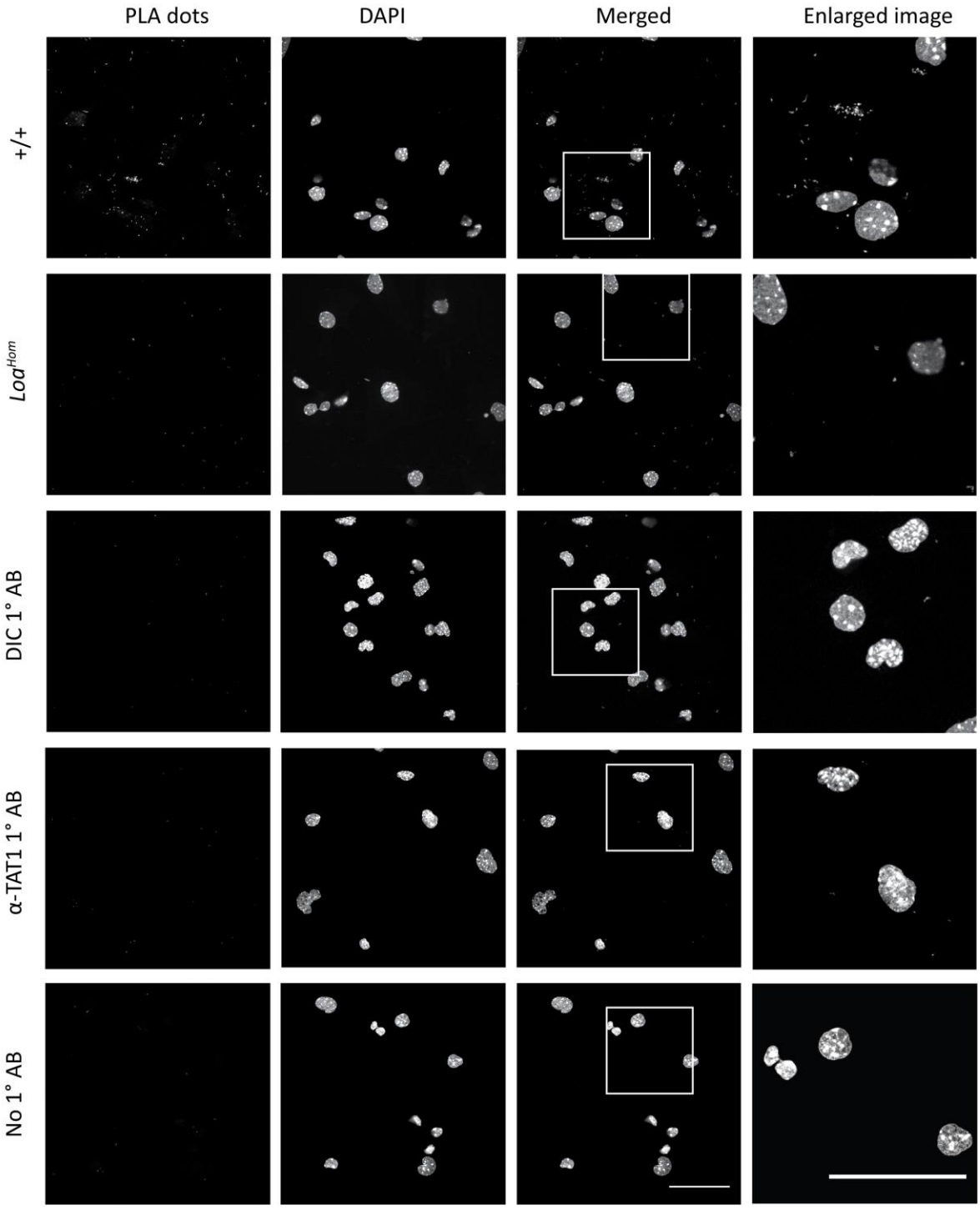
PLA dots
DAPI
Merged
Enlarged image
+/+
Loa^Hom
DIC 1° AB
α-TAT1 1° AB
No 1° AB

Figure 3.5 Altered interaction between DIC and α-TAT1 in Loa^{Hom} motor neuron culture. Mouse MNs (DIV7) were fixed, and PLA was performed using mouse anti-DIC and rabbit anti-α-TAT1 antibodies. The nuclei stained with DAPI. The representative images are shown as maximum projections of Z-stacks of confocal images and white dots represent PLA signal. Negative controls of PLA are presented with DIC antibody only, α-TAT1 antibody only or without primary antibodies. The enlarged images are from the boxed areas of the merged micrographs for better view of PLA signals. Scale bar, 50 μm.

3.2.6 The α-TAT1 interacts with dynein intermediate chain

Since the earlier results indicated the proximity of DIC and α-TAT1 by PLA, it was sought to evaluate the general interaction biochemically as well. First, the interaction between endogenous DIC and α-TAT1 was assessed in HEK293 cells by co-immunoprecipitation, using DIC antibody to pull down α-TAT1. Western blot was performed using DIC, α-TAT1 and dynein light chain (DLC) antibodies. The DLC was used as a control for the co-immunoprecipitation. The immunoblotting analysis showed that DLC was pulled down, indicating that the co-immunoprecipitation assay worked while the α-TAT1 was not pulled down. This apparent lack of interaction between endogenous DIC and α-TAT1 in the HEK293 cells might be due to a low abundance and transient nature of this interaction (**Figure 3.6 A**).

Then, the interaction between exogenously expressed α-TAT1 with DIC was examined. NIH3T3 cells were transfected with V5 tagged α-TAT1 plasmid. After 24 hours, transfected cells were lysed, and the V5-α-TAT1 was pulled down with the antibody against V5. Western blot was performed using DIC and V5 antibodies. The western blot analysis showed that immunoprecipitates from cells transfected with V5 tagged α-TAT1 include DIC and α-TAT1. Thus, the result of the co-immunoprecipitation assay demonstrated that endogenous DIC interacts with exogenous α-TAT1, confirming α-TAT1-DIC interaction and suggesting a role for dynein in the recruitment of α-TAT1 onto the MT surface (**Figure 3.6 B**). Moreover, NIH3T3 cells were co-transfected with V5 tagged α-TAT1 plasmid and siRNA to α-TAT1. Then, V5-α-TAT1 was pulled down with the V5 antibody. After performing western blot, the immunoprecipitants of DIC was not detected, suggesting that the knockdown of α-TAT1 attenuated the interaction between DIC and α-TAT1. Combined, these results confirmed the result of PLA, showing an interaction between DIC and α-TAT1 (**Figure 3.6 C**).

Figure 3.6

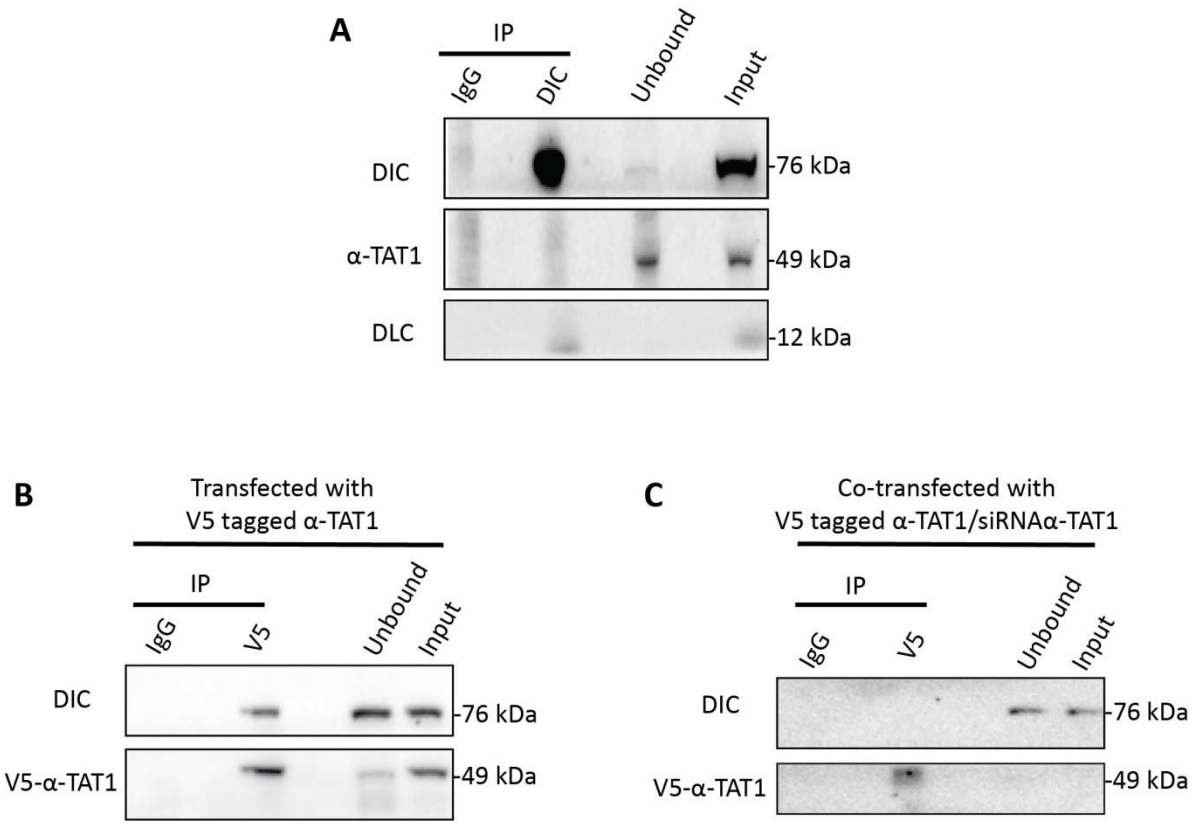

Figure 3.6 Immunoprecipitation of DIC and V5-tagged α-TAT1. (**A**) The HEK293 cells were lysed and protein extracted and immunoprecipitated with beads coated with dynein intermediate chain (DIC) antibody. Immunoprecipitates were separated on SDS-PAGE, and probed with anti-DIC (top panel) or anti- α-TAT1 (middle panel) and anti-dynein light chain (DLC). (**B**) Co-immunoprecipitation analysis of interaction between endogenous DIC and V5-α-TAT. NIH3T3 cells were transfected with V5-tagged α-TAT1 as indicated. Protein extracted and immunoprecipitated with beads coated with V5 antibody. Immunoprecipitates were separated on SDS-PAGE, and probed with anti-DIC (top panel) or anti-V5 (bottom panel). (**C**) The NIH3T3 cells were transfected with V5-tagged α-TAT1 and siRNA-α-TAT1 as indicated. The immunoprecipitation and immunoblotting were carried out as described above. In all experiments, rabbit immunoglobulin G (IgG) was used as negative control.

3.2.7 Levels of α-TAT1 are not changed in fibroblasts with dynein mutation

Since there was a decreased interaction between DIC and α-TAT1 in Loa^{Hom} MEFs and D338N^{Het} human fibroblasts, it was asked whether dynein mutations would affect the expression of α-TAT1 in the mutant fibroblasts. The levels of α-TAT1 were examined in protein extracts obtained from primary wild-type MEFs, Loa^{Hom} MEFs, wild-type and D338N^{Het} human fibroblasts by western blotting. For the western blot analyses, an antibody was used against α-TAT1, which detected three isoforms of α-TAT1 and antibody against β-actin as a loading control (**Figure 3.7 A**). Statistical analysis by unpaired t-test demonstrated no significant difference in the levels of α-TAT1 in Loa^{Hom} MEFs compared to wild-type MEFs counterparts (**Figure 3.7 B)**.

Furthermore, the western blot analysis of protein contents of D338N^{Het} fibroblasts and wild-type human fibroblasts showed a similar level of α-TAT1 protein (**Figure 3.7 C**) and no significant difference was seen in the levels of α-TAT1 using the unpaired t-test across the genotypes (**Figure 3.7 D**).

In these experiments, western blot analysis revealed that *DYNC1H1* mutations result in the reduction of MT acetylation without affecting the expression levels of α-TAT1. Consequently, it confirms that alteration of MT acetylation is a result of reduction of the interaction of DIC and α-TAT1 in Loa^{Hom} MEFs and D338N^{Het} fibroblasts and not because of having less α-TAT1 available in the cells.

Figure 3.7

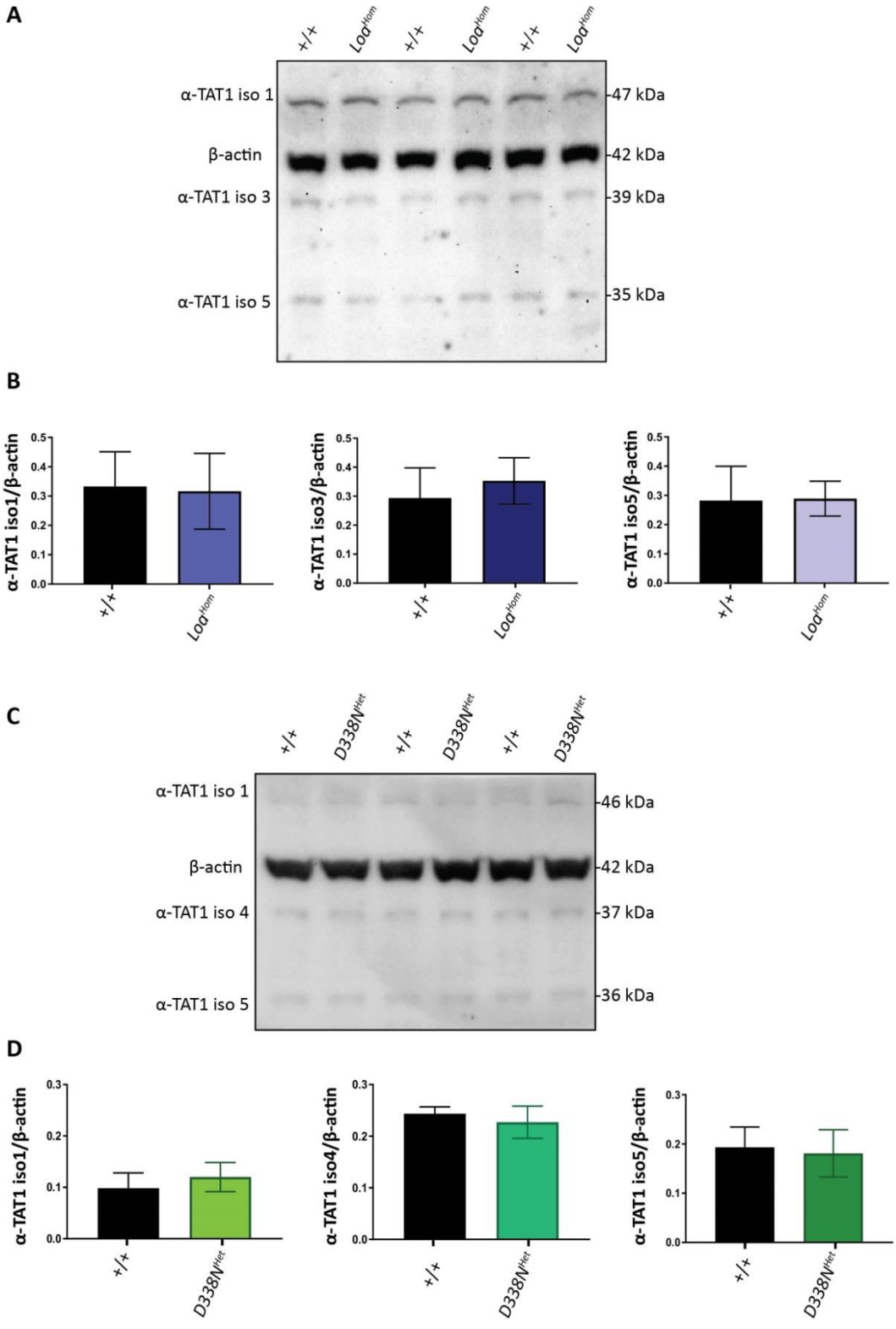
A
+/+
Loa Hom
+/+
Loa Hom
+/+
Loa Hom
α-TAT1 iso 1
β-actin
α-TAT1 iso 3
α-TAT1 iso 5
47 kDa
42 kDa
39 kDa
35 kDa
B
α-TAT1 iso1/β-actin
α-TAT1 iso3/β-actin
α-TAT1 iso5/β-actin
0.0
0.1
0.2
0.3
0.4
0.5
+/+
Loa Hom
C
+/+
D338N Het
+/+
D338N Het
+/+
D338N Het
α-TAT1 iso 1
β-actin
α-TAT1 iso 4
α-TAT1 iso 5
46 kDa
42 kDa
37 kDa
36 kDa
D
α-TAT1 iso1/β-actin
α-TAT1 iso4/β-actin
α-TAT1 iso5/β-actin
0.0
0.1
0.2
0.3
+/+
D338N Het

Figure 3.7 Normal level of α-TAT1 in Loa^{Hom} MEFs and D338N^{Het} fibroblasts. (**A**) Western blot was performed to detect α-TAT1 in extracts obtained from wild-type and Loa^{Hom} MEFs. The protein extracts immunostained with antibody against α-TAT1 detecting three isoforms (Isoform 1, 3, and 5 corresponding to 47, 39, and 35 kDa respectively) of α-TAT1. β-actin was used as a loading control. (**B**) Data is presented as the mean ± SEM; where N = 3, biological repeats for each genotype. Statistics were performed with unpaired t-test ($P > 0.05$). (**C**) Western blot was performed to detect α-TAT1 isoforms in extracts obtained from wild-type and D338N^{Het} human fibroblasts. The protein extracts immunostained with antibody against α-TAT1 detecting three isoforms of α-TAT1 (Isoform 1, 4, and 5 corresponding to 46, 37, and 36 kDa respectively) and β-actin was used as a loading control. (**D**) Data is presented as the mean ± SEM; where N = 3 and N = 6, independent experimental repeats for R339G^{Hom} and D338N^{Het} fibroblasts respectively. Statistics were performed with unpaired t-test ($P > 0.05$).

3.2.8 Recovery of α-tubulin deacetylation following HDAC6 inhibition demonstrates a similar rate of MT deacetylation in both Loa^{Hom} MEFs and D338N^{Het} human fibroblasts compared to wild-type fibroblasts

For further investigation, *DYNC1H1* mutations were checked to see whether these mutations affect the function of HDAC6. HDAC6 is the main α-tubulin deacetylase responsible for removal of the acetyl group from Lys40 residues of α-tubulin, modulating the acetylation of MT. It was investigated whether dynein deficiency affects the activity of HDAC6 and subsequently, HDAC6 alters the levels of MT acetylation. Tubastatin (TBA) was used to inhibit HDAC6 activity in both wild-type and mutant fibroblasts. The cell cultures were treated with TBA for 4 hours, and then after removal of TBA, cells were recovered up to 5 hours. Cells were lysed and western blot was performed using antibodies of acetylated tubulin (AC α-tubulin) and total tubulin. The signal of AC- α-tubulin was normalised to the signal of total tubulin in the same lane. The western blot analysis of protein extracts obtained from untreated and treated fibroblasts revealed that upon inhibition of HDAC6, levels of α-tubulin acetylation in MEFs and human fibroblasts were increased regardless of genetic mutations compared to the cells treated with DMSO (vehicle) (**Figure 3.8, A-C, lanes 2 and 9**). After washout of TBA, cells were recovered for distinct time points up to 5 hours to check the level of α-tubulin acetylation. During the recovery period, levels of acetylation of α-tubulin decreased gradually into basal levels at a similar rate (**Figure 3.8, A-C**) with no difference in the rate of recovery in Loa^{Hom} MEFs and D338N^{Het} human fibroblasts in comparison to the rate of recovery in their wild-type counterparts (**Figure 3.8 B-D**). These data suggest that the difference in the levels of α-tubulin acetylation in Loa^{Hom} MEFs and D338N^{Het} human fibroblasts is mainly because of a difference in the function of α-TAT1 as the main acetyltransferase rather than the function of HADC6 as a main α-tubulin deacetylase.

Figure 3.8

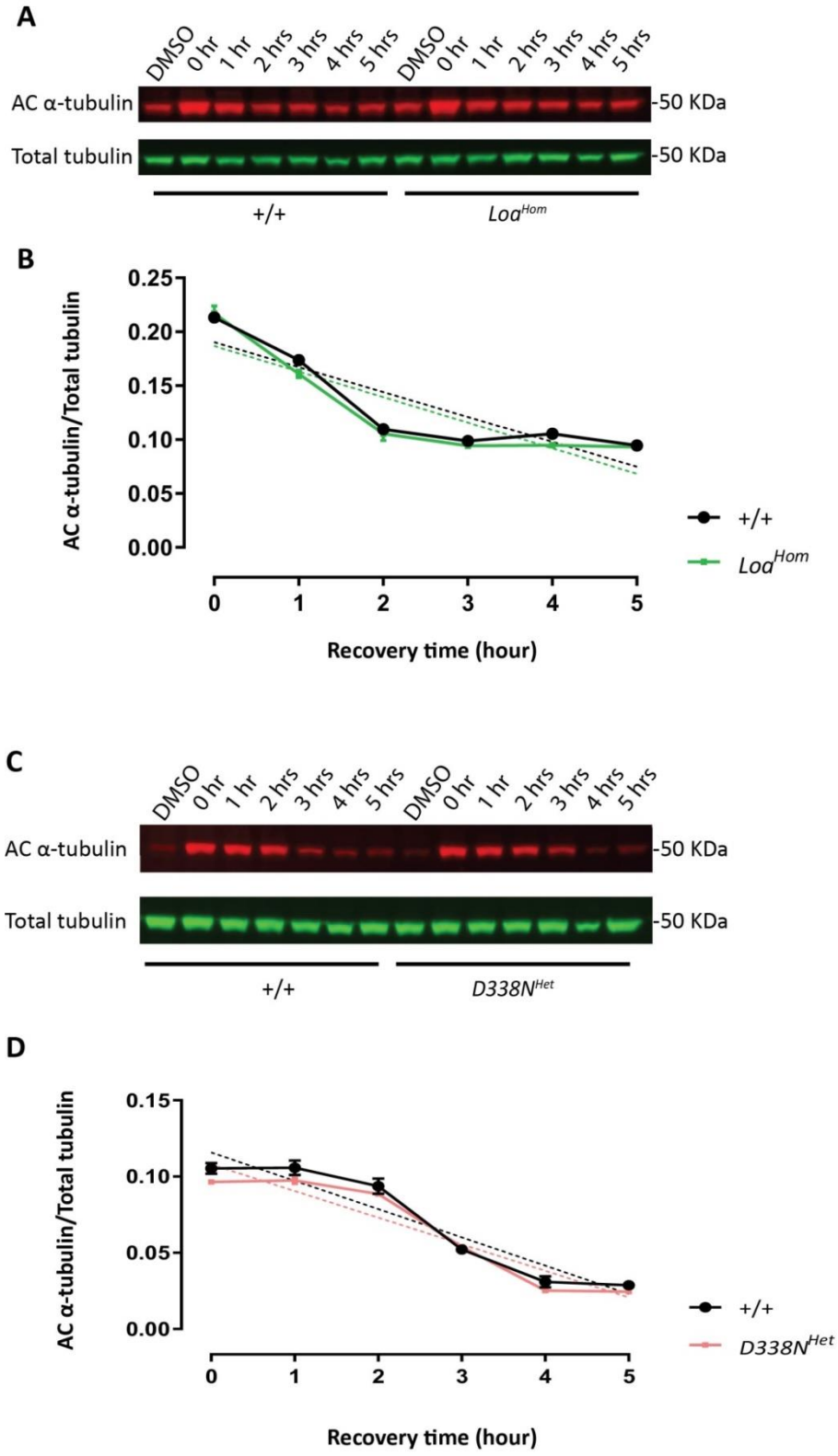
A
DMSO
0 hr
1 hr
2 hrs
3 hrs
4 hrs
5 hrs
DMSO
0 hr
1 hr
2 hrs
3 hrs
4 hrs
5 hrs
AC α-tubulin
-50 KDa
Total tubulin
-50 KDa
+/+
Loa^Hom
B
AC α-tubulin/Total tubulin
0.25
0.20
0.15
0.10
0.05
0.00
0
1
2
3
4
5
Recovery time (hour)
+/+
Loa^Hom
C
DMSO
0 hr
1 hr
2 hrs
3 hrs
4 hrs
5 hrs
DMSO
0 hr
1 hr
2 hrs
3 hrs
4 hrs
5 hrs
AC α-tubulin
-50 KDa
Total tubulin
-50 KDa
+/+
D338N^Het
D
AC α-tubulin/Total tubulin
0.15
0.10
0.05
0.00
0
1
2
3
4
5
Recovery time (hour)
+/+
D338N^Het

Figure 3.8 The rate of α-tubulin deacetylation after HDAC6 inhibition shows similar pattern regardless of genotype. (**A**) Western blot was performed using anti acetylated α-tubulin and anti α-tubulin antibodies. Cell lysate was prepared from wild-type and Loa^{Hom} MEFs treated with HDAC6 inhibitor (TBA) for 4 hours followed by washout and then recovering in complete media for different time points. Total tubulin was used as a loading control. (**B**) Data is presented as the mean ± SEM; where N = 2, biological repeats for each genotype. Linear regression analysis of levels of acetylated α-tubulin with recovery time in MEFs (wild-type and Loa^{Hom}) (*P* = 0.9516). (**C**) Western blot was performed using anti acetylated α-tubulin and anti α-tubulin antibodies. Cell lysate was prepared from wild-type and $D338N^{Het}$ fibroblasts treated with TBA for 4 hours followed by washout and then recovering in complete media for different time points. Total tubulin was used as a loading control. (**D**) Data is presented as the mean ± SEM; where N = 2, experimental repeats. Linear regression analysis of levels of acetylated α-tubulin with recovery time in human fibroblasts (wild-type and $D338N^{Het}$) (*P* = 0.7971).

3.2.9 The interaction between DIC and HDAC6 in MEFs

The interaction between DIC and HDAC6 was also checked to see if dynein mutation changes its interaction with HDAC6. Previously, it was reported that dynein interacts with HDAC6 directly (Kawaguchi et al., 2003). To examine this interaction in the mutant cells, PLA was performed in wild-type and Loa^{Hom} MEFs using the primary antibodies of HDAC6 and DIC. The PLA signals in confocal images revealed in similar pattern in wild-type and Loa^{Hom} MEFs (**Figure 3.9**).

Figure 3.9

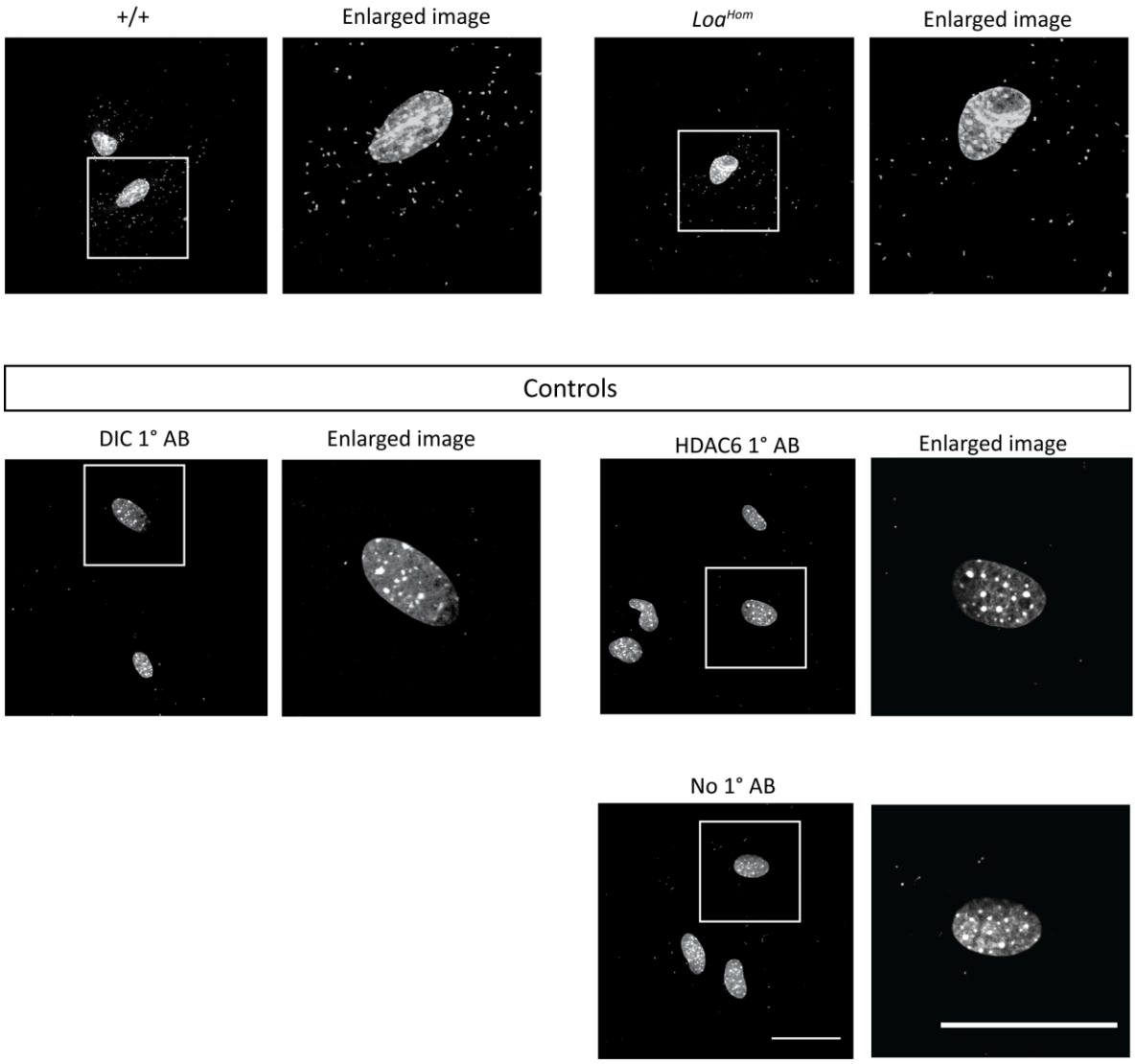

Figure 3.9 The interaction between DIC and HDAC6 in Loa^{Hom} MEFs. The wild-type and Loa^{Hom} MEFs were fixed, and PLA was performed using mouse anti-DIC and rabbit anti-HDAC6 antibodies. The nuclei stained with DAPI. The representative images of PLA are shown as maximum projections of Z-stacks of confocal images and white dots represent PLA signal. Negative controls of PLA are presented with DIC antibody only, HDAC6 antibody only or without primary antibodies. The enlarged images are from the boxed areas of the merged micrographs for the better view of PLA signals. Scale bar, 50 µm.

3.2.10 Mutation of dynein's heavy chain does not change the interaction between dynein and Golgin160

Golgi ministacks are made of small Golgi membrane vesicles, which form into cisternae that then undergo stacking. This process is MT dependant, and the motor dynein is required to form a continuous Golgi ribbon. Furthermore, the requirement of dynein on the Golgi membrane is mediated through Golgin160. Previously, a former PhD student in Hafezparast lab showed that the Golgi apparatus was dispersed in R399G^{Hom} human fibroblasts. Thus, the aim was to find whether *DYNC1H1* mutations impact the interaction between dynein and Golgin160 on Golgi membrane. Previously interaction between DIC and Golgin160 was reported (Yadav et al., 2012). Therefore, the interaction was checked between DIC and Golgin160 by PLA. To ensure the validity of PLA signals, the negative controls were included.

First, *in situ* PLA was conducted in wild-type and Loa^{Hom} MEFs. The negative controls displayed very low background signal. The PLA signals showing interaction between DIC and Golgin160 were detected throughout the cells both in wild-type and mutant fibroblasts (**Figure 3.10 A**). Although the Golgi fragmentation was not reported in D338N^{Het} human fibroblasts, PLA was also performed in D338N^{Het} human fibroblasts. The PLA signals were detected throughout the cells similar to the pattern found in Loa^{Hom} MEFs (**Figure 3.10 B**).

Figure 3.10

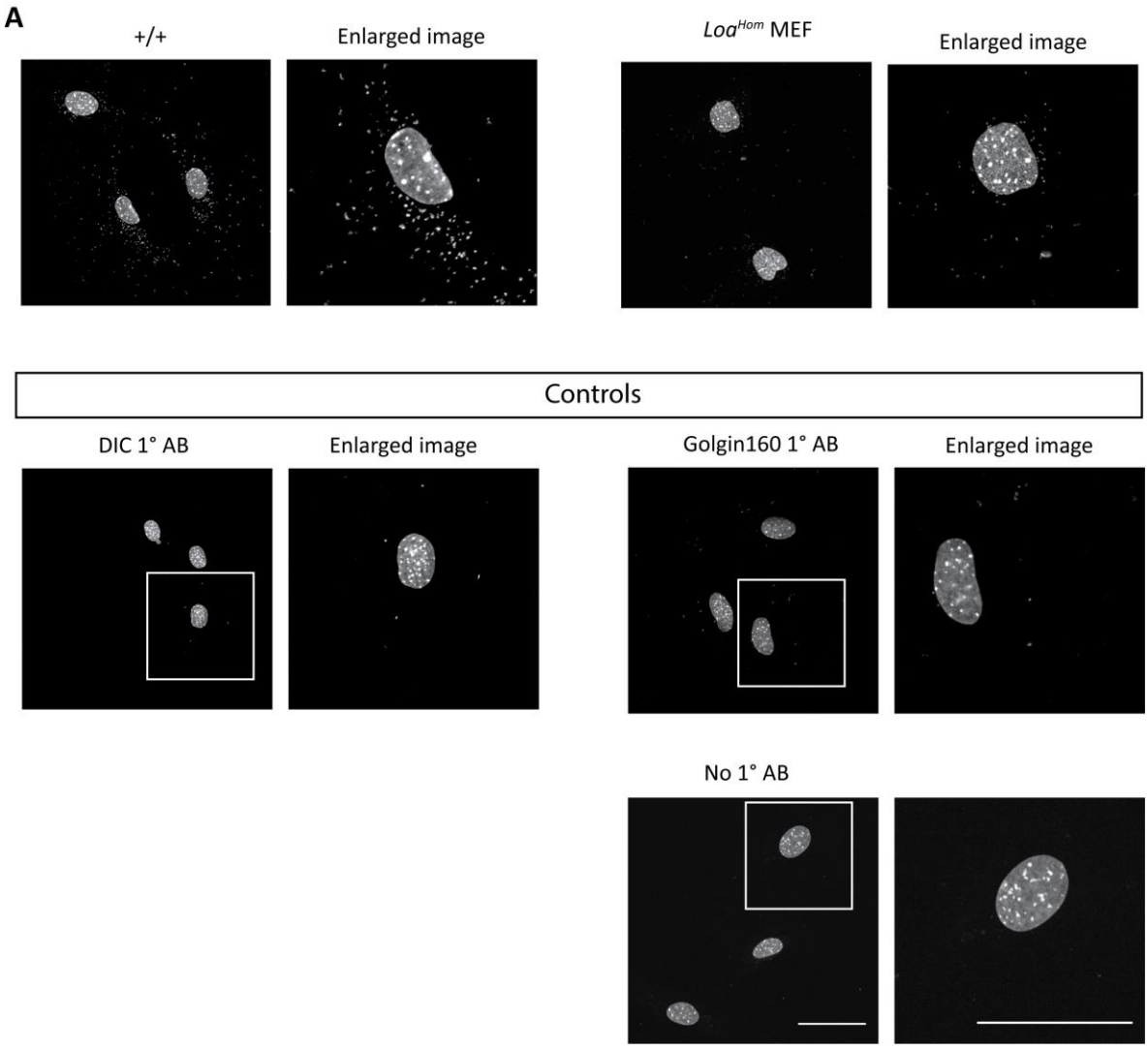
A
+/+
Enlarged image
Loa^Hom MEF
Enlarged image
Controls
DIC 1° AB
Enlarged image
Golgin160 1° AB
Enlarged image
No 1° AB

Figure 3.10 continued

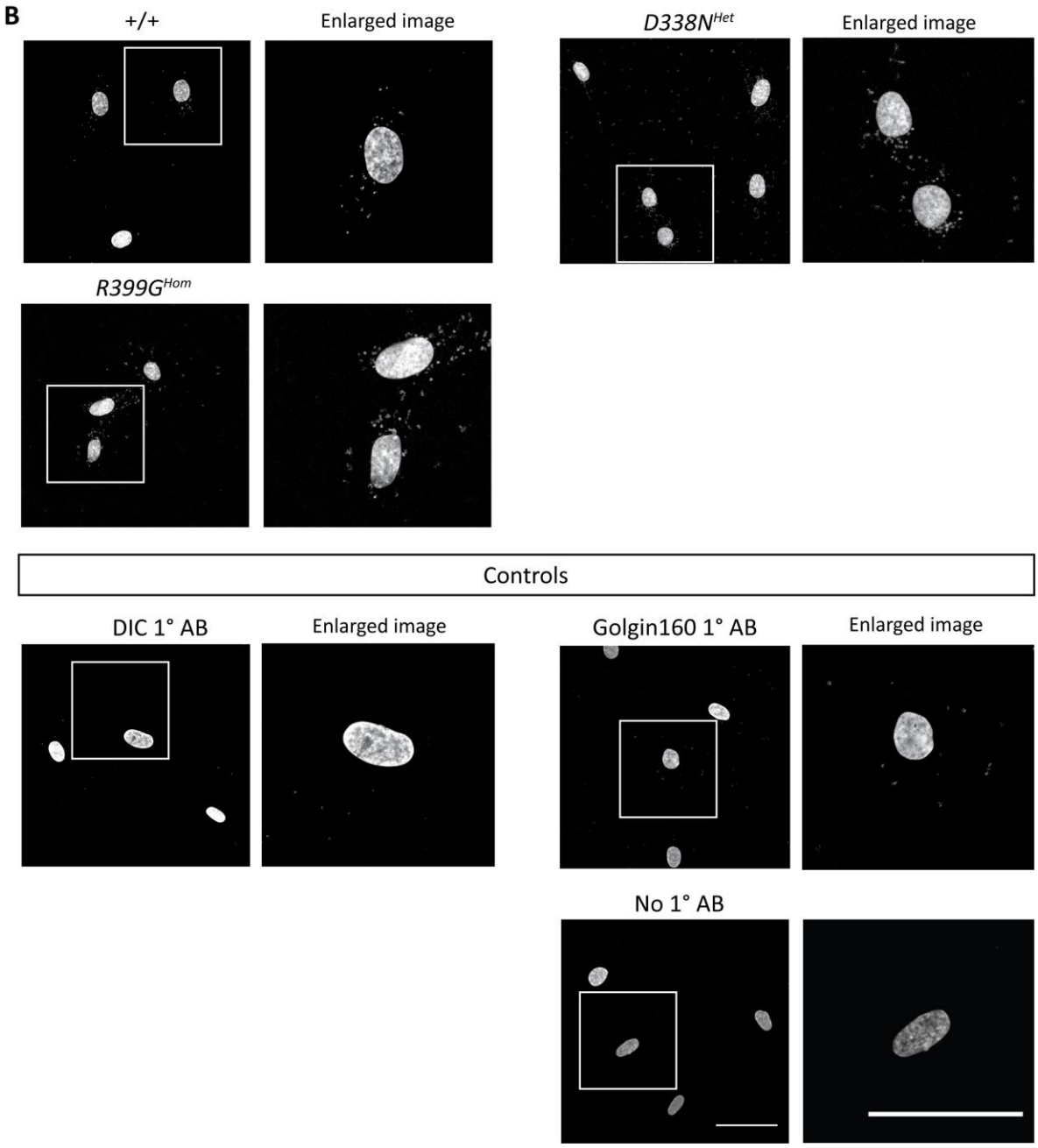

Figure 3.10 Proximity ligation assay represents interaction between DIC and Golgin160 is not changed in mutant fibroblasts. (**A**) The wild-type and Loa^{Hom} MEFs were fixed, and PLA was performed using mouse anti-DIC and rabbit anti-Golgin160 antibodies. The representative images of PLA are shown as maximum projections of Z-stacks of confocal images and white dots representing PLA signals. The enlarged images are from the boxed areas of the merged micrographs for better view of PLA signals. Scale bar 50 µm. (**B**) The PLA was performed D338N^{Het} and R399G^{Hom} human fibroblasts using mouse anti-DIC and rabbit anti-Golgin160 antibodies and negative controls were included. The nuclei were stained with DAPI. The representative images of PLA are shown as maximum projections of Z-stacks of confocal images and white dots represent PLA signal. Negative controls are presented with DIC antibody only, Golgin160 antibody only or without primary antibodies. The enlarged images are from the boxed areas of the merged micrographs for better view of PLA signals. Scale bar, 50 µm.

3.2.11 Summary

Of the experiments which measured the levels of acetylated α-tubulin, apart from the experiment for R399G^{Hom} fibroblasts, all confirmed the previous results showing the significant effect of the dynein on the levels of acetylated α-tubulin in mutant human fibroblasts and MEFs.

Importantly, for the first time, it was found that there is an interaction between dynein and α-TAT1. Moreover, this interaction was found to be significantly reduced in Loa^{Hom} MEFs and D338N^{Het} compared to the wild-type counterparts. This interaction was also observed in neurons. The results of experiment also showed no difference in levels of α-TAT1 between genotypes. Additionally, experiments which measured the interaction between dynein and HDAC6 showed no difference in this interaction across the genotypes. Furthermore, it was observed that interaction between dynein and Golgin160 was unchanged in Loa^{Hom} MEFs and D338N^{Het} compared to the wild-type counterparts.

Chapter 4: Dynein dysfunction impairs autophagy and synergizes with TBK1 inhibition/knockdown to induce protein aggregates

4.1 Introduction

ALS is characterized by the protein aggregates in affected MNs and several constituents of ALS-linked aggregates including FUS, TDP-43, OPTN, p62 and UBQLN have been identified (Blokhuis et al., 2013). P62 has been considered as a common component of ALS-associated protein aggregates and mutations affecting functional domain of p62 have been recognized in ALS patients (Ramesh & Pandey, 2017). Moreover, p62 is involved in protein degradation pathways, including autophagy and ubiquitin proteasome system. P62 as an autophagy adaptor facilitates sequestration of ubiquitinated proteins and organelles such as mitochondria into the autophagosomes for their degradation (Peng et al., 2017). Importantly, p62 mutations have been found to modulate efficiency of autophagy and contribute to the pathogenesis of ALS (Vicencio et al., 2020). Depletion of p62 level also results in accumulation of ubiquitinated proteins (Seibenhener et al., 2004).

Of note, TBK1 phosphorylates p62 on Ser-403 increasing its affinity for recruitment of ubiquitinated substrates into the autophagosomes and this phosphorylation is essential for autophagic clearance (Pilli et al., 2012). Consequently, inhibition or knockdown of TBK1 impacts the recruitment of ubiquitinated proteins to the autophagosome and subsequent degradation and TBK1 mutations have been linked to ALS (de Majo et al., 2018). More importantly, dynein is essential for fusion of autophagosome and lysosome and it has been reported that dynein inhibition impairs autophagosome-lysosome fusion resulting in accumulation of autophagosomes increasing level of LC3II and accumulation of aggregation-prone proteins (De Vos et al., 2008; Ravikumar et al., 2005; Yamamoto, Suzuki, & Himeno, 2010).

This study aimed to investigate whether dysfunction of dynein makes cells prone to protein aggregation pathology when accompanied by deficiencies in TBK1 functions. This would test the two-hit model in ALS pathology, where dynein deficiency in presence of second stress promotes or exacerbates protein aggregation. It was hypothesised that due to the role of dynein in autophagy and removal of protein aggregates, dynein mutation may cause cellular susceptibility leading to accumulation of protein aggregates.

4.2 Results

4.2.1 The location of point mutations in *DYNC1H1* determines its effects on autophagy impairment

LC3II is a lipidated form of LC3I, which is incorporated into the autophagic membranes and it is a well-known marker of autophagic flux. Its increased levels indicate the blockage of degradation of the autophagosomes. Li and co-investigators have shown that dynein knockdown results in an increased level of LC3II (D. Li et al., 2013). Furthermore, it has been reported that the *Loa* point mutation in *Dync1h1* causes an elevated level of LC3II, suggesting autophagy dysregulation (Ravikumar et al., 2005). In this research, the levels of LC3II in both wild-type and Loa^{Hom} MEFs were checked which confirmed the previous results showing a significant increase in the level of LC3II in Loa^{Hom} MEFs (**Figure 4.1 A-B**).

The level of LC3II in human fibroblasts of patients diagnosed with SMA-LED carrying mutations in *DYNC1H1* ($D338N^{Het}$ and $R399G^{Hom}$) was also tested. The quantification of the levels of LC3II in $D338N^{Het}$ fibroblasts exhibited no significant changes. However, the quantification of immunoblot revealed a significant reduction in the levels of LC3I (**Figure 4.1 C-D**). The immunoblot analysis of homogenates of $R399G^{Hom}$ fibroblasts also revealed that the point mutation of *DYNC1H1* resulted in no significant changes in the levels of LC3II (**Figure 4.1 E-F**).

These results suggest that the location of point mutations and how these mutations would affect the dimerization and binding ability of dynein to its cargoes could determine the effect of dynein on autophagic removal and degradation of LC3II.

Figure 4.1

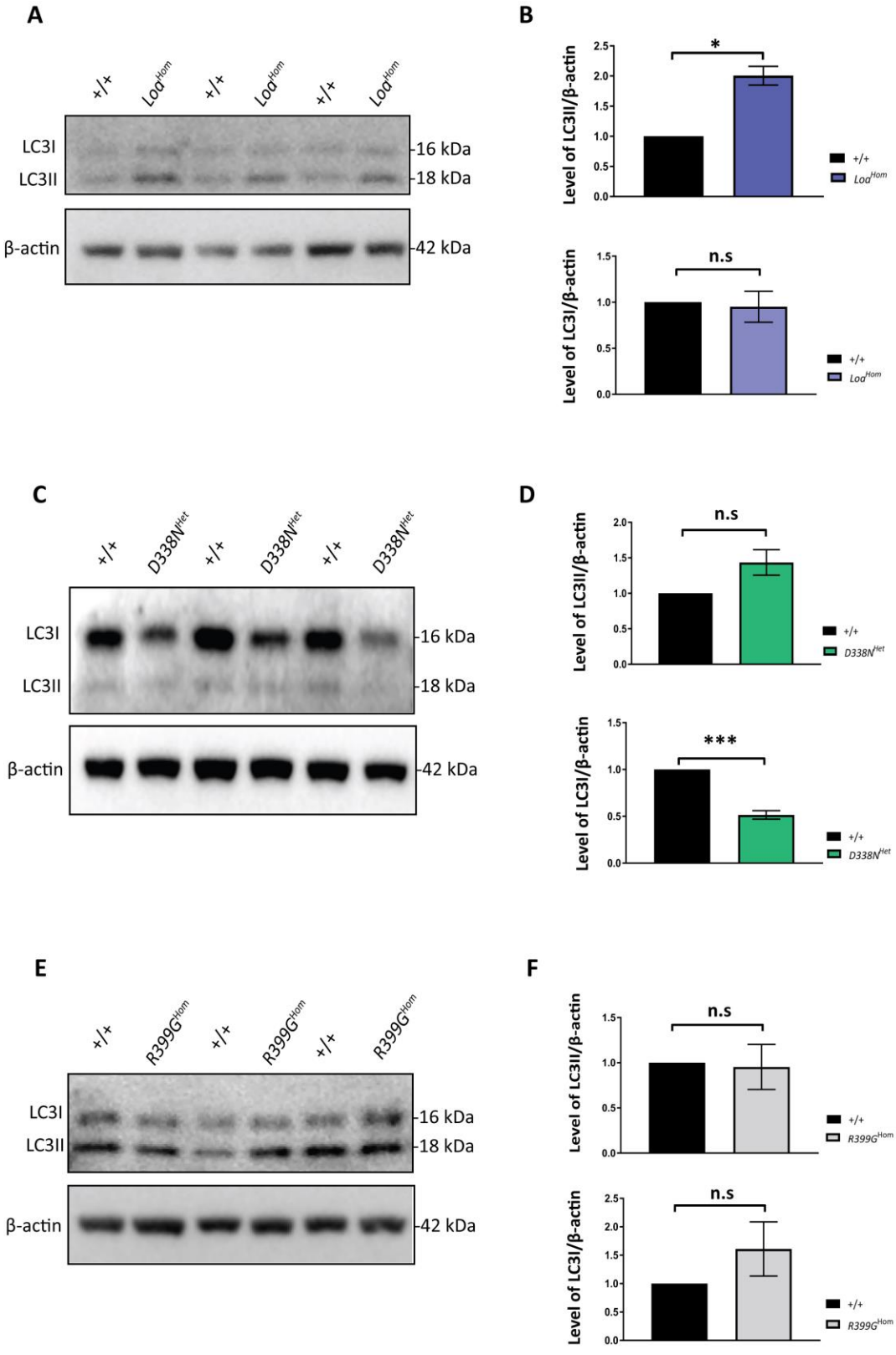
A
+/+
Loa Hom
+/+
Loa Hom
+/+
Loa Hom
LC3I
LC3II
16 kDa
18 kDa
β-actin
42 kDa
B
Level of LC3II/β-actin
*
+/+
Loa Hom
Level of LC3I/β-actin
n.s
+/+
Loa Hom
C
+/+
D338N Het
+/+
D338N Het
+/+
D338N Het
LC3I
LC3II
16 kDa
18 kDa
β-actin
42 kDa
D
Level of LC3II/β-actin
n.s
+/+
D338N Het
Level of LC3I/β-actin
***
+/+
D338N Het
E
+/+
R399G Hom
+/+
R399G Hom
+/+
R399G Hom
LC3I
LC3II
16 kDa
18 kDa
β-actin
42 kDa
F
Level of LC3II/β-actin
n.s
+/+
R399G Hom
Level of LC3I/β-actin
n.s
+/+
R399G Hom

Figure 4.1 Altered level of LC3II in Loa^{Hom} MEFs. (**A**) Western blot analysis shows level of LC3II and LC3I in wild-type and Loa^{Hom} MEFs. β-actin was used as a loading control. (**B**) Data is presented as the mean ± SEM; where N = 3, biological repeats, and N = 3, technical repeats for each genotype. Statistic was performed with unpaired t-test (* $P < 0.05$). (**C**) Western blot analysis shows level of LC3II and LC3I in wild-type and D338N^{Het} fibroblasts. (**D**) Data is presented as the mean ± SEM; where N = 3, technical repeats. Statistic was performed with unpaired t-test (*** $P < 0.001$). (**E**) Western blot analysis shows level of LC3II and LC3I in wild-type and R399G^{Hom} fibroblasts. (**F**) Data is presented as the mean ± SEM; where N = 3, technical repeats for each genotype. Statistic was performed with unpaired t-test ($P = 0.1$).

4.2.2 Ciliobrevin D inhibition of dynein accelerates the formation of p62 puncta in Loa^{Hom} MEFs

Dynein-mediated retrograde transport is an important step in autophagosome maturation and autophagic degradation of protein aggregates. Importantly, it has been reported that dysfunctions in basal autophagy are sufficient to cause neurodegeneration in animal models (Hara et al., 2006).

This set of experiment aimed to assess the effect of non-functional dynein using CilD on accumulation of aggregation-prone protein in wild-type and Loa^{Hom} MEFs. It was hypothesised that mutant dynein might not be sufficient to result in aggregated proteins but it might cause the susceptibility when mild inhibition of dynein is applied leads to protein aggregates. For this purpose, the wild-type and Loa^{Hom} MEFs were treated with a mild concentration of dynein inhibitor (CilD, 30 µM) and a higher concentration (CilD, 50 µM) for 6 hours followed by fixing, and immunostaining of the cells using anti-p62 antibody. The quantification of p62 puncta indicated that the mild treatment of CilD in Loa^{Hom} MEFs increased the number of p62 puncta significantly, whereas the wild-type MEFs did not show significant alterations in p62 puncta (**Figure 4.2 A, second row**). Subsequently, the effect of the higher concentration of CilD treatment on the number of p62-positive aggregates was checked. The higher concentration of CilD caused the increased number of p62 aggregates in Loa^{Hom} MEFs, and also the number of p62 aggregates was significantly increased in wild-type MEFs (**Figure 4.2 A, third row**). After quantification of number of p62 aggregates, a two-way ANOVA was carried out to determine the effect of CilD treatment and genotype on the number of p62 aggregates (N > 80 number of cells per genotype). The results showed that there was a significant interaction between CilD treatment and genotype (P = 0.0219, F = 4.69), indicating that effect of CilD treatment on p62 accumulation is dependent on the genotype. Moreover, there was a significant main effect of CilD treatment (P < 0.0001, F = 36.83) and a significant main effect of genotype (P < 0.0001, F = 17.14) on number of p62 aggregates (**Figure 4.2 B**).

Furthermore, it was demonstrated that CilD treatment increases the size of p62 puncta both in wild-type and Loa^{Hom} MEFs. However, p62 puncta in Loa^{Hom} MEFs were on average significantly larger compared to those in wild-type MEFs. A two-way ANOVA showed that there was a significant interaction between CilD treatment and genotype (P = 0.003, F = 9.102) on the size of p62 aggregates. Moreover, there was a significant main effect of CilD treatment (P < 0.0001, F = 49.1) and a significant main effect of genotype (P < 0.0001, F = 38.72) on size of p62 aggregates (**Figure 4.2 C**).

This set of data demonstrates a dynein-dependent susceptibility in Loa^{Hom} MEFs in which mild treatment with CilD enhanced the number of p62 puncta significantly. In contrast, the wild-type MEFs exhibited the p62 aggregates only upon treatment with a higher concentration of dynein inhibitor.

Figure 4.2

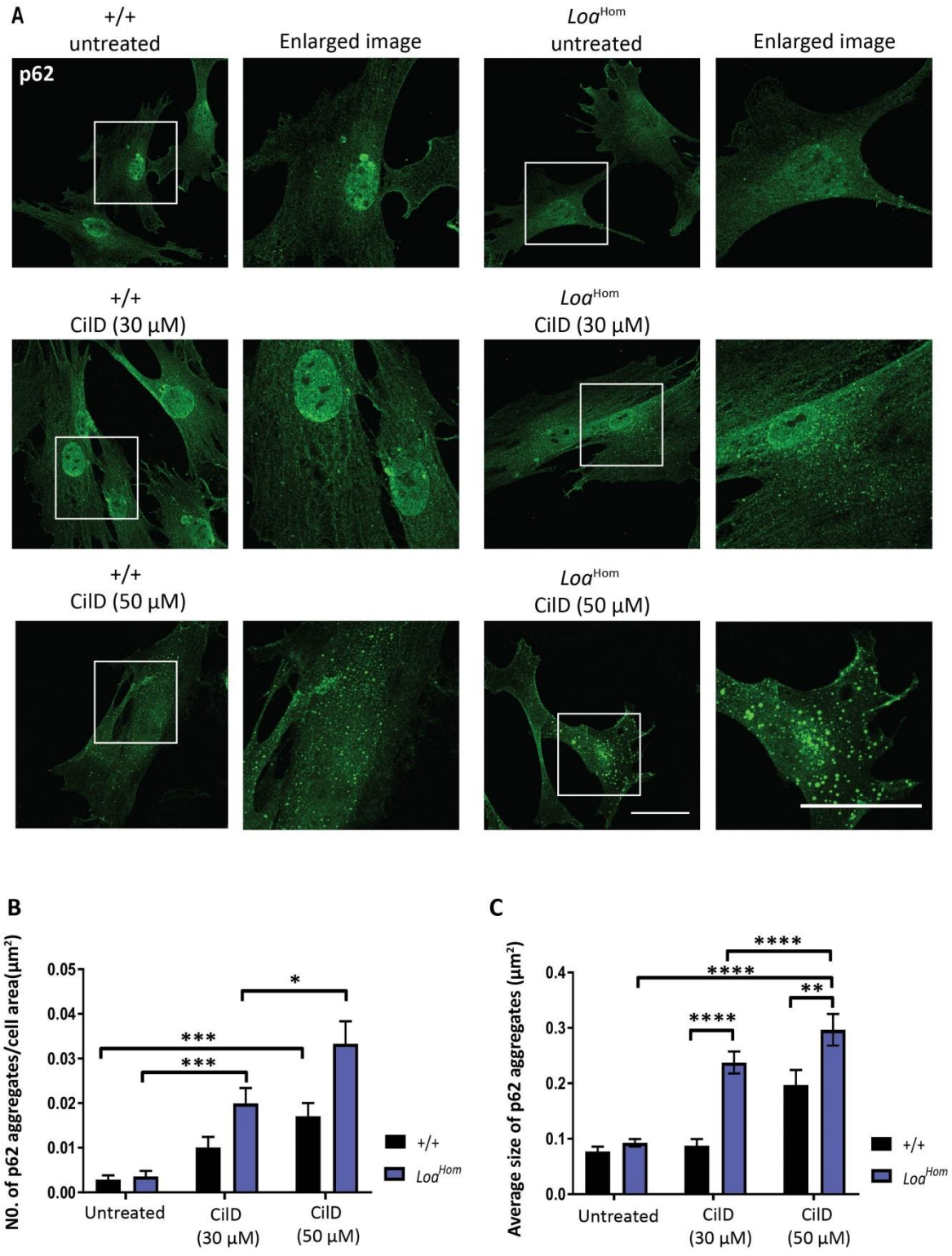
A
+/+
untreated
Enlarged image
Loa Hom
untreated
Enlarged image
p62
+/+
CilD (30 µM)
Loa Hom
CilD (30 µM)
+/+
CilD (50 µM)
Loa Hom
CilD (50 µM)
B
N0. of p62 aggregates/cell area(µm²)
0.05
0.04
0.03
0.02
0.01
0.00
***
***
*
Untreated
CilD (30 µM)
CilD (50 µM)
+/+
Loa Hom
C
Average size of p62 aggregates (µm²)
0.4
0.3
0.2
0.1
0.0
****
****
****
**
Untreated
CilD (30 µM)
CilD (50 µM)
+/+
Loa Hom

Figure 4.2 Low concentration of dynein inhibitor elevates the number of p62 accumulation significantly in Loa^{Hom} MEFs. (**A**) Wild-type and Loa^{Hom} MEFs were treated with dynein inhibitor (CilD, 30 and 50 µM). Immunostaining was performed using anti-p62 antibody. The representative images are shown as maximum projections of Z-stacks of confocal images. Images were taken at 63 X magnification. The enlarged images are the boxed areas shown for better view of p62 puncta. Scale bar, 50 µm. (**B**) Data is presented as the mean ± SEM; where N > 80 number of cells, N = 3 biological repeats per genotype, and N = 3 technical repeats. For all experiment, quantification was performed in at least 30 images per genotype. Two-way ANOVA showed significant interaction between genotype and CilD treatment (* P = 0.0123, F (2, 67) = 4.69) followed by Tukey's post-test. Moreover, there were significant main effects of CilD treatment and genotype on number of p62 accumulation (**** P < 0.0001, F (2, 67) = 36.83) and **** P < 0.0001, F (1, 67) = 17.14 respectively). (**C**) Data is presented as the mean ± SEM; where N > 80 number of cells, N = 3 biological repeats per genotype, and N = 3 technical repeats. Two-way ANOVA showed significant interaction between genotype and CilD treatment (*** P = 0.003, F (2, 80) = 9.102) followed by Tukey's post-test. Additionally, there were significant main effects of CilD treatment and genotype on size of p62 accumulation (**** P < 0.0001, F (2, 80) = 49.1 and **** P < 0.0001, F (1, 80) = 38.72 respectively).

4.2.3 TBK1 inhibition exacerbates the autophagy impairments in MEFs harbouring dysfunctional dynein and results in accumulation of p62

P62, a key autophagy adaptor, has been reported as a good marker of autophagic maturation, matching or exceeding in performance LC3-based assays (Larsen et al., 2010). TBK1 phosphorylates Ser402 in the UBA domain of p62, which increases its affinity for K48 and K63-linked ubiquitin chains. Phosphorylation of p62 is also essential to enable the entry of p62 into the autophagic degradative pathway and efficient autophagosome engulfment (Matsumoto et al., 2015, 2011). P62 co-localises with TBK1 and LC3 in basal conditions and after the induction of autophagy, it is shown that activation of autophagy upon starvation enhances the clearance of p62 (Pilli et al., 2012).

Based on autophagic clearance of p62 aggregates and effect of dynein mutation on autophagic degradation (mentioned above), the aim was to investigate whether different concentrations of TBK1 inhibitor (BX795) affect the accumulation of p62-positive puncta in wild-type and Loa^{Hom} MEFs differentially or not. For this purpose, the wild-type and Loa^{Hom} MEFs were treated with two doses of BX795 (5 and 10 µM) for 6 hours. The low concentration of TBK1 inhibitor (5 µM) was used to partially inhibit TBK1 kinase activity. Using immunocytochemistry and confocal imaging techniques, the number of p62 puncta were quantified before and after treatment. In the basal condition, in untreated cells, the p62 was diffused in the cytoplasm both in wild-type and Loa^{Hom} MEFs with no obvious p62 puncta. The quantification of p62-positive puncta revealed a significant increase in number of p62 accumulations only in Loa^{Hom} MEFs upon the low concentration treatment of BX795 but not in treated wild-type MEFs (**Figure 4.3 A, second row**).

Furthermore, with increasing the dose of BX795 to 10 µM, a significant number of p62 puncta was detected in the treated wild-type MEFs. Moreover, the Loa^{Hom} MEFs treated with a higher concentration of BX795 showed a higher number of p62 puncta compared to the wild-type counterparts. Therefore, accumulation of protein upon treatment with low concentration of TBK1 inhibitor in Loa^{Hom} MEFs showed that mutant dynein causes

susceptibility when another partner of autophagy system is defected, in this case TBK1, results in accumulation of p62-positive puncta. In contrast, only treatment with higher concentration of BX795 resulted in accumulation of p62 in wild-type MEFs (**Figure 4.3 A right, third row**). A two-way ANOVA was carried out to determine the effect of TBK1 treatment and genotype on the number of p62 puncta (N > 80 number of cells per genotype). These results showed that there was a significant interaction between TBK1 treatment and genotype ($P = 0.0012$, F = 7.383), indicating that effect of TBK1 treatment on p62 puncta is dependent on the genotype. Moreover, there was a significant main effect of TBK1 treatment ($P < 0.0001$, F = 39.39) and a significant main effect of genotype ($P < 0.0001$, F = 18.89) on number of p62 puncta (**Figure 4.3 B**).

Furthermore, it was demonstrated that TBK1 treatment increases the size of p62 puncta both in wild-type and Loa^{Hom} MEFs. However, p62 puncta in Loa^{Hom} MEFs were on average significantly larger compared to those in wild-type MEFs. A two-way ANOVA showed that there was a significant interaction between TBK1 treatment and genotype ($P = 0.0001$, F = 19.1) on the size of p62 puncta. Moreover, there was a significant main effect of TBK1 treatment ($P < 0.0001$, F = 125.3) and a significant main effect of genotype ($P < 0.0001$, F = 94.61) on size of p62 accumulation (**Figure 4.3 C**).

The above results were further validated biochemically by western blot analysis of BX795-treated wild-type and Loa^{Hom} MEFs, which demonstrated the level of LC3II was elevated significantly in the Loa^{Hom} MEFs (**Figure 4.3 D**). These results also showed the susceptibility of Loa^{Hom} MEFs in which further dysfunction of autophagy pathway mediated by TBK1 inhibition results in increased level of LC3II. A two-way ANOVA showed that there was a significant interaction between TBK1 treatment and genotype ($P = 0.0374$, F = 6.208), indicating that effect of TBK1 treatment on level of LC3II is dependent on the genotype. Furthermore, there was a significant main effect of TBK1 treatment ($P < 0.0001$, F = 64.34) and a significant main effect of genotype ($P < 0.0001$, F = 70.69) on level of LC3II (**Figure 4.3 E**). Moreover, western blot analysis of levels of p62 showed no alteration in the levels of p62 upon BX795 treatment ($P = 0.4777$, F = 0.57) (**Figure 4.3 F**). No changes in the level

of p62 showed that increased number of p62 after BX795 treatment is not due to the increased p62 expression.

Pertinent to the above results, when serum starvation, as biological stressor and inducer of autophagy, was used on its own or in combination with the TBK1 inhibitor, western blot analysis demonstrated increased levels of LC3II in both genotypes but the increase was significantly higher in Loa^{Hom} MEFs than in the wild-type MEFs. A two-way ANOVA showed no significant interaction between TBK1 treatment and genotype ($P = 0.5940$, $F = 0.56$) on the level of LC3II. However, there was a significant main effect of TBK1 treatment ($P < 0.0001$, $F = 184.6$) and a significant main effect of genotype ($P = 0.0001$, $F = 70.69$) on level of LC3II. Additionally, TBK1 inhibition in serum-starved MEFs enhanced the level of LC3II in both genotypes but the increase was significantly higher in Loa^{Hom} MEFs than in the wild-type MEFs (**Figure 4.3 G-H**). This set of results also supports that dynein causes cellular vulnerability, when combined with further defects in autophagy system, results in increased level of LC3II. Moreover, western blot analysis showed no alteration in the levels of p62 upon starvation and BX795 treatment ($P = 0.5896$, $F = 0.55$) (**Figure 4.3 I**).

Figure 4.3

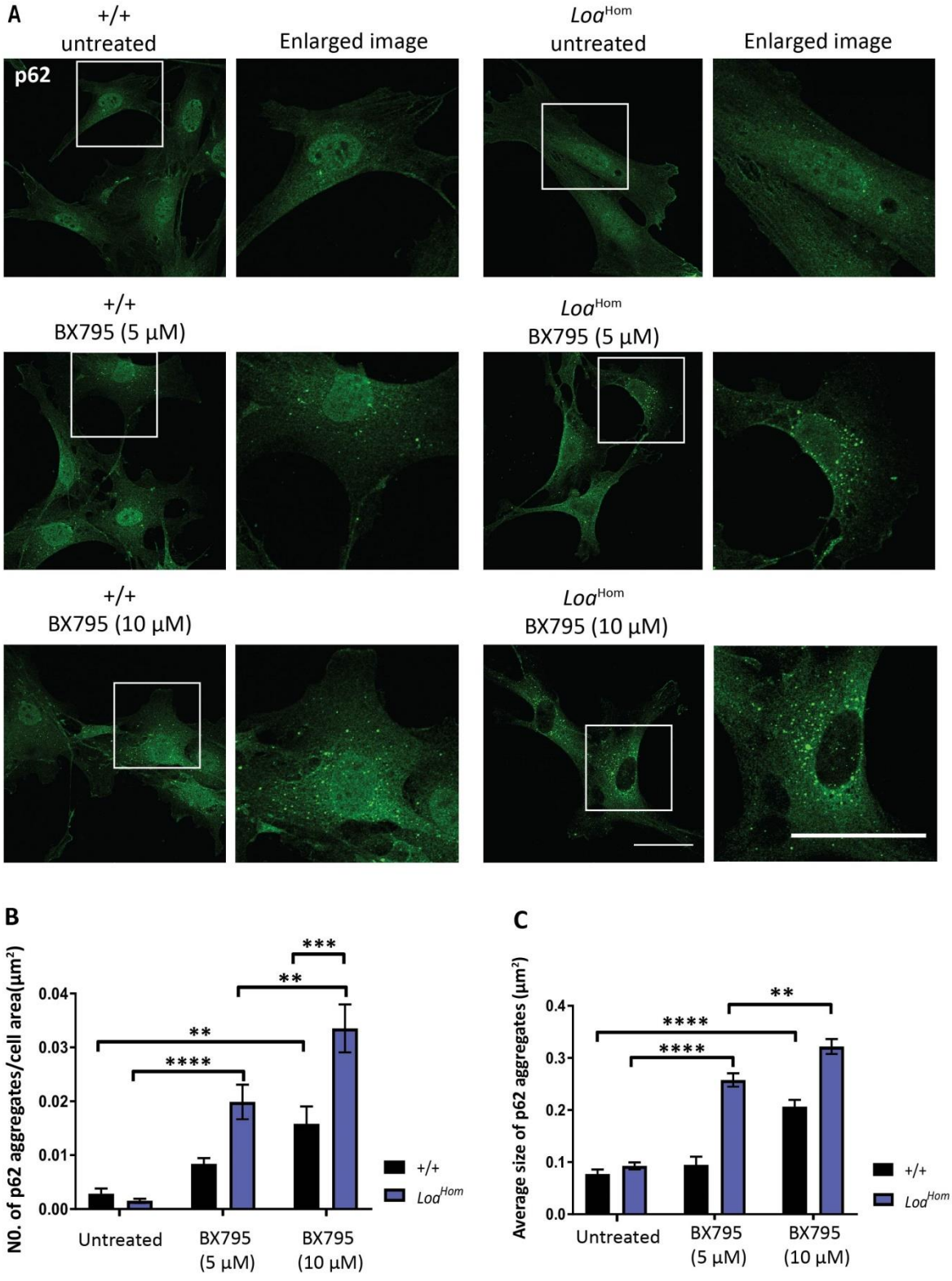
A
+/+
untreated
Enlarged image
Loa^Hom
untreated
Enlarged image
p62
+/+
BX795 (5 µM)
Loa^Hom
BX795 (5 µM)
+/+
BX795 (10 µM)
Loa^Hom
BX795 (10 µM)
B
N0. of p62 aggregates/cell area(µm²)
0.04
0.03
0.02
0.01
0.00
***
**
**
****
Untreated
BX795 (5 µM)
BX795 (10 µM)
+/+
Loa^Hom
C
Average size of p62 aggregates (µm²)
0.4
0.3
0.2
0.1
0.0
**
****
****
Untreated
BX795 (5 µM)
BX795 (10 µM)
+/+
Loa^Hom

Figure 4.3 continued

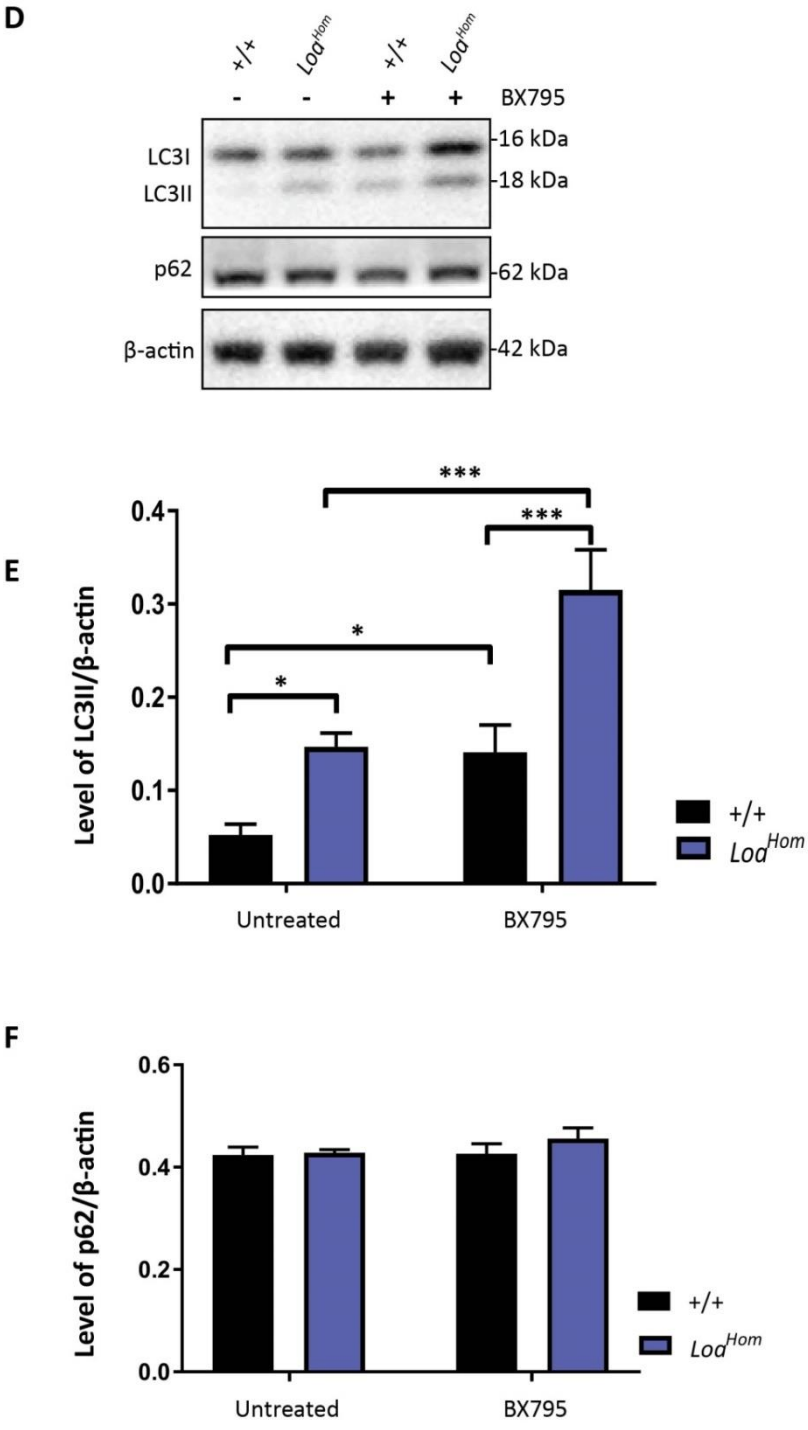

Figure 4.3 continued

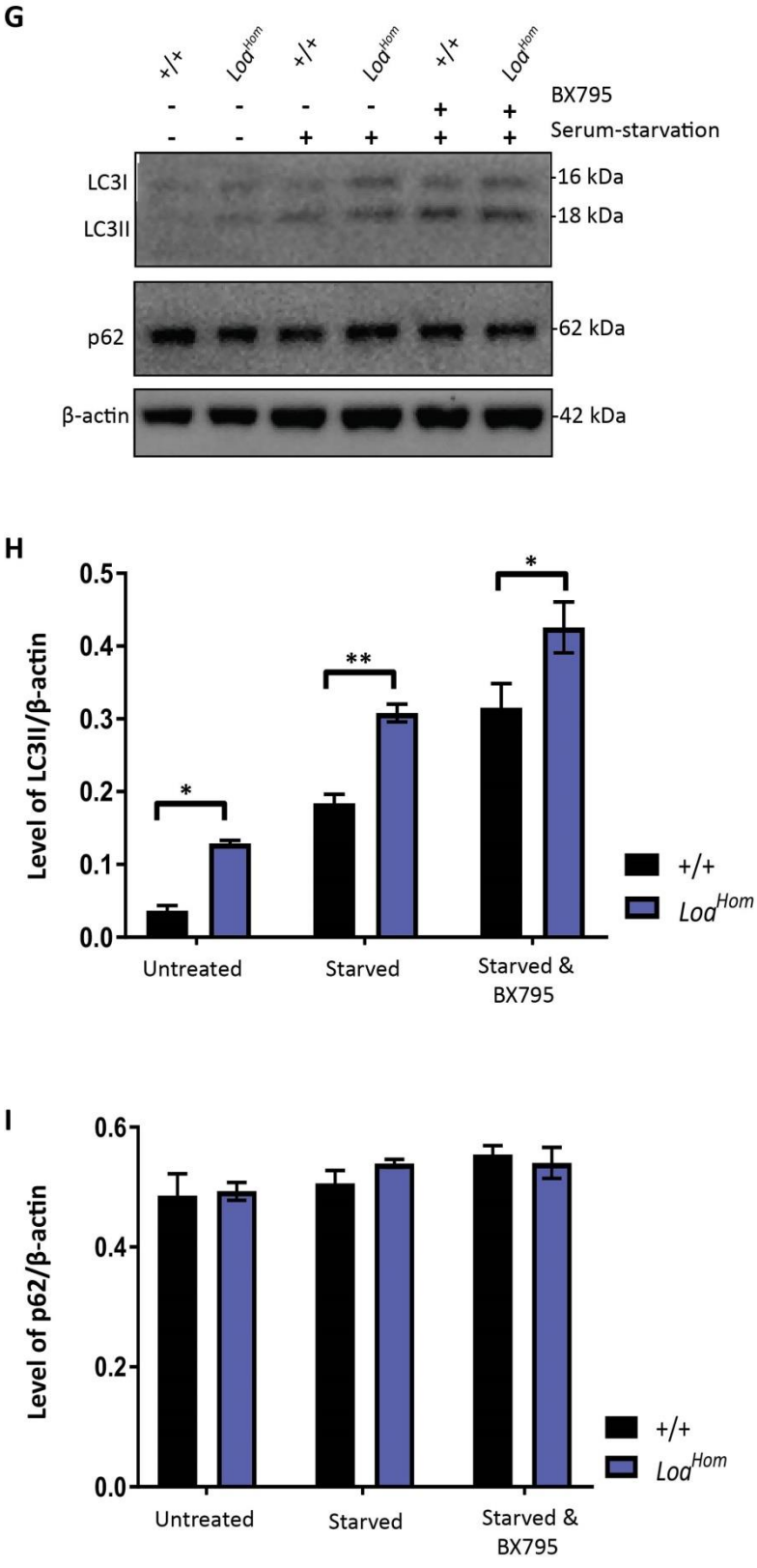

Figure 4.3 Mild inhibition of TBK1 markedly compromises the autophagy pathway in Loa^{Hom} MEFs. (**A**) Wild-type and Loa^{Hom} MEFs were treated with TBK1 inhibitor (BX795, 5 and 10 µM). Immunostaining was performed using anti-p62 antibody. The representative images are shown as maximum projections of Z-stacks of confocal images. Images were taken at 63 X magnification. The enlarged images are the boxed areas shown for better view of p62 puncta. Scale bar, 50 µm. (**B**) Data is presented as the mean ± SEM; where N > 80 number of cells per genotype, N = 3 biological repeats, and N = 3 technical repeats for each genotype. For all experiments, quantification was performed in at least 30 images. A two-way ANOVA showed significant interaction between genotype and BX795 treatment (** P = 0.0012, F (2, 72) = 7.38) followed by Tukey's post-test. Moreover, there were significant main effects of BX795 treatment and genotype on number of p62 puncta (**** P < 0.0001 and F (2, 72) = 39.39, and **** P < 0.0001 and F (1, 72) = 18.89 respectively). (**C**) Data is presented as the mean ± SEM; where N > 80 cells per genotype, N = 3 biological repeats, and N = 3 technical repeats for each genotype. A two-way ANOVA showed significant interaction between genotype and BX795 treatment (*** P = 0.0001, F (2, 101) = 19.1) followed by Tukey's post-test. Additionally, there were significant main effects of BX795 treatment and genotype on size of p62 puncta (**** P < 0.0001, F (2, 101) = 125.3 and **** P < 0.0001, F (1, 101) = 94.61 respectively). (**D**) Western blot analysis represents level of LC3II in wild-type and Loa^{Hom} MEFs before and after treatment with BX795. β-actin was used as a loading control. (**E**) Data is presented as the mean ± SEM; where N = 3 biological repeats for each genotype, and N = 3 technical repeats for each genotype. A two-way ANOVA showed significant interaction between genotype and BX795 treatment (* P = 0.0374, F (1, 8) = 6.208) followed by Tukey's post-test. There were significant main effects of BX795 treatment and genotype on level of LC3II (**** P < 0.0001, F (1, 8) = 64.34) and **** P < 0.0001, F (1, 8) = 70.69). (**F**) Data is presented as the mean ± SEM; where N = 3, biological repeats, and N = 3 technical repeats for each genotype. A two-way ANOVA showed no significant interaction between genotype and BX795 treatment (P = 0. 4777, F (2, 12) = 0.57). (**G**) Western blot analysis represents level of LC3II in wild-type and Loa^{Hom} MEFs before and after starvation and treatment with BX795. (**H**) Data is presented as the mean ± SEM; where N = 3 biological repeats, and N = 3 technical repeats for each genotype. A two-way ANOVA showed no interaction between genotype and BX795 treatment (P = 0.5940, F (2, 6) = 0.56) on the level of LC3II. However, there were significant main effects of BX795 treatment and genotype on level of LC3II (**** P < 0.0001, F (2, 6) = 184.6 and *** P = 0.0001, F (1, 6) = 78.98 respectively). (**I**) Data is presented as the mean ± SEM. A two-way ANOVA showed no significant interaction between genotype and BX795 treatment (P = 0.5896, F (2, 12) = 0.55) on the level of p62.

4.2.4 Combined pharmacological inhibition of TBK1 and dynein confirms the synergy in the pernicious impacts of defective dynein and TBK1 functions on autophagy

To further assess the interrelated functions of dynein and TBK1 in the removal of protein aggregates through autophagy pathway, the wild-type MEFs were co-treated with dynein and TBK1 inhibitors (CilD 50 μM and BX795 10 μM respectively) for 6 hours. Then, cells were fixed and immunostained for p62 followed by confocal microscopy. The quantification of p62 puncta in Z-stacks of confocal images showed an increased number of aggregates in the MEFs co-treated with CilD and BX795, indicating the synergistic impact of defective dynein and TBK1 on the accumulation of p62, most likely through disrupting the autophagy-lysosome pathway (**Figure 4.4 A**). A one-way ANOVA was performed with Tukey's multiple comparison test. The one-way ANOVA showed a significant increase in number of p62 puncta between untreated and treated MEFs (P < 0.0001, F = 29.77). Tukey's multiple comparison test showed a significant increase in number of p62 puncta between untreated MEFs and BX795-treated MEFs (P = 0.0182), untreated MEFs and CilD-treated MEFs (P < 0.0001), and untreated MEFs and BX795/CilD-treated MEFs (P < 0.0001) (**Figure 4.4 B**). Moreover, the size of p62 puncta after co-treatment of dynein and TBK1 inhibitors showed the significant increase, which suggests the inefficient removal of accumulated protein corroborating the previous data as demonstrated in Loa^{Hom} MEFs treated with the TBK1 inhibitor. A one-way ANOVA showed a significant increase in size of p62 puncta between untreated and treated MEFs (P < 0.0001, F = 66.39). Tukey's multiple comparison test showed a significant increase in size of p62 puncta between untreated and BX795-treated MEFs (P < 0.0001), untreated and CilD-treated MEFs (P < 0.0001), and untreated and BX895/CilD-treated MEFs (P < 0.0001) (**Figure 4.4 C**).

To investigate the effects of dynein and TBK1 inhibitions in neuronal cell line, Neuro2A cells were treated with BX795 and CilD (10 μM and 50 μM respectively) for 6 hours. The analysis of western blot demonstrated a slight increase in the level of LC3II upon TBK1

inhibition or dynein inhibition. In contrast, cells co-treated with the TBK1 and dynein inhibitors showed a significant increase in the level of LC3II, indicating exacerbated impairment of the autophagy flux and a defective autophagy-lysosome pathway in neuro2A cells, similar to that in the MEFs (**Figure 4.4 D**). A one-way ANOVA was performed with Tukey's multiple comparison test. The one-way ANOVA showed a significant increase in levels of LC3II between untreated and treated MEFs ($P < 0.0001$, $F = 46.77$). Tukey's multiple comparison test showed a significant increase in Levels of LC3II between untreated and CilD-treated MEFs ($P < 0.0007$), untreated and BX795/CilD-treated MEFs ($P < 0.0001$), and CilD-treated and BX795/CilD-treated MEFs ($P = 0.0085$) (**Figure 4.4 E**).

The data also suggest that the accumulation of p62 is a consequence of the autophagy dysregulation and defects in the autophagy-dependent removal of aggregates, which cannot be removed through other degradative systems.

Figure 4.4

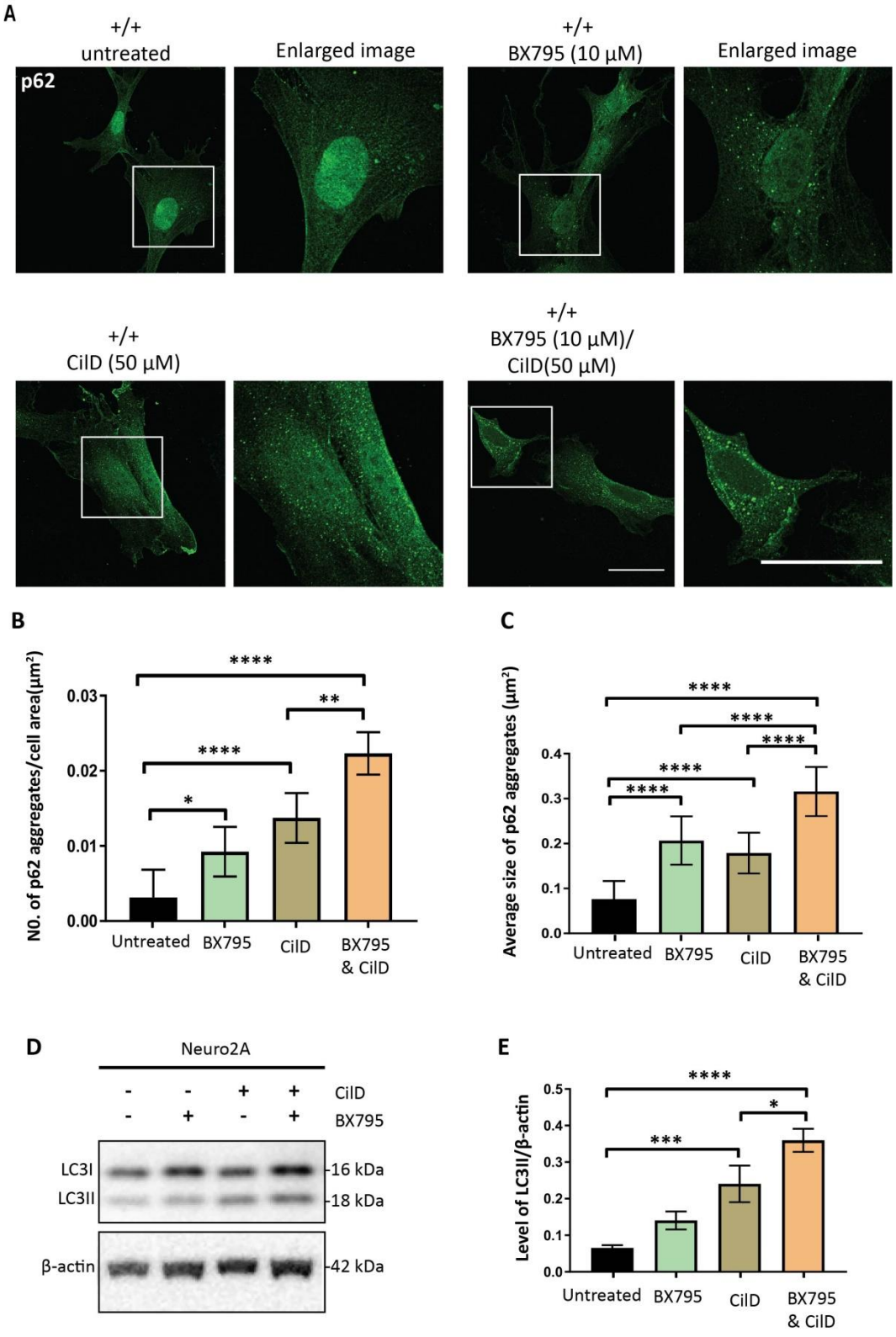
A
+/+
untreated
Enlarged image
+/+
BX795 (10 μM)
Enlarged image
p62
+/+
CilD (50 μM)
+/+
BX795 (10 μM)/
CilD(50 μM)
B
N0. of p62 aggregates/cell area(μm²)
0.03
0.02
0.01
0.00
****
**
****
*
Untreated
BX795
CilD
BX795
& CilD
C
Average size of p62 aggregates (μm²)
0.4
0.3
0.2
0.1
0.0
****
****
****
****
****
Untreated
BX795
CilD
BX795
& CilD
D
Neuro2A
-
-
+
+
CilD
-
+
-
+
BX795
LC3I
LC3II
16 kDa
18 kDa
β-actin
42 kDa
E
Level of LC3II/β-actin
0.5
0.4
0.3
0.2
0.1
0.0
****
*
***
Untreated
BX795
CilD
BX795
& CilD

Figure 4.4 Co-treatment of dynein and TBK1 inhibitors exacerbates the number of p62 aggregates. (**A**) Wild-type MEFs were treated with TBK1 inhibitor (BX795, 10 µM) and dynein inhibitor (CilD, 50 µM). Immunostaining was performed using anti-p62 antibody. The representative images are shown as maximum projections of Z-stacks of confocal images. Images were taken at 63 X magnification. The enlarged images are boxed areas shown for the better view of p62 puncta. Scale bar, 50 µm. (**B**) Data is presented as the mean ± SEM; where N > 80 number of cells, N = 3 biological repeats, and N = 3 technical repeats for each genotype. For this experiment, quantification was performed in at least 30 images. A one-way ANOVA showed a significant difference in number of p62 puncta between untreated and treated wild-type MEFs (**** $P < 0.0001$, F (3, 45) = 29.77). Tukey's multiple comparison test showed a significant increase in this measurement in MEFs treated with BX795 (* $P < 0.0182$), CilD (**** $P < 0.0001$), and BX795/CilD (**** $P < 0.0001$) compared to the untreated MEFs. (**C**) Data is presented as the mean ± SEM; where N > 80 cells, N = 3 biological repeats, and N = 3 technical repeats for each genotype. A one-way ANOVA showed a significant difference in size of p62 puncta between untreated and treated wild-type MEFs (**** $P < 0.0001$, F (3, 60) = 66.39). Tukey's multiple comparison test showed a significant increase in this measurement in MEFs treated with BX795 (**** $P < 0.0001$), CilD (**** $P < 0.0001$) and BX795/CilD (**** $P < 0.0001$) compared to the untreated MEFs. (**D**) Western blot analysis shows increased level of LC3II in Neuro2A co-treated with BX795 and CilD. β-actin was used as a loading control. (**E**) Data is presented as the mean ± SEM; where N = 3, experimental repeat. A one-way ANOVA showed a significant difference in size of p62 puncta between untreated and treated wild-type MEFs (**** $P < 0.0001$, F (3, 8) = 46.77). Tukey's multiple comparison test showed a significant increase in this measurement in MEFs treated with CilD (*** $P = 0.0007$) and BX795/CilD (**** $P < 0.0001$) compared to the untreated MEFs.

4.2.5 Genetic knockdown of TBK1 in Loa^{Hom} MEFs also shows a synergy between defective TBK1 and impaired dynein functions in increased p62 aggregation

It has been reported that TBK1 knockdown suppresses the autophagosome maturation and autophagic flux (Pilli et al., 2012). Thus, effect of TBK1 knockdown on the p62 puncta in wild-type and Loa^{Hom} MEFs was checked. To confirm that TBK1 deficiency exacerbates accumulation of p62 in Loa^{Hom}, both wild-type and Loa^{Hom} MEFs were transiently transfected with scrambled shRNA (non-targeting shRNA) and TBK1-shRNA (**Figure 4.5 A**). The TBK1 knockdown enhanced the number of p62 puncta significantly in Loa^{Hom} MEFs compared to the wild-type MEFs transfected with Scr-shRNA (**Figure 4.5 B**). After quantification of number of p62 puncta, a two-way ANOVA was carried out to determine the effect of TBK1 knockdown and genotype on the number of p62 puncta (N > 80 number of cells per genotype). The results showed that there was a significant interaction between TBK1 knockdown and genotype (P = 0.0236, F = 5.69), indicating that effect of TBK1 knockdown on p62 accumulation is dependent on the genotype (**Figure 4.5 C**). Moreover, there was a significant main effect of TBK1 knockdown (P = 0.0011, F = 13.05) and a significant main effect of genotype (P = 0.0437, F = 4.43) on number of p62 puncta. These results suggest that TBK1 knockdown exacerbates the effect of dynein mutation in autophagic degradation of p62 and results in p62 accumulation.

Furthermore, it was demonstrated that TBK1 knockdown increases the size of p62 puncta both in wild-type and Loa^{Hom} MEFs. However, p62 puncta in Loa^{Hom} MEFs were on average significantly larger compared to those in wild-type (**Figure 4.5 D**). A two-way ANOVA showed that there was a significant interaction between TBK1 knockdown and genotype (P = 0.0445, F = 4.279) on the size of p62 puncta. Moreover, there was a significant main effect of TBK1 knockdown (P < 0.0001, F = 246.2) and a significant main effect of genotype (P = 0.0002, F = 16.11) on size of p62 puncta.

Besides, the effect of TBK1 knockdown on the number and size of p62 puncta is relatively lower compared to the effect of TBK1 inhibition. Moreover, this set of data also showed that TBK1 knockdown caused similar impact to the pharmacological inhibition of TBK1 on the exacerbation of number of p62-positive puncta in Loa^{Hom} MEFs. Furthermore, these results suggest that loss of kinase activity of TBK1 combined with deficiency of dynein exacerbates the accumulation of protein.

Figure 4.5

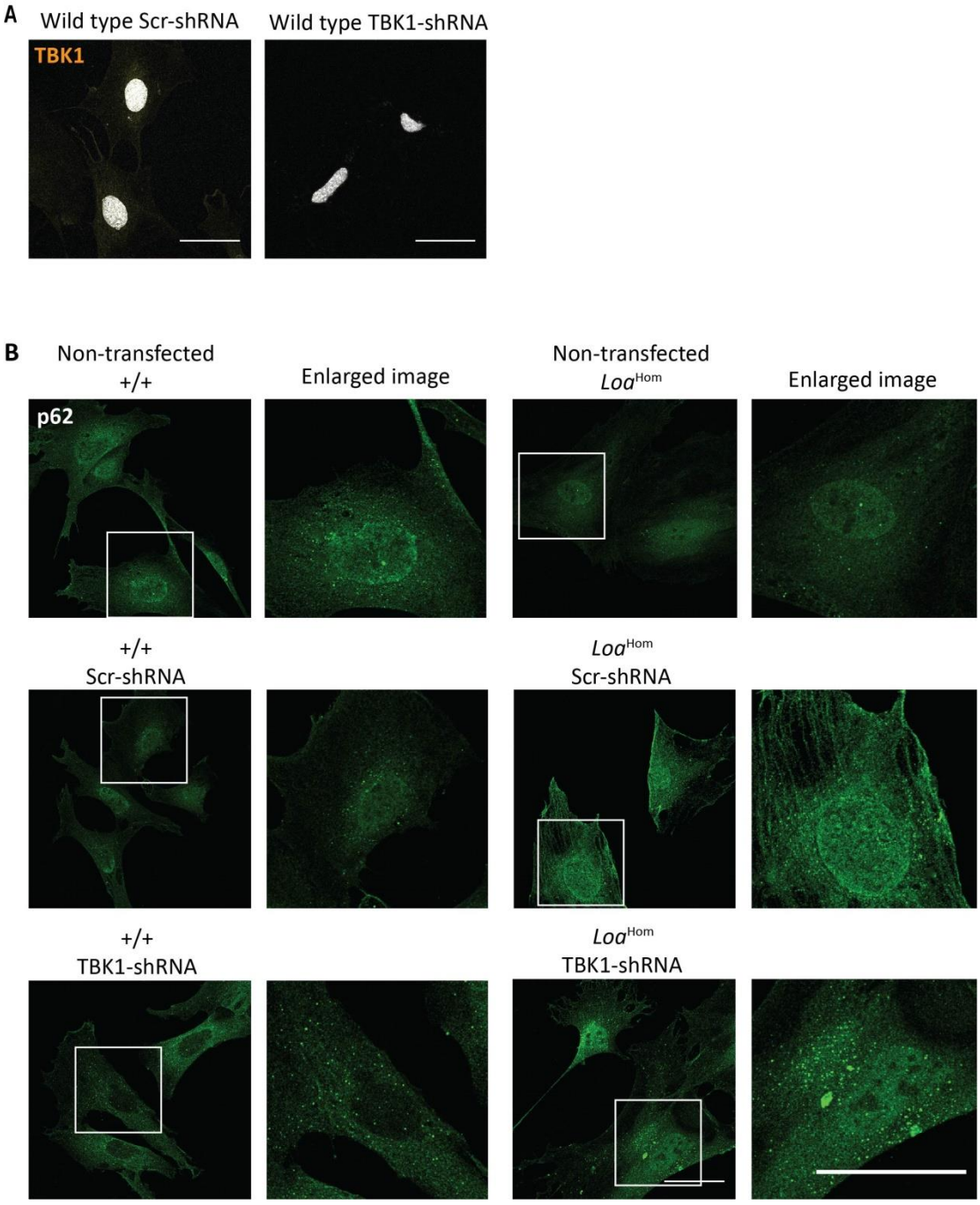
A
Wild type Scr-shRNA
Wild type TBK1-shRNA
TBK1
B
Non-transfected
+/+
Enlarged image
Non-transfected
Loa Hom
Enlarged image
p62
+/+
Scr-shRNA
Loa Hom
Scr-shRNA
+/+
TBK1-shRNA
Loa Hom
TBK1-shRNA

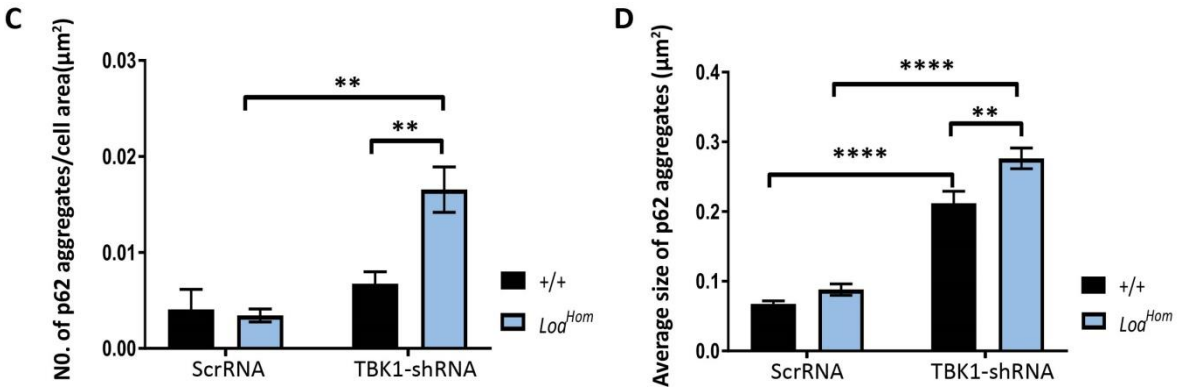

Figure 4.5 Genetic knockdown of TBK1 causes significant increase in number of p62 puncta in Loa^{Hom} MEFs. (**A**) Wild-type MEFs were transfected with Scrambled shRNA (Scr-shRNA) or TBK1-shRNA. Images show merged yellow (TBK1) and gray (nucleus) channels. Scale bar, 50 µm (**B**) Wild-type and Loa^{Hom} MEFs were transfected with Scr-shRNA or TBK1-shRNA. Immunostaining was performed using anti-p62 antibody. The representative images are shown as maximum projections of Z-stacks of confocal images. Images were taken at 63 X magnification. The enlarged images are boxed areas shown for the better view of p62 puncta. Scale bar, 50 µm. (**C**) Data is presented as the mean ± SEM; where N > 80, number of cells per genotype, N = 3 biological repeats, and N = 3 technical repeats for each genotype. For all experiments, quantification was performed in at least 30 images per genotype. A two way ANOVA showed significant interaction between genotype and TBK1 knockdown (* P = 0.0236, F (1, 30) = 5.69) on number of p62 puncta followed by Tukey's post-test. Moreover, there were significant main effects of TBK1 knockdown and genotype on number of p62 puncta (**** P < 0.0011, F (1, 30) = 13.05 and * P = 0.0437, F (1, 30) = 4.43 respectively). (**D**) Data is presented as the mean ± SEM; where N > 80, number of cells per genotype, N = 3 biological repeats, and N = 3 technical repeats for each genotype. A two way ANOVA showed significant interaction between genotype and TBK1 knockdown (* P = 0.0445, F (1, 44) = 4.279) on size of p62 puncta followed by Tukey's post-test. Additionally, there were significant main effects of TBK1 knockdown and genotype on size of p62 puncta (**** P < 0.0001, F (1, 44) = 246.2 and *** P = 0.0002, F (1, 44) = 16.11 respectively).

4.2.6 Proteasome inhibition overloads the autophagy-lysosome pathway in cells with impaired dynein function

It is well established that for the maintenance of cellular homeostasis, both functional autophagy-lysosome pathway and UPS are necessary (Ramesh & Pandey, 2017). Besides, impaired proteasome function has been implicated in neurodegenerative disorders, including ALS (Dantuma & Bott, 2014; Zheng et al., 2016). Moreover, the autophagy system and UPS work coordinately and inactivation or inhibition of UPS induces autophagy, but the reverse is not true and deficiency of autophagy eventuate in the accumulation of protein aggregates highlighting the importance of functional autophagy in degradation of protein aggregates (Bao, Gu, Ta, Wang, & Xu, 2016; Wang et al., 2019).

In this research, the aim was to determine the impact of defective autophagy mediated by dynein when combined with impaired proteasome system as secondary stress, on accumulation of the aggregation-prone proteins. Moreover, the two-hit hypothesis implicated in pathology of ALS was tested to check whether defective dynein causes cellular susceptibility in the cell, which when UPS is dysregulated results in protein accumulation. First, wild-type MEFs were utilized to simultaneously inhibit dynein and the 26S proteasome, using CilD and MG132, respectively. It has been shown that CilD by inhibiting dynein ATPase activity inhibits axonal transport and axon tension (Roossien, Miller, & Gallo, 2015). The primary MEFs were treated with 10 µM of MG132 and 50 µM of CilD for 6 hours. MEFs were also treated with MG132 and higher concentrations of CilD (60 and 100 µM) for 6 hours. The cells were analysed by performing immunocytochemistry. In the non-treated cells, p62 was diffusely distributed in the cytoplasm. Whereas, proteasome inhibition resulted in a significant accumulation of p62 in the cytoplasm (**Figure 4.6 A**). While MG132 treatment resulted in the formation of p62 puncta, simultaneous treatment with CilD increased the number of p62 puncta significantly as a result of deficient dynein-mediated autophagy pathway in the clearance of accumulated proteins. A one-way ANOVA was performed with Tukey's multiple comparison test. The one-way ANOVA showed a significant increase in number of p62

puncta between MG132-treated and MG132/CilD-treated MEFs (P = 0.0054, F = 9.961). Tukey's multiple comparison test showed a significant increase in number of p62 puncta between MG132-treated MEFs and MG132/CilD (50 μM)-treated MEFs (P = 0.0035), MG132-treated MEFs and MG132/CilD (60 μM)-treated MEFs (P = 0.0011), and MG132-treated MEFs and MG132/CilD (100 μM)-treated MEFs (P < 0.0001). However, increasing concentration of CilD (60 and 100 μM) did not exacerbate the p62 puncta upon MG132 treatment (**Figure 4.6 B**). Moreover, the one-way ANOVA showed a significant increase in size of p62 puncta between MG132-treated and MG132/CilD-treated MEFs (P = 0.0054, F = 4.551). Tukey's multiple comparison test showed a significant increase in size of p62 puncta between MG132-treated MEFs and MG132/CilD (60 μM)-treated MEFs (P = 0.0264), and MG132-treated MEFs and MG132/CilD (100 μM)-treated MEFs (P = 0.0474) (**Figure 4.6 C**). These results showed that defective autophagy due to the failure of dynein enhanced size of protein puncta and exacerbated cytoplasmic protein accumulation upon inhibition of proteasome system.

Figure 4.6

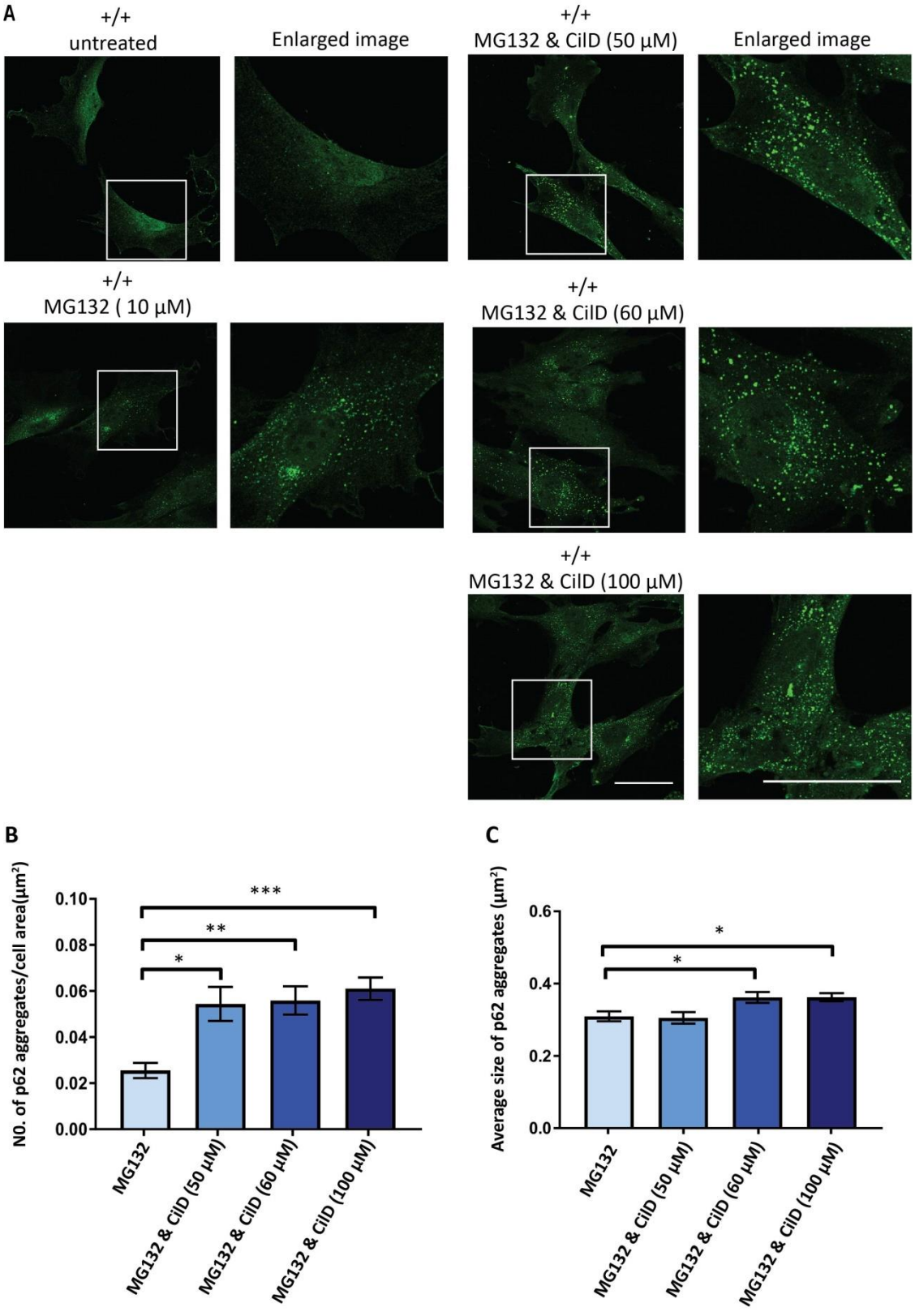
A
+/+
untreated
Enlarged image
+/+
MG132 & CilD (50 µM)
Enlarged image
+/+
MG132 (10 µM)
+/+
MG132 & CilD (60 µM)
+/+
MG132 & CilD (100 µM)
B
N0. of p62 aggregates/cell area(µm²)
0.10
0.08
0.06
0.04
0.02
0.00
***
**
*
MG132
MG132 & CilD (50 µM)
MG132 & CilD (60 µM)
MG132 & CilD (100 µM)
C
Average size of p62 aggregates (µm²)
0.6
0.4
0.2
0.0
*
*
MG132
MG132 & CilD (50 µM)
MG132 & CilD (60 µM)
MG132 & CilD (100 µM)

Figure 4.6 Co-inhibition of dynein and the proteasome pharmacologically increases p62 accumulation (**A**) Wild-type MEFs were treated with proteasome and dynein inhibitors (MG132, 10 μM, CilD, 50, 60 and 100 μM). Immunostaining was performed using anti-p62 antibody. The representative images are shown as maximum projections of Z-stacks of confocal images. Images were taken at 63 X magnification. The enlarged images are the boxed areas shown for better view of p62 puncta. Scale bar, 50 μm. (**B**) Data is presented as the mean ± SEM; where N > 80 cells per genotype, N = 3 biological repeats, and N = 3 technical repeats for each genotype. For all experiments, quantification was performed in at least 30 images per genotype. A one-way ANOVA showed a significant difference in number of p62 puncta between MG132-treated and MG132/CilD-treated wild-type MEFs (**** $P < 0.0001$, F (3, 61) = 9.961). Tukey's multiple comparison test showed a significant increase in this measurement in MEFs co-treated with MG132/CilD (50 μM) (** $P < 0.0035$), MG132/CilD (60 μM) (** $P = 0.0011$), and MG132/CilD (100 μM) (**** $P < 0.0001$) compared to the MEFs treated with MG132. (**C**) Data is presented as the mean ± SEM; where N > 80 cells per genotype, N = 3 biological repeats, and N = 3 technical repeats for each genotype. (**C**) A one-way ANOVA showed a significant difference in size of p62 puncta between MG132-treated and MG132/CilD- treated wild-type MEFs (** $P = 0.0054$, F (3, 78) = 4.551). Tukey's multiple comparison test shows a significant increase in this measurement in MEFs co-treated with MG132/CilD (60 μM) (* $P = 0.0264$), MG132/CilD (100 μM) (* $P = 0.0474$) compared to the MEFs treated with MG132.

4.2.7 TBK1 inhibition or knockdown increases the number and size of MG132-induced p62 puncta in Loa^{Hom} MEFs

Based on our results showing that dynein inhibition upon proteasome inhibition exacerbates the accumulation of protein, the aim was to establish how TBK1 inhibition or knockdown in combination with dynein deficiency upon proteasome inhibition alters protein accumulation. As phosphorylation of p62 by TBK1 is critical for recruitment of ubiquitinated proteins into the autophagosomes for degradation, deficiency of TBK1 results in accumulation of p62-positive puncta. To test how disturbance in TBK1 function caused by TBK1 inhibitor in mutant dynein fibroblasts upon proteasome inhibition impacts the protein puncta, the wild-type and Loa^{Hom} MEFs were treated with proteasome inhibitor (MG132, 10 µM) and TBK1 inhibitor (BX795, 10 µM) simultaneously. After cell fixation, the immunostaining was performed using anti- p62 antibody. Quantifications of p62 puncta in wild-type MEFs co-treated with TBK1 and proteasome inhibitors demonstrated a slight increase in the number of p62 puncta in the wild-type MEFs (**Figure 4.7 A, right column, third row**). While a significant increase in the number of p62 puncta upon proteasome and TBK1 inhibition was detected in the Loa^{Hom} MEFs. These results suggest that inhibition of TBK1 affecting recruitment of ubiquitinated proteins into the autophagosome combined with deficiency of dynein in Loa^{Hom} MEFs following proteasome inhibition exacerbated p62-positive puncta (**Figure 4.7 A, left column third row**). After quantification of number of p62 puncta, a two-way ANOVA was carried out to determine the effect of MG132/BX795 treatment and genotype on the number of p62 puncta (N > 100 number of cells per genotype). The results showed that there was a significant interaction between MG132/BX795 treatment and genotype (P = 0.0122, F = 4.925), indicating that effect of MG132/BX795 treatment on p62 puncta is dependent on the genotype (**Figure 4.7 B**). Furthermore, there was a significant main effect of MG132/BX795 treatment (P = 0.0034, F = 7.219) and a significant main effect of genotype (P = 0.0002, F =19.54) on number of p62 puncta. Moreover, the quantification of the size of puncta revealed that concurrent inhibition of TBK1 and proteasome increased the size

of puncta across the genotype checked. However, the p62 puncta formed in Loa^{Hom} MEFs co-treated with the proteasome and TBK1 inhibitors were distinct and more extensive compared to those in wild-type MEFs. A two-way ANOVA showed that there was not a significant interaction between MG132/BX795 treatment and genotype (P = 0.8635, F = 0.029) on the size of p62 puncta. However, there was a significant main effect of MG132/BX795 treatment (P < 0.0001, F = 33.38) and a significant main effect of genotype (P < 0.0001, F = 24.03) on size of p62 puncta (**Figure 4.7 C**).

For the further validation of results obtained from inhibition of TBK1 and proteasome system and to confirm that vulnerability of Loa^{Hom} MEFs in combination with of TBK1 deficiency results in exacerbation of p62 puncta, the wild-type and Loa^{Hom} MEFs were transfected with Scr-shRNA and TBK1-shRNA. After 42 hours, cells were treated with MG132 (10 µM) for 6 hours. They were then fixed, and immunocytochemistry was performed and analysed the images obtained from confocal microscopy.

In agreement with the previous results, quantification of the number of p62-positive puncta showed a significant increase in number of p62 in TBK1-shRNA transfected Loa^{Hom} MEFs treated with proteasome inhibitors. After quantification of number of p62 puncta, a two-way ANOVA was carried out to determine the effect of TBK1 knockdown/MG132 treatment and genotype on the number of p62 puncta (N > 100 number of cells per genotype) (**Figure 4.7 D**). The results showed that there was a significant interaction between TBK1 knockdown/MG132 treatment and genotype (P = 0.0492, F = 4.44), indicating that effect of TBK1 knockdown/MG132 treatment on p62 accumulation is dependent on the genotype. This increase in number of p62-positive aggregates was significantly higher in the Loa^{Hom} when compared with the wild-type MEFs, demonstrating that the dynein mutation increases the vulnerability of primary MEFs to any perturbation in the autophagy-lysosome degradation pathway. Furthermore, there was a significant main effect of TBK1 knockdown/MG132 treatment (P = 0.0277, F = 5.74) and a significant main effect of genotype (P < 0.0001, F = 74.68) on number of p62 puncta (**Figure 4.7 E**).

Moreover, the quantification of the size of puncta revealed that concurrent TBK1 knockdown and MG132 treatment increased the size of puncta across the genotype. However, the p62 puncta formed in Loa^{Hom} MEFs transfected with TBK1-shRNA and treated with MG132 were distinct and more extensive compared to those in wild-type MEFs. A two-way ANOVA showed that there was not a significant interaction between TBK1-knockdown/BX795 treatment and genotype (P = 0.9832, F = 0.0004) on the size of p62 puncta. However, there was a significant main effect of TBK1-knockdown/MG132 treatment (P = 0.0002, F = 17.05) and a significant main effect of genotype (P = 0.0001, F = 17.83) on size of p62 puncta (**Figure 4.7 F**).

Together, these data suggest that cells under normal condition through the activation of compensatory mechanisms such as chaperons tolerate the deficiencies of autophagy through promoting the solubility of proteins and aggregate formation. However, cells with deficiencies in dynein and another protein component of the autophagy process might fail to tolerate double hit, leading to the protein accumulation that cannot be cleared and finally leading to cell death.

Figure 4.7

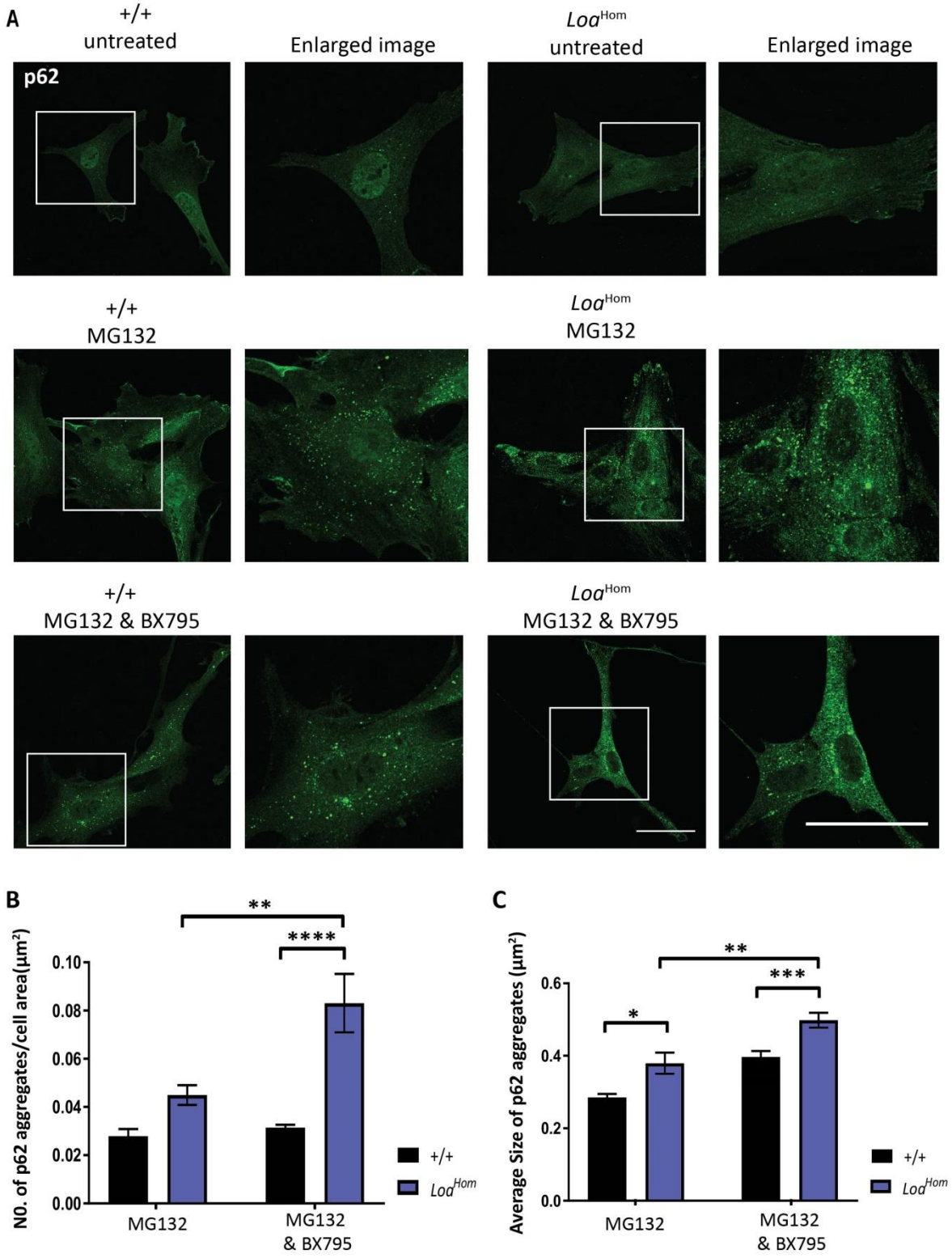
A
+/+
untreated
Enlarged image
Loa Hom
untreated
Enlarged image
p62
+/+
MG132
Loa Hom
MG132
+/+
MG132 & BX795
Loa Hom
MG132 & BX795
B
NO. of p62 aggregates/cell area(μm²)
0.10
0.08
0.06
0.04
0.02
0.00
**
****
MG132
MG132
& BX795
+/+
Loa Hom
C
Average Size of p62 aggregates (μm²)
0.6
0.4
0.2
0.0
**
***
*
MG132
MG132
& BX795
+/+
Loa Hom

Figure 4.7 continued

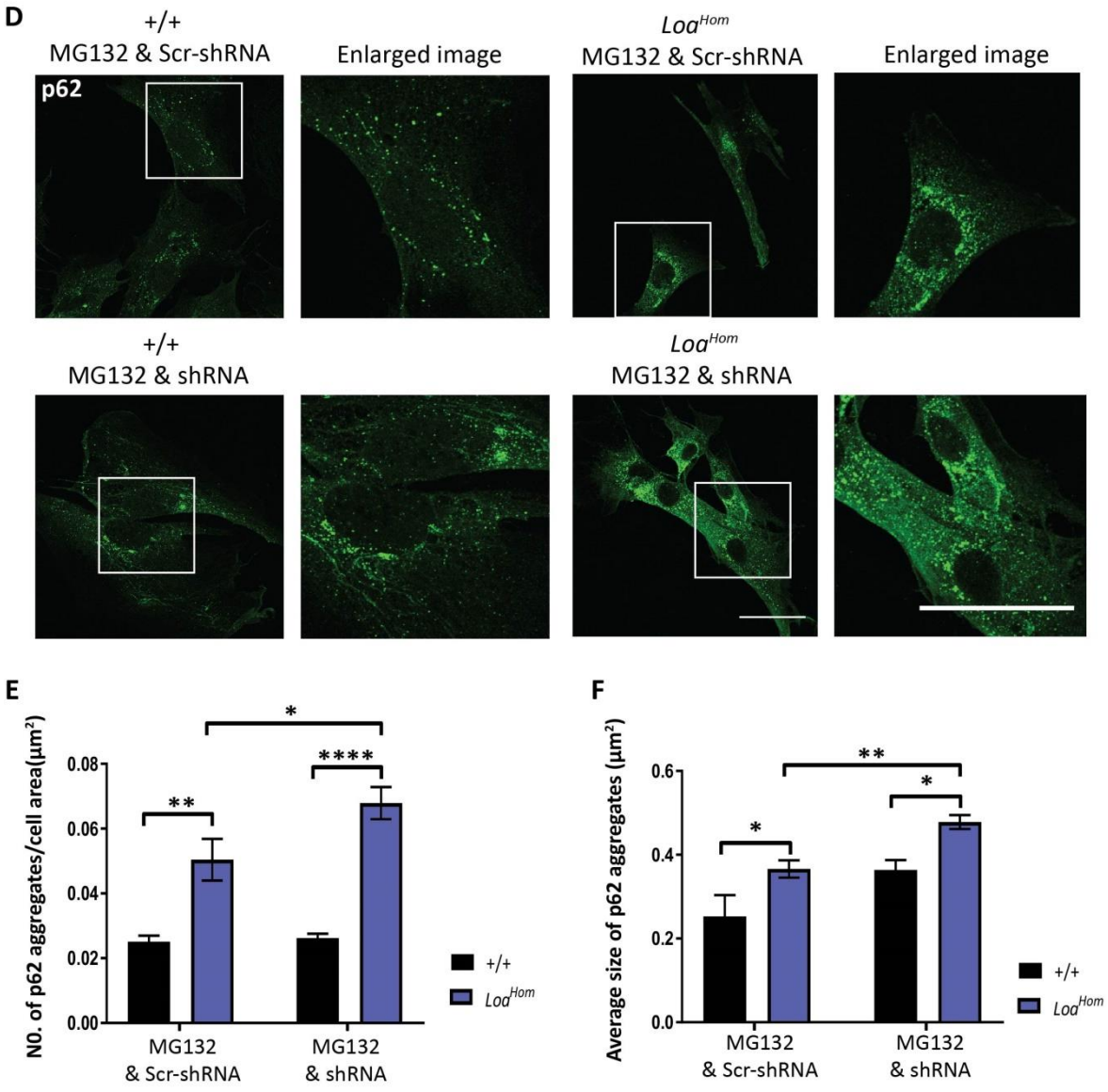

Figure 4.7 TBK1 knockdown or inhibition increases number and size of p62 puncta upon proteasome inhibition. (**A**) Wild-type and Loa^{Hom} MEFs were treated with proteasome and TBK1 inhibitors (MG132, 10 µM, BX795, 10 µM, respectively). Immunostaining was performed using anti-p62 antibody. The representative images are shown as maximum projections of Z-stacks of confocal images. Images were taken at 63 X magnification. The enlarged images are boxed areas shown for the better view of p62 puncta. Scale bar, 50 µm. (**B**) Data is presented as the mean ± SEM; where N > 100, number of cells, N = 3 biological repeats, and N = 3 technical repeats for each genotype. For all experiments, quantification was performed in at least 30 images per genotype. A two-way ANOVA showed significant interaction between genotype and MG132/BX795 treatment (* $P = 0.0122$, F (1, 64) = 4.92) on number of p62 puncta followed by Tukey's post-test. Moreover, there were significant main effects of MG132/BX795 treatment and genotype on number of p62 puncta (** $P < 0.0034$, F (1, 64) = 7.219 and ** $P = 0.0002$, F (1, 64) = 19.54 respectively). (**C**) Data is presented as the mean ± SEM; where N > 100, number of cells, N = 3 biological repeats, and N = 3 technical repeats for each genotype. A two-way ANOVA showed no significant interaction between genotype and MG132/BX795 treatment ($P = 0.8635$ F (1, 67) = 0.029) on size of p62 puncta followed by Tukey's post-test. Additionally, there were significant main effects of MG132/BX795 treatment and genotype on size of p62 puncta (**** $P < 0.0001$, F (1, 67) = 33.38 and **** $P < 0.0001$, F (1, 67) = 24.03 respectively). (**D**) Wild-type and Loa^{Hom} MEFs were transfected with Scr-shRNA and TBK1-shRNA followed by proteasome inhibitor treatment. Immunostaining was performed using anti-p62 antibody. The representative images are shown as maximum projections of Z-stacks of confocal images. Images were taken at 63 X magnification. The enlarged images are boxed areas shown for the better view of p62 puncta. Scale bar, 50 µm. (**E**) Data is presented as the mean ± SEM; where N > 100 number of cells, N = 3 biological repeats, and N = 6 technical repeats for each genotype. A two-way ANOVA showed significant interaction between genotype and TBK1 knockdown/MG132 treatment (* $P = 0.0492$, F (1, 18) = 4.44) followed by Tukey's post-test. There were significant main effects of TBK1 knockdown/MG132 treatment and genotype on number of p62 puncta (* $P = 0.0277$, F (1, 18) = 5.74 and **** $P < 0.0001$, F (1, 18) = 74.68 respectively). (**F)** Data is presented as the mean ± SEM; where N > 100 number of cells, N = 3 biological repeats, and N = 3 technical repeats for each genotype. A two-way ANOVA showed no significant interaction between genotype and TBK1 knockdown/MG132 treatment ($P = 0.9832$, F (1, 38) = 0.0004) on size of p62 puncta followed by Tukey's post-test. Additionally, there were significant main effects of TBK1 knockdown/MG132 treatment and genotype on size of p62 puncta (*** $P = 0.0002$, F (1, 38) = 17.05 and *** $P = 0.0001$, F (1, 38) = 17.83 respectively).

4.2.8 Summary

In this chapter, it was shown that D338N^{Het}, R399G^{Hom} fibroblasts and Loa^{Hom} MEFs impact the level of LC3II differentially, suggesting that the location of point mutation contributing to conformational changes, which affect the dynein function and its contribution to level of LC3II distinctively. Moreover, it was shown that combined defects in the key autophagy proteins such as dynein and TBK1 resulted in enhanced formation of protein aggregates. Furthermore, the results obtained in this research supported the two-hit hypothesis contributing to the ALS pathology. At the first step, mutant dynein on its own is not enough to induce protein accumulation. However, exposure to a second detrimental insult such as inhibition or knockdown of TBK1 leads to a significant accumulation of protein, a hallmark of ALS. The cellular susceptibility also was supported by partial inhibition of dynein leading to significant increase in p62-positive puncta. Moreover, deficiencies in autophagy-related proteins such as TBK1 and dynein following inhibition of the proteasome system enhanced formation of protein puncta in Loa^{Hom} MEFs support the two-hit hypothesis contributing to the pathogenesis of ALS.

Chapter 5: Effect of the *Loa* *DYNC1H1* mutation on cytoplasmic mislocalisation of TDP-43 linked to inhibition or knockdown of TBK1

5.1 Introduction

TDP-43, an RNA/DNA binding protein, is mainly localised in the nucleus but also shuttles to the cytoplasm for some of its cellular functions (Ayala et al., 2008). Importantly, TDP-43 has been identified as a key component of cytoplasmic inclusions in neurodegenerative disease such as ALS (Neumann et al., 2006). In ALS, mislocalisation of the RNA-binding protein TDP-43 is highly conserved and recognised as a contributor to the susceptibility of MNs (Weskamp et al., 2020). Moreover, the cytoplasmic mislocalisation of mutant TDP-43 and formation of aggregates have been reported to lead to a toxic gain of function or a loss of TDP-43 function (Barmada et al., 2010; Polymenidou et al., 2011). Although the effects of TDP-43 aggregates have been studied from different aspects, the underlying mechanisms for TDP-43 mislocalisation remain to be examined**.**

Importantly, an oligogenic basis and two-hit hypothesis have been suggested contributing to the pathogenetic mechanisms in fALS and sALS respectively. In two-hit hypothesis, deficiencies of more than one factor contribute to the pathogenesis of ALS. In this model, dysfunction of one factor causes susceptibility and presence of second deleterious event or second hit leads to disease pathogenesis (Pesiridis, Tripathy, Tanik, Trojanowski, & Lee, 2011; Renton et al., 2014).

Furthermore, the stress response mechanisms, including the formation of SGs, are among the mechanisms contributing to neurodegeneration. SGs are composed of RNA and proteins formed when translation initiation is inhibited to reduce stress-related damage and promote cell survival. SGs are dynamic intracellular structures, which degrade after removal of stressor. Degradation of SGs is highly regulated through various mechanisms including autophagy that plays a key role in the elimination of SGs (Buchan et al., 2013; Wheeler et al., 2016). Importantly, disruptions in protein degradation processes result in prolonged persistence of SG in the cytoplasm leading to intractable aggregates and cell death (Guerrero et al., 2016; Khalfallah et al., 2018). Interestingly, dynein is involved in both formation of SGs and autophagy-dependent clearance of SGs; however, there is little evidence about dynein function in autophagy contributing to SGs dynamics.

This work was aimed to investigate whether dynein dysfunction under specific conditions is capable of altering the localisation of TDP-43 and exploring potential effects of dynein deficiency on the dynamics of SGs. In line with the multi-hit hypothesis of ALS, I hypothesised that dynein dysfunction renders cells more susceptible to any genetic defect or cellular insult leading to TDP-43 mislocalisation. Moreover, based on significant role of dynein in SG dynamic, it was hypothesised that deficiency of dynein function might modulate the dynamics of SGs by hampering disassembly of SGs with cumulative effect on protein aggregation over course of time or when exposed to environmental stress, contributing to the pathogenesis of ALS.

5.2 Results

5.2.1 Inhibition of TBK1 in Loa^{Hom} MEFs leads to mislocalisation of TDP-43

To obtain a better insight in TDP-43 pathogenesis, a major pathological protein in ALS, identification of pathways and factors that could contribute to the mislocalisation and aggregation of TDP-43 and its neurotoxicity is critical. Of note, TBK1 mutation or loss of function has been implicated in multiple neurodegenerative diseases, particularly in ALS (Gijselinck et al., 2015; Herman et al., 2012; Oakes et al., 2017). Recently, it has been reported that TBK1 regulates and induces autophagic degradation of TDP-43 (Foster et al., 2020).

Based on the two-hit hypothesis, it was aimed to test whether deficiency in dynein coupled with inhibition of TBK1 kinase activity, lead to TDP-43 pathology.

To investigate this, the wild-type and Loa^{Hom} MEFs were plated in 6-well plate and treated with TBK1 inhibitor (BX795, 10 µM) for 6 hours. Then, cells were fixed with 4 % formaldehyde and immunostained with anti-TDP-43 antibody and processed for confocal microscopy. Concordant with the mainly nuclear localisation of TDP-43, immunostaining by anti-TDP-43 antibody showed a similar diffused cytoplasmic staining with distinct localisation in the nucleus in vehicle-treated MEFs (**Figure 5.1 A, top two rows**). In contrast, the TDP-43 intensity in wild-type and Loa^{Hom} MEFs treated with TBK1 inhibitor showed cytoplasmic mislocalisation of TDP-43 in Loa^{Hom} MEFs but not in wild-type MEFs (**Figure 5.1 A, bottom two rows**) suggesting that dynein deficiency by itself is not sufficient for TDP-43 mislocalisation; however, coupled with TBK1 deficiency impacts TDP-43 localisation. After quantification of cytoplasmic and nuclear TDP-43 intensity, a two-way ANOVA was carried out to determine the effect of BX795 treatment and genotype on the localisation of TDP-43 (N > 80 number of cells per genotype). The results showed that there was a significant interaction between BX795 treatment and genotype (P = 0.0453, F = 4.104), indicating that the effect of BX795 on the cytoplasmic TDP-43 mislocalisation is

dependent on the genotype. Moreover, there was a significant main effect of BX795 treatment ($P < 0.0001$, F = 23.99) and a significant main effect of genotype ($P = 0.0239$, F = 5.253) on cytoplasmic TDP-43 mislocalisation (**Figure 5.1 B**). Moreover, quantification of nuclear TDP-43 showed that there was a significant interaction between BX795 treatment and genotype ($P = 0.0453$, F = 4.104). Furthermore, there were significant main effects of BX795 treatment ($P < 0.0001$, F = 23.99) and genotype ($P = 0.0239$, F = 5.253) on nuclear TDP-43 (**Figure 5.1 C**). Figure 5.1 D demonstrates the alterations in the proportion of cytoplasmic TDP-43 to nuclear TDP-43 before and after treatment with BX795.

Figure 5.1

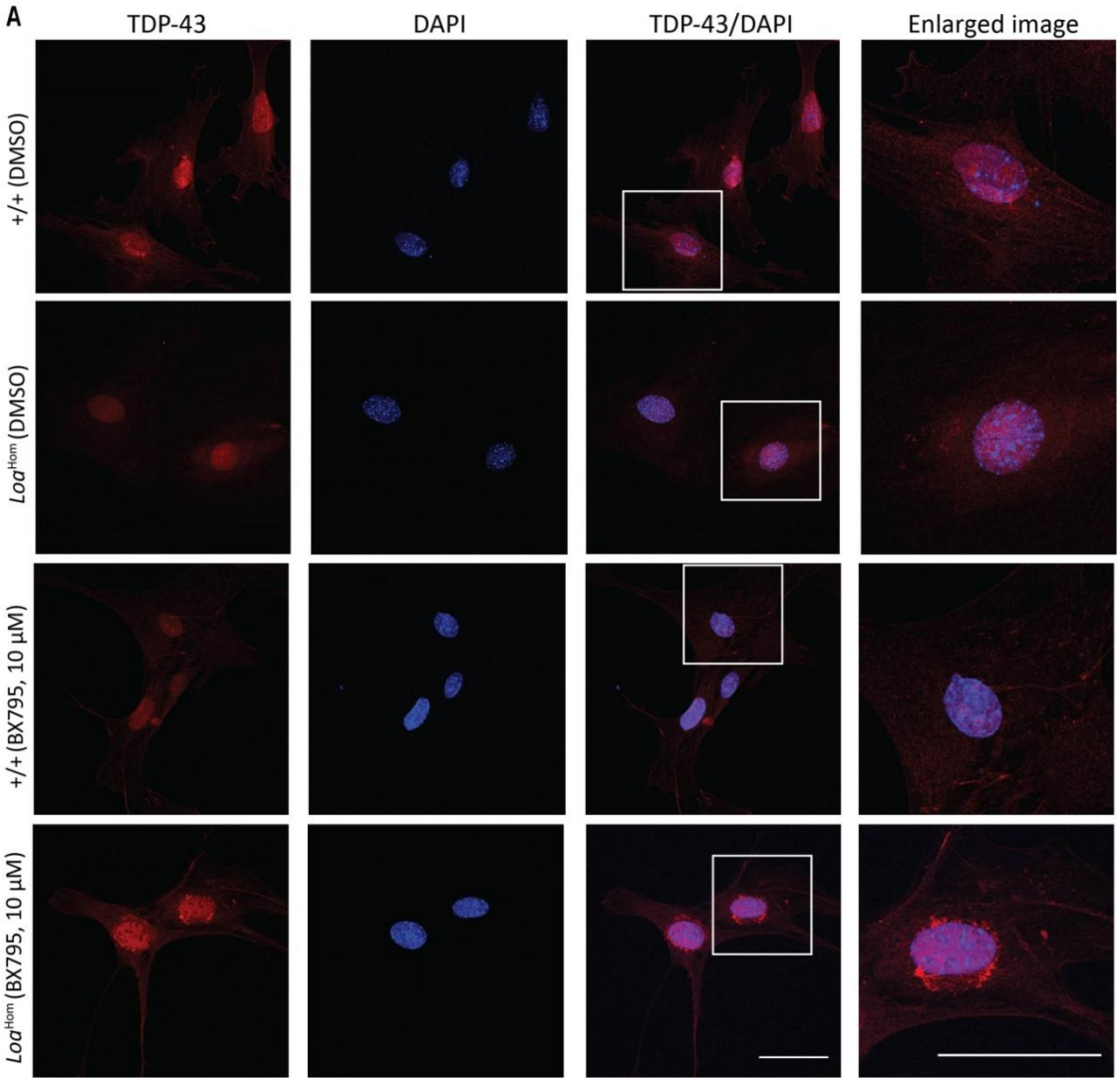

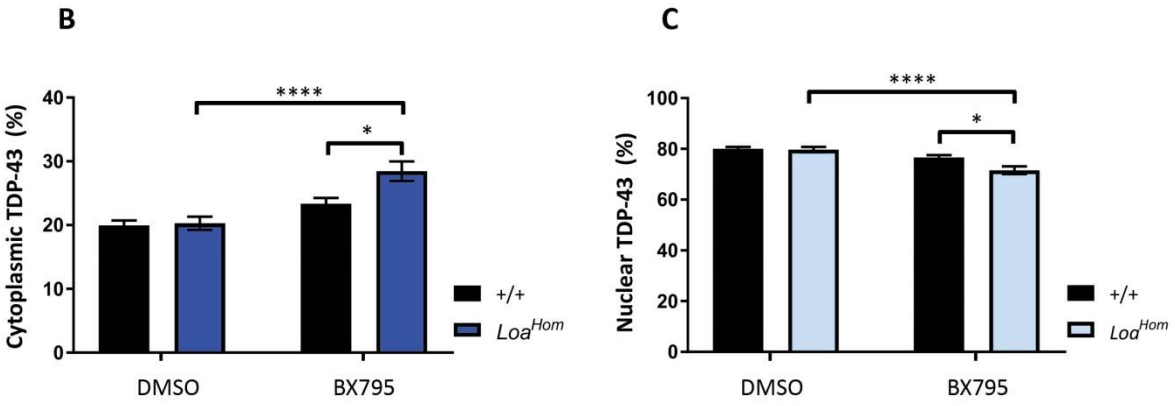
B
Cytoplasmic TDP-43 (%)
40
30
20
10
0
****
*
DMSO
BX795
+/+
Loa^Hom
C
Nuclear TDP-43 (%)
100
80
60
40
20
0
****
*
DMSO
BX795
+/+
Loa^Hom

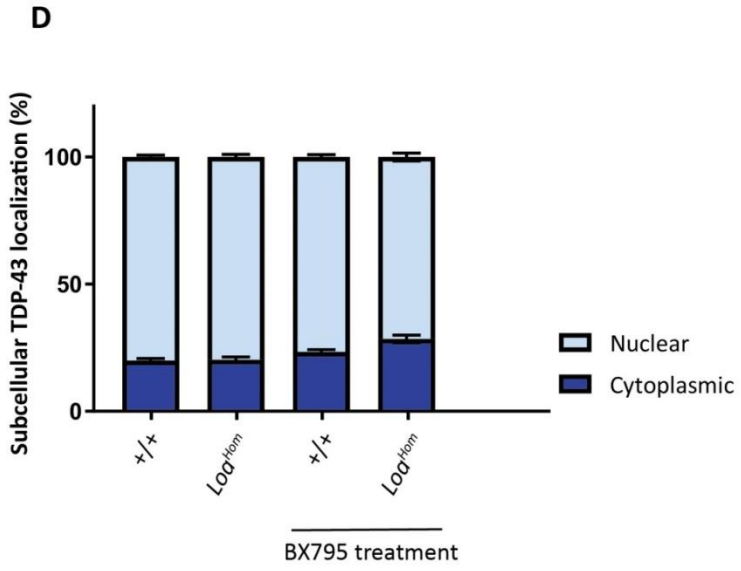
D
Subcellular TDP-43 localization (%)
100
50
0
+/+
Loa^Hom
+/+
Loa^Hom
BX795 treatment
Nuclear
Cytoplasmic

Figure 5.1 TBK1 inhibition leads to TDP-43 mislocalisation in primary Loa^{Hom} MEFs. (**A**) Primary MEFs were treated with vehicle (DMSO) or TBK1 inhibitor (BX795) and then stained with anti-TDP-43 antibody to assess its subcellular distribution, and DAPI for nuclear staining. TDP-43 localises mainly to the nucleus upon treatment with DMSO. In contrast, BX795 treatment induces cytoplasmic accumulation of TDP-43 in Loa^{Hom} MEFs. Representative images are shown. The enlarged images are the boxed areas shown for better view. Scale bar, 50 µm. (**B**) Data is presented as the mean ± SEM; where N > 80 number of cells per genotype, N = 3 biological repeats, and N = 3 technical repeats for each genotype. For this experiment, quantification was performed in at least 30 images per genotype. A two-way ANOVA showed significant interaction between genotype and BX795 treatment (* P = 0.0453, F (1, 104) = 4.104) followed by Tukey's post-test. Additionally, there were significant main effects of BX795 treatment and genotype on cytoplasmic TDP-43 (**** P < 0.0239, F (1, 104) = 23.99 and * P = 0.0019, F (1, 104) = 5.25 respectively). (**C**) Data is presented as the mean ± SEM; where N > 80 number of cells per genotype, N = 3 biological repeats, and N = 3 technical repeats for each genotype. A two-way ANOVA showed significant interaction between genotype and BX795 treatment (* P = 0.0453, F (1, 104) = 4.104) followed by Tukey's post-test. There were significant main effects of BX795 treatment and genotype on nuclear TDP-43 (**** P < 0.0239, F (1, 104) = 23.99 and * P = 0.0019, F (1, 104) = 5.25 respectively). (**D**) The ratio of fluorescence intensities of nuclear TDP-43 (light blue) versus cytoplasmic TDP-43 (dark blue) in the primary MEFs untreated or treated with BX795.

5.2.2 Knockdown of TBK1 causes TDP-43 mislocalisation in Loa^{Hom} MEFs

Aforementioned, pharmacological inhibition of TBK1 resulted in the TDP-43 mislocalisation in Loa^{Hom} MEFs. Based on those results, it was aimed to investigate if TBK1-knockdown in combination with dynein dysfunction impacts localisation of TDP-43. As pharmacological inhibitor of TBK1 might potentially affect other enzymes unrelated to the autophagy, knockdown of TBK1 using shRNA decreases level of TBK1 more specifically. To test this, both wild-type and Loa^{Hom} MEFs were transfected with Scr-shRNA or TBK1-shRNA. After 48 hours, cells were fixed with 4 % formaldehyde, and then immunofluorescent staining was performed, which proceeded to the confocal microscopy. For the analysis of TDP-43 mislocalisation, the intensity of cytoplasmic and nuclear TDP-43 staining was quantified in confocal images.

ShRNA knockdown of TBK1 induced cytoplasmic mislocalisation of TDP-43 in Loa^{Hom} MEFs but not in wild-type MEFs, where TDP-43 remained localised in the nucleus after TBK1-knockdown (**Figure 5.2 A**). Collectively, these data corroborated results of previous experiment showing aberrant mislocalisation of TDP-43 in the cytoplasm following TBK1 inhibition in Loa^{Hom} MEFs. Therefore, inhibition of TBK1 activity or loss of TBK1 function in MEFs coupled with impaired function of dynein caused cytoplasmic mislocalisation of TDP-43. A two-way ANOVA was carried out to ascertain the effect of genotype and the TBK1-knockdown on the level of TDP-43 (N > 80). The results showed a significant interaction between the effect of genotype and TBK1-knockdown on the cytoplasmic TDP-43 (P = 0.0001, F = 16.66). Furthermore, both TBK1 knockdown (P = 0.0001, F = 40.37) and genotype (P = 0.0001, F = 23.38) had a significant main effect on cytoplasmic TDP-43 (**Figure 5.2 B**). Moreover, the statistical analysis revealed a significant interaction between the effect of genotype and TBK1 knockdown on the nuclear TDP-43 (P = 0.0001, F = 5.909) and both TBK1 knockdown (P = 0.0001, F = 17) and genotype (P = 0.0001, F = 9.12) had a significant main effect on nuclear TDP-43 (**Figure 5.2 C**). Figure 5.3 D demonstrates the alterations in the proportion of cytoplasmic TDP-43 versus nuclear TDP-43 before and after knockdown of TBK1.

Figure 5.2

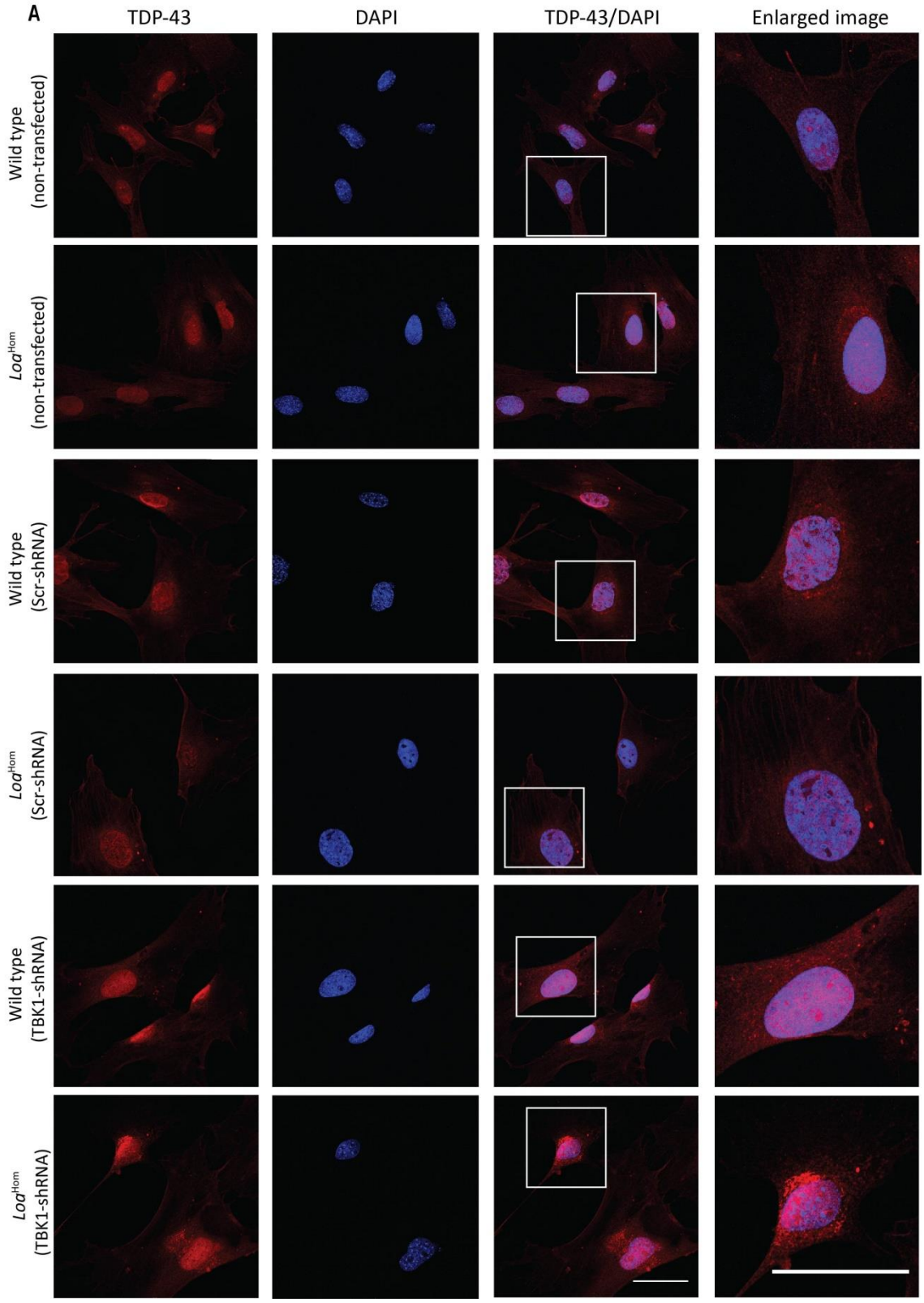
A
TDP-43
DAPI
TDP-43/DAPI
Enlarged image
Wild type (non-transfected)
Loa^Hom (non-transfected)
Wild type (Scr-shRNA)
Loa^Hom (Scr-shRNA)
Wild type (TBK1-shRNA)
Loa^Hom (TBK1-shRNA)

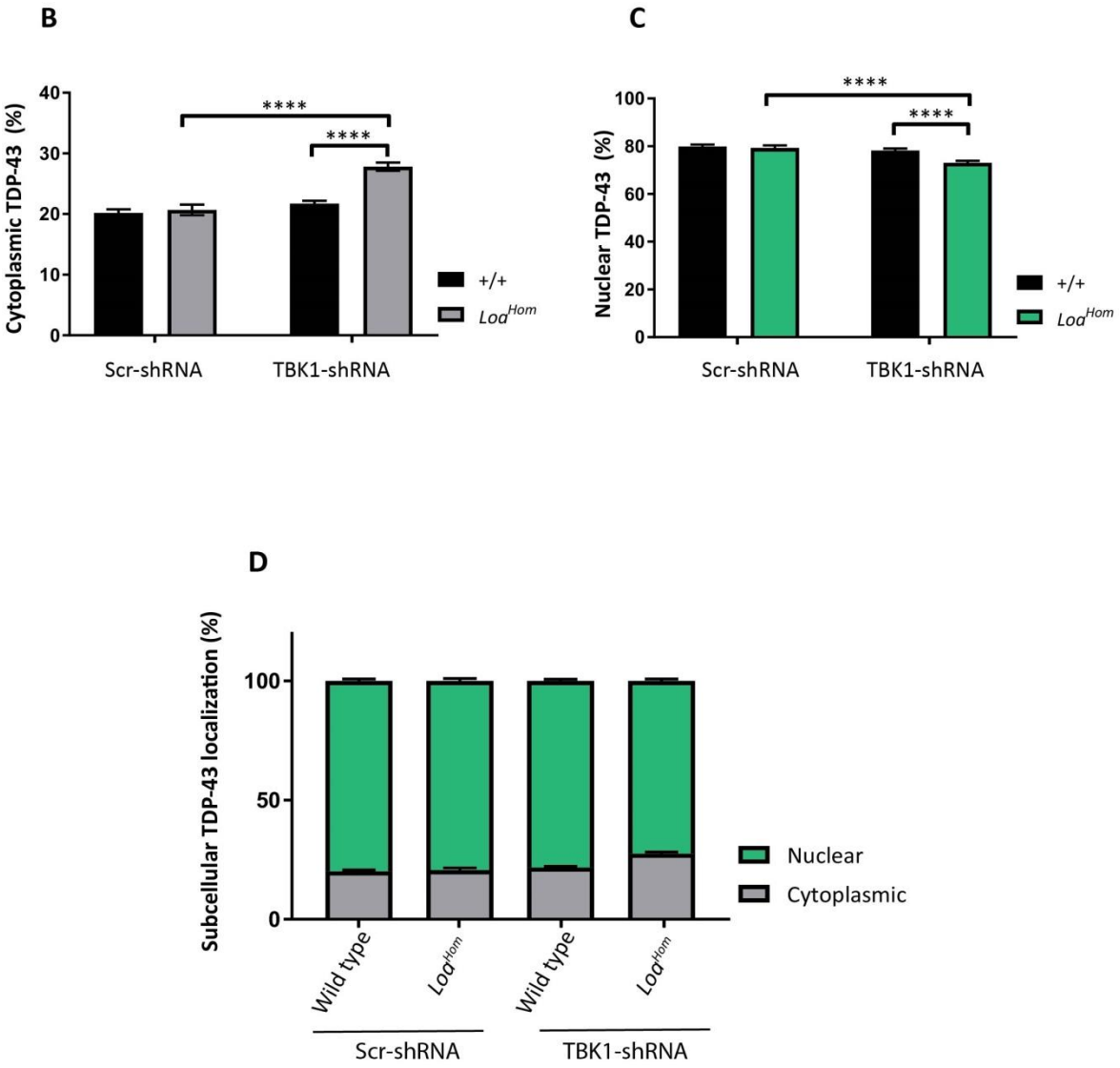
B
Cytoplasmic TDP-43 (%)
40
30
20
10
0
****
****
+/+
Loa^Hom
Scr-shRNA
TBK1-shRNA
C
Nuclear TDP-43 (%)
100
80
60
40
20
0
****
****
+/+
Loa^Hom
Scr-shRNA
TBK1-shRNA
D
Subcellular TDP-43 localization (%)
100
50
0
Nuclear
Cytoplasmic
Wild type
Loa^Hom
Wild type
Loa^Hom
Scr-shRNA
TBK1-shRNA

Figure 5.2 TBK1 knockdown results in mislocalisation of TDP-43 in Loa^{Hom} MEFs. (**A**) Primary MEFs were transfected with Scr-shRNA and TBK1-shRNA, and then stained with anti-TDP-43 antibody to assess its subcellular distribution, and DAPI for nuclear staining. TDP-43 localises mainly to the nucleus upon treatment with DMSO. In contrast, TBK1 knockdown induces TDP-43 mislocalisation in Loa^{Hom} MEFs but not wild-type MEFs. Representative images are shown. The enlarged images are the boxed areas shown for better view. Scale bar, 50 µm. (**B**) Data is presented as the mean ± SEM; where N > 80 number of cells per genotype, N = 3 biological repeats, and N = 3 technical repeats for each genotype. For this experiment, quantification was performed in at least 30 images per genotype. Two-way ANOVA showed significant interaction between genotype and TBK1 knockdown (**** P = 0.0001, F (1, 88) = 16.6) followed by Tukey's post-test. There were significant main effects of knockdown and genotype on cytoplasmic TDP-43 (**** P = 0.0001, F (1, 88) = 40.37 and **** P = 0.0001, F (1, 88) = 23.38 respectively). (**C**) Data is presented as the mean ± SEM; where N > 100 number of cells per genotype, N = 3 biological repeats, and N = 3 technical repeats for each genotype. Two-way ANOVA showed significant interaction between genotype and TBK1 knockdown on nuclear TDP-43 (**** P = 0.0001, F (1, 83) = 5.909) followed by Tukey's post-test. Additionally, there were significant main effects of knockdown and genotype (**** P = 0.0001, F (1, 83) = 17 and **** P = 0.0001, F (1, 83) = 9.12 respectively). (**D**) The ratio of fluorescence intensities of nuclear TDP-43 (green) versus cytoplasmic TDP-43 (gray) in the primary MEFs transfected with Scr-shRNA or TBK1-shRNA.

5.2.3 The normal cytoplasmic localisation of TDP-43 is disrupted in wild-type and Loa^{Hom} MEFs treated with dynein inhibitor

Our data elucidated mislocalisation of TDP-43 in Loa^{Hom} MEFs upon modification of TBK1 function either pharmacologically or genetically, suggesting the vulnerability of Loa^{Hom} MEFs to the second hit.

Based on these data, it was aimed to further interrogate the potential involvement of motor activity of dynein in the localisation of TDP-43 and assess whether inhibition of ATPase activity of dynein by itself could impact the TDP-43 localisation. To test this, the wild-type and Loa^{Hom} MEFs were treated with CilD (CilD, 50 µM) for 6 hours. After treatments, cells were fixed with 4 % formaldehyde and then stained with anti-TDP-43 antibody. The images were taken with the confocal microscope and the results obtained from two independent biological replicates.

It was found that dynein inhibition resulted in TDP-43 mislocalisation both in wild-type and Loa^{Hom} MEFs. However, the dynein inhibition led to a higher level of mislocalisation in Loa^{Hom} MEFs in comparison to the wild-type counterpart, which may suggest that dynein deficiency caused by the *Loa* mutation in the tail domain of *Dync1h*1 by its own was not sufficient to cause TDP-43 mislocalisation; however, CilD inhibition of the ATPase activity of dynein in the motor domain of dynein heavy chain resulted in mislocalisation of TDP-43 (**Figure 5.3 A**). A two-way ANOVA was carried out to determine the effect of genotype and the CilD treatment on the level of TDP-43 (N > 100 number of cells per genotype). The results showed a significant interaction between the effect of genotype (wild-type or Loa^{Hom}) and CilD treatment on the cytoplasmic TDP-43 (P = 0.0295, F = 4.443). Furthermore, both genotype (P = 0.0126, F = 28.36) and CilD treatment (P < 0.0001, F = 5.98) had significant main effect on cytoplasmic TDP-43 (**Figure 5.3 B**).

Moreover, quantification of nuclear TDP-43 showed a significant interaction between the effect of genotype and CilD treatment (P = 0.0295, F = 4.906) with both CilD treatment (P < 0.0001, F = 26.64) and genotype (P = 0.0126, F = 5.98) having significant main effect on

nuclear TDP-43 (**Figure 5.3 C**). Figure 5.4 D demonstrates the alterations in the proportion of cytoplasmic TDP-43 versus nuclear TDP-43 before and after inhibition of dynein motor activity.

Figure 5.3

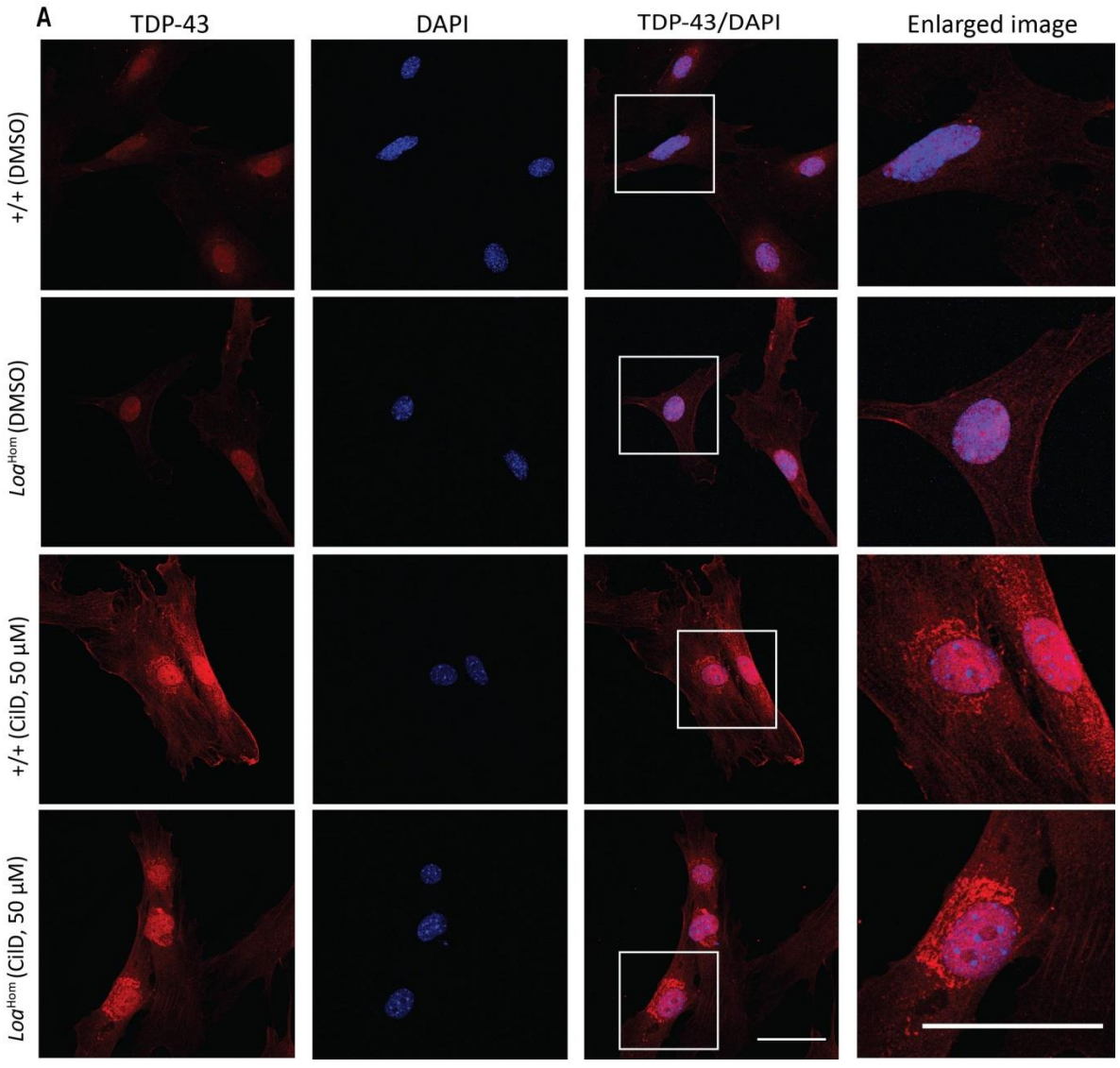

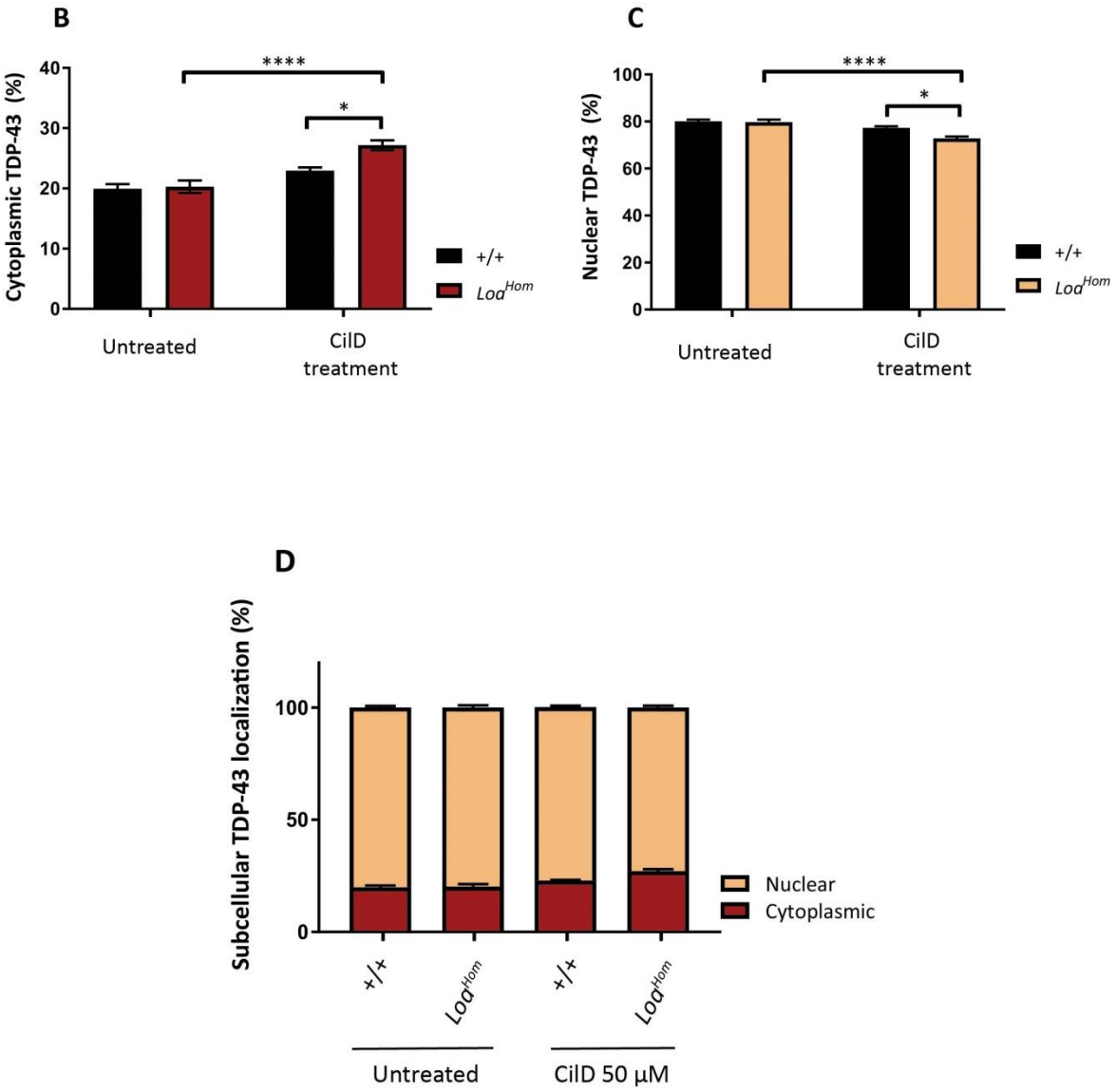
B
Cytoplasmic TDP-43 (%)
40
30
20
10
0
****
*
+/+
Loa^Hom
Untreated
CilD
treatment
C
Nuclear TDP-43 (%)
100
80
60
40
20
0
****
*
+/+
Loa^Hom
Untreated
CilD
treatment
D
Subcellular TDP-43 localization (%)
100
50
0
Nuclear
Cytoplasmic
+/+
Loa^Hom
+/+
Loa^Hom
Untreated
CilD 50 µM

Figure 5.3 Dynein inhibition leads to a higher level of TDP-43 mislocalisation in Loa^{Hom} MEFs. (**A**) Primary MEFs were treated with dynein inhibitor (CilD, 50 µM), and then stained with anti-TDP-43 antibody to assess its subcellular distribution, and DAPI for nuclear staining. TDP-43 localises mainly to the nucleus upon treatment with DMSO. In contrast, dynein inhibition causes cytoplasmic accumulation of TDP-43 in wild-type and Loa^{Hom} MEFs, while the mislocalisation in Loa^{Hom} MEFs is more significant. Representative images are shown. The enlarged images are the boxed areas shown for better view. Scale bar, 50 µm. (**B**) Data is presented as the mean ± SEM; where N > 80 number of cells per genotype, N = 3 biological repeats, and N = 3 technical repeats for each genotype. For this experiment, quantification was performed in at least 30 images per genotype. Two-way ANOVA showed significant interaction between genotype and CilD treatment (* P = 0.029, F (1, 82) = 4.443) followed by Tukey's post-test. Additionally, there were significant main effects of treatment and genotype on cytoplasmic TDP-43 (**** P < 0.0001, F (1, 82) = 28.36 and * P = 0.0126, F (1, 82) = 5.98 respectively). (**C**) Data is presented as the mean ± SEM; where N > 80 number of cells per genotype, N = 3 biological repeats, and N = 6 technical repeats for each genotype. Two-way ANOVA showed significant interaction between genotype and CilD treatment (* P = 0.0295, F (1, 82) = 4.906) followed by Tukey's post-test. There were significant main effects of CilD treatment and genotype on nuclear TDP-43 (**** P < 0.0001, F (1, 82) = 26.64 and * P = 0.0126, F (1, 82) = 6.504 respectively). (**D**) The ratio of fluorescence intensities of nuclear TDP-43 (pink) versus cytoplasmic TDP-43 (red) in the primary MEFs untreated or treated with CilD.

5.2.4 The concurrent inhibition of dynein and TBK1 leads to TDP-43 mislocalisation in wild-type MEFs

To elucidate that TDP-43 mislocalisation is associated with the synergistic effect of dynein deficiency and reduction in TBK1 functions, the primary wild-type MEFs were co-treated with TBK1 and dynein inhibitors (CilD, 50 µM and BX795, 10 µM respectively) for 6 hours. Then, cells were fixed and stained with anti-TDP-43 antibody. The confocal images were used to quantify the intensity of nuclear and cytoplasmic TDP-43.

The analysis of images showed that TBK1 inhibition by itself did not alter the localisation of TDP-43 as observed previously. However, the dynein inhibition induced TDP-43 mislocalisation in wild-type MEFs, when was accompanied by TBK1 inhibition (**Figure 5.4 A**). A one-way ANOVA showed a significant difference between untreated and treated wild-type MEFs on cytoplasmic TDP-43 ($P < 0.0001$, $F = 8.271$). Tukey's multiple comparison test showed a significant increase in cytoplasmic TDP-43 between untreated MEFs and CilD-treated MEFs ($P = 0.0314$) and between untreated MEFs and BX795/CilD ($P = 0.0001$). Moreover, there was a significant increase in cytoplasmic TDP-43 between CilD-treated MEFs and BX795/CilD treated MEFs ($P = 0.0124$). No difference was seen between untreated and BX795-treated wild-type MEFs ($P = 0.7433$) (**Figure 5.4 B**).

Furthermore, the one-way ANOVA showed a significant difference between untreated and treated wild-type MEFs on intensity of nuclear TDP-43 ($P = 0.0001$, $F = 7.882$). Tukey's multiple comparison test showed a significant reduction in nuclear TDP-43 between untreated MEFs and CilD-treated MEFs ($P = 0.0474$), and between untreated MEFs and BX795/CilD-treated MEFs ($P = 0.0001$) (**Figure 5.4 C**). Figure 5.4 D demonstrates the alterations in the proportion of cytoplasmic TDP-43 versus nuclear TDP-43 in untreated wild-type MEFs and wild-type MEFs co-treated with TBK1 and dynein inhibitors.

These data highlight the importance of dynein function in the maintenance of a balanced localisation of TDP-43 and also as both dynein and TBK1 are key players in autophagy, it

suggests that association of dynein and TBK1 with TDP-43 homeostasis is via their functional link with the autophagy pathway.

Figure 5.4

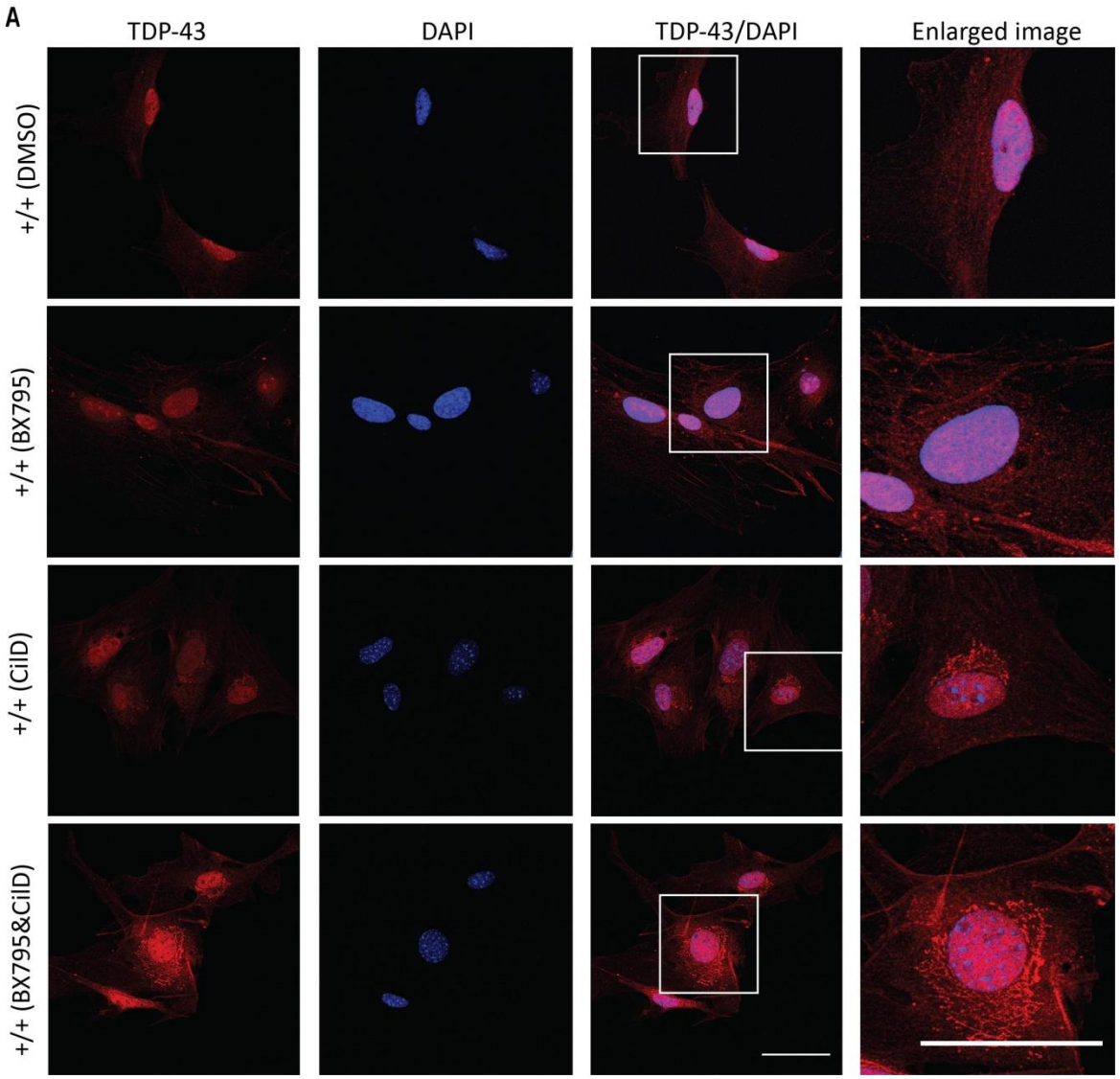

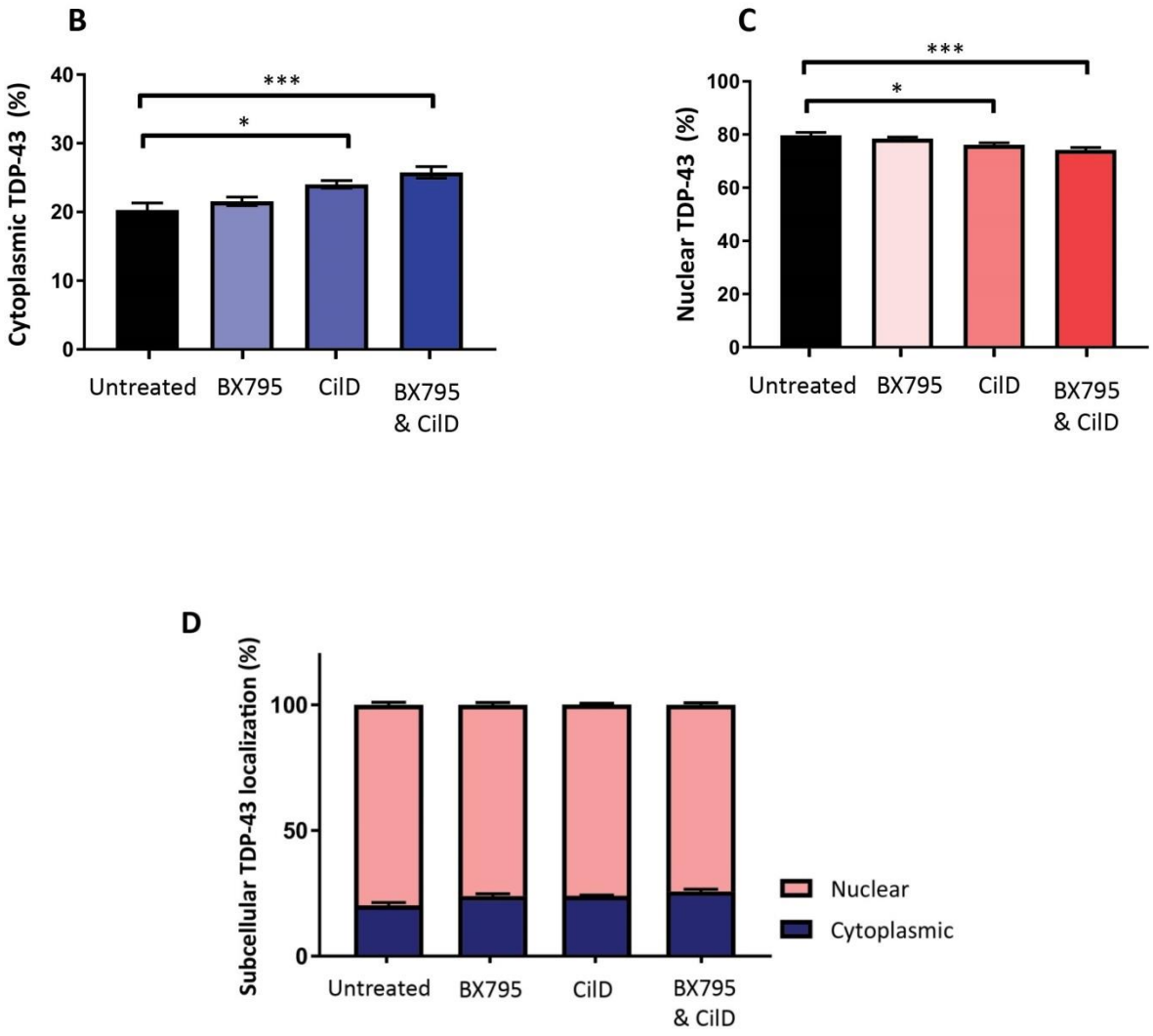
B
Cytoplasmic TDP-43 (%)
40
30
20
10
0
***
*
Untreated
BX795
CilD
BX795 & CilD
C
Nuclear TDP-43 (%)
100
80
60
40
20
0
***
*
Untreated
BX795
CilD
BX795 & CilD
D
Subcellular TDP-43 localization (%)
100
50
0
Untreated
BX795
CilD
BX795 & CilD
Nuclear
Cytoplasmic

Figure 5.4 Co-treatment of dynein and TBK1 inhibitors increases TDP-43 cytoplasmic localisation. (**A**) Wild-type MEFs were treated with TBK1 inhibitor (BX795) with or without dynein inhibitor (CilD) and then stained with anti-TDP-43 antibody. Nuclei were stained with DAPI. The co-treatment of BX795 and CilD resulted in TDP-43 mislocalisation. Representative images are shown. The enlarged images are the boxed areas shown for better view. Scale bar, 50 µm. (**B**) Data is presented as the mean ± SEM; where N > 80 number of cells per genotype, N = 3 biological repeats, and N = 6 technical repeats for each genotype. For this experiment, quantification was performed in at least 30 images per genotype. A one-way ANOVA showed a significant difference in cytoplasmic TDP-43 between untreated and treated wild-type MEFs (****P* = 0.0001, F (3, 69) = 8.271). Tukey's multiple comparison test showed a significant increase in this measurement in MEFs treated with CilD, and co-treated with BX795/CilD in comparison to the untreated MEFs (* *P* = 0.0314, and *** *P* = 0.0001 respectively). (**C**) Data is presented as the mean ± SEM; where N > 80 number of cells per genotype, N = 3 biological repeats, and N = 3 technical repeats for each genotype. A one-way ANOVA showed a significant difference in nuclear TDP-43 between untreated and treated wild-type MEFs (*** *P* = 0.0001, F (3, 69) = 7.882). Tukey's multiple comparison test showed a significant decrease in this measurement in MEFs treated with CilD and co-treated with BX795/CilD compared to the untreated MEFs (* *P* = 0.0474, and *** *P* = 0.0001 respectively). (**D**) The ratio of fluorescence intensities of nuclear TDP-43 (pink) versus cytoplasmic TDP-43 (dark blue) in the primary MEFs untreated or treated with BX795 and CilD.

5.2.6 Inhibition of the proteasome system causes almost complete loss of nuclear TDP-43 in Loa^{Hom} MEFs

The translocation of TDP-43 from the nucleus to the cytoplasm is a typical neuropathological feature recognised in neurons of the brain and spinal cord slices from ALS cases (Neumann et al., 2006). The subcellular localisation of TDP-43 is regulated through various cellular systems such as the proteasome system, which when dysregulated lead to the aberrant localisation of TDP-43. In addition, it has been reported that proteasome inhibition causes the re-distribution of TDP-43 in primary neurons (van Eersel et al., 2011). It was aimed to test whether the Loa^{Hom} MEFs are more prone to TDP-43 mislocalisation when the proteasome system is compromised too.

Primary MEFs plated in 6-well plate were treated with 26S proteasome inhibitor (MG132, 10 µM) for 6 hours. After cell fixation, the immunocytochemistry was performed using anti-TDP-43 antibody. In vehicle-treated controls, TDP-43 was localised tightly to the nucleus, as observed by overlay with DAPI staining, while proteasome inhibition increased intensity of cytoplasmic TDP-43 together with a decline in the nuclear TDP-43 staining (**Figure 5.5 A, top two rows**).

Interestingly, we noticed that proteasome inhibition in Loa^{Hom} MEFs had a much more significant effect on TDP-43 mislocalisation than in the wild-type cells, resulting in almost clearing all TDP-43 from the nucleus (**Figure 5.5 A, bottom two rows**). A two-way ANOVA was carried out to determine the effect of genotype and MG132 treatment on the TDP-43 mislocalisation ($N > 80$). The results showed that there was a significant interaction between the effect of genotype and MG132 treatment on the cytoplasmic level of TDP-43 ($P < 0.0001$, $F = 64$). Moreover, both MG132 treatment ($P < 0.0001$, $F = 142.3$) and genotype ($P < 0.0001$, $F = 70.18$) had significant main effect on cytoplasmic TDP-43 mislocalisation (**Figure 5.5 B**). Moreover, quantification of nuclear TDP-43 intensity showed that there was a significant interaction between the effect of genotype and MG132 treatment on the nuclear TDP-43 ($P < 0.0001$, $F = 53.14$). Furthermore, both

MG132 treatment ($P < 0.0001$, F = 121.4) and genotype ($P < 0.0001$, F = 58.31) had significant main effect on nuclear TDP-43 (**Figure 5.5 C**). Figure 5.5 D demonstrates the alterations in proportion of cytoplasmic TDP-43 versus nuclear TDP-43 in untreated wild-type MEFs and wild-type MEFs treated with Proteasome inhibitor.

It was also investigated whether TBK1 or proteasome inhibition alters the solubility of TDP-43. To examine this, wild-type and Loa^{Hom} MEFs were plated in 100 mm dish and treated with BX795 or MG132 for 6 hours followed by fractionation. Although there is a transfer issue in lane 2 for the level of insoluble TDP-43 but generally the protein contents of the soluble and insoluble fractions upon TBK1 and proteasome inhibition showed that, while the soluble fraction of TDP-43 remains unchanged, the insoluble fraction of TDP-43 was markedly increased in Loa^{Hom} MEFs (**Figure 5.5 E**). This might show that upon treatment with TBK1 and proteasome inhibitors, the level of insoluble TDP-43 increases which is in correlation with increased level of cytoplasmic TDP-43 as reported previously (**Figure 5.1 A and 5.5 A**).

Interestingly, short-term proteasome system inhibition is also involved in the formation of SGs and cellular stress responses (Mazroui, Di Marco, Kaufman, & Gallouzi, 2007). Accordingly, for further investigation, localisation of FUS, as a marker of SGs, upon proteasome inhibition was checked. No change in FUS localisation was found following proteasome inhibition in primary MEFs, which suggests that inhibition of proteasome system affects localisation of RNA-binding proteins differentially (**Figure 5.5 F**).

Figure 5.5

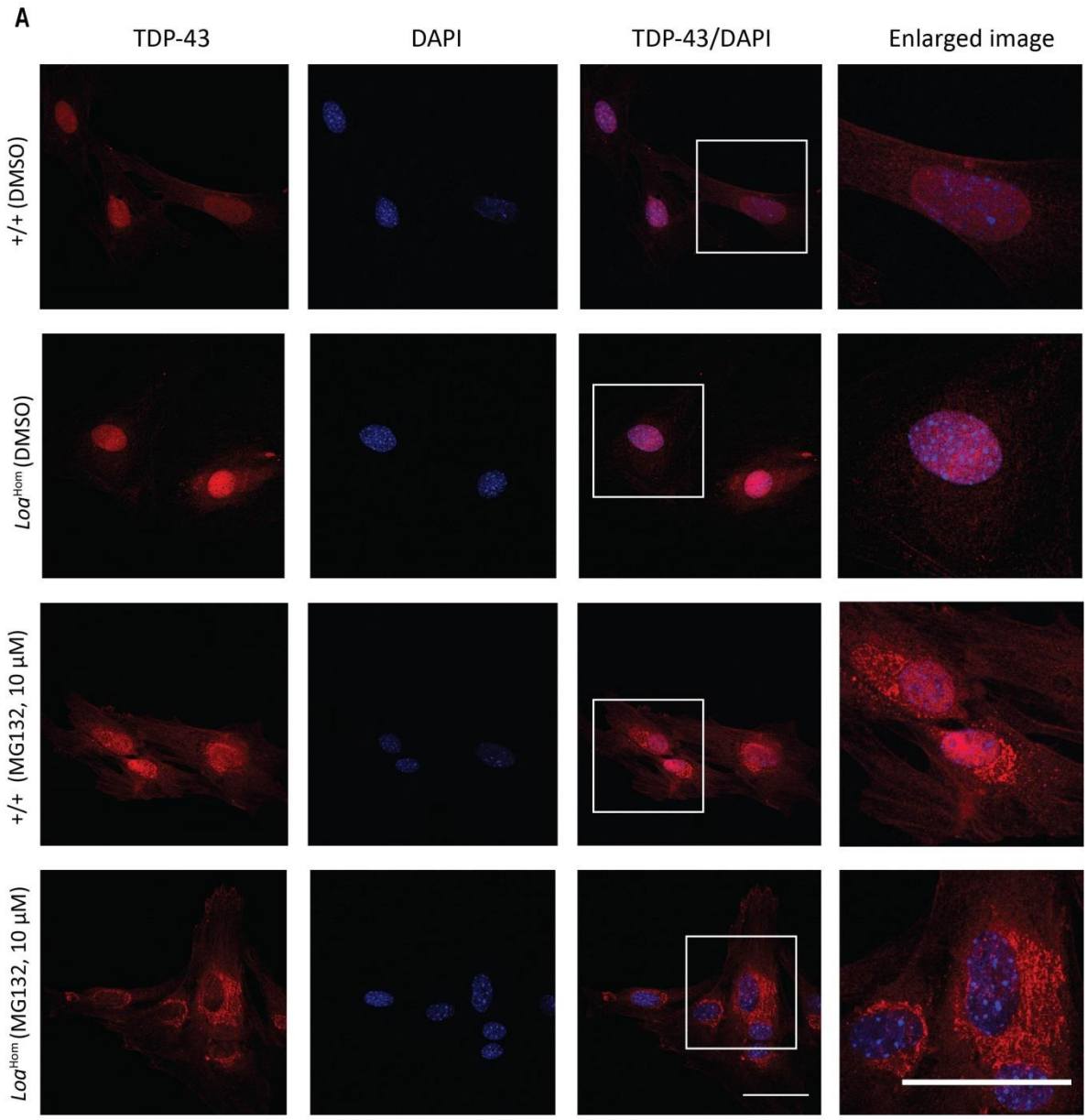
A
TDP-43
DAPI
TDP-43/DAPI
Enlarged image
+/+ (DMSO)
Loa^Hom (DMSO)
+/+ (MG132, 10 µM)
Loa^Hom (MG132, 10 µM)

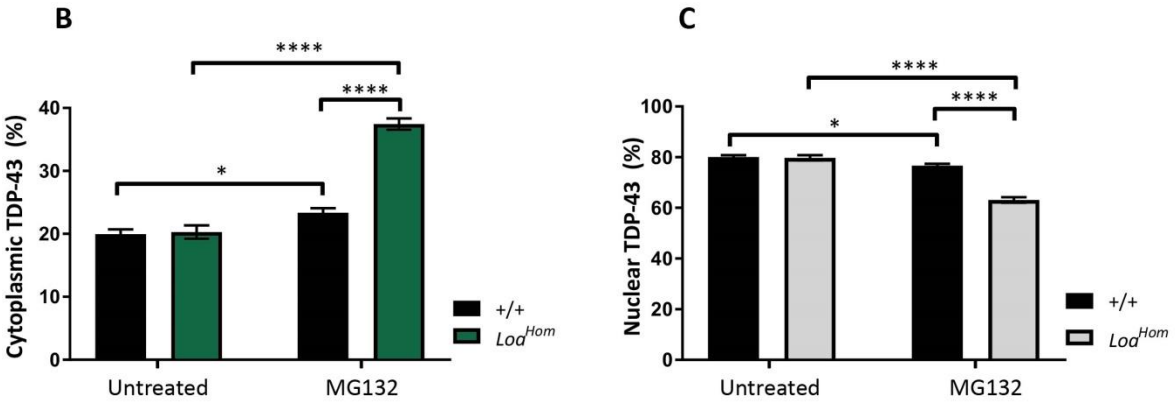
B
Cytoplasmic TDP-43 (%)
40
30
20
10
0
****
****
*
+/+
Loa^Hom
Untreated
MG132
C
Nuclear TDP-43 (%)
100
80
60
40
20
0
****
****
*
+/+
Loa^Hom
Untreated
MG132

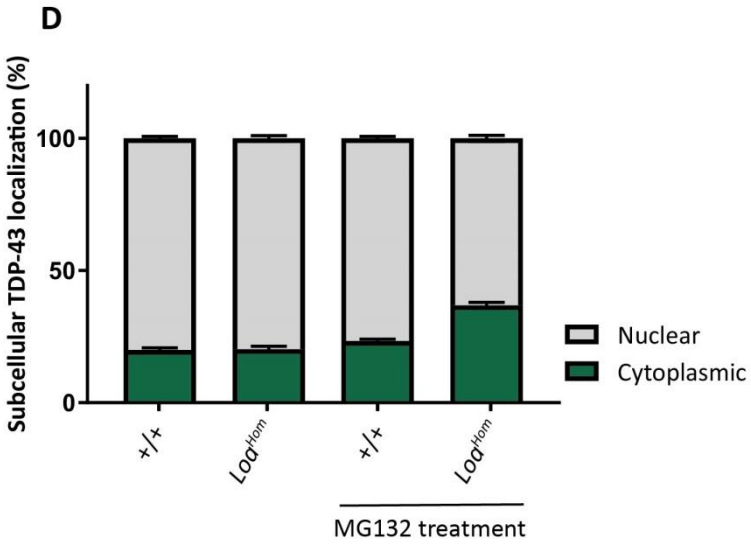
D
Subcellular TDP-43 localization (%)
100
50
0
Nuclear
Cytoplasmic
+/+
Loa^Hom
+/+
Loa^Hom
MG132 treatment

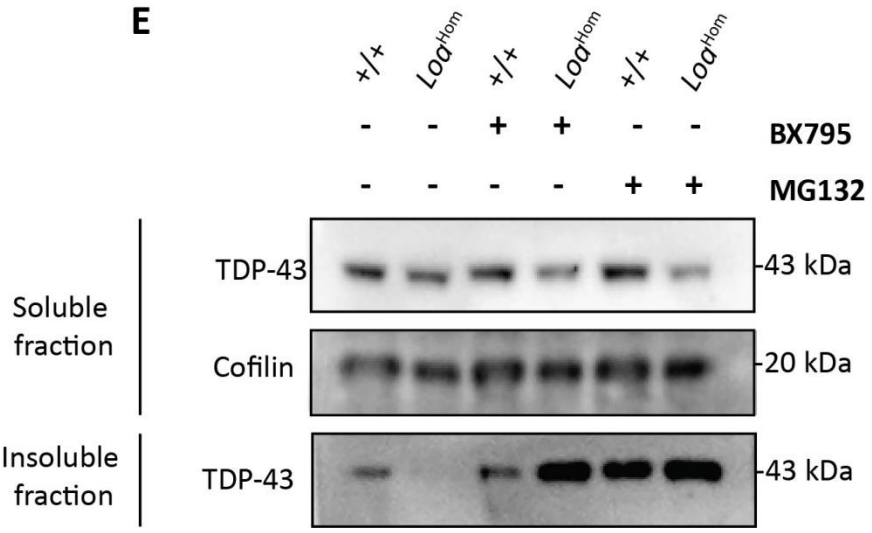
E
+/+
Loa^Hom
+/+
Loa^Hom
+/+
Loa^Hom
BX795
MG132
Soluble fraction
TDP-43
43 kDa
Cofilin
20 kDa
Insoluble fraction
TDP-43
43 kDa

Figure 5.5 continued

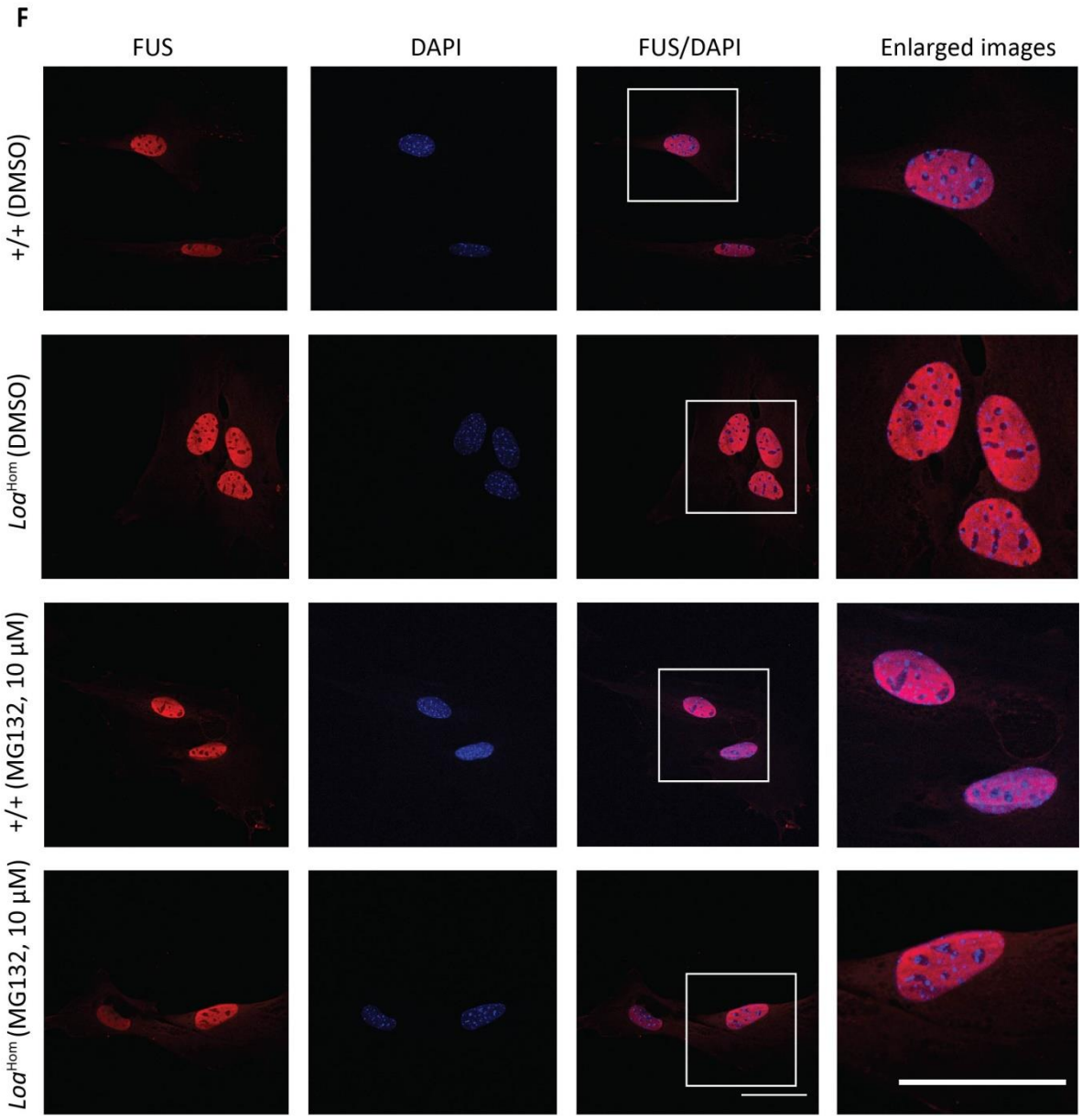

Figure 5.5 Proteasome inhibitor induces mislocalisation of TDP-43, but not FUS, in primary MEFs. (**A**) TDP-43 is localised in the nucleus in DMSO-treated MEFs, with a weak staining in the cytoplasm. Treatment with 10 µM MG132 for 6 hours, however, results in cytoplasmic mislocalisation of TDP-43, together with the significant nucleic loss of TDP-43 in Loa^{Hom} MEFs. Cell nuclei were counterstained with DAPI. Representative images are shown. The enlarged images are the boxed areas shown for better view. Scale bar, 50 µm. (**B**) Data is presented as the mean ± SEM; where N > 80 number of cells, N = 3 biological repeats, and N = 3 technical repeats for each genotype. For this experiment, quantification was performed in at least 30 images per genotype. A two-way ANOVA showed significant interaction between genotype and MG132 treatment (**** P < 0.0001, F (1, 98) = 64) followed by Tukey's post-test. Additionally, there were significant main effects of MG132 treatment and genotype on cytoplasmic TDP-43 (**** P < 0.0001, F (1, 98) = 142.3 and **** P < 0.0001, F (1, 98) = 70.18 respectively). (**C**) Data is presented as the mean ± SEM; where N > 80 number of cells, N = 3 biological repeats, and N = 3 technical repeats for each genotype. A two-way ANOVA showed significant interaction between genotype and MG132 treatment (**** P < 0.0001, F (1, 105) = 53.14) followed by Tukey's post-test. There were significant main effects of MG132 treatment and genotype on nuclear TDP-43 (**** P < 0.0001, F (1, 105) = 121.4 and **** P < 0.0001, F (1, 105) = 58.31 respectively). (**D**) The ratio of fluorescence intensities of nuclear TDP-43 (gray) versus cytoplasmic TDP-43 (green) in the primary MEFs untreated or treated with MG132. (**E**) Wild-type and Loa^{Hom} MEFs were treated with BX795 or MG132, followed by cell fractionation. Soluble and insoluble fractions were subjected to immunoblot analysis with the indicated antibodies, N = 2 biological repeats. (**F**) FUS expression is restricted to the nucleus in vehicle treated primary MEFs, while being absent from the cytoplasm. Treatment with MG132 did not alter the localisation of FUS and after treatment, FUS remains in the nucleus in both wild-type and Loa^{Hom} MEFs. FUS staining performed with antibody to FUS. Nuclei were stained with DAPI. Representative images are shown. The enlarged images are the boxed areas shown for better view. Scale bar, 50 µm.

5.2.6 Inhibition of dynein function exacerbated the mislocalisation of TDP-43 in wild-type MEFs treated with the proteasome inhibitor

The proteasome inhibition resulted in TDP-43 mislocalisation in both wild-type and Loa^{Hom} MEFs. However, Loa^{Hom} MEFs showed a higher level of mislocalised TDP-43. Thus, the aim was to check whether concurrent inhibition of dynein and proteasome system exacerbates the mislocalisation of TDP-43 in the wild-type MEFs.

Wild-type MEFs were treated simultaneously with a single concentration of proteasome inhibitor (MG132, 10 µM) and three different concentrations of dynein inhibitor (CilD, 50, 60 and 100 µM) for 6 hours. Then, cells were fixed with 4 % formaldehyde, followed by TDP-43 staining. The intensity of nuclear and cytoplasmic TDP-43 was quantified in confocal images, which showed an increased level of TDP-43 mislocalisation in MEFs co-treated with MG132/CilD (**Figure 5.6 A**). A one-way ANOVA was performed with Tukey's multiple comparison test. The one-way ANOVA for the intensity of cytoplasmic TDP-43 showed a significant difference between single treatment and co-treatment in wild-type MEFs (P = 0.0443, F = 9.317). Tukey's multiple comparison test showed a significant increase in cytoplasmic TDP-43 between MG132-treated MEFs and MG132/CilD (100 µM)-treated MEFs (P < 0.0001) (**Figure 5.6 B**). Collectively, the data showed that inhibition of ATPase activity of dynein, upon inhibition of proteasome system enhances TDP-43 mislocalisation upon proteasome inhibition.

Furthermore, the one-way ANOVA for the intensity of nuclear TDP-43 showed a significant difference between single treatment and co-treatment in wild-type MEFs (P < 0.0001, F = 9.317). Tukey's multiple comparison test showed a significant reduction in nuclear TDP-43 between MG132-treated MEFs and MG132/CilD (100 µM)-treated MEFs (P < 0.0001) (**Figure 5.6 C**). Figure 5.6 D demonstrates the alterations in proportion of cytoplasmic TDP-43 versus nuclear TDP-43 in MG132-treated and MG132/CilD treated wild-type MEFs.

Figure 5.6

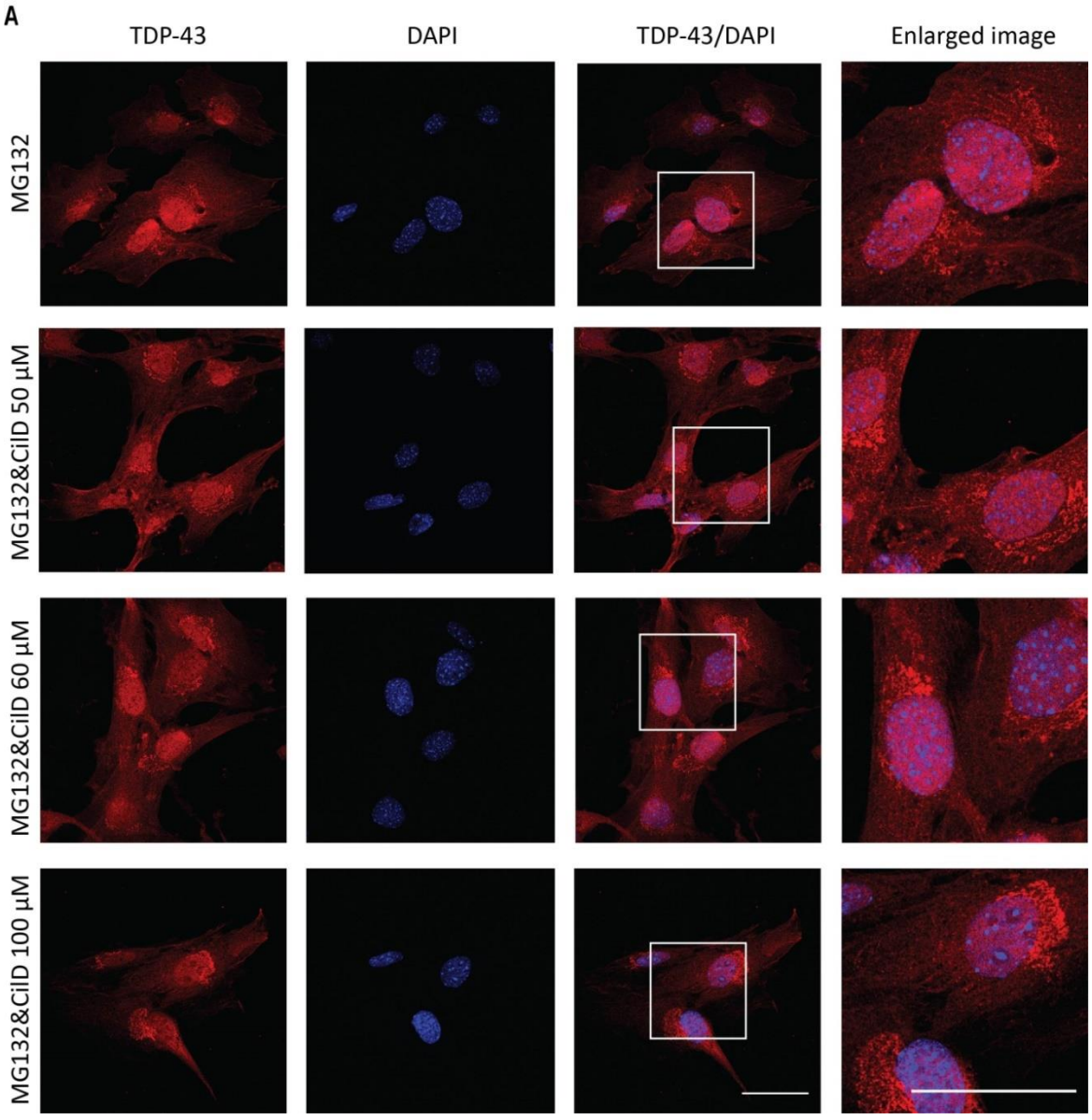
A
TDP-43
DAPI
TDP-43/DAPI
Enlarged image
MG132
MG132&CilD 50 µM
MG132&CilD 60 µM
MG132&CilD 100 µM

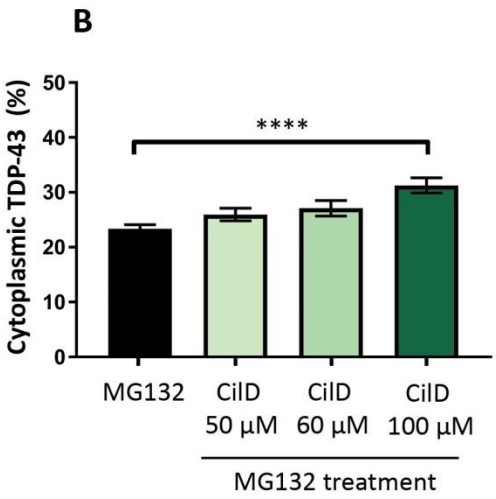
B
Cytoplasmic TDP-43 (%)
50
40
30
20
10
0
****
MG132
CilD 50 µM
CilD 60 µM
CilD 100 µM
MG132 treatment

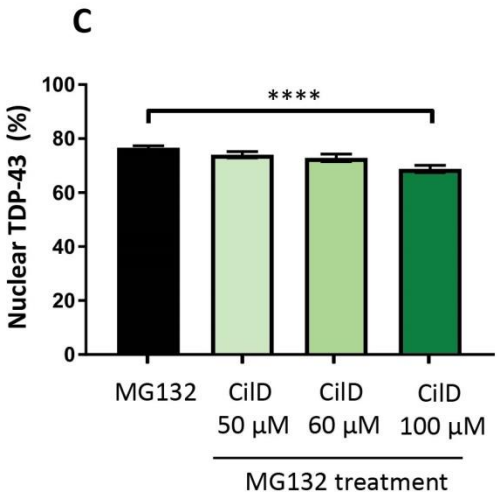
C
Nuclear TDP-43 (%)
100
80
60
40
20
0
****
MG132
CilD 50 µM
CilD 60 µM
CilD 100 µM
MG132 treatment

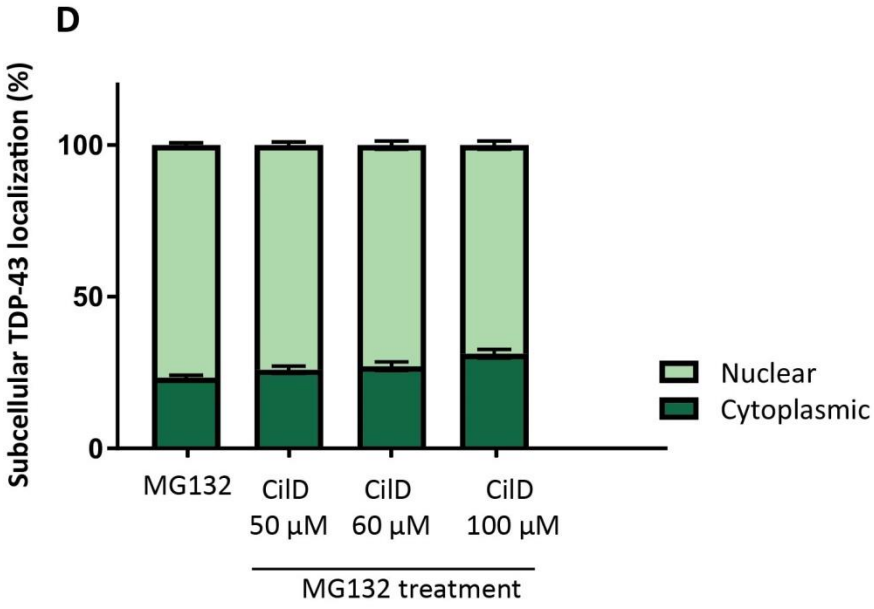
D
Subcellular TDP-43 localization (%)
100
50
0
MG132
CilD 50 µM
CilD 60 µM
CilD 100 µM
MG132 treatment
Nuclear
Cytoplasmic

Figure 5.6 Dynein inhibition exacerbates the effect of proteasome inhibition on TDP-43 mislocalisation. (**A**) Wild-type MEFs were co-treated with dynein and proteasome inhibitors and then stained with anti-TDP-43 antibody. Nuclei were stained with DAPI. The co-treatment of dynein and proteasome inhibitors resulted in creased level of TDP-43 mislocalisation. Representative images are shown. The enlarged images are the boxed areas shown for better view. Scale bar, 50 µm. (**B**) Data is presented as the mean ± SEM; where N > 80 number of cells per genotype, N = 3 biological repeats, and N = 3 technical repeats for each genotype. For this experiment, quantification was performed in at least 30 images per genotype. A one-way ANOVA showed a significant difference in cytoplasmic TDP-43 between MG132-treated and MG132/CilD-treated MEFs (**** $P < 0.0001$, F (3, 79) = 9.317). Tukey's multiple comparison test showed a significant increase in this measurement in MEFs co-treated with MG132/CilD (100 µM) compared to the MEFs treated with MG132 (**** $P < 0.0001$). (**C**) Data is presented as the mean ± SEM; where N > 100 number of cells per genotype, N = 3 biological repeats, and N = 3 technical repeats for each genotype. A one-way ANOVA showed a significant difference in nuclear TDP-43 between MG132-treated and MG132/CilD-treated MEFs (**** $P < 0.0001$, F (3, 79) = 9.317). Tukey's multiple comparison test showed a significant decrease in this measurement in MEFs co-treated with MG132/CilD (100 µM) compared to the MEFs treated with MG132 (**** $P < 0.0001$). (**D**) The ratio of fluorescence intensities of nuclear TDP-43 (light green) versus cytoplasmic TDP-43 (green) in the primary MEFs treated with MG132 and co-treated with MG132/CilD.

5.2.7 Disrupted dynamics of stress granules in primary Loa^{Hom} MEFs

Formation of SGs is one of the immediate responses upon cellular stress that might constitute a vital feature to regulate the expression of genes in cellular stress. SGs are highly dynamic compartments, but during the ageing and other environmental stresses, they convert to aggregate-like inclusions (Alberti, Mateju, Mediani, & Carra, 2017).

It has also been reported that dynein is involved in the formation of SGs and impairment of dynein motor proteins and disruption of MTs arrays could prevent the formation of SGs (Kwon et al., 2007). Additionally, dynein is involved in the autophagy-dependent removal of SG. Based on the importance of dynein function in SG dynamics, it was sought to investigate whether dynein deficiency caused by *Loa* mutation would affect the dynamics of SGs.

To induce SG, wild-type and Loa^{Hom} MEFs plated in 6-well plate were treated with 1 mM sodium arsenite (SA) for 1 hour. Then, cells were fixed with 4 % formaldehyde, which followed by FUS staining and confocal microscopy. In the control group, both wild-type and Loa^{Hom} fibroblasts, FUS was mainly localised in the nucleus. In the arsenite-induced cells, FUS-positive punctate granules (ranging from 1 μm to 15 μm) appeared in the cytoplasm, and the quantification of number of SGs showed a significant reduction in the number of SGs in Loa^{Hom} MEFs (**Figure 5.7 A-B**).

The dynamics of SG during the recovery period was also investigated. Here, after induction of SG, SA was removed, and cells were washed with DPBS and recovered in complete media, and fixed after 10, 20, and 30 minutes followed by immunostaining of FUS. The quantification of microscopic images showed an initial reduction in SGs after 10 minutes in wild-type MEFs while in the Loa^{Hom} MEFs reduction in the number of SG started 20 minutes after releasing of stress treatment suggesting the delayed resolution of SGs in Loa^{Hom} MEFs (**Figure 5.7 A-B**). Furthermore, after 30 minutes of recovery, ~ 50 % of wild-type MEFs were free of SGs with complete clearance. However, more than 80 % of Loa^{Hom} MEFs were SG-positive, and SGs persisted late post-removal of SA (**Figure 5.7 C)**.

Figure 5.7

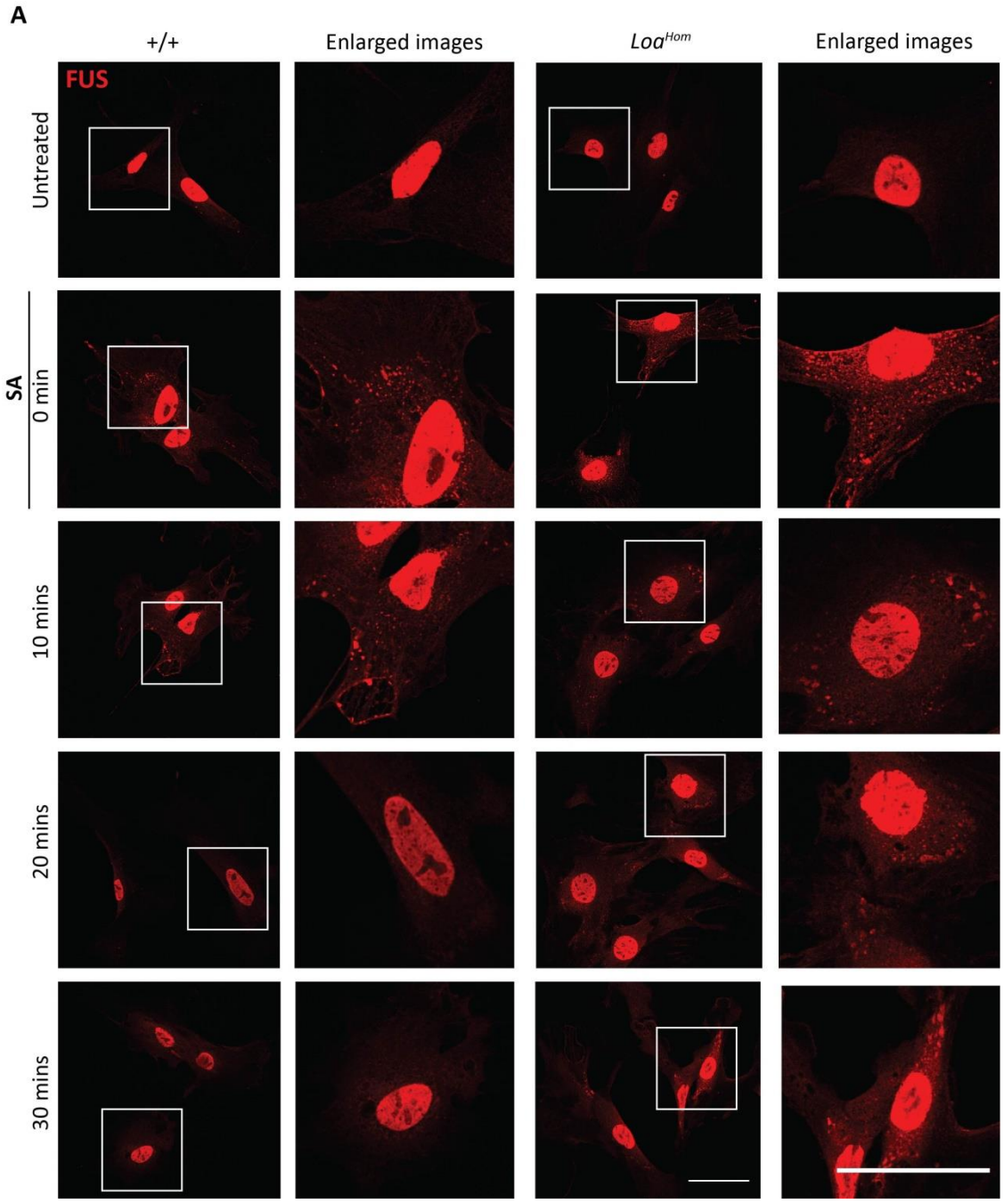
A
+/+
Enlarged images
Loa^Hom
Enlarged images
FUS
Untreated
SA
0 min
10 mins
20 mins
30 mins

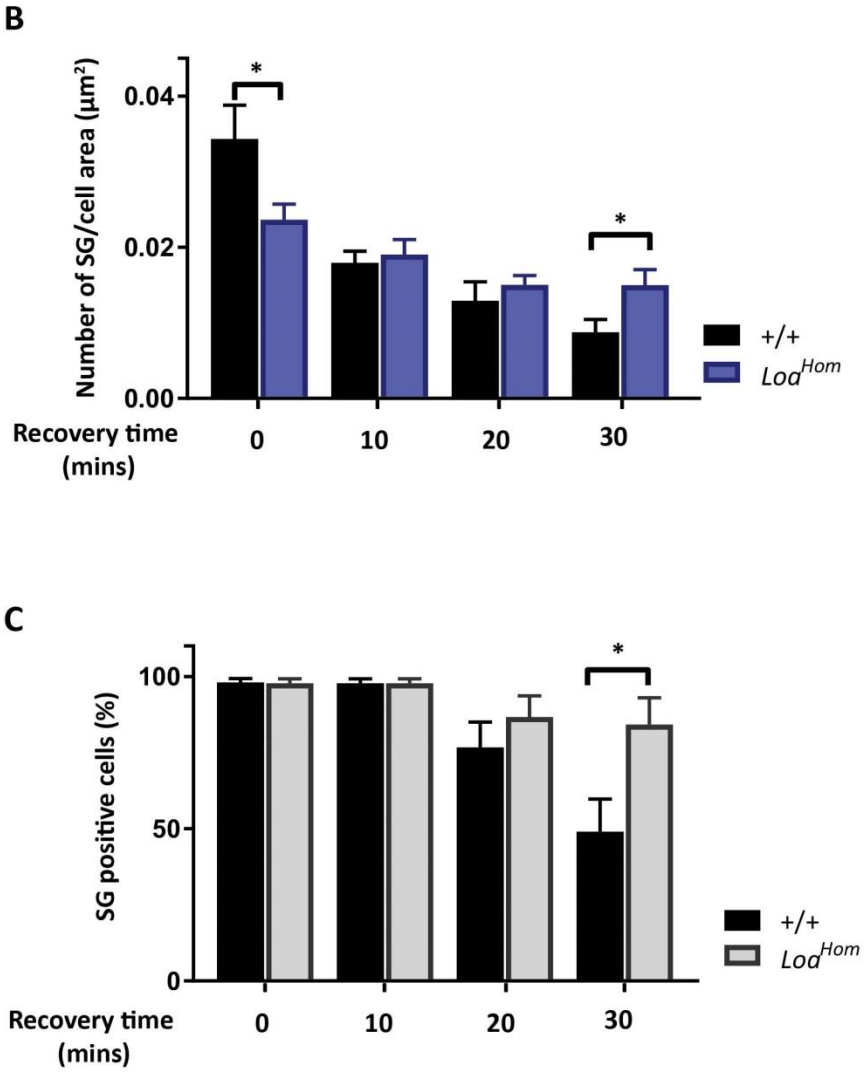

Figure 5.7 Dynein alters the assembly and disassembly of SGs. (**A**) Primary culture of MEFs treated (or not) with 1 mM sodium arsenite (SA) for 1 hour, followed by washout and then recovering in complete media and fixed at different time points. Cytoplasmic SGs were labelled with an antibody against FUS. Representative images are shown. The enlarged images are the boxed areas shown for better view. Sale bar, 50 µm. (**B**) Quantification was performed by normalizing number of SGs to the cell area of wild-type and Loa^{Hom} MEFs at the indicated time points. Data is presented as the mean ± SEM; where N > 80 number of cells per genotype, N = 3 biological repeats, and N = 3 technical repeats for each genotype. For this experiment, quantification was performed in at least 30 images per genotype. Statistic was performed with Multiple t-test (* $P < 0.05$). (**C**) The percent of SG-positive fibroblast are also shown. Data is presented as the mean ± SEM; Multiple t-test was performed (* $P < 0.05$).

Furthermore, the different composition of SGs due to various stresses has been reported (Aulas et al., 2017). Based on the different content of SG, dynamics of SGs was also checked by *in situ* hybridisation using Cy5-oligo (dT) probe since polyadenylated mRNA is recruited into the SGs after cellular stress regardless of the stressor and cell type (Khalfallah et al., 2018).

SGs were induced in primary MEFs as mentioned previously and the number of SGs and their dynamics during recovery period studied by scoring oligo dT-positive granules. In correlation with the previous experiment, the quantification of the number of SGs represented the reduction in the number of SGs in Loa^{Hom} MEFs (**Figure 5.8 A-B**).

Moreover, during the recovery period, SGs persisted longer in Loa^{Hom} MEFs, as evident from the data in Figure 5.8 B and C. Interestingly, comparing the rate of recovery, indicated that removal of FUS protein was faster compared to the rate of oligo (dT) suggesting that removal of RNA-binding proteins starts earlier compared to the release of mRNA trapped in the SGs compartment. However, quantification of number of SG-positive cells after 30 minutes recovery showed a higher number of Loa^{Hom} MEFs, in comparison to the wild-type, similar to the number of FUS-positive Loa^{Hom} MEFs reported previously.

Collectively, this set of data indicated the attenuated number of SGs and their resolution in Loa^{Hom} MEFs, suggesting that dynein mutation perturb the SG dynamics, which may compromise their response to cellular stress and enhance the likelihood of formation of protein aggregates.

Figure 5.8

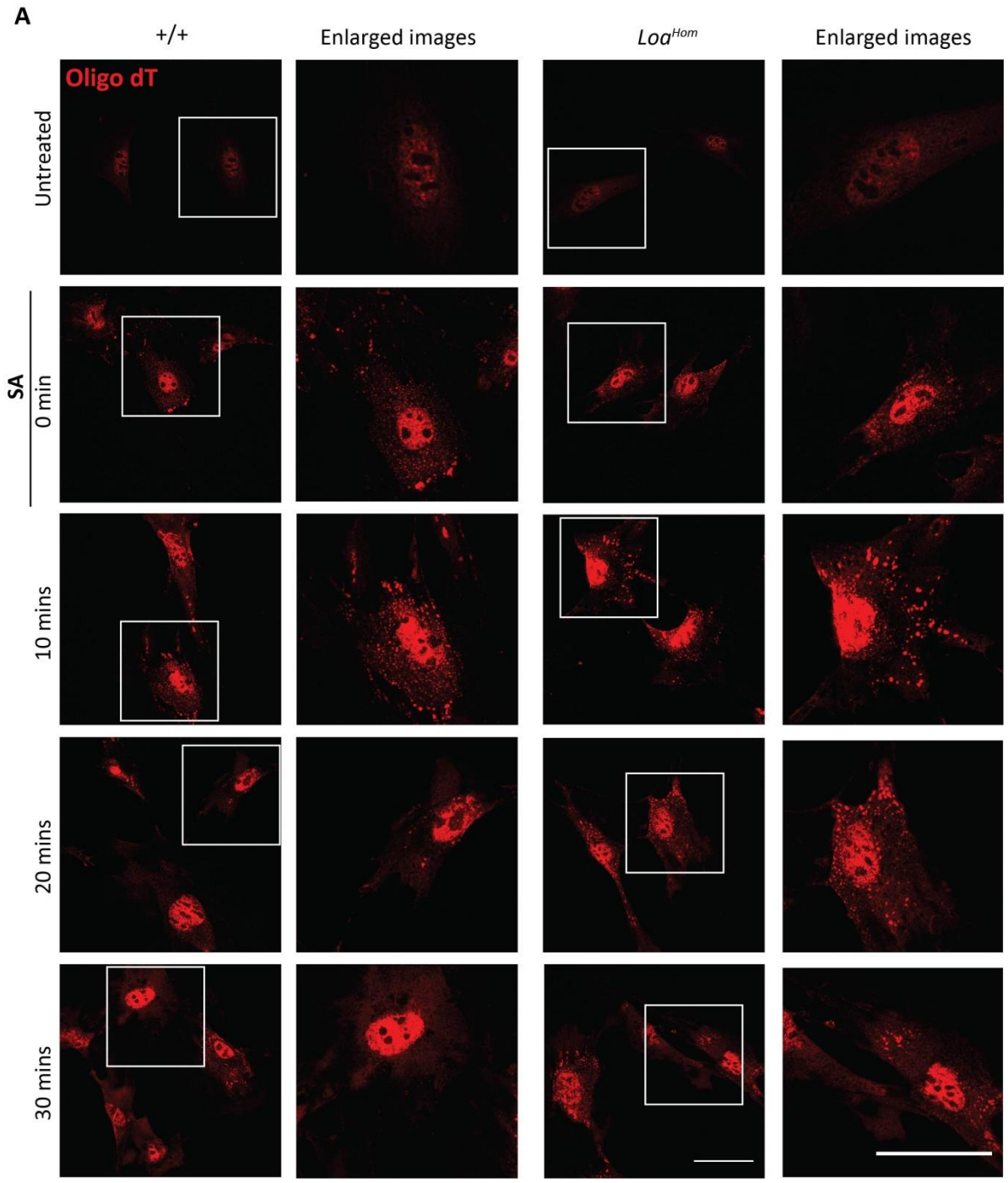
A
+/+
Enlarged images
Loa^Hom
Enlarged images
Oligo dT
Untreated
SA
0 min
10 mins
20 mins
30 mins

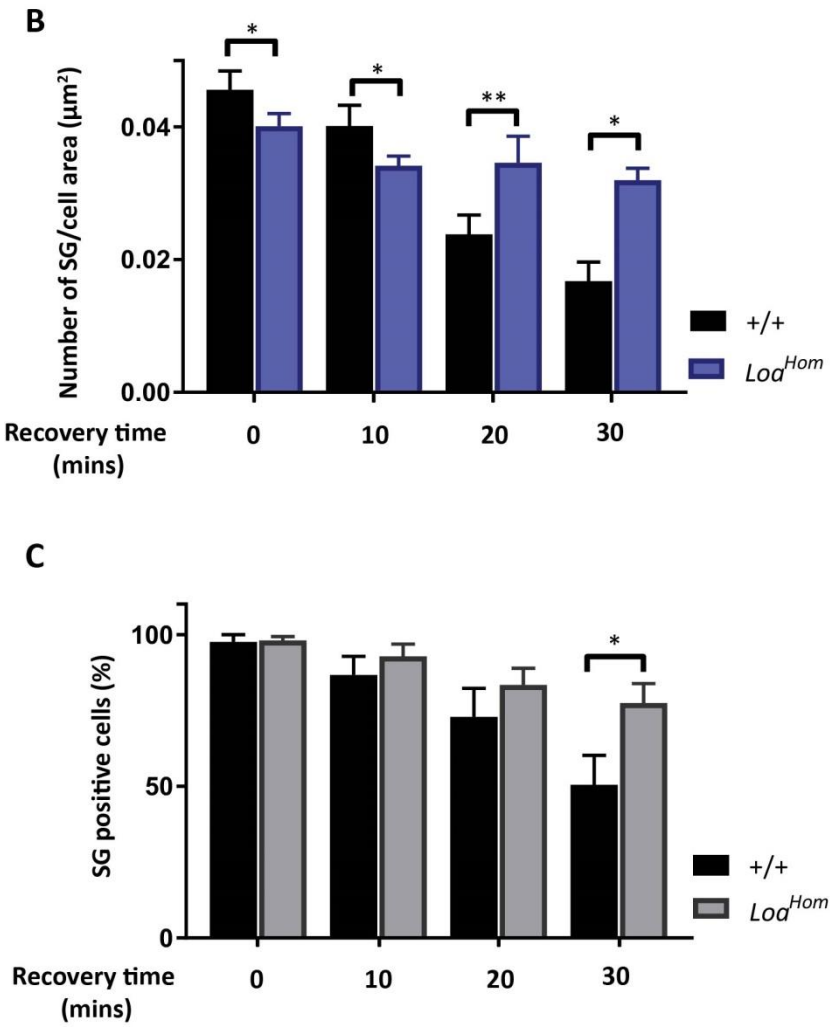

Figure 5.8 Dynein mutation reduces the formation of SGs and delays removal of SG during recovery phase. (**A**) Primary culture of MEFs treated (or not) with 1 mM sodium arsenite (SA) for 1 hour followed by washout and then recovering in complete media and fixed at different time points. Cytoplasmic SGs were labelled with a Cy5-oligo (dT) probe. Representative images are shown. The enlarged images are the boxed areas shown for better view. Sale bar, 50 µm. (**B**) Quantification was performed by normalizing number of SGs to the cell area of wild-type and Loa^{Hom} MEFs at the indicated time points. Data is presented as the mean ± SEM; where N > 80 number of cells per genotype, N = 3 biological repeats, and N = 3 technical repeats for each genotype. For this experiment, quantification was performed in at least 30 images per genotype. Statistic was performed with Multiple t-test (* $P < 0.05$, and ** $P < 0.002$). (**C**) The percent of SG-positive fibroblasts are also shown. Data is presented as the mean ± SEM; Multiple t-test was performed (* $P < 0.05$).

5.2.8 Reduced number of SGs in Loa^{Hom} motor neuron culture

Given the alterations in the SGs dynamic in Loa^{Hom} MEFs, potential effect of dynein mutations on the formation of SGs in MNs was assessed. Primary MNs were treated with 0.5 µM SA for 1 hour, and the formation of SGs was detected by labelling of SG with oligo (dT) probe (**Figure 5.9 A**).

In support of data from the MEFs, SG formation was reduced in Loa^{Hom} MNs when compared to that in wild-type MNs (**Figure 5.9 B**). Moreover, the formation of SGs was analysed in the hippocampal neurons. Primary hippocampal neurons were treated with 0.5 µM SA for 1 hour, and the formation of SGs was detected by labelling of SG with oligo (dT) probe (**Figure 5.9 C**). Quantification of these results showed a significant reduction in number of SGs in Loa^{Het} hippocampal neurons compare to the wild-type neurons (**Figure 5.9 D**). Additionally, the hippocampal neurons were allowed to recover following the SA treatment. Quantification of number of SGs showed the latency in resolution of SGs in Loa^{Het} hippocampal neurons (**Figure 5.9 D**). Overall, these results support the notion that mutant dynein delays the clearance of SGs leading to persistent SGs.

Figure 5.9

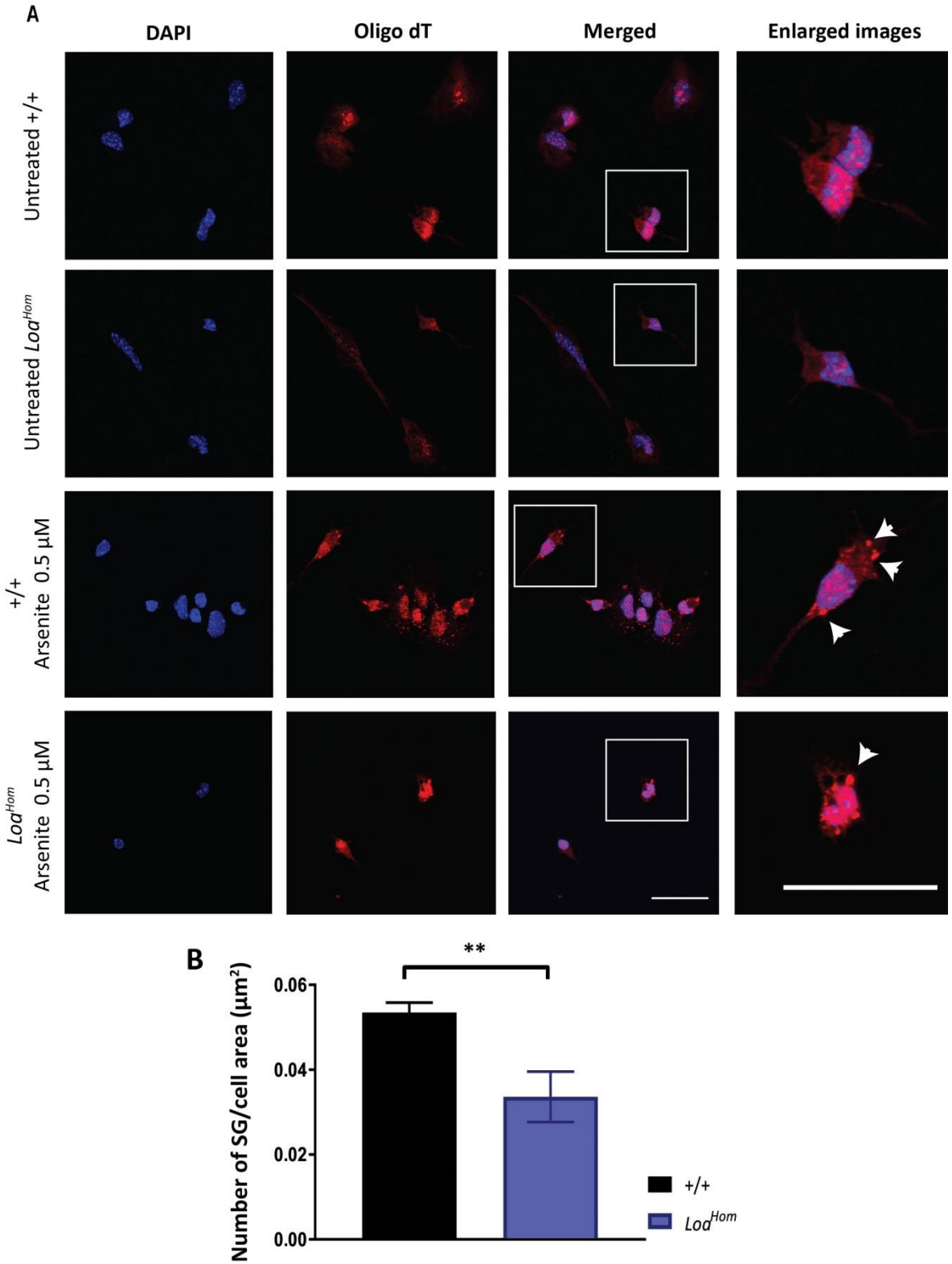
A
DAPI
Oligo dT
Merged
Enlarged images
Untreated +/+
Untreated Loa^Hom
+/+ Arsenite 0.5 µM
Loa^Hom Arsenite 0.5 µM
B
**
Number of SG/cell area (µm²)
0.06
0.04
0.02
0.00
+/+
Loa^Hom

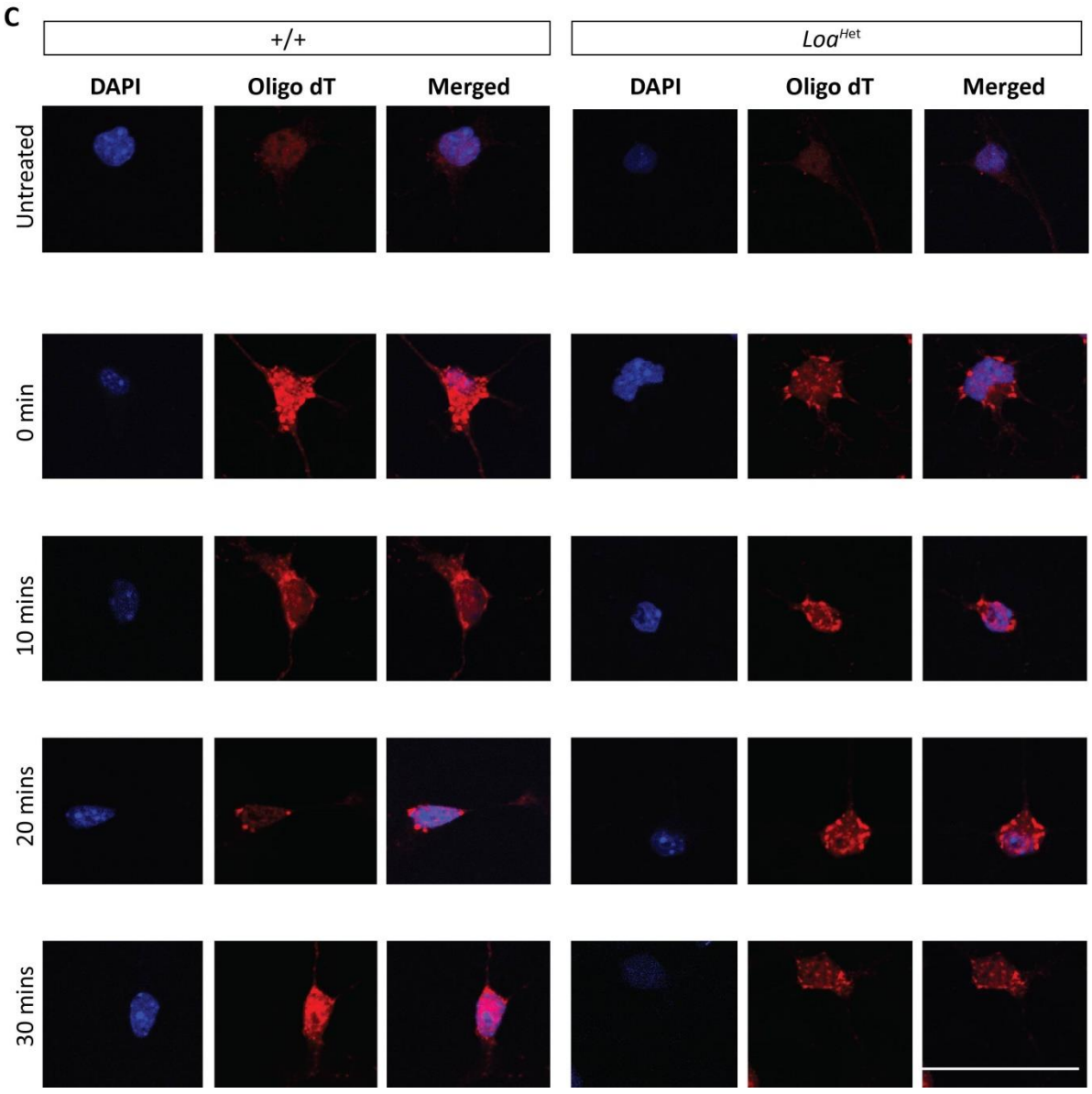
C
+/+
Loa^Het
DAPI
Oligo dT
Merged
DAPI
Oligo dT
Merged
Untreated
0 min
10 mins
20 mins
30 mins

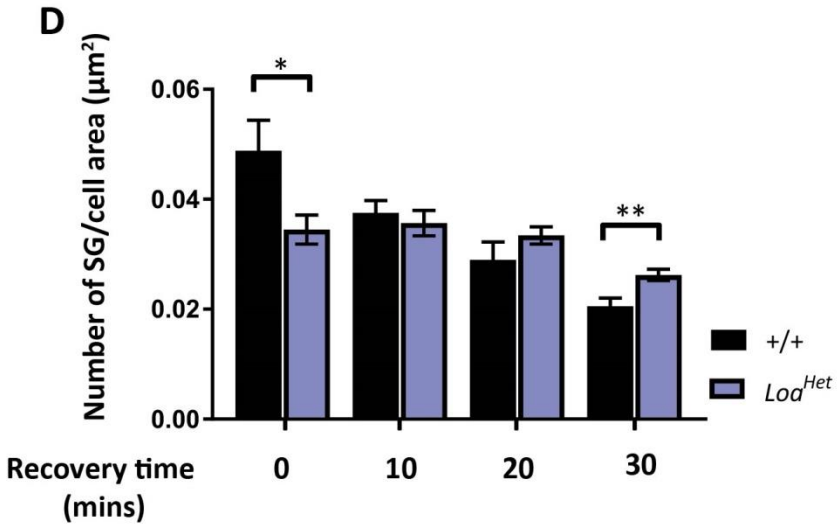

Figure 5.9 Dynein mutation impairs formation of SGs in motor neurons and hippocampal neurons. (**A**) Primary MNs were treated (or not) with 0.5 mM sodium arsenite (SA) for 1 hour. Cytoplasmic SGs were labelled with a Cy5-oligo (dT) probe. Representative images are shown. The enlarged images are the boxed areas shown for better view. Sale bar, 50 µm. (**B**) Quantification was performed by normalizing number of SGs to the cell area of wild-type and Loa^{Hom} MNs. Data is presented as the mean ± SEM; where N > 30 number of cells per genotype, N = 3 biological repeats, and N = 3 technical repeats for each genotype. For this experiment, quantification was performed in at least 20 images per genotype. Unpaired t-test was performed (** P = 0.0051). (**C**) Primary hippocampal neurons were treated (or not) with 0.5 mM sodium arsenite (SA) for 1 hour, followed by washout and then recovering in complete media and fixed at different time points. (**D**) Quantification was performed by normalizing number of SGs to the cell area of wild-type and Loa^{Het} hippocampal neurons at the indicated time points. Data is presented as the mean ± SEM; where N > 30 number of cells per genotype, N = 3 biological repeats, and N = 3 technical repeats for each genotype. Multiple t-test was performed (* P = 0.02, and ** P = 0.006).

5.2.9 Inhibition of TBK1 in Loa^{Hom} MEFs causes the formation of oligo (dT) positive stress granules but not FUS-positive granules

TDP-43 and FUS are mainly localised in the nucleus with distinct functions in mRNA processing. Loss of nuclear TDP-43 and FUS and cytoplasmic localisation are implicated in pathogenesis of ALS (Ling et al., 2013). As enhanced formation of SGs was reported in Loa^{Hom} MEFs and due to the mislocalisation of TDP-43 in Loa^{Hom} MEFs after TBK1 inhibition, it was aimed to investigate whether aberrant function of dynein compounded with TBK1 deficiency contributes to the FUS mislocalisation. It has been shown that upon cellular stress condition, FUS mislocalises into the cytoplasm, forming FUS-positive granules, a hallmark of ALS (Tyzack et al., 2019).

Here, primary MEFs (wild-type and Loa^{Hom}) were treated with TBK1 inhibitor (BX795, 10 µM) for 6 hours and then fixed and stained with anti-FUS antibody. The microscopic images of cells treated with BX795 did not represent the significant changes in the FUS localisation, and FUS remained localised in the nucleus. These results may suggest the distinct impact of TBK1 and dynein deficiencies on the mislocalisation of RNA-binding proteins (**Figure 5.10 A**).

Additionally, it was checked whether combined deficiencies in dynein and TBK1 cause cellular stress responses and formation of SGs contributing to TDP-43 aberrant localisation in cytoplasm. To test this, the wild-type and Loa^{Hom} MEFs were treated with the BX795 (10 µM) and fixed at different time points (1, and 5 hours) to capture either the rapid formation of SGs upon exposure of cellular stress after 1 hour or after 5 hours for those SGs that are formed at a slower rate. After fixation, *in situ* hybridisation using Cy5-oligo (dT) probe was performed to detect SGs. The oligo (dT)-positive SGs were found in the Loa^{Hom} MEFs treated with BX795 for 5 hours but not in wild-type MEFs (**Figure 5.10 B**). The detection of SGs may represent the potential correlation between the appearance of SG and robust mislocalisation of TDP-43 in Loa^{Hom} MEFs.

Figure 5.10

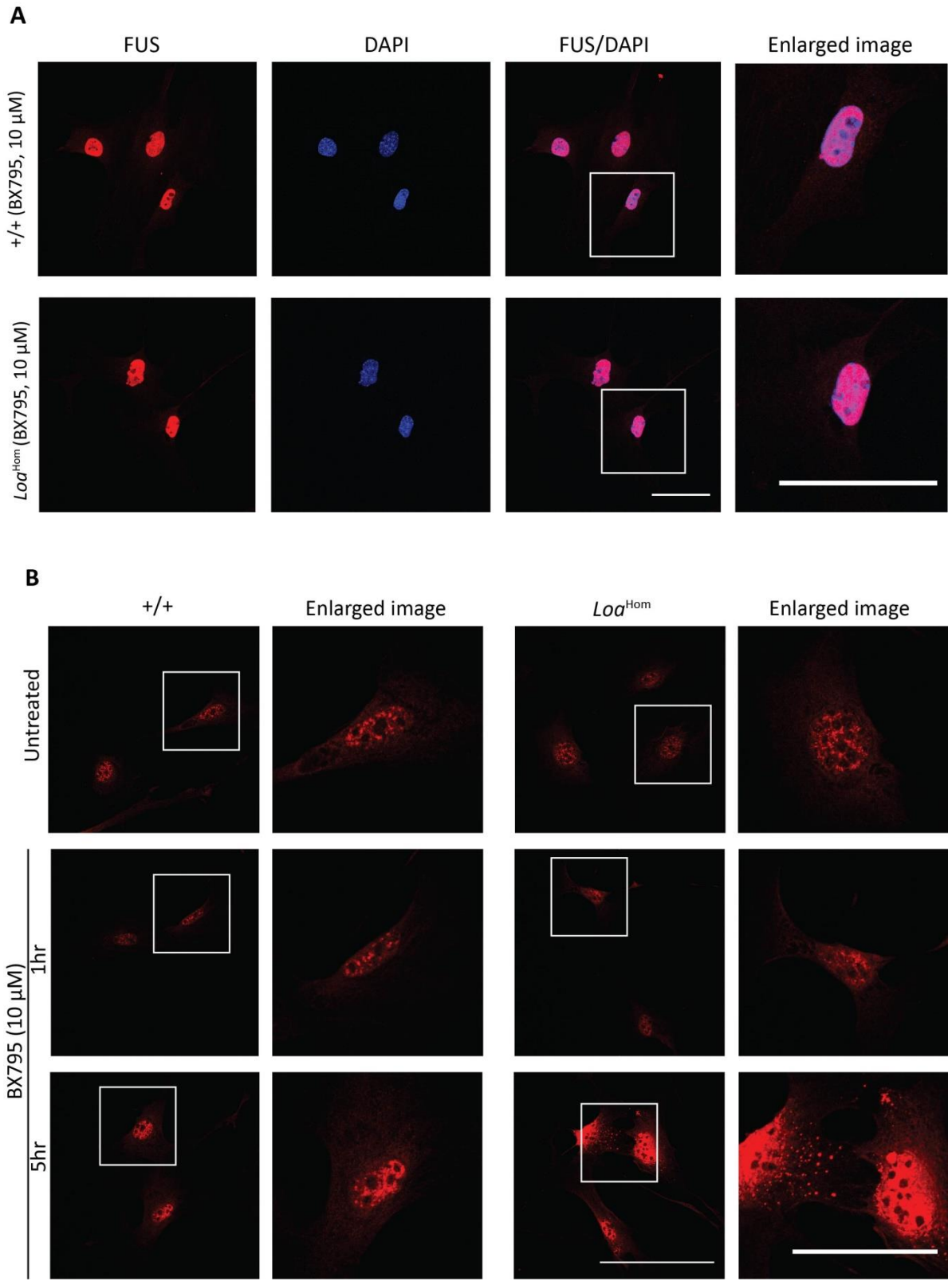
A
FUS
DAPI
FUS/DAPI
Enlarged image
+/+ (BX795, 10 µM)
Loa^Hom (BX795, 10 µM)
B
+/+
Enlarged image
Loa^Hom
Enlarged image
Untreated
BX795 (10 µM)
1hr
5hr

Figure 5.10 TBK1 inhibitor induces oligo (dT)-positive granules but not FUS-positive granule in primary Loa^{Hom} MEFs. (**A**) Primary MEFs were treated with TBK1 inhibitor (BX795, 10 μM) and then stained with antibodies to FUS and DAPI was used for nuclear staining. TBK1 inhibition did not induce formation of FUS-positive granule in wild-type and Loa^{Hom} MEFs. Representative images are shown. The enlarged images are the boxed areas for better view. Scale bar, 50 μm. (**B**) Primary MEFs were treated with TBK1 inhibitor and then cells were fixed at different time points followed by *in situ* hybridization. TBK1 inhibition induced formation of oligo (dT)-positive granule in Loa^{Hom} MEFs but not in wild-type MEFs. Representative images are shown. The enlarged images are the boxed areas shown for better view. Scale bar, 50 μm.

5.2.10 Summary

In this chapter, for the first time, it was shown that dynein deficiency causes susceptibility that upon further dysregulation in protein quality control pathway leads to TDP-43 mislocalisation. The cytoplasmic mislocalisation of TDP-43 was found in Loa^{Hom} MEFs following TBK1 inhibition using BX795 or TBK1 knockdown with TBK1-shRNA. Moreover, cytoplasmic mislocalisation of TDP-43 was detected after inhibition of proteasome system using MG132. This was found to be significantly different between genotypes where the higher level of TDP-43 mislocalisation was detected in Loa^{Hom} MEFs. Furthermore, susceptibility of Loa^{Hom} MEFs to the secondary detrimental insults was confirmed by concurrent treatment of proteasome and TBK1 or dynein inhibitors that showed enhanced cytoplasmic mislocalisation of TDP-43 in Loa^{Hom} MEFs.

Interestingly, reduction in number of arsenite-induced SGs was reported in Loa^{Hom} MEFs showing that dynein deficiency attenuated formation of SGs in Loa^{Hom} MEFs. Moreover, the increase in number of persistent SGs after removal of arsenite was shown in Loa^{Hom} MEFs and neurons. This suggests that dynein deficiency impairs the clearance of SGs resulting in persistent SGs that may lead to formation of aggregates when coupled with secondary insult.

Chapter 6: Discussion

6.1 Discussion

6.1.1 Altered level of α-tubulin acetylation in dynein mutant fibroblasts

To find the mechanisms participating in the pathology of SMA-LED caused by dynein mutations, the potential cellular mechanisms contributing to the pathology of disease were studied in human fibroblasts carrying the $D338N^{Het}$ and $R399G^{Hom}$ mutations and embryonic fibroblasts from *Loa* mouse model of SMA-LED. Dynein mutations have been classified based on their effects on cellular functions, and alterations of MT compartments have been recognised as the most common effect of the majority of *DYNC1H1* mutations (Sivagurunathan et al., 2012).

Dynein interconnects with plus-end of MTs, leading to MT stabilisation, which enables efficient retrograde transport (Yogev et al., 2017). Consequently, dynein inhibition impairs axonal transport, which also modulates MT acetylation (Even et al., 2019). Importantly, MT acetylation modulates the function and recruitment of motor proteins such as dynein onto MT and regulates axonal transport (Janke & Bulinski, 2011; Song & Brady, 2015). It has been shown that increased level of α-tubulin acetylation accelerates the dynein-dependent retrograde trafficking, in contrast, promoting MT deacetylation, attenuates motor processivity and movement of vesicles (Gao, Hubbert, & Yao, 2010; Reed et al., 2006). Moreover, acetylation of MT promotes the conformational changes in the MT, increasing affinity of MT-binding motor proteins (Skiniotis et al., 2004). Enhancing acetylation of MT has been shown to compensate for the deficits of axonal transport in the fly, mouse, and animal model of sALS (Morelli et al., 2018).

Furthermore, defects in MT components have been found in a range of neurological disorders including Huntington's disease, which impairs MT-dependant vesicular transport (Dompierre et al., 2007). Defects in dynactin, the most complex regulator of dynein, have also been shown to cause susceptibility to ALS (Münch et al., 2004) and also cause distal hereditary neuropathy (OMIM: 608634) (Puls et al., 2005) and Perry syndrome (OMIM:

168605) (Konno et al., 2017). Based on the regulatory effects of dynein on MT stability and in turn importance of dynamicity of MT in function and processivity of dynein, the level of α-tubulin acetylation has been analysed in R399G^{Hom} and D338N^{Het} fibroblasts and Loa^{Hom} MEFs.

In this research, the decreased MT acetylation was further validated using secondary fluorescent antibody in D338N^{Het} fibroblasts and Loa^{Hom} MEFs reported previously in Hafezparast lab. However, no significant change in the levels of MT acetylation was detected in the R399G^{Hom} fibroblasts, which contradicts the previous observation. Alteration of α-tubulin acetylation in D338N^{Het} fibroblasts but not in R399G^{Hom} fibroblasts might suggest that the location of mutations determine dynein contribution to the MT acetylation due to the extent and nature of the conformational changes in the dynein. As an example, it has been shown that conformational changes caused by the *nud*AR3086C mutation, which does not reside in ATP binding or hydrolysis region, alters dynein's ATPase activity leading to compromised function of dynein. Therefore, conformational changes caused by mutations may influence the function of other domains (Zhuang, Zhang, & Xiang, 2007). Furthermore, the reported heterogeneity of symptoms associated with *DYNC1H1* mutations could be proposed to be a result of distinct effects of different dynein mutations on the broad spectrum of its functions (Peeters et al., 2015).

To confirm the above results, the effect of dynein on MT acetylation, wild-type fibroblasts were treated with the chemical inhibitor of dynein (CilD), which decreased levels of MT acetylation. Therefore, the activity of dynein is crucial for the level of MT acetylation, and the inhibition of ATPase activity of dynein leads to disruption of MT acetylation.

Collectively, these results suggest that dynein and acetylated MT mutually regulate each other's functions. Therefore, the *DYNC1H1* mutations could contribute to neurodegeneration through affecting functionality of dynein and altering MT acetylation and stability. It can also be proposed that dynein dysfunction might not lead to neurodegeneration but enhancing susceptibility to genetic variations or cellular stresses.

As MNs are the most affected neurons in MND, the focus of future study will be investigating levels of MT acetylation in the MNs.

6.1.2 A novel interaction of dynein with the major mammalian K40 α-tubulin acetyltransferase (α-TAT1)

To unravel the mechanisms of dynein contribution to α-tubulin acetylation, the potential interaction between α-TAT1 and dynein was studied. It has been shown that α-TAT1 through diffusion into the lumen of MTs induces acetylation of α-tubulin (Coombes et al., 2016). In this context, it is interesting that a large pool of α-TAT1 on the surface of motile vesicles, such as lysosomes and synaptic vesicles have been detected suggesting motile vesicles bring α-TAT1 in close vicinity of MT ends (Even et al., 2019).

In this study, a novel protein-protein interaction between dynein and α-TAT1 was introduced for the first time. Robust PLA signals between DIC and α-TAT1 in primary MEFs and human fibroblasts were detected. Moreover, the decreased interaction of IC and α-TAT1 was found in Loa^{Hom} MEFs and $D338N^{Het}$ human fibroblasts. These observations were indeed in agreement with data on the decreased level of α-tubulin acetylation in Loa^{Hom} MEFs and $D338N^{Het}$ human fibroblasts. This finding describes regulatory role of dynein on recruitment of α-TAT1 onto the MT contributing to MT acetylation. Therefore, the data obtained in this research, provide a mechanistic explanation for the reduction in acetylation in $D338N^{Het}$ fibroblasts and Loa^{Hom} MEFs as a result of compromised access of α-TAT1 to the MT leading to reduced level of acetylation in MT.

The interaction of dynein and α-TAT1 was also examined in MNs culture, which showed a significant reduction in the interaction of dynein and α-TAT1 in Loa^{Hom} MNs. The function of α-TAT1 as the main acetyltransferase is vital to maintain the stable MT in neuronal processes by providing stable tracks for long-lived neuronal cells (Shida et al., 2010). Moreover, loss of α-TAT1 in neurons disrupts MT structural integrity, defects in axonal morphology and consequently axonal degeneration and neuromuscular defects (Akella et al., 2010; Neumann & Hilliard, 2014). Thus, data of this work demonstrating decreased interaction between dynein and α-TAT1 in neuronal culture are in line with published data

showing that disruption in MT stability and MT-dependent axonal transport in Loa^{Hom} MNs could contribute to the pathogenicity observed in SMA-LED (Garrett et al., 2014). After discovering the novel protein-protein interaction between dynein and α-TAT1 by PLA, we also examined this interaction biochemically by co-immunoprecipitation after overexpression of V5-tagged α-TAT1. These experiments revealed the co-pull-down of DIC with α-TAT1, confirming the interaction between these proteins. This protein-protein interaction is either direct or mediated by yet another protein. Although, as the maximum distance between the proteins for obtaining a positive PLA signal is 40 nm, this interaction is likely to be a direct interaction, but further work is required to ascertain this notion.

6.1.3 The recruitment of HDAC6 on dynein remains unchanged in mutant fibroblasts

The HDAC6-dependant regulation of MT deacetylation is vital for a balance of MT acetylation (Li, Shin, & Kwon, 2013). To investigate whether the reduction in dynein-α-TAT1 interaction is the key determinants in the MT acetylation, the interaction between dynein and HDAC6 was studied via performing PLA. Previously, it was reported that dynein interacts with HDAC6 directly (Kawaguchi et al., 2003). In this set of experiments, no significant changes in the number of PLA signals were found in Loa^{Hom} MEFs compared to the wild-type. Therefore, our data suggest that the interaction between mutant dynein with HDAC6 remains unchanged.

The potential effect of dynein mutation on HDAC6 function was also investigated. Interestingly, it has been suggested that the competing acetyltransferase and deacetylase activities of α-TAT1 and HDAC6 controls the α-tubulin acetylation (Wong et al., 2018). For further investigation of effect of α-TAT1 and HDAC6 on level of MT acetylation, both wild-type and mutant fibroblasts were treated with Tubastatin, a chemical inhibitor of HDAC6, to increase the level of MT acetylation. Then, cells were recovered for 5 hours following removal of Tubastatin. The analysis of the rate of MT acetylation recovery in Loa^{Hom} MEFs and D338N^{Het} fibroblasts showed no significant difference compared to the corresponding

wild-type cells. Accordingly, these data validated the pivotal role of dynein-α-TAT1 complex in the regulation of MT acetylation. Thus, it could be suggested that the *DYNC1H1* mutation by affecting the efficient interaction between dynein with its binding partner α-TAT1 reduces MT acetylation level. One of the possible explanations in differential binding affinity of dynein to other proteins might be due to the conformational changes. For example, it has been shown that *Loa* mutation enhances the binding affinity between HC and IC, which also affects the interaction between dynein and dynactin (W. Deng et al., 2010). Therefore, conformational changes in HC and subsequent alteration in IC and dynactin binding might result in less efficient interaction between dynein and α-TAT1.

As the unchanged interaction of dynein and HDAC6 was reported, it can be proposed that the decreased level of MT acetylation observed in the mutant cells is a result of restricted dynein-dependent recruitment of α-TAT1 onto the MT surface rather than an enhanced HDAC6 activity

The data obtained from western blot analysis also demonstrated that the levels of α-TAT1 were similar across all studied genotypes. The *DYNC1H1* mutation did not change the levels of any of α-TAT1 isoforms in mutant fibroblasts. These findings verified that the decreased interaction between dynein-α-TAT1 is not as a consequence of decreased availability of α-TAT1 in the cells; rather it is due to a decreased interaction caused by the attenuated binding affinity of dynein to its partner. Importantly, the decreased interaction between dynein and α-TAT1 suggests reduced incorporation of α-TAT1 onto the MT, affecting the dynamicity of MT, which is independent of its acetyltransferase activity. A study has shown that presence of α-TAT1 on the surface of MT is necessary for effective modifications of tubulin and even interaction between α-TAT1 and MT is more critical in the regulation of MT stability rather than acetylation (Kalebic, Martinez, et al., 2013). Due to the effect of α-TAT1 on the acceleration of MT dynamics, it may also contribute to the processivity of dynein on the MT, which requires further *in vitro* and *in vivo* studies to reveal the details of these processes. Therefore, the novel interaction between dynein and

α-TAT1 found in this study highlights a crucial mechanism for MT dynamic and stability and suggests a potentially important role for α-TAT1 in MT-associated diseases.

6.1.4 *Dync1h1* mutation causes no changes in interaction between dynein and Golgin160

Golgi fragmentation has been reported in several neurodegenerative disorders. Golgi fragmentation has been considered as an early event even before cytoskeletal degeneration during neurodegeneration (Nakagomi et al., 2008). A study showed that perturbation of Golgi impairs processing and sorting of several proteins, contributing to the development of Alzheimer's disease (Joshi, Bekier, & Wang, 2015). It has been suggested that morphological alterations of Golgi and consequent functional changes result in the neurotoxicity and neurodegenerative disease. Furthermore, another study demonstrated neuromuscular denervation and axon retraction as consequent of Golgi fragmentation (van Dis et al., 2014).

Importantly, dynein plays a role not only in the positioning of the Golgi apparatus but also dynein is involved in the motility of Golgi membranes (Jaarsma & Hoogenraad, 2015). In addition, some regulatory factors of dynein such as dynactin subunit p150 Glued, BICD2 and Lis1 contribute to Golgi function and positioning (Lam, Vergnolle, Thorpe, Woodman, & Allan, 2010). Indeed, incorporation of Golgi-associated proteins into Golgi structure is mediated through dynein (Kim, Takahashi, Matsuo, & Ono, 2007). Dynein is also recruited to the Golgi apparatus through binding to Golgin160, a Golgi adaptor protein (Yadav et al., 2012).

Thus, another potential pathological mechanism for SMA-LED caused by *DYNC1H1* point mutations could be Golgi fragmentation as a result of decreased recruitment of dynein on Golgi structure. The previous data obtained in Hafezparast lab showed fragmented Golgi phenotype in $R399G^{Hom}$ fibroblasts. However, Golgi fragmentation was not detected in the $D338N^{Het}$ fibroblasts. To find out the potential effect of dynein mutation on its binding to Golgin160, the *in situ* PLA was performed, and the quantification of PLA signal

demonstrated that the interaction between dynein and Golgin160 remained unchanged in mutant fibroblasts compared to the wild-type counterparts. As no change in interaction between dynein and Golgin160 was detected, it could be suggested that other mechanisms such as activation of caspase-mediated cleavage of Golgin160, ROS and ER stress contribute to the Golgi dispersal (Nakagomi et al., 2008). Additionally, despite no significant changes in the interaction of Golgin160-dynein, the conformational changes in the dynein and the potential alterations in MT stability could cause the cellular vulnerability leading to morphological changes in Golgi.

Furthermore, Golgi fragmentation has not been reported in the Loa^{Hom} MEFs, however, the delayed reconstitution of the Golgi ribbon following nocodazole washout has been shown (Hafezparast et al., 2003). In this research, the quantification of PLA signals showed a reduction trend for dynein-Golgin160 interaction in Loa^{Hom} MEFs but it was not statistically significant. On the basis of this set of data, it can be proposed that mutant dynein may not be sufficient to cause Golgi fragmentation but may contribute to cellular vulnerability compounded with the secondary stress like nocodazole resulting in delayed recovery of Golgi structure.

Moreover, the $R399G^{Hom}$ fibroblasts, despite showing Golgi fragmentation, neither showed the alteration of Golgin160-dynein interaction nor changes in MT acetylation, which might propose the heterogeneity of effect of dynein mutations on downstream target and illustrates the differences in pathogenic mechanisms between these two mutants studied in this thesis.

6.2 Combined deficiencies of dynein and degradation pathways exacerbate mislocalisation of proteins and accumulation of aggregation-prone proteins

6.2.1 *Dync1h1* mutation modulates level of LC3II in Loa^{Hom} MEFs and combined with inhibition of ATPase activity of dynein contributes to formation of p62-positive aggregates

Protein misfolding and aggregation underlie many human diseases including ALS. The ubiquitin-proteasome and autophagy-lysosome pathways are two major mechanisms implicated in degradation of intracellular proteins, which are cooperative and complementary to maintain homeostasis (Lilienbaum, 2013). In familial cases of ALS, disease-causing mutations contribute to misfolding and aggregation of the mutant proteins. *TDP-43*, *FUS*, *OPTN*, *SQSTM1*, *UBQLN*, *C9orf72*, *DCTN1* and *VCP* are ALS-associated genes and mutations in these genes lead to the formation of protein aggregates (Ramesh & Pandey, 2017).

Importantly, the behaviour of mutant proteins is affected by the cellular environment and only selected subsets of cells such as MNs are the most affected and particularly vulnerable neurons in ALS (Fu, Hardy, & Duff, 2018). Moreover, variants in individuals' genetic background act as modifier, which could affect proteins and regulatory pathways interacting with the disease-causing mutant proteins and exacerbates the effects of mutant protein. Additionally, modifiers could modulate different aspect of disease such as onset of disease, severity of disease or duration of disease (Lamar & McNally, 2014).

Of note, cytoplasmic dynein, as the main retrograde motor protein mediates a variety of functions regulated by different subsets of subunits whose dysfunction lead to the distinct defects in cellular mechanisms (Sasaki et al., 2000). Moreover, interruption of the dynein-dynactin complex by overexpressing dynamitin in transgenic mice triggers late-onset MN degeneration similar to human ALS, causing phenotypes such as a staggering gait (LaMonte et al., 2002). Importantly, one possible mechanism contributing to

neurodegeneration is deficiency of dynein-dependent transport resulting in accumulation of autophagosome and protein aggregates (Ravikumar et al., 2005).

In the first set of experiment, due to the importance of dynein-dependents retrograde transport and its contribution to the degradation of protein inclusions, the aim was to investigate whether variations in dynein function modulates formation of protein aggregation. Furthermore, based on the multiple-hit hypothesis of neurodegeneration in ALS, this study aimed to investigate compounded effects of dynein deficiencies on accumulation of aggregation-prone proteins when secondary stress in degradative pathways exists.

Aforementioned, our analysis of the level of MT acetylation revealed that the point mutations in *DYNC1H1* in D338N^{Het} human fibroblasts and Loa^{Hom} MEFs caused the decreased level of MT acetylation. However, the R399G^{Hom} mutation did not impact the level of MT acetylation. Of note, MT acetylation plays a significant role in regulation to MT properties such as stability as well as its function in intracellular trafficking (Hammond, Cai, & Verhey, 2008). Moreover, increasing MT acetylation has been shown to rescue the axonal transport (Godena et al., 2014) and enhances retrograde transport of autophagosomes toward the lysosomes (Bánréti, Sass, & Graba, 2013). Another study (Xie, Nguyen, McKeehan, & Liu, 2010) also showed that MT acetylation is required for LC3II degradation and removal of autophagosomes, but non-acetylated MT appeared having no role in the process of autophagosome maturation. Therefore, MT and dynein involved in different phases of the autophagosome-lysosome pathway, contribute to the degradation of misfolded or aggregated proteins preventing cellular stress or death.

Here, in this research, the increased level of LC3II in Loa^{Hom} MEFs was confirmed, which was reported previously (Ravikumar et al., 2005). Moreover, the levels of LC3II in R399G^{Hom} and D338N^{Het} human fibroblasts were assessed. The results of this set of experiments showed a considerable trend toward an increased level of LC3II in D338N^{Het} human fibroblasts, which also showed a decreased level of MT acetylation. However, the analysis of levels of LC3II in R399G^{Hom} fibroblasts did not exhibit any changes in the level of

LC3II as well as no alteration in the level of MT acetylation. These findings suggest the heterogeneity of dynein's effect on retrograde transport and autophagy degradation.

Further investigation of the role of dynein in modulating formation of protein aggregates demonstrated that dynein deficiency in Loa^{Hom} MEFs is not sufficient to cause p62 aggregate formation as untreated Loa^{Hom} MEFs showed no protein aggregates with diffuse staining of p62. However, a very low concentration of CilD, mild inhibition of dynein ATPase activity, led to a significant accumulation of p62 aggregates. P62 was used as a marker as it is a well-validated UPS and autophagy substrate and accumulates as a result of proteasome inhibition and can be degraded through the autophagy. Additionally, p62 is an autophagy receptor involved in sequestering damaged or unwanted proteins into the autophagosome for degradation (Pankiv et al., 2007).

Therefore, these findings suggest that the dynein mutation might not be sufficient to cause p62 aggregate formations by its own, however, very mild stress or partial inhibition, in this case, a low concentration of CilD, promotes the formation of aggregates. Nevertheless, this very mild inhibition of dynein did not induce any changes in the number of p62 puncta in wild-type MEFs. In wild-type MEFs, p62-positive aggregates were detected only after treatment with a higher concentration of CilD. This set of data suggests the susceptibility of Loa^{Hom} MEFs, which when dynein is partially inhibited results in significant accumulation of protein aggregates. Interestingly, the selective interaction of p62 with the mutant proteins such as ALS-linked SOD1 mutants rather than wild-type protein has been shown leading to the further accumulation of p62 (Gal et al., 2007). This might also explain the cellular susceptibility in Loa^{Hom} MEFs in which the rapid formation of p62 aggregates in Loa^{Hom} MEFs upon very mild exposure to CilD might result from the presence of misfolded or unfolded protein oligomers (unidentified) due to the dynein mutation, which may contribute to the further accumulation of p62. Whereas the normal distribution of p62 upon mild treatment of CilD might suggest that the existence of unidentified misfolded proteins could be necessary for the fast formation of p62-positive aggregates in Loa^{Hom} MEFs, but further work is required to support this notion.

Therefore, impairment of dynein function as a result of mutations or ageing could be considered as an important risk factor for the accumulation of misfolded proteins when accompanied by proteostasis deficiencies. Future studies into these possibilities could provide further insights into the underlying molecular mechanisms of late-onset neurodegenerative disease.

6.2.2 Dynein deficiency compounded with TBK1 malfunction leads to accumulation of p62-positive aggregates

Dynein dysfunction has been linked to the impairment of autophagy flux, although it is not fully established whether the alterations in dynein function make the cells more prone to formation of protein aggregates. P62 accumulation after autophagy inhibition disturbs subsequent degradation of ubiquitinated proteins destined for proteasome through delaying their delivery to the proteasome's proteases (Korolchuk, Mansilla, Menzies, & Rubinsztein, 2009). Therefore, the formation of p62 aggregates not only affects cellular transport but also decreases the degradation of ubiquitinated proteins, which might lead to formation of further aggregations. Furthermore, autophagy inhibition not only affects the degradation of long-lived proteins but also compromises the ubiquitin-proteasome system and results in accumulation of aggregation-prone proteins as proteasome is not able to compensate failure in autophagy degradation (Korolchuk et al., 2009).

TANK-binding kinase 1 (TBK1) is involved in the phosphorylation of autophagy adaptors such as p62 and OPTN contributing to the efficient sequestration of ubiquitinated substrates into the autophagosomes (Oakes et al., 2017). TBK1 inhibition or loss of TBK1 function causes the formation of p62-positive aggregates, which results in inefficient recruitment of p62 into the autophagosome and consequently p62 accumulation (Pilli et al., 2012; Ye et al., 2019). In the current study, treatment with different concentrations of TBK1 inhibitor revealed that a very mild inhibition of TBK1 in Loa^{Hom} MEFs was sufficient for the formation of significant numbers of p62 puncta. In contrast, with mild inhibition of TBK1 in the wild-type MEFs, the formation of p62-positive aggregates was not detected.

The wild-type MEFs only upon treatment with a higher concentration of TBK1 inhibitor showed significant numbers of p62 puncta compared to the untreated cells but even then they were relatively lower in comparison to the number of p62 aggregates in Loa^{Hom} MEFs. These findings suggest that mutant dynein causes susceptibility in Loa^{Hom} MEFs and when compounded with partial inhibition of TBK1, it results in accumulation of p62 aggregates, while the low concentration of TBK1 inhibitor is not sufficient to induce the formation of protein aggregates in wild-type MEFs. Consequently, the accumulation of protein aggregates overloads UPS, which is not able to compensate for the deficiency of autophagy. These results suggest that dynein deficiency by its own might not cause significant protein aggregation, but a concomitant perturbation in the autophagy-lysosome pathway, in case of this study TBK1 dysfunction, exacerbates the deficiency of dynein leading to the significant increase in the number of cytoplasmic aggregates.

For further analysis, the effect of TBK1 inhibition on the level of LC3Il was investigated in western blots. Previously, it was shown that TBK1 inhibition increases the level of LC3II (Pilli et al., 2012). The treatment of the primary fibroblasts with TBK1 inhibitor also led to increased levels of LC3II. Furthermore, the western blot analysis revealed the significant increase in the level of LC3II in treated Loa^{Hom} MEFs compared to the treated wild-type MEFs, which confirms the vulnerability of the autophagy pathway in Loa^{Hom} MEFs. However, the analysis of soluble p62 showed no changes in untreated and treated cells regardless of genotype confirming that TBK1 inhibition did not affect the expression of p62 and validated the accumulation of p62 occurs as a result of autophagy deficiencies and not to the increased level of protein.

Moreover, the genetic knockdown of TBK1 resulted in accumulation of p62 puncta, which were significantly higher in the Loa^{Hom} MEFs than their wild-type counterparts. Therefore, knockdown of TBK1 recapitulating loss of TBK1 function, which also might be more closely related to the TBK1 level in human diseases, corroborated the results of the pharmacological inhibition of TBK1.

Importantly, it has been shown that loss of TBK1 function or mutation affecting the kinase activity of TBK1 results in p62-positive accumulation (Oakes et al., 2017). Moreover, loss of function in TBK1 or its ALS-associated variants affecting the kinase domain impacts the phosphorylation of p62 and thus compromising its ubiquitin-binding function and leading to dysregulated autophagy and mitophagy (Foster et al., 2020). Therefore, our data suggest that decreased activity of TBK1 concomitant with variations in function of dynein might contribute to the accumulation of pathological aggregates and consequently neurodegeneration.

Moreover, simultaneous inhibitions of dynein and TBK1 resulted in the formation of larger p62 inclusions, which might propose that malfunction of two proteins involved in a degradation system such as autophagy leads to the formation of large aggregates that other degradation systems such as UPS are unable to remove. Interestingly, it has been shown that reduced autophagy may induce the UPS and chaperon activities to maintain the solubility of proteins and thus preventing the increase in the size of protein inclusions (Nishikawa, Fewell, Kato, Brodsky, & Endo, 2001; Wang & Qin, 2013). This set of data also suggest that pathological consequences of deficiency in one autophagic component either dynein or TBK1 could be compensated by chaperon mediated degradation or UPS, whereas, impairments of both dynein and TBK1 is likely to overwhelm the UPS, rendering cells unable to maintain the proteostasis balance and resulting in p62 aggregation and subsequently its further accumulation and formation of large inclusions. Furthermore, results showed that combined inhibition of dynein and TBK1 caused the significant increase in the level of LC3II, which also confirm that the concurrent inhibition of two autophagic players leads to a higher level of LC3II supporting the dysfunction of autophagic removal.

Moreover, a previous study (Bjorkoy et al., 2005) suggested the coordinated incorporation of LC3II and p62 into the autophagic machinery to facilitate the clearance of aggregates, which is also supported by the findings of research presented here where absence of efficient recruitment of p62 or LC3II into autophagic compartment was shown to lead to protein accumulation and thereby could contribute to formation of toxic aggregates.

6.2.3 Effects of dynein and TBK1 on formation of aggregates synergizes with proteasome inhibition

Due to the coordinated function of autophagy and the proteasome system, in this research, it was examined whether defective autophagy pathway mediated by mutant dynein in Loa^{Hom} MEFs exacerbates MG132-mediated accumulation of p62. The formation of aggregates of ubiquitinated proteins around the p62 bodies has been reported as a consequence of proteasome inhibition (Bjorkoy et al., 2005). Consequently, p62 bodies facilitate the removal of protein aggregates through the autophagy (You et al., 2019). Moreover, MG132-mediated inhibition of proteasome has been shown to result in the activation of autophagy (D. Wang et al., 2019). Additionally, proteasome activity declines with age and reduced activity of proteasome has been reported in neurodegenerative disorders (Tai & Schuman, 2008). Thus, a robust autophagic clearance seems crucial for cellular proteostasis. The results of treatment with the proteasome inhibitor showed p62 accumulation in both wild-type and Loa^{Hom} MEFs, however, the number of p62 puncta was significantly higher in the Loa^{Hom} MEFs. This suggests that the dynein mutation renders Loa^{Hom} MEFs more susceptible to accumulation of p62-positive aggregates when proteasome is dysregulated.

Moreover, to further assess the effect of deficiencies of autophagy caused by dynein dysfunction on the accumulation of ubiquitinated proteins upon proteasome inhibition, wild-type MEFs were co-treated with proteasome and dynein inhibitors. The results of this set of experiments showed that upon dynein inhibition and subsequent deficiency of autophagy, the number of p62 aggregates increased significantly when proteasome was inhibited.

Therefore, concurrent inhibition of proteasome degradation and autophagy dysfunction synergizes accumulation of protein aggregates. However, the quantification of p62 aggregates represented that the increasing concentration of dynein inhibitor did not result in a higher number of aggregates; although the size of p62-positive aggregates enhanced significantly. These findings show that delay in clearance of protein aggregates

due to the impaired function of autophagy causes coalescence of p62 aggregates resulting in formation of larger aggregates. Moreover, it was shown that proteasome inhibition activates autophagy by inducing expression of autophagy genes, which promotes cell survival through clearance of Ub-conjugated proteins (Sha, Schnell, Ruoff, & Goldberg, 2018). In other words, the robust autophagic system has been shown to promote cell survival through compensating age-dependent reduction in proteasome system. Therefore, lack of efficient proteasome degradation and concurrent reduction of dynein functionality as a consequence of mutations or genetic variations might modulate the accumulation of aggregation-prone proteins leading to the cellular dysfunction and degeneration.

To further investigate the effects of autophagy dysregulation on the exacerbations of accumulation of proteins upon proteasomal dysfunction, the TBK1 inhibitor was used concomitant with the proteasome inhibitor in wild-type and Loa^{Hom} MEFs. The data demonstrated a significant increase in the number of p62 aggregates in Loa^{Hom} MEFs co-treated with TBK1 and proteasome inhibitors. In contrast, the wild-type MEFs showed a slight change in the number of p62 aggregates. This set of data suggests that deficiencies in more than one protein involved in autophagy exacerbate the autophagy deficits leading to the formation of larger aggregates. Thus, malfunction of autophagy leads to formation of large inclusions that cannot be degraded through other protein degradation systems rather than autophagy and thus end up in further accumulation, which interferes with the normal cellular trafficking and results in degeneration. In another word, proteasome inhibition results in the formation of protein aggregates and at the same time activation of the autophagy system to induce clearance of aggregated protein to prevent cellular stress or cell death. Therefore, genetic variations or defects in proteins regulating various stages of autophagy, which by their own are not detrimental; in combination with failure of proteasome system could contribute to the formation of toxic protein aggregates and ALS pathogenesis.

Results of these experiments support the multistep hypothesis in ALS. This set of data showed that coexistence of multiple risk factors involved in autophagy pathway, dynein

and TBK1 in this study, and reduced function of proteasome results in exacerbation of protein aggregation, which triggers the pathology in neurodegenerative disease such as ALS. Moreover, ALS has been suggested to be an oligogenic disease. In fact, combined effects of mutations in different ALS-related genes contribute to the disease progression rate and pathology (Fogh et al., 2016). Additionally, genetic variations have been reported in ALS patients and some of these variations contribute to the early-onset of symptoms. (Chiò et al., 2018). Therefore, findings of this study suggest that cryptic natural variants in genes encoding components of the proteostasis systems, even though not causing detectable phenotype in healthy individuals, can have profound effects on formation of protein aggregates upon a second hit, leading to neurodegeneration.

6.3 Aberrant dynein function causes susceptibility synergizes with impairment of degradation system leads to TDP-43 mislocalisation

6.3.1 Combined deficiencies of dynein and TBK1 lead to TDP-43 mislocalisation

TDP-43 mislocalisation is a relatively widespread feature in distinct neurodegenerative disease, particularly ALS; however, the majority of studies focused mainly on TDP-43 aggregation rather than wild-type TDP-43 mislocalisation, for which the underlying molecular mechanism of neurotoxicity is not fully understood.

Here, TDP-43 mislocalisation was studied across primary MEFs in wild-type and Loa^{Hom} mice. The aim was to investigate the impact of dynein malfunction on cellular susceptibility and its potential participation in TDP-43 mislocalisation in combination with TBK1 deficiency, representing a second hit.

After treatment of wild-type and Loa^{Hom} MEFs with a pharmacological inhibitor of TBK1, significant cytoplasmic mislocalisation of TDP-43 was reported in Loa^{Hom} MEFs with no alteration in localisation of TDP-43 in the wild-type MEFs. Moreover, knockdown of TBK1 led to mislocalisation of TDP-43 in Loa^{Hom} MEFs, which corroborated previous result,

showing that stress-provoked phenotypes of Loa^{Hom} MEFs with dynein deficiency cause aberrant mislocalisation of TDP-43 when combined with dysfunction of TBK1. These results were further supported by co-inhibition of dynein and TBK1 in wild-type MEFs showing that combined defects of dynein and TBK1 contribute to TDP-43 mislocalisation. The quantification of TDP-43 intensity revealed the significant level of TDP-43 mislocalisation, which further validated the previous result showing that simultaneous perturbation in dynein and TBK1 functions results is TDP-43 mislocalisation.

These findings showed that dynein dysfunction or reduction of TBK1 function by itself is not sufficient for the TDP-43 mislocalisation in wild-type MEFs. However, the combined effect of dynein and TBK1 malfunctions altered the localisation of TDP-43 in Loa^{Hom} MEFs. These results suggest a two-hit hypothesis for the TDP-43 mislocalisation in Loa^{Hom} MEFs wherein a second deleterious event or second hit is required to cause TDP-43 mislocalisation following the dynein dysfunction.

Interestingly, TBK1 controls the MT dynamics and also regulates the cytoplasmic level of dynein. It has been reported that reduction of TBK1 function or TBK1 inhibition alters the level of cytoplasmic dynein. In addition, TBK1 phosphorylates the NuMA, a mitotic protein, which binds to dynein and knockdown of TBK1 by affecting the phosphorylation of NuMA decreases dynein recruitment (Pillai et al., 2014). Therefore, TBK1 deficits not only affect the phosphorylation of autophagy adaptors and subsequent sequestration of ubiquitinated proteins into autophagosomes but also could exacerbate dynein deficiency contributing to the cellular stress and aberrant mislocalisation of TDP-43.

Pointing to the autophagy dysregulation and consequently reduced removal of protein aggregates, TBK1 mutations result in the cytoplasmic TDP-43 and p62 inclusions in the brain of ALS patients (Pottier et al., 2015). In contrast, another study reported that heterozygous deletion of mouse *Tbk1*, corresponding to the *Tbk1* loss of function mutation, did not cause the MND phenotype and TDP-43 pathology in early stages. Besides, the overexpression of mutant SOD1 with heterozygous deletion of *Tbk1* mice resulted in pathological symptoms (Brenner et al., 2019). Thus, it has been speculated that

Tbk1 loss of function mutations in the presence of deficiency in one or more factors as secondary hit might show the pathological phenotype. This is of particular importance as current finding that TBK1 inhibition or knockdown only upon exposure to the second factor, which in this study was a dynein-related deficiency, caused the TDP-43 mislocalisation. Given the varied and crucial roles of TBK1 and cytoplasmic dynein in autophagy, further investigations into the link between dynein and TBK1 functions will extend our understanding of the underlying molecular mechanisms of ALS.

6.3.2 Dynein inhibition results in TDP-43 mislocalisation in wild-type and Loa^{Hom} MEFs

As regards to the role of autophagy in the maintenance of TDP-43 localisation and cytoplasmic level and importance of dynein for the efficiency of autophagy; the potential effect of dynein inhibition on TDP-43 mislocalisation was assessed. Both wild-type and Loa^{Hom} MEFs treated with dynein inhibitor exhibited the mislocalisation of TDP-43. However, the Loa^{Hom} MEFs showed a higher level of TDP-43 mislocalisation, which is likely due to the presence of primary defect of dynein in Loa^{Hom} MEFs with the potential failure of autophagy rendering the cells susceptible to dynein inhibition contributing to the higher level of mislocalisation after inhibition of dynein.

Interestingly, TDP-43 modulates axonal transport and also regulates the axonal transcriptome of MNs (Fratta et al., 2018). Therefore, not only deficiency of intracellular transport could result in TDP-43 pathology, but also in turn, TDP-43-dependant pathology could contribute to further deficiency in this system as ALS-linked mutations in *TARDBP* have been reported to cause pre-symptomatic defects in axonal transport (Gordon et al., 2019; Sleigh et al., 2020). Importantly, loss of TDP-43 has been shown to decrease expression of dynactin subunit p150 Glued and impair autophagosome-lysosome fusion resulting in accumulation of immature autophagic vesicles (Xia et al., 2015). Therefore, dynein deficiency with subsequent TDP-43 mislocalisation causing further disturbances in

autophagosome-lysosome fusion could explain the accumulation of p62-positive aggregates in Loa^{Hom} MEFs.

6.3.3 Proteasome inhibition exacerbated the TDP-43 mislocalisation in Loa^{Hom} MEFs

Under normal conditions, UPS degrades the ubiquitinated proteins rapidly. Thus, upon failure of proteasome function, proteins such TDP-43 have the potential to build up oligomers, which are small protein aggregates (Johnson et al., 2009). Consequently, the presence of TDP-43 deposition and increased protein inclusions in the degenerating neurons induces further impairment of proteasome. Additionally, overexpression and abnormal accumulation of TDP-43 inhibit the enzymatic activity of the proteasome (Tashiro et al., 2012). Then, the balance in degradation system for removal of protein aggregates shifts toward the autophagy pathway where autophagosomes engulf these aggregates and through fusion with lysosome remove them. Therefore, the decline in UPS function such as described in sporadic cases of ALS, resulting in an increased level of ubiquitinated proteins, induces the overloaded autophagy (Bendotti et al., 2012; Lee et al., 2019). Moreover, in wild-type MEFs, the UPS has been highlighted as the main pathway for degradation of TDP-43, which when inhibited results in TDP-43 accumulation in ALS/FTD brains (Lee et al., 2019; Rutherford et al., 2008). It has also been reported that proteasome inhibition in cells expressing either wild-type or mutant TDP-43 accelerates the accumulation of TDP-43 in the cytoplasm (Winton, Igaz, et al., 2008).

Furthermore, autophagy is critical for degradation of TDP-43, and the aberrant function of each partner in this pathway impairs proper autophagic degradation of TDP-43 and results in the formation of TDP-43 inclusions (S. M. Lee et al., 2019). Recognition of several ALS-associated proteins such as p62, VCP, OPTN, ubiquilin, and TBK1 linked to degradation process of ubiquitinated proteins, also revealed the critical role of autophagy and its contribution to the pathology of ALS (Renton et al., 2014).

Here, in this study, it was demonstrated that pharmacological inhibition of the proteasome in Loa^{Hom} MEFs promotes TDP-43 mislocalisation with a significant loss of nuclear TDP-43 in comparison to their wild-type counterpart suggesting that mutation in *Dync1h1* gene makes cells more vulnerable. While the proteasome inhibition was sufficient to promote the TDP-43 mislocalisation both in wild-type and Loa^{Hom} MEFs, dynein mutation exacerbated the nuclear loss of TDP-43 supporting the two-hit hypothesis in which the combined deficiency of dynein, an autophagy component (first hit), and proteasome inhibition (second hit) promoted further mislocalisation of TDP-43 in Loa^{Hom} MEFs.

In contrast to TDP-43, FUS persisted within the nucleus after proteasome inhibition which could be explained by the difference in the rate that they are shuttled between nucleus and cytoplasm (Kim & Taylor, 2017). In other words, the mislocalisation of TDP-43 may show a much higher rate of transfer, which causes TDP-43 to be more prone to accumulate in the cytoplasm due to the proteasome inhibition in comparison to FUS.

Altogether, this set of data suggests that TDP-43 subcellular distribution is regulated by both proteasome and autophagy systems, which confirm the result of other study showing that both proteasome and autophagy are involved in the regulation of the cytoplasmic level of TDP-43 (Wang et al., 2010). As recycling of TDP-43 is highly controlled through more than one protein turnover pathway, concurrent inhibition of the proteasome system and autophagy impairment in the Loa^{Hom} MEFs augments loss of nuclear TDP-43. Moreover, *DYNC1H1* variations such as p.Asp1991Asn, p.Leu3508lle, p.Ser4603lle, and p.Thr4394Met that have been recognised in both sALS cases and healthy controls might suggest that dynein-dependent deficiency affecting distinct pathways including proteostasis system might not be sufficient to result in pathological phenotype such as TDP-43 mislocalisation but renders the cells susceptible to the subsequent insult leading to neurodegenerative pathology.

These data might also suggest that the prolonged exposure to the proteasome inhibitor in Loa^{Hom} MEFs might lead to the formation of protein aggregates after mislocalisation of TDP-43, which needs further investigation.

6.3.4 Dynein mutation delays resolution of SGs

Here, in this study, mislocalisation of TDP-43 was reported in Loa^{Hom} MEFs following inhibition of kinase activity of TBK1 or TBK1 knockdown. TDP-43 and FUS contain low-complexity domain (LCD) and prion-like domain, which mediate the localisation of these proteins with SG marker and also promote protein aggregation. In pathological condition, possibly owing to diverse genetic and environmental factors, TDP-43 and FUS turn into the persistent cytoplasmic aggregates which are not readily cleared after severe stress, consequently inhibiting physiological stress responses (Aulas & Vande Velde, 2015).

As both TDP-43 and FUS are RNA-binding proteins and involved in cellular stress responses, it was investigated whether TBK1 inhibition coupled with dynein deficiency in Loa^{Hom} MEFs results in mislocalisation of FUS similar to TDP-43 reported in Loa^{Hom} MEFs. The analysis of microscopic images showed no changes in the localisation of FUS after treatment, and FUS remained localised in the nucleus. Although after TBK1 inhibition, performing *in situ* hybridisation, oligo (dT) positive granules in the Loa^{Hom} MEFs were scored, supporting the hypothesis that concurrent deficiencies of dynein and TBK1 could be attributed to cellular stress and contribute to the formation of SGs. Consequently, the assembly of SGs in the Loa^{Hom} MEFs promoted the mislocalisation of proteins such as TDP-43 and subsequent localisation of TDP-43 with SG components. It is noteworthy that TDP-43 and FUS do not have overlapping functions in SG assembly and assembly of SGs (Aulas, Stabile, & Vande Velde, 2012). Role of TDP-43 in regulation of SG assembly is more specific compared to the FUS and assembly of SGs occurs in absence of FUS which also might explain the cytoplasmic absence of FUS upon TBK1 inhibition.

Importantly, contribution of SG to the pathogenesis of many human diseases has stimulated great interest in the biology and dynamics of SG. Disruption of SG dynamics has

been implicated in the pathogenesis of several diseases, including neurodegenerative disease (Panas et al., 2016). Thus, due to the importance of SGs in the cellular stress responses and the cellular homeostasis, the effect of dynein on the dynamics of SGs via scoring the FUS, an essential component of SGs and the oligo (dT) a general marker of SG were examined.

Here, the reduction in the number of SGs in Loa^{Hom} MEFs and also persistent SGs in Loa^{Hom} MEFs during the recovery period after removal of stressors was shown. We also investigated the dynamic of SGs in the hippocampal neurons. The quantifications of number of SGs revealed a significant reduction in the number of SGs in Loa^{Het} neurons. Of note, formation of SGs has been considered as a protective mechanism that enables the cells to respond to stresses by regulation of its activities. Thus, the reduction in the number of SGs in Loa^{Hom} MEFs suggests cellular vulnerability, which might influence the susceptibility to stresses (Tsai et al., 2009).

Furthermore, dynein could impact process of SG formation indirectly through alteration of MT stability. Interestingly, it has been reported that MT instability modulates SG formation (Chernov et al., 2009). Therefore, these data might suggest that the reduced MT acetylation in Loa^{Hom} MEFs could be also involved in reduced number of SGs.

This work also showed that dynein malfunction in Loa^{Hom} MEFs causes a significant delay in the removal of FUS and oligo (dT) containing SGs in comparison to relatively quick removal of SGs in the wild-type counterparts. In response to cellular stress, cells can form transient SGs, but functional impairment of SGs and impaired SG dynamics drive neurodegeneration (Wolozin, 2014). Formation of SGs occurs through the liquid-liquid phase separation (LLPS), a biochemical property of some RNA-binding proteins, where SGs proteins form a liquid phase distinct from the cytosol (Protter & Parker, 2016). The persistent SGs by inhibiting the protein translation, loss of essential components necessary for cellular function, and also the accumulation of toxic components disturb the cellular homeostasis. Additionally, the persistence of stable SG-like aggregates has been characterised by pathological inclusions in MNs, brain, muscle, and bone cells, causing

multisystem proteinopathy (Kim et al., 2013). Moreover, disturbances in low-complexity sequence domain (LCD) in RNA-binding proteins such as TDP-43 undergo LLPS, which facilitate the formation of liquid-like droplets, may subsequently convert to static assemblies (Babinchak et al., 2019). In addition, LCD-mediated LLPS has been suggested to contribute to the SGs assembly and provide a link between persistent SGs and pathological protein fibrillisation (Molliex et al., 2015). Furthermore, FUS and TDP-43 contain prion-like domain mediating their assembly into high-order structures. Alterations in prion-like domain lead to hyperassembly of SGs and perturbed SG dynamics, which increase persistence of proteins in SGs (Ramaswami, Taylor, & Parker, 2013). More importantly, appearance of persistent pathological SGs prior to TDP-43 deposition has been implicated in the aberrant SGs response, which drives TDP-43 proteinopathy in ALS (Chew et al., 2019).

Therefore, aberrant persistence of SGs in Loa^{Hom} MEFs could be considered as a pathological mechanism prior to mislocalisation of TDP-43 and also render cells more susceptible to the subsequent insult leading to protein accumulation.

One of the mechanisms that possibly could explain delayed SGs recovery is the decreased level of MT acetylation reported in the Loa^{Hom} MEFs affecting the dynein-dependant removal of SGs. Moreover, autophagy dysregulation caused by dynein mutation could be considered as another potential mechanism involved in the delayed recovery of SG. The importance of autophagy in SGs clearance has been reported previously in which autophagy regulates the removal of FUS-positive SGs through VCP-containing proteins and autophagy impairment, which is common in the ALS, leading to SG persistence (Buchan et al., 2013; Soo et al., 2015).

In addition, FUS contributes to both autophagy initiation and autophagic flux, and the expression of ALS-associated mutant FUS impaired the autophagy resulting in the increased number of LC3-positive vesicles and modulation of SGs dynamic by increasing their cytoplasmic persistence (Monahan et al., 2016; Soo et al., 2015). Moreover, the pathological persistence of SGs results in formation of stable structures which are largely

irreversible in cells (Y. R. Li et al., 2013). Thus, the persistent of FUS-positive SGs in the Loa^{Hom} MEFs may induce further defects in autophagy-dependent removal of SGs and protein aggregation. Subsequently, the accumulation of stable structures SG-like assemblies alters RNA biogenesis, signaling pathways, and axonal transport, which triggers cell death (Ramaswami et al., 2013).

Collectively, these data provide better insight into the importance of the role of dynein, contributing to the maintenance of cellular homeostasis through regulating the formation of SGs and autophagy-dependent removal of SG. Moreover, result of this research describes how intrinsic vulnerabilities within the cellular system such as presence of genetic variants might lead to the pathological aggregation when SGs become persistent, accelerating the neurotoxicity and neurodegeneration. On the other hand, as activation of autophagy has been reported to reduce the number of FUS-positive SGs and resulting in the reduction of neurites fragmentation and neuronal death (Ryu et al., 2014). Thus, it can be suggested that activation of the autophagic system might restore the disrupted SG dynamic in Loa^{Hom} MEFs and can be considered as a potential therapeutic approach.

6.2 Conclusion

Data in this thesis confirmed the reduction in MT acetylation in one of *DYNC1H1* mutations reported previously in Hafezparast lab. Reduced MT acetylation validated in this thesis indicates the importance of dynein in pathogenic mechanism contributory to SMA-LED, which could be targeted by therapeutics. Furthermore, the novel protein-protein interaction between dynein and α-TAT1 introduced in this thesis provides a better understanding of mechanism through which dynein modulate MT acetylation. The decreased interaction between dynein and α-TAT1 detected in both D338N^{Het} fibroblasts and Loa^{Hom} MEFs explains the underlying mechanism for curtailing MT acetylation in mutant fibroblasts. Additionally, no alteration in interaction between HDAC6 and dynein and no changes in function of HDAC6 were reported in D338N^{Het} fibroblasts and Loa^{Hom} MEFs confirm the importance of dynein-α-TAT1 interaction in regulation of MT acetylation.

Moreover, previous data in Hafezparast lab showed decreased recruitment of dynein on Golgi membrane and Golgi fragmentation in R339G^{Het} fibroblasts suggesting a pathological mechanism contributing to SMA-LED. However, in this work, no change in interaction of dynein and Golgin160 was found in R339G^{Het} and D338N^{Het} fibroblasts, which propose that interaction between dynein and Golgin160 does not underlie the Golgi fragmentation. However, to ascertain this notion, further experiments are required to check the interaction between dynein and Golgin160 on the Golgi membrane.

Furthermore, the research work presented in this thesis showed that dynein deficiency in combination with TBK1 or proteasome inhibition significantly modulates level of LC3II and had a cumulative effect on formation of p62-positive aggregates and aberrant localisation of TDP-43. Interestingly, variations in *DYNC1H1* have been reported in both ALS and control groups suggest that dysfunction of dynein coupled with further deficiencies in mechanisms such as protein quality control system contribute to the appearance of pathological phenotype in ALS cases.

Therefore, data of this study fit the two-hit model for the pathogenicity of ALS and its progress. The dynein variation could be considered as the first hit causing the susceptibility. The second hit could be deficiency in protein degradation pathway including lack of functional ubiquitin-proteasome system, and loss of TBK1 function leading to the aberrant protein mislocalisation and accumulation of protein aggregates. The Loa^{Hom} MEFs upon presence of second detrimental event or stress showed a higher susceptibility and recapitulated relevant cellular features of sALS. Thus, variations in function of dynein might render cells intrinsically susceptible to cellular ageing and overlying genetic variations, which trigger p62 aggregation and mislocalisation of TDP-43. As TDP-43 mislocalisation has a significant role in cellular dysfunction and increasingly, the field has been focusing on the regulatory mechanisms involved in TDP-43 mislocalisation.

Importantly, data of this thesis provide the insight into the mechanism driving TDP-43 proteinopathy and further support for importance of dynein's function in maintenance of cellular homeostasis through modulating formation of protein aggregates and clearance of toxic protein inclusions. Importantly, protein mislocalisation is a reversible process in comparison to protein aggregation. Therefore, understanding of regulatory mechanisms in TDP-43 subcellular localisation will be beneficial for therapy development especially those therapeutics that have the potential to be more efficacious earlier in disease and more pertinent to the most cases to prevent progression of ALS. Furthermore, as TDP-43 pathology in most cases coexists with other aggregate-prone proteins such as p62, a better understanding of role of TDP-43 mislocalisation will serve the broader insight in pathology and modes of degeneration across a spectrum of neurodegenerative disease.

Moreover, the findings of this research showed latency in clearance of SGs after removal of stressor suggesting that the persistent SGs in Loa^{Hom} MEFs and neurons might seed the formation of toxic protein aggregation acting as a hub that initiates pathological formation of protein aggregation. Moreover, formation of SGs upon TBK1 inhibition in Loa^{Hom} MEFs indicates the cellular response to oxidative stress that might explain aberrant TDP-43 cytoplasmic mislocalisation in the mutant fibroblasts. These results open new avenues for therapeutic strategies targeting dynein and autophagy at earlier stages of disease, critical

for SG dynamics to prevent pathological accumulation of protein aggregates and mislocalisation.

In summary, finding interaction between dynein and α-TAT1 and role of dynein in regulation of MT acetylation advance our understanding of molecular consequences of *DYNC1H1* mutations causing SMA-LED and the *Dync1h1* mutation in SMA-LED mouse model. Moreover, data presented in this thesis further expose effects of dynein genetic variations on cellular susceptibility, which may serve as triggers for protein aggregates and TDP-43 mislocalisation contributing to the pathology of ALS. As importance of genetic variations recognised in ALS cases, findings of this thesis, provide the better insight into understanding of consequences of *DYNC1H1* variations on pathological inclusion which may lead to therapeutic interventions targeting the dynein-dependent pathways. It seems restoring dynein functionality in combination with other treatment targeting the disease-associated mechanism such as protein aggregation would be of benefit.

In the future study, further effort is needed to study interaction between dynein and α-TAT1 onto the MT in MNs to provide better insight recognising effect of decreased interaction of dynein-α-TAT1 on MN degeneration in MND. Such comprehensions could pave the way towards procedures to modulate dynein-dependent regulation of MT acetylation. Moreover, it will be of particular interest to investigate consequences of other dynein variations coupled with variations in ALS-linked genes to provide better insight into the molecular mechanisms underlying ALS pathogenesis.

References

Adams, J. 2003. The proteasome: structure, function, and role in the cell. ***Cancer treatment reviews***, 29 Suppl 1: 3–9.

Aiken, J., Moore, J. K. & Bates, E. A. 2019. TUBA1A mutations identified in lissencephaly patients dominantly disrupt neuronal migration and impair dynein activity. ***Human molecular genetics***, 28(8): 1227–1243.

Ajroud-Driss, S. & Siddique, T. 2015. Sporadic and hereditary amyotrophic lateral sclerosis (ALS). ***Biochimica Et Biophysica Acta (BBA)-Molecular Basis of Disease***, 1852(4): 679–684.

Akella, J. S., Wloga, D., Kim, J., Starostina, N. G., Lyons-Abbott, S., Morrissette, N. S., et al. 2010. MEC-17 is an α-tubulin acetyltransferase. ***Nature***, 467(7312): 218–222.

Akhmanova, A. & Steinmetz, M. O. 2015. Control of microtubule organization and dynamics: two ends in the limelight. ***Nature reviews Molecular cell biology***, 16(12): 711–726.

Al-Chalabi, A. & Hardiman, O. 2013. The epidemiology of ALS: a conspiracy of genes, environment and time. ***Nature reviews. Neurology***, 9(11): 617–628.

Al-Chalabi, A., Jones, A., Troakes, C., King, A., Al-Sarraj, S. & van den Berg, L. H. 2012. The genetics and neuropathology of amyotrophic lateral sclerosis. ***Acta neuropathologica***, 124(3): 339–352.

Alami, N. H., Smith, R. B., Carrasco, M. A., Williams, L. A., Winborn, C. S., Han, S. S., et al. 2014. Axonal transport of TDP-43 mRNA granules is impaired by ALS-causing mutations. ***Neuron***, 81(3): 536–543.

Alberti, S., Mateju, D., Mediani, L. & Carra, S. 2017. Granulostasis: protein quality control of RNP granules. ***Frontiers in molecular neuroscience***, 10(84): 1–18.

Alemu, E. A., Lamark, T., Torgersen, K. M., Birgisdottir, A. B., Larsen, K. B., Jain, A., et al. 2012. ATG8 family proteins act as scaffolds for assembly of the ULK complex sequence requirements for LC3-interacting region (LIR) motifs. ***Journal of Biological Chemistry***, 287(47): 39275–39290.

Alonso, A., Logroscino, G., Jick, S. S. & Hernán, M. A. 2009. Incidence and lifetime risk of motor neuron disease in the United Kingdom: a population-based study. ***European journal of neurology : the official journal of the European Federation of Neurological Societies***, 16(6): 745–751.

Altan-Bonnet, N., Sougrat, R. & Lippincott-Schwartz, J. 2004. Molecular basis for Golgi maintenance and biogenesis. ***Current opinion in cell biology***, 16(4): 364–372.

Amick, J., Roczniak-Ferguson, A. & Ferguson, S. M. 2016. C9orf72 binds SMCR8, localizes to lysosomes, and regulates mTORC1 signaling. ***Molecular biology of the cell***, 27(20): 3040–3051.

Amick, J., Tharkeshwar, A. K., Amaya, C. & Ferguson, S. M. 2018. WDR41 supports lysosomal response to changes in amino acid availability. ***Molecular biology of the cell***, 29(18): 2213–2227.

Andersen, P. M. 2006. Amyotrophic lateral sclerosis associated with mutations in the CuZn superoxide dismutase gene. ***Current neurology and neuroscience reports***, 6(1): 37–46.

Andersen, P. M. & Al-Chalabi, A. 2011. Clinical genetics of amyotrophic lateral sclerosis: what do we really know? ***Nature reviews. Neurology***, 7(11): 603–615.

Anderson, P. & Kedersha, N. 2008. Stress granules: the Tao of RNA triage. ***Trends in biochemical sciences***, 33(3): 141–150.

Anderson, P. & Kedersha, N. 2009. RNA granules: post-transcriptional and epigenetic modulators of gene expression. ***Nature reviews Molecular cell biology***, 10(6): 430–436.

Andersson, M. K., Ståhlberg, A., Arvidsson, Y., Olofsson, A., Semb, H., Stenman, G., et al. 2008. The multifunctional FUS, EWS and TAF15 proto-oncoproteins show cell type-

specific expression patterns and involvement in cell spreading and stress response. ***BMC cell biology***, 9(1): 1–17.

Anguiano, J., Garner, T. P., Mahalingam, M., Das, B. C., Gavathiotis, E. & Cuervo, A. M. 2013. Chemical modulation of chaperone-mediated autophagy by retinoic acid derivatives. ***Nature chemical biology***, 9(6): 374–382.

Arimoto-Matsuzaki, K., Saito, H. & Takekawa, M. 2016. TIA1 oxidation inhibits stress granule assembly and sensitizes cells to stress-induced apoptosis. ***Nature communications***, 7(1): 1–10.

Aschenbrenner, L., Naccache, S. N. & Hasson, T. 2004. Uncoated endocytic vesicles require the unconventional myosin, Myo6, for rapid transport through actin barriers. ***Molecular biology of the cell***, 15(5): 2253–2263.

Ash, P. E. A., Bieniek, K. F., Gendron, T. F., Caulfield, T., Lin, W.-L., Dejesus-Hernandez, M., et al. 2013. Unconventional translation of C9ORF72 GGGGCC expansion generates insoluble polypeptides specific to c9FTD/ALS. ***Neuron***, 77(4): 639–646.

Asthana, J., Kuchibhatla, A., Jana, S. C., Ray, K. & Panda, D. 2012. Dynein light chain 1 (LC8) association enhances microtubule stability and promotes microtubule bundling. ***Journal of Biological Chemistry***, 287(48): 40793–40805.

Audebert, S., Desbruyères, E., Gruszczynski, C., Koulakoff, A., Gros, F., Denoulet, P., et al. 1993. Reversible polyglutamylation of alpha- and beta-tubulin and microtubule dynamics in mouse brain neurons. ***Molecular biology of the cell***, 4(6): 615–626.

Aulas, A., Fay, M. M., Lyons, S. M., Achorn, C. A., Kedersha, N., Anderson, P., et al. 2017. Stress-specific differences in assembly and composition of stress granules and related foci. ***J Cell Sci***, 130(5): 927–937.

Aulas, A., Stabile, S. & Vande Velde, C. 2012. Endogenous TDP-43, but not FUS, contributes to stress granule assembly via G3BP. ***Molecular neurodegeneration***, 7(54): 1–14.

Aulas, A. & Vande Velde, C. 2015. Alterations in stress granule dynamics driven by TDP-43 and FUS: a link to pathological inclusions in ALS? ***Frontiers in cellular neuroscience***, 9(423): 1–13.

Ayaki, T., Ito, H., Fukushima, H., Inoue, T., Kondo, T., Ikemoto, A., et al. 2014. Immunoreactivity of valosin-containing protein in sporadic amyotrophic lateral sclerosis and in a case of its novel mutant. ***Acta neuropathologica communications***, 2(172): 1–14.

Ayala, Y. M., Zago, P., D'Ambrogio, A., Xu, Y.-F., Petrucelli, L., Buratti, E., et al. 2008. Structural determinants of the cellular localization and shuttling of TDP-43. ***Journal of cell science***, 121(22): 3778–3785.

Baas, P. W., Rao, A. N., Matamoros, A. J. & Leo, L. 2016. Stability properties of neuronal microtubules. ***Cytoskeleton***, 73(9): 442–460.

Babinchak, W. M., Haider, R., Dumm, B. K., Sarkar, P., Surewicz, K., Choi, J.-K., et al. 2019. The role of liquid-liquid phase separation in aggregation of the TDP-43 low-complexity domain. ***Journal of Biological Chemistry***, 294(16): 6306–6317.

Balendra, R. & Isaacs, A. M. 2018. C9orf72-mediated ALS and FTD: multiple pathways to disease. ***Nature Reviews Neurology***, 14(9): 544–558.

Bánréti, A., Sass, M. & Graba, Y. 2013. The emerging role of acetylation in the regulation of autophagy. ***Autophagy***, 9(6): 819–829.

Bao, W., Gu, Y., Ta, L., Wang, K. & Xu, Z. 2016. Induction of autophagy by the MG-132 proteasome inhibitor is associated with endoplasmic reticulum stress in MCF-7 cells. ***Molecular medicine reports***, 13(1): 796–804.

Barmada, S. J., Skibinski, G., Korb, E., Rao, E. J., Wu, J. Y. & Finkbeiner, S. 2010. Cytoplasmic mislocalization of TDP-43 is toxic to neurons and enhanced by a mutation associated with familial amyotrophic lateral sclerosis. ***Journal of Neuroscience***, 30(2): 639–649.

Beale, R., Wise, H., Stuart, A., Ravenhill, B. J., Digard, P. & Randow, F. 2014. A LC3-interacting motif in the influenza A virus M2 protein is required to subvert autophagy and maintain virion stability. ***Cell host & microbe***, 15(2): 239–247.

Behrends, C., Sowa, M. E., Gygi, S. P. & Harper, J. W. 2010. Network organization of the human autophagy system. ***Nature***, 466(7302): 68–76.

Belzil, V. V., Bauer, P. O., Prudencio, M., Gendron, T. F., Stetler, C. T., Yan, I. K., et al. 2013. Reduced C9orf72 gene expression in c9FTD/ALS is caused by histone trimethylation, an epigenetic event detectable in blood. ***Acta neuropathologica***, 126(6): 895–905.

Bendotti, C., Marino, M., Cheroni, C., Fontana, E., Crippa, V., Poletti, A., et al. 2012. Dysfunction of constitutive and inducible ubiquitin-proteasome system in amyotrophic lateral sclerosis: implication for protein aggregation and immune response. ***Progress in neurobiology***, 97(2): 101–126.

Berning, B. A. & Walker, A. K. 2019. The pathobiology of TDP-43 C-terminal fragments in ALS and FTLD. ***Frontiers in neuroscience***, 13(335): 1–27.

Bertos, N. R., Gilquin, B., Chan, G. K., Yen, T. J., Khochbin, S. & Yang, X.-J. 2004. Role of the tetradecapeptide repeat domain of human histone deacetylase 6 in cytoplasmic retention. ***Journal of Biological Chemistry***, 279(46): 48246–48254.

Bhabha, G., Johnson, G. T., Schroeder, C. M. & Vale, R. D. 2016. How dynein moves along microtubules. ***Trends in biochemical sciences***, 41(1): 94–105.

Bhuwania, R., Castro-Castro, A. & Linder, S. 2014. Microtubule acetylation regulates dynamics of KIF1C-powered vesicles and contact of microtubule plus ends with podosomes. ***European journal of cell biology***, 93(10-12): 424–437.

Bilsland, L. G., Sahai, E., Kelly, G., Golding, M., Greensmith, L. & Schiavo, G. 2010. Deficits in axonal transport precede ALS symptoms in vivo. ***Proceedings of the National Academy of Sciences of the United States of America***, 107(47): 20523–20528.

Bjorkoy, G., Lamark, T., Brech, A., Outzen, H., Perander, M., Overvatn, A., et al. 2005. p62/SQSTM1 forms protein aggregates degraded by autophagy and has a protective effect on huntingtin-induced cell death. ***The Journal of cell biology***, 171(4): 603–614.

Bjørkøy, G., Lamark, T. & Johansen, T. 2006. p62/SQSTM1: a missing link between protein aggregates and the autophagy machinery. ***Autophagy***, 2(2): 138–139.

Blokhuis, A. M., Groen, E. J. N., Koppers, M., van den Berg, L. H. & Pasterkamp, R. J. 2013. Protein aggregation in amyotrophic lateral sclerosis. ***Acta neuropathologica***, 125(6): 777–794.

Bodakuntla, S., Jijumon, A., Villablanca, C., Gonzalez-Billault, C. & Janke, C. 2019. Microtubule-associated proteins: structuring the cytoskeleton. ***Trends in cell biology***, 29(10): 804–819.

Bogucki, A., Pigo'nska, J., Szadkowska, I. & Gajos, A. 2016. Unilateral progressive muscular atrophy with fast symptoms progression. ***Neurologia i Neurochirurgia Polska***, 50(1): 52–54.

Boland, B., Kumar, A., Lee, S., Platt, F. M., Wegiel, J., Yu, W. H., et al. 2008. Autophagy induction and autophagosome clearance in neurons: relationship to autophagic pathology in Alzheimer's disease. ***Journal of Neuroscience***, 28(27): 6926–6937.

Boland, B., Yu, W. H., Corti, O., Mollereau, B., Henriques, A., Bezard, E., et al. 2018. Promoting the clearance of neurotoxic proteins in neurodegenerative disorders of ageing. ***Nature reviews Drug discovery***, 17(9): 660–688.

Bonnet, C., Boucher, D., Lazereg, S., Pedrotti, B., Islam, K., Denoulet, P., et al. 2001. Differential binding regulation of microtubule-associated proteins MAP1A, MAP1B, and MAP2 by tubulin polyglutamylation. ***Journal of Biological Chemistry***, 276(16): 12839–12848.

Bornens, M. 2008. Organelle positioning and cell polarity. ***Nature Reviews Molecular Cell Biology***, 9(11): 874–886.

Bose, J. K., Huang, C.-C. & Shen, C.-K. J. 2011. Regulation of autophagy by neuropathological protein TDP-43. ***Journal of Biological Chemistry***, 286(52): 44441–44448.

Bounedjah, O., Desforges, B., Wu, T.-D., Pioche-Durieu, C., Marco, S., Hamon, L., et al. 2014. Free mRNA in excess upon polysome dissociation is a scaffold for protein multimerization to form stress granules. ***Nucleic acids research***, 42(13): 8678–8691.

Boyault, C., Gilquin, B., Zhang, Y., Rybin, V., Garman, E., Meyer-Klaucke, W., et al. 2006. HDAC6-p97/VCP controlled polyubiquitin chain turnover. ***The EMBO journal***, 25(14): 3357–3366.

Boyault, C., Zhang, Y., Fritah, S., Caron, C., Gilquin, B., Kwon, S. H., et al. 2007. HDAC6 controls major cell response pathways to cytotoxic accumulation of protein aggregates. ***Genes & development***, 21(17): 2172–2181.

Brenner, D., Sieverding, K., Bruno, C., Lüningschrör, P., Buck, E., Mungwa, S., et al. 2019. Heterozygous Tbk1 loss has opposing effects in early and late stages of ALS in mice. ***Journal of Experimental Medicine***, 216(2): 1–12.

Brenner, D., Yilmaz, R., Müller, K., Grehl, T., Petri, S., Meyer, T., et al. 2018. Hot-spot KIF5A mutations cause familial ALS. ***Brain***, 141(3): 688–697.

Breuer, A. C. & Atkinson, M. B. 1988. Fast axonal transport alterations in amyotrophic lateral sclerosis (ALS) and in parathyroid hormone (PTH)-treated axons. ***Cell motility and the cytoskeleton***, 10(1-2): 321–330.

Brown, A. K., Hunt, S. D. & Stephens, D. J. 2014. Opposing microtubule motors control motility, morphology and cargo segregation during ER-to-Golgi transport. ***Biology open***, 3(5): 307–313.

Brunden, K. R., Lee, V. M., Smith III, A. B., Trojanowski, J. Q. & Ballatore, C. 2017. Altered microtubule dynamics in neurodegenerative disease: Therapeutic potential of microtubule-stabilizing drugs. ***Neurobiology of disease***, 105: 328–335.

Buchan, J. R., Kolaitis, R.-M., Taylor, J. P. & Parker, R. 2013. Eukaryotic stress granules are cleared by autophagy and Cdc48/VCP function. ***Cell***, 153(7): 1461–1474.

Buchan, J. R. & Parker, R. 2009. Eukaryotic stress granules: the ins and outs of translation. ***Molecular cell***, 36(6): 932–941.

Budini, M., Buratti, E., Stuani, C., Guarnaccia, C., Romano, V., De Conti, L., et al. 2012. Cellular model of TAR DNA-binding protein 43 (TDP-43) aggregation based on its C-terminal Gln/Asn-rich region. ***Journal of Biological Chemistry***, 287(10): 7512–7525.

Burgess, S. A., Walker, M. L., Sakakibara, H., Knight, P. J. & Oiwa, K. 2003. Dynein structure and power stroke. ***Nature***, 421(6924): 715–718.

Byrne, S., Elamin, M., Bede, P. & Hardiman, O. 2012. Absence of consensus in diagnostic criteria for familial neurodegenerative diseases. ***Journal of neurology, neurosurgery, and psychiatry***, 83(4): 365–367.

Cai, D., McEwen, D. P., Martens, J. R., Meyhofer, E. & Verhey, K. J. 2009. Single molecule imaging reveals differences in microtubule track selection between Kinesin motors. ***PLoS biology***, 7(10): 1–14.

Cai, Q., Lu, L., Tian, J.-H., Zhu, Y.-B., Qiao, H. & Sheng, Z.-H. 2010. Snapin-regulated late endosomal transport is critical for efficient autophagy-lysosomal function in neurons. ***Neuron***, 68(1): 73–86.

Calderwood, S. K., Murshid, A. & Prince, T. 2009. The shock of aging: molecular chaperones and the heat shock response in longevity and aging-a mini-review. ***Gerontology***, 55(5): 550–558.

Carter, A. P. 2013. Crystal clear insights into how the dynein motor moves. ***Journal of cell science***, 126(3): 705–713.

Cascella, R., Fani, G., Capitini, C., Rusmini, P., Poletti, A., Cecchi, C., et al. 2017. Quantitative assessment of the degradation of aggregated TDP-43 mediated by the ubiquitin proteasome system and macroautophagy. ***The FASEB Journal***, 31(12): 5609–

5624.

Cemma, M., Grinstein, S. & Brumell, J. H. 2016. Autophagy proteins are not universally required for phagosome maturation. ***Autophagy***, 12(9): 1440–1446.

Cha-Molstad, H., Lee, S. H., Kim, J. G., Sung, K. W., Hwang, J., Shim, S. M., et al. 2018. Regulation of autophagic proteolysis by the N-recognin SQSTM1/p62 of the N-end rule pathway. ***Autophagy***, 14(2): 359–361.

Cha-Molstad, H., Yu, J. E., Feng, Z., Lee, S. H., Kim, J. G., Yang, P., et al. 2017. p62/SQSTM1/Sequestosome-1 is an N-recognin of the N-end rule pathway which modulates autophagosome biogenesis. ***Nature communications***, 8(1): 1–17.

Chen, S., Owens, G. C., Makarenkova, H. & Edelman, D. B. 2010. HDAC6 regulates mitochondrial transport in hippocampal neurons. ***PloS one***, 5(5): 1–11.

Chen, X.-J., Levedakou, E. N., Millen, K. J., Wollmann, R. L., Soliven, B. & Popko, B. 2007. Proprioceptive sensory neuropathy in mice with a mutation in the cytoplasmic Dynein heavy chain 1 gene. ***Journal of Neuroscience***, 27(52): 14515–14524.

Chen, Y. & Klionsky, D. J. 2011. The regulation of autophagy-unanswered questions. ***Journal of cell science***, 124(2): 161–170.

Chen, Y., Zheng, Z.-Z., Chen, X., Huang, R., Yang, Y., Yuan, L., et al. 2014. SQSTM1 mutations in Han Chinese populations with sporadic amyotrophic lateral sclerosis. ***Neurobiology of aging***, 35(3): 726–728.

Cheng, X.-T., Zhou, B., Lin, M.-Y., Cai, Q. & Sheng, Z.-H. 2015. Axonal autophagosomes recruit dynein for retrograde transport through fusion with late endosomes. ***J Cell Biol***, 209(3): 377–386.

Chernov, K. G., Barbet, A., Hamon, L., Ovchinnikov, L. P., Curmi, P. A. & Pastré, D. 2009. Role of microtubules in stress granule assembly microtubule dynamical instability favors the formation of micrometric stress granules in cells. ***Journal of Biological Chemistry***, 284(52): 36569–36580.

Cherra III, S. J., Kulich, S. M., Uechi, G., Balasubramani, M., Mountzouris, J., Day, B. W., et al. 2010. Regulation of the autophagy protein LC3 by phosphorylation. ***Journal of Cell Biology***, 190(4): 533–539.

Chew, J., Cook, C., Gendron, T. F., Jansen-West, K., Del Rosso, G., Daughrity, L. M., et al. 2019. Aberrant deposition of stress granule-resident proteins linked to C9orf72-associated TDP-43 proteinopathy. ***Molecular neurodegeneration***, 14(1): 1–15.

Chew, J., Gendron, T. F., Prudencio, M., Sasaguri, H., Zhang, Y.-J., Castanedes-Casey, M., et al. 2015. C9ORF72 repeat expansions in mice cause TDP-43 pathology, neuronal loss, and behavioral deficits. ***Science***, 348(6239): 1151–1154.

Chiò, A., Mazzini, L., D'Alfonso, S., Corrado, L., Canosa, A., Moglia, C., et al. 2018. The multistep hypothesis of ALS revisited: the role of genetic mutations. ***Neurology***, 91(7): 635–642.

Chitiprolu, M., Jagow, C., Tremblay, V., Bondy-Chorney, E., Paris, G., Savard, A., et al. 2018. A complex of C9ORF72 and p62 uses arginine methylation to eliminate stress granules by autophagy. ***Nature communications***, 9(1): 1–18.

Chou, C.-C., Alexeeva, O. M., Yamada, S., Pribadi, A., Zhang, Y., Mo, B., et al. 2015. PABPN1 suppresses TDP-43 toxicity in ALS disease models. ***Human molecular genetics***, 24(18): 5154–5173.

Chowdhury, S., Ketcham, S. A., Schroer, T. A. & Lander, G. C. 2015. Structural organization of the dynein-dynactin complex bound to microtubules. ***Nature structural & molecular biology***, 22(4): 345–347.

Chu, C.-W., Hou, F., Zhang, J., Phu, L., Loktev, A. V., Kirkpatrick, D. S., et al. 2011. A novel acetylation of β-tubulin by San modulates microtubule polymerization via down-regulating tubulin incorporation. ***Molecular biology of the cell***, 22(4): 448–456.

Cianfrocco, M. A., DeSantis, M. E., Leschziner, A. E. & Reck-Peterson, S. L. 2015. Mechanism and regulation of cytoplasmic dynein. ***Annual review of cell and***

developmental biology, 31: 83–108.

Ciechanover, A. & Kwon, Y. T. 2015. Degradation of misfolded proteins in neurodegenerative diseases: therapeutic targets and strategies. ***Experimental & molecular medicine***, 47(3): 147–162.

Ciuffa, R., Lamark, T., Tarafder, A. K., Guesdon, A., Rybina, S., Hagen, W. J., et al. 2015. The selective autophagy receptor p62 forms a flexible filamentous helical scaffold. ***Cell reports***, 11(5): 748–758.

Clark, J. A., Yeaman, E. J., Blizzard, C. A., Chuckowree, J. A. & Dickson, T. C. 2016. A Case for Microtubule Vulnerability in Amyotrophic Lateral Sclerosis: Altered Dynamics During Disease. ***Frontiers in Cellular Neuroscience***, 10(204): 1–16.

Cohen, T. J., Hwang, A. W., Restrepo, C. R., Yuan, C.-X., Trojanowski, J. Q. & Lee, V. M. 2015. An acetylation switch controls TDP-43 function and aggregation propensity. ***Nature communications***, 6(1): 1–13.

Colacurcio, D. J. & Nixon, R. A. 2016. Disorders of lysosomal acidification-The emerging role of v-ATPase in aging and neurodegenerative disease. ***Ageing research reviews***, 32: 75–88.

Coombes, C., Yamamoto, A., McClellan, M., Reid, T. A., Plooster, M., Luxton, G. G., et al. 2016. Mechanism of microtubule lumen entry for the α-tubulin acetyltransferase enzyme αTAT1. ***Proceedings of the National Academy of Sciences***, 113(46): 7176–7184.

Cooper-Knock, J., Hewitt, C., Highley, J. R., Brockington, A., Milano, A., Man, S., et al. 2012. Clinico-pathological features in amyotrophic lateral sclerosis with expansions in C9ORF72. ***Brain : a journal of neurology***, 135(Pt 3): 751–764.

Crawley, O., Opperman, K. J., Desbois, M., Adrados, I., Borgen, M. A., Giles, A. C., et al. 2019. Autophagy is inhibited by ubiquitin ligase activity in the nervous system. ***Nature communications***, 10(1): 1–17.

Crippa, V., Carra, S., Rusmini, P., Sau, D., Bolzoni, E., Bendotti, C., et al. 2010. A role of small heat shock protein B8 (HspB8) in the autophagic removal of misfolded proteins responsible for neurodegenerative diseases. ***Autophagy***, 6(7): 958–960.

Cuervo, A. M., Stefanis, L., Fredenburg, R., Lansbury, P. T. & Sulzer, D. 2004. Impaired degradation of mutant α-synuclein by chaperone-mediated autophagy. ***Science***, 305(5688): 1292–1295.

Cueva, J. G., Hsin, J., Huang, K. C. & Goodman, M. B. 2012. Posttranslational acetylation of α-tubulin constrains protofilament number in native microtubules. ***Current biology***, 22(12): 1066–1074.

Da Cruz, S. & Cleveland, D. W. 2011. Understanding the role of TDP-43 and FUS/TLS in ALS and beyond. ***Current opinion in neurobiology***, 21(6): 904–919.

Daigle, J. G., Krishnamurthy, K., Ramesh, N., Casci, I., Monaghan, J., McAvoy, K., et al. 2016. Pur-alpha regulates cytoplasmic stress granule dynamics and ameliorates FUS toxicity. ***Acta neuropathologica***, 131(4): 605–620.

Dantuma, N. P. & Bott, L. C. 2014. The ubiquitin-proteasome system in neurodegenerative diseases: precipitating factor, yet part of the solution. ***Frontiers in molecular neuroscience***, 7(10): 70–87.

Dao, T. P., Kolaitis, R.-M., Kim, H. J., O'Donovan, K., Martyniak, B., Colicino, E., et al. 2018. Ubiquitin modulates liquid-liquid phase separation of UBQLN2 via disruption of multivalent interactions. ***Molecular cell***, 69(6): 965–978.

De Majo, M., Topp, S. D., Smith, B. N., Nishimura, A. L., Chen, H.-J., Gkazi, A. S., et al. 2018. ALS-associated missense and nonsense TBK1 mutations can both cause loss of kinase function. ***Neurobiology of aging***, 71: 266–275.

De Vos, K. J., Grierson, A. J., Ackerley, S. & Miller, C. C. 2008. Role of axonal transport in neurodegenerative diseases. ***Annu. Rev. Neurosci.***, 31: 151–173.

DeJesus-Hernandez, M., Mackenzie, I. R., Boeve, B. F., Boxer, A. L., Baker, M., Rutherford, N. J., et al. 2011. Expanded GGGGCC hexanucleotide repeat in noncoding region of C9ORF72 causes chromosome 9p-linked FTD and ALS. ***Neuron***, 72(2): 245–256.

Deng, H., Gao, K. & Jankovic, J. 2014. The role of FUS gene variants in neurodegenerative diseases. ***Nature reviews. Neurology***, 10(6): 337–348.

Deng, H.-X., Klein, C. J., Yan, J., Shi, Y., Wu, Y., Fecto, F., et al. 2010. Scapuloperoneal spinal muscular atrophy and CMT2C are allelic disorders caused by alterations in TRPV4. ***Nature genetics***, 42(2): 165–178.

Deng, H.-X., Zhai, H., Bigio, E. H., Yan, J., Fecto, F., Ajroud, K., et al. 2010. FUS-immunoreactive inclusions are a common feature in sporadic and non-SOD1 familial amyotrophic lateral sclerosis. ***Annals of neurology***, 67(6): 739–748.

Deng, W., Garrett, C., Dombert, B., Soura, V., Banks, G., Fisher, E. M., et al. 2010. Neurodegenerative mutation in cytoplasmic dynein alters its organization and dynein-dynactin and dynein-kinesin interactions. ***Journal of Biological Chemistry***, 285(51): 39922–39934.

Deng, Z., Lim, J., Wang, Q., Purtell, K., Wu, S., Palomo, G. M., et al. 2020. ALS-FTLD-linked mutations of SQSTM1/p62 disrupt selective autophagy and NFE2L2/NRF2 anti-oxidative stress pathway. ***Autophagy***, 16(5): 917–931.

Dent, E. W. & Gertler, F. B. 2003. Cytoskeletal Dynamics and Transport in Growth Cone Motility and Axon Guidance. ***Neuron***, 40(2): 209–227.

Deretic, V. 2012. Autophagy as an innate immunity paradigm: expanding the scope and repertoire of pattern recognition receptors. ***Current opinion in immunology***, 24(1): 21–31.

DeSantis, M. E., Cianfrocco, M. A., Htet, Z. M., Tran, P. T., Reck-Peterson, S. L. & Leschziner, A. E. 2017. Lis1 has two opposing modes of regulating cytoplasmic dynein. ***Cell***, 170(6): 1197–1208.

Devoy, A., Kalmar, B., Stewart, M., Park, H., Burke, B., Noy, S. J., et al. 2017. Humanized mutant FUS drives progressive motor neuron degeneration without aggregation in “FUSDelta14”knockin mice. ***Brain***, 140(11): 2797–2805.

Dewey, C. M., Cenik, B., Sephton, C. F., Dries, D. R., Mayer, P., Good, S. K., et al. 2011. TDP-43 is directed to stress granules by sorbitol, a novel physiological osmotic and oxidative stressor. ***Molecular and cellular biology***, 31(5): 1098–1108.

DeWitt, M. A., Cypranowska, C. A., Cleary, F. B., Belyy, V. & Yildiz, A. 2015. The AAA3 domain of cytoplasmic dynein acts as a switch to facilitate microtubule release. ***Nature structural & molecular biology***, 22(1): 73–82.

Dikic, I. & Elazar, Z. 2018. Mechanism and medical implications of mammalian autophagy. ***Nature reviews Molecular cell biology***, 19(6): 349–364.

Dompierre, J. P., Godin, J. D., Charrin, B. C., Cordelieres, F. P., King, S. J., Humbert, S., et al. 2007. Histone deacetylase 6 inhibition compensates for the transport deficit in Huntington’s disease by increasing tubulin acetylation. ***Journal of Neuroscience***, 27(13): 3571–3583.

Dormann, D., Madl, T., Valori, C. F., Bentmann, E., Tahirovic, S., Abou-Ajram, C., et al. 2012. Arginine methylation next to the PY-NLS modulates Transportin binding and nuclear import of FUS. ***The EMBO journal***, 31(22): 4258–4275.

Dum, R. P. & Strick, P. L. 1991. The origin of corticospinal projections from the premotor areas in the frontal lobe. ***The Journal of neuroscience : the official journal of the Society for Neuroscience***, 11(3): 667–689.

Dupuis, L., Fergani, A., Braunstein, K. E., Eschbach, J., Holl, N., Rene, F., et al. 2009. Mice with a mutation in the dynein heavy chain 1 gene display sensory neuropathy but lack motor neuron disease. ***Experimental neurology***, 215(1): 146–152.

Ederle, H. & Dormann, D. 2017. TDP-43 and FUS en route from the nucleus to the cytoplasm. ***FEBS letters***, 591(11): 1489–1507.

Elbaum-Garfinkle, S., Kim, Y., Szczepaniak, K., Chen, C. C.-H., Eckmann, C. R., Myong, S., et al. 2015. The disordered P granule protein LAF-1 drives phase separation into droplets with tunable viscosity and dynamics. ***Proceedings of the National Academy of Sciences***, 112(23): 7189–7194.

Elshenawy, M. M., Canty, J. T., Oster, L., Ferro, L. S., Zhou, Z., Blanchard, S. C., et al. 2019. Cargo adaptors regulate stepping and force generation of mammalian dynein-dynactin. ***Nature chemical biology***, 15(11): 1093–1101.

Elshenawy, M. M., Kusakci, E., Volz, S., Baumbach, J., Bullock, S. L. & Yildiz, A. 2020. Lis1 activates dynein motility by modulating its pairing with dynactin. ***Nature Cell Biology***, 22: 1–20.

Eschbach, J., Sinniger, J., Bouitbir, J., Fergani, A., Schlagowski, A.-I., Zoll, J., et al. 2013. Dynein mutations associated with hereditary motor neuropathies impair mitochondrial morphology and function with age. ***Neurobiology of disease***, 58: 220–230.

Eshun-Wilson, L., Zhang, R., Portran, D., Nachury, M. V., Toso, D. B., Löhr, T., et al. 2019. Effects of α-tubulin acetylation on microtubule structure and stability. ***Proceedings of the National Academy of Sciences***, 116(21): 10366–10371.

Evans, C. G., Wisén, S. & Gestwicki, J. E. 2006. Heat shock proteins 70 and 90 inhibit early stages of amyloid β-(1-42) aggregation in vitro. ***Journal of Biological Chemistry***, 281(44): 33182–33191.

Evans, C. S. & Holzbaur, E. L. 2019. Autophagy and mitophagy in ALS. ***Neurobiology of disease***, 122: 35–40.

Even, A., Morelli, G., Broix, L., Scaramuzzino, C., Turchetto, S., Gladwyn-Ng, I., et al. 2019. ATAT1-enriched vesicles promote microtubule acetylation via axonal transport. ***Science Advances***, 5(12): 2705–2718.

Falkenberg, K. J. & Johnstone, R. W. 2014. Histone deacetylases and their inhibitors in cancer, neurological diseases and immune disorders. ***Nature reviews. Drug discovery***, 13(9): 673–691.

Fanara, P., Banerjee, J., Hueck, R. V., Harper, M. R., Awada, M., Turner, H., et al. 2007. Stabilization of hyperdynamic microtubules is neuroprotective in amyotrophic lateral sclerosis. ***Journal of Biological Chemistry***, 282(32): 23465–23472.

Farg, M. A., Sundaramoorthy, V., Sultana, J. M., Yang, S., Atkinson, R. A., Levina, V., et al. 2014. C9ORF72, implicated in amytrophic lateral sclerosis and frontotemporal dementia, regulates endosomal trafficking. ***Human molecular genetics***, 23(13): 3579–3595.

Fass, E., Shvets, E., Degani, I., Hirschberg, K. & Elazar, Z. 2006. Microtubules support production of starvation-induced autophagosomes but not their targeting and fusion with lysosomes. ***The Journal of biological chemistry***, 281(47): 36303–30316.

Fecto, F., Yan, J., Vemula, S. P., Liu, E., Yang, Y., Chen, W., et al. 2011. SQSTM1 mutations in familial and sporadic amyotrophic lateral sclerosis. ***Archives of neurology***, 68(11): 1440–1446.

Ferreira, J. V., Fôfo, H., Bejarano, E., Bento, C. F., Ramalho, J. S., Girão, H., et al. 2013. STUB1/CHIP is required for HIF1A degradation by chaperone-mediated autophagy. ***Autophagy***, 9(9): 1349–1366.

Fiorillo, C., Moro, F., Yi, J., Weil, S., Brisca, G., Astrea, G., et al. 2014. Novel Dynein DYNC 1 H 1 Neck and Motor Domain Mutations Link Distal Spinal Muscular Atrophy and Abnormal Cortical Development. ***Human mutation***, 35(3): 298–302.

Fischle, W., Kiermer, V., Dequiedt, F. & Verdin, E. 2001. The emerging role of class II histone deacetylases. ***Biochemistry and cell biology*** , 79(3): 337–348.

Fleury, P. & Hageman, G. 1985. A dominantly inherited lower motor neuron disorder presenting at birth with associated arthrogryposis. ***Journal of neurology, neurosurgery, and psychiatry***, 48(10): 1037–1048.

Fogh, I., Lin, K., Tiloca, C., Rooney, J., Gellera, C., Diekstra, F. P., et al. 2016. Association of a locus in the CAMTA1 gene with survival in patients with sporadic amyotrophic lateral

sclerosis. ***JAMA neurology***, 73(7): 812–820.

Foster, A., Downing, P., Figredo, E., Polain, N., Stott, A., Layfield, R., et al. 2020. ALS-associated TBK1 variant p. G175S is defective in phosphorylation of p62 and impacts TBK1-mediated signalling and TDP-43 autophagic degradation. ***Molecular and Cellular Neuroscience***, 108: 103539–103550.

Francelle, L., Outeiro, T. F. & Rappold, G. A. 2020. Inhibition of HDAC6 activity protects dopaminergic neurons from alpha-synuclein toxicity. ***Scientific Reports***, 10(1): 1–14.

Francis, F., Meyer, G., Fallet-Bianco, C., Moreno, S., Kappeler, C., Socorro, A. C., et al. 2006. Human disorders of cortical development: from past to present. ***European Journal of Neuroscience***, 23(4): 877–893.

Franker, M. A. & Hoogenraad, C. C. 2013. Microtubule-based transport-basic mechanisms, traffic rules and role in neurological pathogenesis. ***Journal of cell science***, 126(11): 2319–2329.

Fratta, P., Mizielinska, S., Nicoll, A. J., Zloh, M., Fisher, E. M., Parkinson, G., et al. 2012. C9orf72 hexanucleotide repeat associated with amyotrophic lateral sclerosis and frontotemporal dementia forms RNA G-quadruplexes. ***Scientific reports***, 2: 1016.

Fratta, P., Sivakumar, P., Humphrey, J., Lo, K., Ricketts, T., Oliveira, H., et al. 2018. Mice with endogenous TDP-43 mutations exhibit gain of splicing function and characteristics of amyotrophic lateral sclerosis. ***The EMBO journal***, 37(11): 98684–98698.

Freibaum, B. D., Chitta, R. K., High, A. A. & Taylor, J. P. 2010. Global analysis of TDP-43 interacting proteins reveals strong association with RNA splicing and translation machinery. ***Journal of proteome research***, 9(2): 1104–1120.

Freischmidt, A., Wieland, T., Richter, B., Ruf, W., Schaeffer, V., Müller, K., et al. 2015. Haploinsufficiency of TBK1 causes familial ALS and fronto-temporal dementia. ***Nature neuroscience***, 18(5): 631–636.

French, R. L., Grese, Z. R., Aligireddy, H., Dhavale, D. D., Reeb, A. N., Kedia, N., et al. 2019. Detection of TAR DNA-binding protein 43 (TDP-43) oligomers as initial intermediate species during aggregate formation. ***Journal of Biological Chemistry***, 294(17): 6696–6709.

Friedmann, D. R., Aguilar, A., Fan, J., Nachury, M. V. & Marmorstein, R. 2012. Structure of the α-tubulin acetyltransferase,αTAT1, and implications for tubulin-specific acetylation. ***Proceedings of the National Academy of Sciences***, 109(48): 19655–19660.

Fu, H., Hardy, J. & Duff, K. E. 2018. Selective vulnerability in neurodegenerative diseases. ***Nature neuroscience***, 21(10): 1350–1358.

Fu, M., Nirschl, J. J. & Holzbaur, E. L. 2014. LC3 binding to the scaffolding protein JIP1 regulates processive dynein-driven transport of autophagosomes. ***Developmental cell***, 29(5): 577–590.

Fujita, N., Itoh, T., Omori, H., Fukuda, M., Noda, T. & Yoshimori, T. 2008. The Atg16L complex specifies the site of LC3 lipidation for membrane biogenesis in autophagy. ***Molecular biology of the cell***, 19(5): 2092–2100.

Fulga, T. A., Elson-Schwab, I., Khurana, V., Steinhilb, M. L., Spires, T. L., Hyman, B. T., et al. 2007. Abnormal bundling and accumulation of F-actin mediates tau-induced neuronal degeneration in vivo. ***Nature cell biology***, 9(2): 139–148.

Gal, J., Ström, A.-L., Kwinter, D. M., Kilty, R., Zhang, J., Shi, P., et al. 2009. Sequestosome 1/p62 links familial ALS mutant SOD1 to LC3 via an ubiquitin-independent mechanism. ***Journal of neurochemistry***, 111(4): 1062–1073.

Gal, J., Ström, A.-L., Kilty, R., Zhang, F. & Zhu, H. 2007. p62 accumulates and enhances aggregate formation in model systems of familial amyotrophic lateral sclerosis. ***Journal of Biological Chemistry***, 282(15): 11068–11077.

Gama, J. B., Pereira, C., Simões, P. A., Celestino, R., Reis, R. M., Barbosa, D. J., et al. 2017. Molecular mechanism of dynein recruitment to kinetochores by the Rod-Zw10-Zwilch complex and Spindly. ***Journal of Cell Biology***, 216(4): 943–960.

Gamez, J., Corbera-Bellalta, M., Nogales, G., Raguer, N., Garcia-Arumi, E., Badia-Canto, M., et al. 2006. Mutational analysis of the Cu/Zn superoxide dismutase gene in a Catalan ALS population: should all sporadic ALS cases also be screened for SOD1? ***Journal of the neurological sciences***, 247(1): 21–28.

Ganassi, M., Mateju, D., Bigi, I., Mediani, L., Poser, I., Lee, H. O., et al. 2016. A surveillance function of the HSPB8-BAG3-HSP70 chaperone complex ensures stress granule integrity and dynamism. ***Molecular cell***, 63(5): 796–810.

Gao, F. J., Hebbar, S., Gao, X. A., Alexander, M., Pandey, J. P., Walla, M. D., et al. 2015. GSK-3β Phosphorylation of Cytoplasmic Dynein Reduces Ndel1 Binding to Intermediate Chains and Alters Dynein Motility. ***Traffic***, 16(9): 941–961.

Gao, Y., Hubbert, C. C. & Yao, T.-P. 2010. The microtubule-associated histone deacetylase 6 (HDAC6) regulates epidermal growth factor receptor (EGFR) endocytic trafficking and degradation. ***Journal of Biological Chemistry***, 285(15): 11219–11226.

Garrett, C. A., Barri, M., Kuta, A., Soura, V., Deng, W., Fisher, E. M., et al. 2014. DYNC1H1 mutation alters transport kinetics and ERK1/2-cFos signalling in a mouse model of distal spinal muscular atrophy. ***Brain***, 137: 1883–1893.

Gee, M. A., Heuser, J. E. & Vallee, R. B. 1997. An extended microtubule-binding structure within the dynein motor domain. ***Nature***, 390(60): 636–639.

Geeraert, C., Ratier, A., Pfisterer, S. G., Perdiz, D., Cantaloube, I., Rouault, A., et al. 2010. Starvation-induced hyperacetylation of tubulin is required for the stimulation of autophagy by nutrient deprivation. ***Journal of Biological Chemistry***, 285(31): 24184–24194.

Gendron, T. F., Rademakers, R. & Petrucelli, L. 2013. TARDBP mutation analysis in TDP-43 proteinopathies and deciphering the toxicity of mutant TDP-43. ***Journal of Alzheimer's disease : JAD***, 33 Suppl 1: 35–49.

Geuens, G., Gundersen, G. G., Nuydens, R., Cornelissen, F., Bulinski, J. C. & DeBrabander, M. 1986. Ultrastructural colocalization of tyrosinated and detyrosinated alpha-tubulin in interphase and mitotic cells. ***The Journal of cell biology***, 103(5): 1883–1893.

Gibbs, K. L., Greensmith, L. & Schiavo, G. 2015. Regulation of axonal transport by protein kinases. ***Trends in biochemical sciences***, 40(10): 597–610.

Gijselinck, I., Van Mossevelde, S., van der Zee, J., Sieben, A., Philtjens, S., Heeman, B., et al. 2015. Loss of TBK1 is a frequent cause of frontotemporal dementia in a Belgian cohort. ***Neurology***, 85(24): 2116–2125.

Gilbert, C. E., Sztul, E. & Machamer, C. E. 2018. Commonly used trafficking blocks disrupt ARF1 activation and the localization and function of specific Golgi proteins. ***Molecular biology of the cell***, 29(8): 937–947.

Gillingham, A. K. & Munro, S. 2003. Long coiled-coil proteins and membrane traffic. ***Biochimica et biophysica acta***, 1641(2-3): 71–85.

Giudice, T. L., Lombardi, F., Santorelli, F. M., Kawarai, T. & Orlacchio, A. 2014. Hereditary spastic paraplegia: clinical-genetic characteristics and evolving molecular mechanisms. ***Experimental neurology***, 261: 518–539.

Godena, V. K., Brookes-Hocking, N., Moller, A., Shaw, G., Oswald, M., Sancho, R. M., et al. 2014. Increasing microtubule acetylation rescues axonal transport and locomotor deficits caused by LRRK2 Roc-COR domain mutations. ***Nature communications***, 5(1): 1–11.

Goldman, S. M. 2014. Environmental toxins and Parkinson's disease. ***Annual review of pharmacology and toxicology***, 54: 141–164.

Goncalves, A., Bürckstümmer, T., Dixit, E., Scheicher, R., Górna, M. W., Karayel, E., et al. 2011. Functional dissection of the TBK1 molecular network. ***PloS one***, 6(9): 23971–23983.

Gonçalves, J. C., Dantas, T. J. & Vallee, R. B. 2019. Distinct roles for dynein light intermediate chains in neurogenesis, migration, and terminal somal translocation. ***Journal of Cell Biology***, 218(3): 808–819.

Gong, B., Radulovic, M., Figueiredo-Pereira, M. E. & Cardozo, C. 2016. The ubiquitin-proteasome system: potential therapeutic targets for Alzheimer's disease and spinal cord injury. ***Frontiers in molecular neuroscience***, 9(4): 4–20.

Goode, A., Butler, K., Long, J., Cavey, J., Scott, D., Shaw, B., et al. 2016. Defective recognition of LC3B by mutant SQSTM1/p62 implicates impairment of autophagy as a pathogenic mechanism in ALS-FTLD. ***Autophagy***, 12(7): 1094–1104.

Gordon, D., Dafinca, R., Scaber, J., Alegre-Abarrategui, J., Farrimond, L., Scott, C., et al. 2019. Single-copy expression of an amyotrophic lateral sclerosis-linked TDP-43 mutation (M337V) in BAC transgenic mice leads to altered stress granule dynamics and progressive motor dysfunction. ***Neurobiology of Disease***, 121: 148–162.

Gordon, P., Cheng, B., Katz, I., Pinto, M., Hays, A., Mitsumoto, H., et al. 2006. The natural history of primary lateral sclerosis. ***Neurology***, 66(5): 647–653.

Gosavi, N., Lee, H.-J., Lee, J. S., Patel, S. & Lee, S.-J. 2002. Golgi fragmentation occurs in the cells with prefibrillar α-synuclein aggregates and precedes the formation of fibrillar inclusion. ***Journal of Biological Chemistry***, 277(50): 48984–48992.

Gros-Louis, F., Larivière, R., Gowing, G., Laurent, S., Camu, W., Bouchard, J.-P., et al. 2004. A frameshift deletion in peripherin gene associated with amyotrophic lateral sclerosis. ***Journal of Biological Chemistry***, 279(44): 45951–45956.

Guedes-Dias, P., de Proença, J., Soares, T. R., Leitão-Rocha, A., Pinho, B. R., Duchen, M. R., et al. 2015. HDAC6 inhibition induces mitochondrial fusion, autophagic flux and reduces diffuse mutant huntingtin in striatal neurons. ***Biochimica et Biophysica Acta (BBA)-Molecular Basis of Disease***, 1852(11): 2484–2493.

Guerrero, E. N., Wang, H., Mitra, J., Hegde, P. M., Stowell, S. E., Liachko, N. F., et al. 2016. TDP-43/FUS in motor neuron disease: complexity and challenges. ***Progress in neurobiology***, 145: 78–97.

Guerrini, R., Dobyns, W. B. & Barkovich, A. J. 2008. Abnormal development of the human cerebral cortex: genetics, functional consequences and treatment options. ***Trends in neurosciences***, 31(3): 154–162.

Guo, Q., Lehmer, C., Martinez-Sánchez, A., Rudack, T., Beck, F., Hartmann, H., et al. 2018. In situ structure of neuronal C9orf72 poly-GA aggregates reveals proteasome recruitment. ***Cell***, 172(4): 696–705.

Guo, W., Naujock, M., Fumagalli, L., Vandoorne, T., Baatsen, P., Boon, R., et al. 2017. HDAC6 inhibition reverses axonal transport defects in motor neurons derived from FUS-ALS patients. ***Nature communications***, 8(1): 1–15.

Gupta, R., Lan, M., Mojsilovic-Petrovic, J., Choi, W. H., Safren, N., Barmada, S., et al. 2017. The proline/arginine dipeptide from hexanucleotide repeat expanded C9ORF72 inhibits the proteasome. ***Eneuro***, 4(1): 1–18.

Habura, A., Tikhonenko, I., Chisholm, R. L. & Koonce, M. P. 1999. Interaction Mapping of a Dynein Heavy Chain IDENTIFICATION OF DIMERIZATION AND INTERMEDIATE-CHAIN BINDING DOMAINS. ***Journal of Biological Chemistry***, 274(22): 15447–15453.

Hafezparast, M., Klocke, R., Ruhrberg, C., Marquardt, A., Ahmad-Annuar, A., Bowen, S., et al. 2003. Mutations in dynein link motor neuron degeneration to defects in retrograde transport. ***Science***, 300(5620): 808–812.

Hammond, J. W., Cai, D. & Verhey, K. J. 2008. Tubulin modifications and their cellular functions. ***Current opinion in cell biology***, 20(1): 71–76.

Han, T. W., Kato, M., Xie, S., Wu, L. C., Mirzaei, H., Pei, J., et al. 2012. Cell-free Formation of RNA Granules: Bound RNAs Identify Features and Components of Cellular Assemblies. ***Cell***, 149(4): 768–779.

Han, W., Pan, H., Chen, Y., Sun, J., Wang, Y., Li, J., et al. 2011. EGFR tyrosine kinase inhibitors activate autophagy as a cytoprotective response in human lung cancer cells. ***PloS one***, 6(6): 18691–18702.

Hancock, W. O. 2014. Bidirectional cargo transport: moving beyond tug of war. ***Nature reviews Molecular cell biology***, 15(9): 615–628.

Hara, T., Nakamura, K., Matsui, M., Yamamoto, A., Nakahara, Y., Suzuki-Migishima, R., et al. 2006. Suppression of basal autophagy in neural cells causes neurodegenerative disease in mice. ***Nature***, 441(7095): 885–889.

Harada, A., Takei, Y., Kanai, Y., Tanaka, Y., Nonaka, S. & Hirokawa, N. 1998. Golgi vesiculation and lysosome dispersion in cells lacking cytoplasmic dynein. ***The Journal of cell biology***, 141(1): 51–59.

Harms, M. B., Allred, P., Gardner, R., Fernandes Filho, J. A., Florence, J., Pestronk, A., et al. 2010. Dominant spinal muscular atrophy with lower extremity predominance: linkage to 14q32. ***Neurology***, 75(6): 539–546.

Harms, M., Ori-McKenney, K., Scoto, M., Tuck, E., Bell, S., Ma, D., et al. 2012. Mutations in the tail domain of DYNC1H1 cause dominant spinal muscular atrophy. ***Neurology***, 78(22): 1714–1720.

Hasegawa, M., Arai, T., Nonaka, T., Kametani, F., Yoshida, M., Hashizume, Y., et al. 2008. Phosphorylated TDP-43 in frontotemporal lobar degeneration and amyotrophic lateral sclerosis. ***Annals of Neurology: Official Journal of the American Neurological Association and the Child Neurology Society***, 64(1): 60–70.

He, C. & Klionsky, D. J. 2009. Regulation mechanisms and signaling pathways of autophagy. ***Annual review of genetics***, 43: 67–93.

He, M., Subramanian, R., Bangs, F., Omelchenko, T., Liem, K. F., Kapoor, T. M., et al. 2014. The kinesin-4 protein Kif7 regulates mammalian Hedgehog signalling by organizing the cilium tip compartment. ***Nature cell biology***, 16(7): 663–672.

Heo, J.-M., Ordureau, A., Paulo, J. A., Rinehart, J. & Harper, J. W. 2015. The PINK1-PARKIN mitochondrial ubiquitylation pathway drives a program of TBK1 activation and recruitment of OPTN and NDP52 to promote mitophagy. ***Molecular cell***, 60(1): 7–20.

Hergesheimer, R. C., Chami, A. A., de Assis, D. R., Vourc'h, P., Andres, C. R., Corcia, P., et al. 2019. The debated toxic role of aggregated TDP-43 in amyotrophic lateral sclerosis: a resolution in sight? ***Brain***, 142(5): 1176–1194.

Herhaus, L., Bhaskara, R. M., Lystad, A. H., Gestal-Mato, U., Covarrubias-Pinto, A., Bonn, F., et al. 2020. TBK1-mediated phosphorylation of LC3C and GABARAP-L2 controls autophagosome shedding by ATG4 protease. ***EMBO reports***, 21(1): 1–20.

Herman, M., Ciancanelli, M., Ou, Y.-H., Lorenzo, L., Klaudel-Dreszler, M., Pauwels, E., et al. 2012. Heterozygous TBK1 mutations impair TLR3 immunity and underlie herpes simplex encephalitis of childhoodHuman TBK1 deficiency. ***The Journal of experimental medicine***, 209(9): 1567–1582.

Hershko, A. & Ciechanover, A. 1998. The ubiquitin system. ***Annual review of biochemistry***, 67(1): 425–479.

Herzog, J. J., Deshpande, M., Shapiro, L., Rodal, A. A. & Paradis, S. 2017. TDP-43 misexpression causes defects in dendritic growth. ***Scientific reports***, 7(1): 1–13.

Higelin, J., Demestre, M., Putz, S., Delling, J. P., Jacob, C., Lutz, A.-K., et al. 2016. FUS mislocalization and vulnerability to DNA damage in ALS patients derived hiPSCs and aging motoneurons. ***Frontiers in cellular neuroscience***, 10(290): 1–21.

Hirokawa, N., Niwa, S. & Tanaka, Y. 2010. Molecular motors in neurons: transport mechanisms and roles in brain function, development, and disease. ***Neuron***, 68(4): 610–638.

Hirokawa, N. & Takemura, R. 2005. Molecular motors and mechanisms of directional transport in neurons. ***Nature Reviews Neuroscience***, 6(3): 201–214.

Hirokawa, N. & Tanaka, Y. 2015. Kinesin superfamily proteins (KIFs): Various functions and their relevance for important phenomena in life and diseases. ***Experimental cell research***, 334(1): 16–25.

Hoang, H. T., Schlager, M. A., Carter, A. P. & Bullock, S. L. 2017. DYNC1H1 mutations associated with neurological diseases compromise processivity of dynein-dynactin-cargo adaptor complexes. ***Proceedings of the National Academy of Sciences***, 114(9): 1597–1606.

Howard, J. & Hyman, A. A. 2003. Dynamics and mechanics of the microtubule plus end. ***Nature***, 422(6933): 753–758.

Howes, S. C., Alushin, G. M., Shida, T., Nachury, M. V. & Nogales, E. 2014. Effects of tubulin acetylation and tubulin acetyltransferase binding on microtubule structure. ***Molecular biology of the cell***, 25(2): 257–266.

Hoyle, J. C., Isfort, M. C., Roggenbuck, J. & Arnold, W. D. 2015. The genetics of Charcot-Marie-Tooth disease: current trends and future implications for diagnosis and management. ***The Application of Clinical Genetics***, 8: 235–243.

Htet, Z. M., Gillies, J. P., Baker, R. W., Leschziner, A. E., DeSantis, M. E. & Reck-Peterson, S. L. 2020. Lis1 promotes the formation of activated cytoplasmic dynein-1 complexes. ***Nature Cell Biology***, 22(5): 518–525.

Huang, C.-C., Bose, J. K., Majumder, P., Lee, K.-H., Huang, J.-T. J., Huang, J. K., et al. 2014. Metabolism and mis-metabolism of the neuropathological signature protein TDP-43. ***J Cell Sci***, 127(14): 3024–3038.

Huang, R., Fang, D.-F., Ma, M.-Y., Guo, X.-Y., Zhao, B., Zeng, Y., et al. 2012. TARDBP gene mutations among Chinese patients with sporadic amyotrophic lateral sclerosis. ***Neurobiology of aging***, 33(5): 1015–1022.

Hubbert, C., Guardiola, A., Shao, R., Kawaguchi, Y., Ito, A., Nixon, A., et al. 2002. HDAC6 is a microtubule-associated deacetylase. ***Nature***, 417(6887): 455–458.

Igaz, L. M., Kwong, L. K., Xu, Y., Truax, A. C., Uryu, K., Neumann, M., et al. 2008. Enrichment of C-terminal fragments in TAR DNA-binding protein-43 cytoplasmic inclusions in brain but not in spinal cord of frontotemporal lobar degeneration and

amyotrophic lateral sclerosis. ***The American journal of pathology***, 173(1): 182–194.

Ikeda, F., Hecker, C. M., Rozenknop, A., Nordmeier, R. D., Rogov, V., Hofmann, K., et al. 2007. Involvement of the ubiquitin-like domain of TBK1/IKK-i kinases in regulation of IFN-inducible genes. ***The EMBO journal***, 26(14): 3451–3462.

Ikenaka, K., Kawai, K., Katsuno, M., Huang, Z., Jiang, Y.-M., Iguchi, Y., et al. 2013. dnc-1/dynactin 1 knockdown disrupts transport of autophagosomes and induces motor neuron degeneration. ***PLoS One***, 8(2): 54511–54528.

Iko, Y., Kodama, T. S., Kasai, N., Oyama, T., Morita, E. H., Muto, T., et al. 2004. Domain architectures and characterization of an RNA-binding protein, TLS. ***The Journal of biological chemistry***, 279(43): 44834–44840.

Ilieva, H. S., Yamanaka, K., Malkmus, S., Kakinohana, O., Yaksh, T., Marsala, M., et al. 2008. Mutant dynein (Loa) triggers proprioceptive axon loss that extends survival only in the SOD1 ALS model with highest motor neuron death. ***Proceedings of the National Academy of Sciences***, 105(34): 12599–12604.

Ishikawa, H. & Marshall, W. F. 2011. Ciliogenesis: building the cell's antenna. ***Nature reviews. Molecular cell biology***, 12(4): 222–234.

Ivanov, P. A., Chudinova, E. M. & Nadezhdina, E. S. 2003. Disruption of microtubules inhibits cytoplasmic ribonucleoprotein stress granule formation. ***Experimental cell research***, 290(2): 227–233.

Jaarsma, D. & Hoogenraad, C. C. 2015. Cytoplasmic dynein and its regulatory proteins in Golgi pathology in nervous system disorders. ***Frontiers in neuroscience***, 9(397): 1–9.

Jacquin, E., Leclerc-Mercier, S., Judon, C., Blanchard, E., Fraitag, S. & Florey, O. 2017. Pharmacological modulators of autophagy activate a parallel noncanonical pathway driving unconventional LC3 lipidation. ***Autophagy***, 13(5): 854–867.

Jain, S., Wheeler, J. R., Walters, R. W., Agrawal, A., Barsic, A. & Parker, R. 2016. ATPase-modulated stress granules contain a diverse proteome and substructure. ***Cell***, 164(3):

487–498.

Janke, C. & Bulinski, J. C. 2011. Post-translational regulation of the microtubule cytoskeleton: mechanisms and functions. ***Nature reviews Molecular cell biology***, 12(12): 773–786.

Janke, C. & Kneussel, M. 2010. Tubulin post-translational modifications: encoding functions on the neuronal microtubule cytoskeleton. ***Trends in neurosciences***, 33(8): 362–372.

Janke, C. & Magiera, M. M. 2020. The tubulin code and its role in controlling microtubule properties and functions. ***Nature Reviews Molecular Cell Biology***, 21: 1–20.

Janke, C. & Montagnac, G. 2017. Causes and consequences of microtubule acetylation. ***Current Biology***, 27(23): 1287–1292.

Jha, R. & Surrey, T. 2015. Regulation of processive motion and microtubule localization of cytoplasmic dynein, 43: 48–57.

Jinwal, U. K., Abisambra, J. F., Zhang, J., Dharia, S., O'Leary, J. C., Patel, T., et al. 2012. Cdc37/Hsp90 protein complex disruption triggers an autophagic clearance cascade for TDP-43 protein. ***The Journal of biological chemistry***, 287(29): 24814–24820.

Johnson, B. S., Snead, D., Lee, J. J., McCaffery, J. M., Shorter, J. & Gitler, A. D. 2009. TDP-43 is intrinsically aggregation-prone, and amyotrophic lateral sclerosis-linked mutations accelerate aggregation and increase toxicity. ***Journal of Biological Chemistry***, 284(30): 20329–20339.

Johnson, I. P. 2015. Age-related neurodegenerative disease research needs aging models. ***Frontiers in aging neuroscience***, 7(168): 168–169.

Joshi, G., Bekier, M. I. & Wang, Y. 2015. Golgi fragmentation in Alzheimer's disease. ***Frontiers in neuroscience***, 9(340): 340–347.

Ju, J.-S., Fuentealba, R. A., Miller, S. E., Jackson, E., Piwnica-Worms, D., Baloh, R. H., et al. 2009. Valosin-containing protein (VCP) is required for autophagy and is disrupted in VCP disease. ***Journal of Cell Biology***, 187(6): 875–888.

Kabeya, Y., Mizushima, N., Ueno, T., Yamamoto, A., Kirisako, T., Noda, T., et al. 2000. LC3, a mammalian homologue of yeast Apg8p, is localized in autophagosome membranes after processing. ***The EMBO journal***, 19(21): 5720–5728.

Kalebic, N., Martinez, C., Perlas, E., Hublitz, P., Bilbao-Cortes, D., Fiedorczuk, K., et al. 2013. Tubulin acetyltransferase αTAT1 destabilizes microtubules independently of its acetylation activity. ***Molecular and cellular biology***, 33(6): 1114–1123.

Kalebic, N., Sorrentino, S., Perlas, E., Bolasco, G., Martinez, C. & Heppenstall, P. A. 2013. αTAT1 is the major α-tubulin acetyltransferase in mice. ***Nature communications***, 4(1): 1–10.

Kast, D. J. & Dominguez, R. 2015. WHAMM links actin assembly via the Arp2/3 complex to autophagy. ***Autophagy***, 11(9): 1702–1704.

Kato, M., Han, T. W., Xie, S., Shi, K., Du, X., Wu, L. C., et al. 2012. Cell-free Formation of RNA Granules: Low Complexity Sequence Domains Form Dynamic Fibers within Hydrogels. ***Cell***, 149(4): 753–767.

Kaushik, S. & Cuervo, A. M. 2012. Chaperone-mediated autophagy: a unique way to enter the lysosome world. ***Trends in cell biology***, 22(8): 407–417.

Kaushik, S. & Cuervo, A. M. 2018. The coming of age of chaperone-mediated autophagy. ***Nature Reviews Molecular Cell Biology***, 19(6): 365–381.

Kawaguchi, Y., Kovacs, J. J., McLaurin, A., Vance, J. M., Ito, A. & Yao, T.-P. 2003. The deacetylase HDAC6 regulates aggresome formation and cell viability in response to misfolded protein stress. ***Cell***, 115(6): 727–738.

Kawano-Kawada, M., Kakinuma, Y. & Sekito, T. 2018. Transport of amino acids across the vacuolar membrane of yeast: Its mechanism and physiological role. ***Biological and***

Pharmaceutical Bulletin, 41(10): 1496–1501.

Kegel, K. B., Kim, M., Sapp, E., McIntyre, C., Castano, J. G., Aronin, N., et al. 2000. Huntingtin expression stimulates endosomal-lysosomal activity, endosome tubulation, and autophagy. ***Journal of Neuroscience***, 20(19): 7268–7278.

Ketcham, S. A. & Schroer, T. A. 2018. Role of dynactin in dynein-mediated motility. ***Dyneins***: 502–515. Elsevier.

Khalfallah, Y., Kuta, R., Grasmuck, C., Prat, A., Durham, H. D. & Velde, C. V. 2018. TDP-43 regulation of stress granule dynamics in neurodegenerative disease-relevant cell types. ***Scientific reports***, 8(1): 7551–7562.

Kiehn, O. 2016. Decoding the organization of spinal circuits that control locomotion. ***Nature Reviews Neuroscience***, 17(4): 224–238.

Kiffin, R., Kaushik, S., Zeng, M., Bandyopadhyay, U., Zhang, C., Massey, A. C., et al. 2007. Altered dynamics of the lysosomal receptor for chaperone-mediated autophagy with age. ***Journal of cell science***, 120(5): 782–791.

Kim, G.-W., Li, L., Gorbani, M., You, L. & Yang, X.-J. 2013. Mice lacking α-tubulin acetyltransferase 1 are viable but display α-tubulin acetylation deficiency and dentate gyrus distortion. ***Journal of Biological Chemistry***, 288(28): 20334–20350.

Kim, H. J., Kim, N. C., Wang, Y.-D., Scarborough, E. A., Moore, J., Diaz, Z., et al. 2013. Mutations in prion-like domains in hnRNPA2B1 and hnRNPA1 cause multisystem proteinopathy and ALS. ***Nature***, 495(7442): 467–473.

Kim, H. J. & Taylor, J. P. 2017. Lost in transportation: nucleocytoplasmic transport defects in ALS and other neurodegenerative diseases. ***Neuron***, 96(2): 285–297.

Kim, H.-S., Takahashi, M., Matsuo, K. & Ono, Y. 2007. Recruitment of CG-NAP to the Golgi apparatus through interaction with dynein-dynactin complex. ***Genes to cells : devoted to molecular & cellular mechanisms***, 12(3): 421–434.

Kim, Y. E., Hipp, M. S., Bracher, A., Hayer-Hartl, M. & Hartl, F. U. 2013. Molecular chaperone functions in protein folding and proteostasis. ***Annual review of biochemistry***, 82: 323–355.

Kimura, N., Imamura, O., Ono, F. & Terao, K. 2007. Aging attenuates dynactin-dynein interaction: Down-regulation of dynein causes accumulation of endogenous tau and amyloid precursor protein in human neuroblastoma cells. ***Journal of neuroscience research***, 85(13): 2909–2916.

Kimura, N., Samura, E., Suzuki, K., Okabayashi, S., Shimozawa, N. & Yasutomi, Y. 2016. Dynein Dysfunction Reproduces Age-Dependent Retromer Deficiency: Concomitant Disruption of Retrograde Trafficking Is Required for Alteration in β-Amyloid Precursor Protein Metabolism. ***The American journal of pathology***, 186(7): 1952–1966.

Kimura, S., Noda, T. & Yoshimori, T. 2008. Dynein-dependent movement of autophagosomes mediates efficient encounters with lysosomes. ***Cell structure and function***, 33(1): 109–122.

King, A., Maekawa, S., Bodi, I., Troakes, C. & Al-Sarraj, S. 2011. Ubiquitinated, p62 immunopositive cerebellar cortical neuronal inclusions are evident across the spectrum of TDP-43 proteinopathies but are only rarely additionally immunopositive for phosphorylation-dependent TDP-43. ***Neuropathology***, 31(3): 239–249.

King, A., Troakes, C., Smith, B., Nolan, M., Curran, O., Vance, C., et al. 2015. ALS-FUS pathology revisited: singleton FUS mutations and an unusual case with both a FUS and TARDBP mutation. ***Acta neuropathologica communications***, 3(1): 1–12.

King, S. J. & Schroer, T. A. 2000. Dynactin increases the processivity of the cytoplasmic dynein motor. ***Nature cell biology***, 2(1): 20–24.

King, S. M. 2000. The dynein microtubule motor. ***Biochimica et Biophysica Acta (BBA)-Molecular Cell Research***, 1496(1): 60–75.

Kirkwood, T. B. & Melov, S. 2011. On the programmed/non-programmed nature of ageing within the life history. ***Current Biology***, 21(18): 701–707.

Klinman, E. & Holzbaur, E. L. 2015. Stress-induced CDK5 activation disrupts axonal transport via Lis1/Ndel1/Dynein. ***Cell reports***, 12(3): 462–473.

Klumperman, J. 2011. Architecture of the mammalian Golgi. ***Cold Spring Harbor perspectives in biology***, 3(7): 1–19.

Konishi, Y. & Setou, M. 2009. Tubulin tyrosination navigates the kinesin-1 motor domain to axons. ***Nature neuroscience***, 12(5): 559–567.

Konno, T., Ross, O. A., Teive, H. A., Slawek, J., Dickson, D. W. & Wszolek, Z. K. 2017. DCTN1-related neurodegeneration: Perry syndrome and beyond. ***Parkinsonism & related disorders***, 41: 14–24.

Korolchuk, V. I., Mansilla, A., Menzies, F. M. & Rubinsztein, D. C. 2009. Autophagy inhibition compromises degradation of ubiquitin-proteasome pathway substrates. ***Molecular cell***, 33(4): 517–527.

Kruppa, A. J., Kendrick-Jones, J. & Buss, F. 2016. Myosins, actin and autophagy. ***Traffic***, 17(8): 878–890.

Kubo, T., Yanagisawa, H., Yagi, T., Hirono, M. & Kamiya, R. 2010. Tubulin polyglutamylation regulates axonemal motility by modulating activities of inner-arm dyneins. ***Current Biology***, 20(5): 441–445.

Kuijpers, M., van de Willige, D., Freal, A., Chazeau, A., Franker, M. A., Hofenk, J., et al. 2016. Dynein regulator NDEL1 controls polarized cargo transport at the axon initial segment. ***Neuron***, 89(3): 461–471.

Kumar, S., Gu, Y., Abudu, Y. P., Bruun, J.-A., Jain, A., Farzam, F., et al. 2019. Phosphorylation of syntaxin 17 by TBK1 controls autophagy initiation. ***Developmental cell***, 49(1): 130–144.

Kumar, S., Jain, A., Farzam, F., Jia, J., Gu, Y., Choi, S. W., et al. 2018. Mechanism of Stx17 recruitment to autophagosomes via IRGM and mammalian Atg8 proteins. ***Journal of Cell Biology***, 217(3): 997–1013.

Kumsta, C., Chang, J. T., Lee, R., Tan, E. P., Yang, Y., Loureiro, R., et al. 2019. The autophagy receptor p62/SQST-1 promotes proteostasis and longevity in C. elegans by inducing autophagy. ***Nature Communications***, 10(1): 1–12.

Kwiatkowski, T. J., Bosco, D., Leclerc, A., Tamrazian, E., Vanderburg, C., Russ, C., et al. 2009. Mutations in the FUS/TLS gene on chromosome 16 cause familial amyotrophic lateral sclerosis. ***Science***, 323(5918): 1205–1208.

Kwon, S., Zhang, Y. & Matthias, P. 2007. The deacetylase HDAC6 is a novel critical component of stress granules involved in the stress response. ***Genes & development***, 21(24): 3381–3394.

Laan, L., Pavin, N., Husson, J., Romet-Lemonne, G., van Duijn, M., López, M. P., et al. 2012. Cortical dynein controls microtubule dynamics to generate pulling forces that position microtubule asters. ***Cell***, 148(3): 502–514.

Lagier-Tourenne, C., Polymenidou, M. & Cleveland, D. W. 2010. TDP-43 and FUS/TLS: emerging roles in RNA processing and neurodegeneration. ***Human molecular genetics***, 19(1): 46–64.

Lam, C., Vergnolle, M. A., Thorpe, L., Woodman, P. G. & Allan, V. J. 2010. Functional interplay between LIS1, NDE1 and NDEL1 in dynein-dependent organelle positioning. ***Journal of cell science***, 123(2): 202–212.

Lamar, K.-M. & McNally, E. M. 2014. Genetic modifiers for neuromuscular diseases. ***Journal of neuromuscular diseases***, 1(1): 3–13.

Lamark, T. & Johansen, T. 2010. Autophagy: links with the proteasome. ***Current opinion in cell biology***, 22(2): 192–198.

LaMonte, B. H., Wallace, K. E., Holloway, B. A., Shelly, S. S., Ascaño, J., Tokito, M., et al. 2002. Disruption of dynein/dynactin inhibits axonal transport in motor neurons causing late-onset progressive degeneration. ***Neuron***, 34(5): 715–727.

Larsen, K. B., Lamark, T., \Overvatn, A., Harneshaug, I., Johansen, T. & Bjørkøy, G. 2010. A reporter cell system to monitor autophagy based on p62/SQSTM1. ***Autophagy***, 6(6): 784–793.

Lawrence, R. E. & Zoncu, R. 2019. The lysosome as a cellular centre for signalling, metabolism and quality control. ***Nat. Cell Biol***, 21(2): 133–142.

Lawson, V. H. & Arnold, W. D. 2014. Multifocal motor neuropathy: a review of pathogenesis, diagnosis, and treatment. ***Neuropsychiatric disease and treatment***, 10: 567–576.

Lazarou, M., Sliter, D. A., Kane, L. A., Sarraf, S. A., Wang, C., Burman, J. L., et al. 2015. The ubiquitin kinase PINK1 recruits autophagy receptors to induce mitophagy. ***Nature***, 524(7565): 309–314.

Lazarus, J. E., Moughamian, A. J., Tokito, M. K. & Holzbaur, E. L. F. 2013. Dynactin subunit p150(Glued) is a neuron-specific anti-catastrophe factor. ***PLoS biology***, 11(7): 1001611–1001622.

Le Ber, I., De Septenville, A., Millecamps, S., Camuzat, A., Caroppo, P., Couratier, P., et al. 2015. TBK1 mutation frequencies in French frontotemporal dementia and amyotrophic lateral sclerosis cohorts. ***Neurobiology of aging***, 36(11): 3116–3119.

LeDizet, M. & Piperno, G. 1986. Cytoplasmic microtubules containing acetylated alpha-tubulin in Chlamydomonas reinhardtii: spatial arrangement and properties. ***The Journal of cell biology***, 103(1): 13–22.

Lee, I.-G., Olenick, M. A., Boczkowska, M., Franzini-Armstrong, C., Holzbaur, E. L. & Dominguez, R. 2018. A conserved interaction of the dynein light intermediate chain with dynein-dynactin effectors necessary for processivity. ***Nature communications***,

9(1): 1–12.

Lee, J.-Y., Koga, H., Kawaguchi, Y., Tang, W., Wong, E., Gao, Y.-S., et al. 2010. HDAC6 controls autophagosome maturation essential for ubiquitin-selective quality-control autophagy. ***The EMBO journal***, 29(5): 969–980.

Lee, K.-M., Hwang, S.-K. & Lee, J.-A. 2013. Neuronal autophagy and neurodevelopmental disorders. ***Experimental neurobiology***, 22(3): 133–142.

Lee, S., Jeon, Y.-M., Cha, S. J., Kim, S., Kwon, Y., Jo, M., et al. 2019. PTK2/FAK regulates UPS impairment via SQSTM1/p62 phosphorylation in TARDBP/TDP-43 proteinopathies. ***Autophagy***, 16(8): 1396–1412.

Lee, S. M., Asress, S., Hales, C. M., Gearing, M., Vizcarra, J. C., Fournier, C. N., et al. 2019. TDP-43 cytoplasmic inclusion formation is disrupted in C9orf72-associated amyotrophic lateral sclerosis/frontotemporal lobar degeneration. ***Brain Communications***, 1(1): 1–18.

Lenzi, J., De Santis, R., De Turris, V., Morlando, M., Laneve, P., Calvo, A., et al. 2015. ALS mutant FUS proteins are recruited into stress granules in induced pluripotent stem cell-derived motoneurons. ***Disease models & mechanisms***, 8(7): 755–766.

Levine, B. & Kroemer, G. 2008. Autophagy in the pathogenesis of disease. ***Cell***, 132(1): 27–42.

Li, D., Shi, J.-J., Mao, C.-J., Liu, S., Wang, J.-D., Chen, J., et al. 2013. Alteration of dynein function affects α-synuclein degradation via the autophagosome-lysosome pathway. ***International journal of molecular sciences***, 14(12): 24242–24254.

Li, F., Xie, X., Wang, Y., Liu, J., Cheng, X., Guo, Y., et al. 2016. Structural insights into the interaction and disease mechanism of neurodegenerative disease-associated optineurin and TBK1 proteins. ***Nature Communications***, 7(12078): 1–12.

Li, H.-R., Chen, T.-C., Hsiao, C.-L., Shi, L., Chou, C.-Y. & Huang, J. 2018. The physical forces mediating self-association and phase-separation in the C-terminal domain of TDP-43. ***Biochimica et Biophysica Acta (BBA)-Proteins and Proteomics***, 1866(2): 214–223.

Li, J., Li, J., Miyahira, A., Sun, J., Liu, Y., Cheng, G., et al. 2012. Crystal structure of the ubiquitin-like domain of human TBK1. ***Protein & cell***, 3(5): 383–391.

Li, L., Jayabal, S., Ghorbani, M., Legault, L.-M., McGraw, S., Watt, A. J., et al. 2019. ATAT1 regulates forebrain development and stress-induced tubulin hyperacetylation. ***Cellular and Molecular Life Sciences***, 76(18): 3621–3640.

Li, L., Wei, D., Wang, Q., Pan, J., Liu, R., Zhang, X., et al. 2012. MEC-17 deficiency leads to reduced α-tubulin acetylation and impaired migration of cortical neurons. ***Journal of Neuroscience***, 32(37): 12673–12683.

Li, L. & Yang, X.-J. 2015. Tubulin acetylation: responsible enzymes, biological functions and human diseases. ***Cellular and molecular life sciences***, 72(22): 4237–4255.

Li, W., Li, J. & Bao, J. 2012. Microautophagy: lesser-known self-eating. ***Cellular and Molecular Life Sciences***, 69(7): 1125–1136.

Li, W., Yang, Q. & Mao, Z. 2011. Chaperone-mediated autophagy: machinery, regulation and biological consequences. ***Cellular and molecular life sciences : CMLS***, 68(5): 749–763.

Li, Y. R., King, O. D., Shorter, J. & Gitler, A. D. 2013. Stress granules as crucibles of ALS pathogenesis. ***Journal of cell biology***, 201(3): 361–372.

Li, Y., Shin, D. & Kwon, S. H. 2013. Histone deacetylase 6 plays a role as a distinct regulator of diverse cellular processes. ***The FEBS journal***, 280(3): 775–793.

Liewluck, T. & Saperstein, D. S. 2015. Progressive muscular atrophy. ***Neurologic clinics***, 33(4): 761–773.

Lilienbaum, A. 2013. Relationship between the proteasomal system and autophagy. ***International journal of biochemistry and molecular biology***, 4(1): 1–26.

Lim, J., Lachenmayer, M. L., Wu, S., Liu, W., Kundu, M., Wang, R., et al. 2015. Proteotoxic stress induces phosphorylation of p62/SQSTM1 by ULK1 to regulate selective autophagic clearance of protein aggregates. ***PLoS genetics***, 11(2): 2–28.

Linares, J. F., Duran, A., Reina-Campos, M., Aza-Blanc, P., Campos, A., Moscat, J., et al. 2015. Amino acid activation of mTORC1 by a PB1-domain-driven kinase complex cascade. ***Cell reports***, 12(8): 1339–1352.

Ling, S.-C., Polymenidou, M. & Cleveland, D. W. 2013. Converging mechanisms in ALS and FTD: disrupted RNA and protein homeostasis. ***Neuron***, 79(3): 416–438.

Liu, W. J., Ye, L., Huang, W. F., Guo, L. J., Xu, Z. G., Wu, H. L., et al. 2016. p62 links the autophagy pathway and the ubiqutin-proteasome system upon ubiquitinated protein degradation. ***Cellular & molecular biology letters***, 21(1): 1–14.

Liu-Yesucevitz, L., Lin, A. Y., Ebata, A., Boon, J. Y., Reid, W., Xu, Y.-F., et al. 2014. ALS-linked mutations enlarge TDP-43-enriched neuronal RNA granules in the dendritic arbor. ***Journal of Neuroscience***, 34(12): 4167–4174.

Logroscino, G. & Piccininni, M. 2019. Amyotrophic lateral sclerosis descriptive epidemiology: the origin of geographic difference. ***Neuroepidemiology***, 52(1-2): 93–103.

López-Otin, C., Blasco, M. A., Partridge, L., Serrano, M. & Kroemer, G. 2013. The hallmarks of aging. ***Cell***, 153(6): 1194–1217.

Lord, C., Ferro-Novick, S. & Miller, E. A. 2013. The highly conserved COPII coat complex sorts cargo from the endoplasmic reticulum and targets it to the golgi. ***Cold Spring Harbor Perspectives in Biology***, 5(2): 13367–13379.

Loschi, M., Leishman, C. C., Berardone, N. & Boccaccio, G. L. 2009. Dynein and kinesin regulate stress-granule and P-body dynamics. ***Journal of cell science***, 122(21): 3973–3982.

Ly, N., Elkhatib, N., Bresteau, E., Piétrement, O., Khaled, M., Magiera, M. M., et al. 2016. αTAT1 controls longitudinal spreading of acetylation marks from open microtubules extremities. ***Scientific reports***, 6(1): 1–10.

Mackenzie, I. R., Nicholson, A. M., Sarkar, M., Messing, J., Purice, M. D., Pottier, C., et al. 2017. TIA1 mutations in amyotrophic lateral sclerosis and frontotemporal dementia promote phase separation and alter stress granule dynamics. ***Neuron***, 95(4): 808–816.

Maday, S., Wallace, K. E. & Holzbaur, E. L. 2012. Autophagosomes initiate distally and mature during transport toward the cell soma in primary neurons. ***J Cell Biol***, 196(4): 407–417.

Mahboubi, H. & Stochaj, U. 2017. Cytoplasmic stress granules: Dynamic modulators of cell signaling and disease. ***Biochimica et Biophysica Acta (BBA)-Molecular Basis of Disease***, 1863(4): 884–895.

Mammucari, C. & Rizzuto, R. 2010. Signaling pathways in mitochondrial dysfunction and aging. ***Mechanisms of ageing and development***, 131(7): 536–543.

Mandal, A. & Drerup, K. 2019. Axonal transport and mitochondrial function in neurons. ***Frontiers in cellular neuroscience***, 13(373): 1–11.

Mann, D. M., Rollinson, S., Robinson, A., Callister, J. B., Thompson, J. C., Snowden, J. S., et al. 2013. Dipeptide repeat proteins are present in the p62 positive inclusions in patients with frontotemporal lobar degeneration and motor neurone disease associated with expansions in C9ORF72. ***Acta neuropathologica communications***, 1(1): 1–13.

Marcos, S., Moreau, J., Backer, S., Job, D., Andrieux, A. & Bloch-Gallego, E. 2009. Tubulin tyrosination is required for the proper organization and pathfinding of the growth cone. ***PloS one***, 4(4): 1–16.

Marrone, L., Drexler, H. C., Wang, J., Tripathi, P., Distler, T., Heisterkamp, P., et al. 2019. FUS pathology in ALS is linked to alterations in multiple ALS-associated proteins and rescued by drugs stimulating autophagy. ***Acta neuropathologica***, 138(1): 67–84.

Martinez-Alonso, E., Tomás, M. & Martinez-Menárguez, J. A. 2013. Golgi tubules: their structure, formation and role in intra-Golgi transport. ***Histochemistry and cell biology***, 140(3): 327–339.

Martinez-Carrera, L. A. & Wirth, B. 2015. Dominant spinal muscular atrophy is caused by mutations in BICD2, an important golgin protein. ***Frontiers in neuroscience***, 9(401): 1–9.

Marzo, M. G., Griswold, J. M. & Markus, S. M. 2020. Pac1/LIS1 stabilizes an uninhibited conformation of dynein to coordinate its localization and activity. ***Nature Cell Biology***, 22(5): 559–569.

Massey, A. C., Follenzi, A., Kiffin, R., Zhang, C. & Cuervo, A. M. 2008. Early cellular changes after blockage of chaperone-mediated autophagy. ***Autophagy***, 4(4): 442–456.

Matanis, T., Akhmanova, A., Wulf, P., Del Nery, E., Weide, T., Stepanova, T., et al. 2002. Bicaudal-D regulates COPI-independent Golgi-ER transport by recruiting the dynein-dynactin motor complex. ***Nature cell biology***, 4(12): 986–892.

Matsumoto, G., Shimogori, T., Hattori, N. & Nukina, N. 2015. TBK1 controls autophagosomal engulfment of polyubiquitinated mitochondria through p62/SQSTM1 phosphorylation. ***Human molecular genetics***, 24(15): 4429–4442.

Matsumoto, G., Wada, K., Okuno, M., Kurosawa, M. & Nukina, N. 2011. Serine 403 phosphorylation of p62/SQSTM1 regulates selective autophagic clearance of ubiquitinated proteins. ***Molecular cell***, 44(2): 279–289.

Matsuyama, A., Shimazu, T., Sumida, Y., Saito, A., Yoshimatsu, Y., Seigneurin-Berny, D., et al. 2002. In vivo destabilization of dynamic microtubules by HDAC6-mediated deacetylation. ***The EMBO journal***, 21(24): 6820–6831.

Mattson, M. P. & Magnus, T. 2006. Ageing and neuronal vulnerability. ***Nature Reviews Neuroscience***, 7(4): 278–294.

Maurel, C., Dangoumau, A., Marouillat, S., Brulard, C., Chami, A., Hergesheimer, R., et al. 2018. Causative genes in amyotrophic lateral sclerosis and protein degradation pathways: a link to neurodegeneration. ***Molecular neurobiology***, 55(8): 6480–6499.

Mazroui, R., Di Marco, S., Kaufman, R. J. & Gallouzi, I.-E. 2007. Inhibition of the ubiquitin-proteasome system induces stress granule formation. ***Molecular biology of the cell***, 18(7): 2603–2618.

McDonald, K. K., Aulas, A., Destroismaisons, L., Pickles, S., Beleac, E., Camu, W., et al. 2011. TAR DNA-binding protein 43 (TDP-43) regulates stress granule dynamics via differential regulation of G3BP and TIA-1. ***Human molecular genetics***, 20(7): 1400–1410.

McEwan, D. G., Popovic, D., Gubas, A., Terawaki, S., Suzuki, H., Stadel, D., et al. 2015. PLEKHM1 regulates autophagosome-lysosome fusion through HOPS complex and LC3/GABARAP proteins. ***Molecular cell***, 57(1): 39–54.

McKenney, R. J., Huynh, W., Tanenbaum, M. E., Bhabha, G. & Vale, R. D. 2014. Activation of cytoplasmic dynein motility by dynactin-cargo adapter complexes. ***Science***, 345(6194): 337–341.

McKenney, R. J., Huynh, W., Vale, R. D. & Sirajuddin, M. 2016. Tyrosination of α-tubulin controls the initiation of processive dynein-dynactin motility. ***The EMBO journal***, 35(11): 1175–1185.

McKenney, R. J., Vershinin, M., Kunwar, A., Vallee, R. B. & Gross, S. P. 2010. LIS1 and NudE induce a persistent dynein force-producing state. ***Cell***, 141(2): 304–314.

Mejlvang, J., Olsvik, H., Svenning, S., Bruun, J.-A., Abudu, Y. P., Larsen, K. B., et al. 2018. Starvation induces rapid degradation of selective autophagy receptors by endosomal microautophagy. ***Journal of Cell Biology***, 217(10): 3640–3655.

Mejzini, R., Flynn, L. L., Pitout, I. L., Fletcher, S., Wilton, S. D. & Akkari, P. A. 2019. ALS genetics, mechanisms, and therapeutics: Where are we now? ***Frontiers in Neuroscience***, 13(1310): 1–27.

Menzies, F. M., Fleming, A. & Rubinsztein, D. C. 2015. Compromised autophagy and neurodegenerative diseases. ***Nature Reviews Neuroscience***, 16(6): 345–357.

Mercado, P. A., Ayala, Y. M., Romano, M., Buratti, E. & Baralle, F. E. 2005. Depletion of TDP 43 overrides the need for exonic and intronic splicing enhancers in the human apoA-II gene. ***Nucleic acids research***, 33(18): 6000–6010.

Mercuri, E., Messina, S., Kinali, M., Cini, C., Longman, C., Battini, R., et al. 2004. Congenital form of spinal muscular atrophy predominantly affecting the lower limbs: a clinical and muscle MRI study. ***Neuromuscular Disorders***, 14(2): 125–129.

Millarte, V. & Farhan, H. 2012. The Golgi in cell migration: regulation by signal transduction and its implications for cancer cell metastasis. ***The Scientific World Journal***, 2012: 1–11.

MISSING:reed2006microtubule. 2021. MISSING:reed2006microtubule.

Mizushima, N. 2009. Physiological functions of autophagy. ***Autophagy in infection and immunity***: 71–84. Springer.

Mizushima, N., Levine, B., Cuervo, A. M. & Klionsky, D. J. 2008. Autophagy fights disease through cellular self-digestion. ***Nature***, 451(7182): 1069–1075.

Mizushima, N., Yoshimori, T. & Ohsumi, Y. 2011. The role of Atg proteins in autophagosome formation. ***Annual review of cell and developmental biology***, 27: 107–132.

Molino, D., Zemirli, N., Codogno, P. & Morel, E. 2017. The journey of the autophagosome through mammalian cell organelles and membranes. ***Journal of molecular biology***, 429(4): 497–514.

Molliex, A., Temirov, J., Lee, J., Coughlin, M., Kanagaraj, A. P., Kim, H. J., et al. 2015. Phase separation by low complexity domains promotes stress granule assembly and drives

pathological fibrillization. ***Cell***, 163(1): 123–133.

Monahan, Z., Shewmaker, F. & Pandey, U. B. 2016. Stress granules at the intersection of autophagy and ALS. ***Brain research***, 1649: 189–200.

Moore, A. S. & Holzbaur, E. L. 2016. Dynamic recruitment and activation of ALS-associated TBK1 with its target optineurin are required for efficient mitophagy. ***Proceedings of the National Academy of Sciences***, 113(24): 3349–3358.

Moreau, K., Ravikumar, B., Renna, M., Puri, C. & Rubinsztein, D. C. 2011. Autophagosome precursor maturation requires homotypic fusion. ***Cell***, 146(2): 303–317.

Morelli, G., Even, A., Gladwyn-Ng, I., Le Bail, R., Shilian, M., Godin, J. D., et al. 2018. p27kip1 modulates axonal transport by regulating α-tubulin acetyltransferase 1 stability. ***Cell reports***, 23(8): 2429–2442.

Mori, K., Arzberger, T., Grässer, F. A., Gijselinck, I., May, S., Rentzsch, K., et al. 2013. Bidirectional transcripts of the expanded C9orf72 hexanucleotide repeat are translated into aggregating dipeptide repeat proteins. ***Acta neuropathologica***, 126(6): 881–893.

Mori, K., Weng, S.-M., Arzberger, T., May, S., Rentzsch, K., Kremmer, E., et al. 2013. The C9orf72 GGGGCC repeat is translated into aggregating dipeptide-repeat proteins in FTLD/ALS. ***Science***, 339(6125): 1335–1338.

Moughamian, A. J. & Holzbaur, E. L. 2012. Dynactin is required for transport initiation from the distal axon. ***Neuron***, 74(2): 331–343.

Moughamian, A. J., Osborn, G. E., Lazarus, J. E., Maday, S. & Holzbaur, E. L. 2013. Ordered recruitment of dynactin to the microtubule plus-end is required for efficient initiation of retrograde axonal transport. ***Journal of Neuroscience***, 33(32): 13190–13203.

Mourelatos, Z., Gonatas, N. K., Stieber, A., Gurney, M. E. & Dal Canto, M. C. 1996. The Golgi apparatus of spinal cord motor neurons in transgenic mice expressing mutant Cu, Zn superoxide dismutase becomes fragmented in early, preclinical stages of the disease. ***Proceedings of the National Academy of Sciences***, 93(11): 5472–5477.

Mukai, M., Ikegami, K., Sugiura, Y., Takeshita, K., Nakagawa, A. & Setou, M. 2009. Recombinant mammalian tubulin polyglutamylase TTLL7 performs both initiation and elongation of polyglutamylation on β-tubulin through a random sequential pathway. ***Biochemistry***, 48(5): 1084–1093.

Mukherjee, A., Patel, B., Koga, H., Cuervo, A. M. & Jenny, A. 2016. Selective endosomal microautophagy is starvation-inducible in Drosophila. ***Autophagy***, 12(11): 1984–1999.

Münch, C., Sedlmeier, R., Meyer, T., Homberg, V., Sperfeld, A., Kurt, A., et al. 2004. Point mutations of the p150 subunit of dynactin (DCTN1) gene in ALS. ***Neurology***, 63(4): 724–726.

Nakagomi, S., Barsoum, M. J., Bossy-Wetzel, E., Sütterlin, C., Malhotra, V. & Lipton, S. A. 2008. A Golgi fragmentation pathway in neurodegeneration. ***Neurobiology of disease***, 29(2): 221–231.

Nakamura, N., Wei, J.-H. & Seemann, J. 2012. Modular organization of the mammalian Golgi apparatus. ***Current opinion in cell biology***, 24(4): 467–474.

Nakashima, H., Nguyen, T., Goins, W. F. & Chiocca, E. A. 2015. Interferon-stimulated gene 15 (ISG15) and ISG15-linked proteins can associate with members of the selective autophagic process, histone deacetylase 6 (HDAC6) and SQSTM1/p62. ***Journal of Biological Chemistry***, 290(3): 1485–1495.

Nakatogawa, H. 2013. Two ubiquitin-like conjugation systems that mediate membrane formation during autophagy. ***Essays in biochemistry***, 55: 39–50.

Nakatogawa, H. 2020. Mechanisms governing autophagosome biogenesis. ***Nature Reviews Molecular Cell Biology***, 21: 1–20.

Narayanan, R. K., Mangelsdorf, M., Panwar, A., Butler, T. J., Noakes, P. G. & Wallace, R. H. 2013. Identification of RNA bound to the TDP-43 ribonucleoprotein complex in the adult mouse brain. ***Amyotrophic lateral sclerosis & frontotemporal degeneration***, 14(4): 252–560.

Nassif, M., Woehlbier, U. & Manque, P. A. 2017. The enigmatic role of C9ORF72 in autophagy. ***Frontiers in neuroscience***, 11(442): 1–10.

Negrete-Hurtado, A., Overhoff, M., Bera, S., De Bruyckere, E., Schätzmüller, K., Kye, M., et al. 2020. Autophagy lipidation machinery regulates axonal microtubule dynamics but is dispensable for survival of mammalian neurons. ***Nature communications***, 11(1): 1–19.

Neumann, B. & Hilliard, M. A. 2014. Loss of MEC-17 leads to microtubule instability and axonal degeneration. ***Cell reports***, 6(1): 93–103.

Neumann, M., Kwong, L. K., Lee, E. B., Kremmer, E., Flatley, A., Xu, Y., et al. 2009. Phosphorylation of S409/410 of TDP-43 is a consistent feature in all sporadic and familial forms of TDP-43 proteinopathies. ***Acta neuropathologica***, 117(2): 137–149.

Neumann, M., Sampathu, D. M., Kwong, L. K., Truax, A. C., Micsenyi, M. C., Chou, T. T., et al. 2006. Ubiquitinated TDP-43 in frontotemporal lobar degeneration and amyotrophic lateral sclerosis. ***Science***, 314(5796): 130–133.

Neveling, K., Martinez-Carrera, L. A., Hölker, I., Heister, A., Verrips, A., Hosseini-Barkooie, S. M., et al. 2013. Mutations in BICD2, which encodes a golgin and important motor adaptor, cause congenital autosomal-dominant spinal muscular atrophy. ***The American Journal of Human Genetics***, 92(6): 946–954.

Nezis, I. P., Simonsen, A., Sagona, A. P., Finley, K., Gaumer, S., Contamine, D., et al. 2008. Ref (2) P, the Drosophila melanogaster homologue of mammalian p62, is required for the formation of protein aggregates in adult brain. ***The Journal of cell biology***, 180(6): 1065–1071.

Nieuwenhuis, J., Adamopoulos, A., Bleijerveld, O. B., Mazouzi, A., Stickel, E., Celie, P., et al. 2017. Vasohibins encode tubulin detyrosinating activity. ***Science***, 358(6369): 1453–1456.

Nirschl, J. J., Magiera, M. M., Lazarus, J. E., Janke, C. & Holzbaur, E. L. 2016. α-Tubulin tyrosination and CLIP-170 phosphorylation regulate the initiation of dynein-driven

transport in neurons. ***Cell reports***, 14(11): 2637–2652.

Nishida, Y., Arakawa, S., Fujitani, K., Yamaguchi, H., Mizuta, T., Kanaseki, T., et al. 2009. Discovery of Atg5/Atg7-independent alternative macroautophagy. ***Nature***, 461(7264): 654–659.

Nishikawa, S., Fewell, S. W., Kato, Y., Brodsky, J. L. & Endo, T. 2001. Molecular chaperones in the yeast endoplasmic reticulum maintain the solubility of proteins for retrotranslocation and degradation. ***The Journal of cell biology***, 153(5): 1061–1070.

Niu, Q., Wang, X., Shi, M. & Jin, Q. 2015. A novel DYNC1H1 mutation causing spinal muscular atrophy with lower extremity predominance. ***Neurology Genetics***, 1(2): 1–4.

Nixon, R. A. & Shea, T. B. 1992. Dynamics of neuronal intermediate filaments: a developmental perspective. ***Cell motility and the cytoskeleton***, 22(2): 81–91.

Nixon, R. A. & Yang, D.-S. 2012. Autophagy and neuronal cell death in neurological disorders. ***Cold Spring Harbor perspectives in biology***, 4(10): 8839–8861.

O'rourke, J., Bogdanik, L., Yanez, A., Lall, D., Wolf, A., Muhammad, A., et al. 2016. C9orf72 is required for proper macrophage and microglial function in mice. ***Science***, 351(6279): 1324–1329.

Oakes, J. A., Davies, M. C. & Collins, M. O. 2017. TBK1: a new player in ALS linking autophagy and neuroinflammation. ***Molecular brain***, 10(1): 1–10.

Oates, E. C., Rossor, A. M., Hafezparast, M., Gonzalez, M., Speziani, F., MacArthur, D. G., et al. 2013. Mutations in BICD2 cause dominant congenital spinal muscular atrophy and hereditary spastic paraplegia. ***The American Journal of Human Genetics***, 92(6): 965–973.

Oláh, J., Szunyogh, S., Szénási, T., Szaniszló, T., Szabó, A., Lehotzky, A., et al. 2019. Interactions between two regulatory proteins of microtubule dynamics, HDAC6, TPPP/p25, and the hub protein, DYNLL/LC8. ***Biochimica et Biophysica Acta (BBA)-Molecular Cell Research***, 1866(12): 118556–118568.

Olenick, M. A., Dominguez, R. & Holzbaur, E. L. 2019. Dynein activator Hook1 is required for trafficking of BDNF-signaling endosomes in neurons. ***Journal of Cell Biology***, 218(1): 220–233.

Oliver, P. L. & Davies, K. E. 2012. New insights into behaviour using mouse ENU mutagenesis. ***Human molecular genetics***, 21(1): 72–81.

Ori-McKenney, K. M. & Vallee, R. B. 2011. Neuronal migration defects in the Loa dynein mutant mouse. ***Neural development***, 6(1): 1–13.

Ori-McKenney, K. M., Xu, J., Gross, S. P. & Vallee, R. B. 2010. A cytoplasmic dynein tail mutation impairs motor processivity. ***Nature cell biology***, 12(12): 1228–1234.

Otomo, A., Kunita, R., Suzuki-Utsunomiya, K., Ikeda, J.-E. & Hadano, S. 2011. Defective relocalization of ALS2/alsin missense mutants to Rac1-induced macropinosomes accounts for loss of their cellular function and leads to disturbed amphisome formation. ***FEBS letters***, 585(5): 730–736.

Ouyang, H., Ali, Y. O., Ravichandran, M., Dong, A., Qiu, W., MacKenzie, F., et al. 2012. Protein aggregates are recruited to aggresome by histone deacetylase 6 via unanchored ubiquitin C termini. ***Journal of Biological Chemistry***, 287(4): 2317–2327.

Özdemir, A., Machida, K., Imataka, H. & Catling, A. D. 2016. Identification of the T-complex protein as a binding partner for newly synthesized cytoplasmic dynein intermediate chain 2. ***Biochemical and biophysical research communications***, 469(1): 126–131.

Palmer, K. J., Hughes, H. & Stephens, D. J. 2009. Specificity of cytoplasmic dynein subunits in discrete membrane-trafficking steps. ***Molecular biology of the cell***, 20(12): 2885–2899.

Panas, M. D., Ivanov, P. & Anderson, P. 2016. Mechanistic insights into mammalian stress granule dynamics. ***Journal of Cell Biology***, 215(3): 313–323.

Pandey, U. B., Nie, Z., Batlevi, Y., McCray, B. A., Ritson, G. P., Nedelsky, N. B., et al. 2007. HDAC6 rescues neurodegeneration and provides an essential link between autophagy and the UPS. ***Nature***, 447(7146): 860–864.

Pankiv, S., Clausen, T. H., Lamark, T., Brech, A., Bruun, J.-A., Outzen, H., et al. 2007. p62/SQSTM1 binds directly to Atg8/LC3 to facilitate degradation of ubiquitinated protein aggregates by autophagy. ***Journal of biological chemistry***, 282(33): 24131–24145.

Patel, A., Lee, H. O., Jawerth, L., Maharana, S., Jahnel, M., Hein, M. Y., et al. 2015. A liquid-to-solid phase transition of the ALS protein FUS accelerated by disease mutation. ***Cell***, 162(5): 1066–1077.

Paturle-Lafanechère, L., Manier, M., Trigault, N., Pirollet, F., Mazarguil, H. & Job, D. 1994. Accumulation of delta 2-tubulin, a major tubulin variant that cannot be tyrosinated, in neuronal tissues and in stable microtubule assemblies. ***Journal of Cell Science***, 107(6): 1529–1543.

Peeters, K., Bervoets, S., Chamova, T., Litvinenko, I., De Vriendt, E., Bichev, S., et al. 2015. Novel Mutations in the DYNC 1 H 1 Tail Domain Refine the Genetic and Clinical Spectrum of Dyneinopathies. ***Human mutation***, 36(3): 287–291.

Peeters, K., Litvinenko, I., Asselbergh, B., Almeida-Souza, L., Chamova, T., Geuens, T., et al. 2013. Molecular defects in the motor adaptor BICD2 cause proximal spinal muscular atrophy with autosomal-dominant inheritance. ***The American Journal of Human Genetics***, 92(6): 955–964.

Peng, H., Yang, J., Li, G., You, Q., Han, W., Li, T., et al. 2017. Ubiquitylation of p62/sequestosome1 activates its autophagy receptor function and controls selective autophagy upon ubiquitin stress. ***Cell research***, 27(5): 657–674.

Perdiz, D., Mackeh, R., Poüs, C. & Baillet, A. 2011. The ins and outs of tubulin acetylation: more than just a post-translational modification? ***Cellular signalling***, 23(5): 763–771.

Peris, L., Wagenbach, M., Lafanechère, L., Brocard, J., Moore, A. T., Kozielski, F., et al. 2009. Motor-dependent microtubule disassembly driven by tubulin tyrosination.

Journal of Cell Biology, 185(7): 1159–1166.

Perlson, E., Maday, S., Fu, M., Moughamian, A. J. & Holzbaur, E. L. 2010. Retrograde axonal transport: pathways to cell death? ***Trends in neurosciences***, 33(7): 335–344.

Perrot, R., Berges, R., Bocquet, A. & Eyer, J. 2008. Review of the multiple aspects of neurofilament functions, and their possible contribution to neurodegeneration. ***Molecular neurobiology***, 38(1): 27–65.

Perrot, R. & Eyer, J. 2009. Neuronal intermediate filaments and neurodegenerative disorders. ***Brain research bulletin***, 80(4-5): 282–295.

Pesiridis, G. S., Tripathy, K., Tanik, S., Trojanowski, J. Q. & Lee, V. M.-Y. 2011. A "two-hit" hypothesis for inclusion formation by carboxyl-terminal fragments of TDP-43 protein linked to RNA depletion and impaired microtubule-dependent transport. ***Journal of Biological Chemistry***, 286(21): 18845–18855.

Peters, O. M., Ghasemi, M. & Brown, R. H. 2015. Emerging mechanisms of molecular pathology in ALS. ***The Journal of clinical investigation***, 125(5): 1767–1779.

Pfister, K. K., Shah, P. R., Hummerich, H., Russ, A., Cotton, J., Annuar, A. A., et al. 2006. Genetic analysis of the cytoplasmic dynein subunit families. ***PLoS genetics***, 2(1): 1–17.

Phadwal, K., Kurian, D., Salamat, M. K. F., MacRae, V. E., Diack, A. B. & Manson, J. C. 2018. Spermine increases acetylation of tubulins and facilitates autophagic degradation of prion aggregates. ***Scientific reports***, 8(1): 1–17.

Picci, C., Wong, V. S., Costa, C. J., McKinnon, M. C., Goldberg, D. C., Swift, M., et al. 2020. HDAC6 inhibition promotes α-tubulin acetylation and ameliorates CMT2A peripheral neuropathy in mice. ***Experimental Neurology***, 328: 1–48.

Pillai, S., Nguyen, J., Johnson, J., Haura, E., Coppola, D. & Chellappan, S. 2014. Tank binding kinase 1 is a centrosome-associated kinase necessary for microtubule dynamics and mitosis. ***Nature communications***, 6: 10072–10072.

Pilli, M., Arko-Mensah, J., Ponpuak, M., Roberts, E., Master, S., Mandell, M. A., et al. 2012. TBK-1 promotes autophagy-mediated antimicrobial defense by controlling autophagosome maturation. ***Immunity***, 37(2): 223–234.

Polymenidou, M., Lagier-Tourenne, C., Hutt, K. R., Huelga, S. C., Moran, J., Liang, T. Y., et al. 2011. Long pre-mRNA depletion and RNA missplicing contribute to neuronal vulnerability from loss of TDP-43. ***Nature neuroscience***, 14(4): 459–568.

Pongrakhananon, V., Saito, H., Hiver, S., Abe, T., Shioi, G., Meng, W., et al. 2018. CAMSAP3 maintains neuronal polarity through regulation of microtubule stability. ***Proceedings of the National Academy of Sciences***, 115(39): 9750–9755.

Portran, D., Schaedel, L., Xu, Z., Théry, M. & Nachury, M. V. 2017. Tubulin acetylation protects long-lived microtubules against mechanical ageing. ***Nature cell biology***, 19(4): 391–398.

Pottier, C., Bieniek, K. F., Finch, N., van de Vorst, M., Baker, M., Perkersen, R., et al. 2015. Whole-genome sequencing reveals important role for TBK1 and OPTN mutations in frontotemporal lobar degeneration without motor neuron disease. ***Acta neuropathologica***, 130(1): 77–92.

Prasad, A., Bharathi, V., Sivalingam, V., Girdhar, A. & Patel, B. K. 2019. Molecular mechanisms of TDP-43 misfolding and pathology in amyotrophic lateral sclerosis. ***Frontiers in molecular neuroscience***, 12(25): 1–36.

Priest, M. D., Navarro, M. F., Bremer, J. & Granato, M. 2019. Dynein promotes sustained axonal growth and Schwann cell remodeling early during peripheral nerve regeneration. ***PLoS genetics***, 15(2): 1–16.

Protter, D. S. & Parker, R. 2016. Principles and properties of stress granules. ***Trends in cell biology***, 26(9): 668–679.

Puls, I., Jonnakuty, C., LaMonte, B. H., Holzbaur, E. L., Tokito, M., Mann, E., et al. 2003. Mutant dynactin in motor neuron disease. ***Nature genetics***, 33(4): 455–456.

Puls, I., Oh, S. J., Sumner, C. J., Wallace, K. E., Floeter, M. K., Mann, E. A., et al. 2005. Distal spinal and bulbar muscular atrophy caused by dynactin mutation. ***Annals of neurology***, 57(5): 687–694.

Puri, C., Renna, M., Bento, C. F., Moreau, K. & Rubinsztein, D. C. 2013. Diverse autophagosome membrane sources coalesce in recycling endosomes. ***Cell***, 154(6): 1285–1299.

Purves, D., Augustine, G., Fitzpatrick, D., Hall, W., LaMantia, A., McNamara, J., et al. 2004. Neuroscience Third Edtion. ***Sinauer, Massachusetts***.

Puthenveedu, M. A., Bachert, C., Puri, S., Lanni, F. & Linstedt, A. D. 2006. GM130 and GRASP65-dependent lateral cisternal fusion allows uniform Golgi-enzyme distribution. ***Nature cell biology***, 8(3): 238–248.

Ragagnin, A. M., Shadfar, S., Vidal, M., Jamali, S. & Atkin, J. D. 2019. Motor neuron susceptibility in ALS/FTD. ***Frontiers in neuroscience***, 13(532): 1–37.

Rakhit, R. & Chakrabartty, A. 2006. Structure, folding, and misfolding of Cu, Zn superoxide dismutase in amyotrophic lateral sclerosis. ***Biochimica et Biophysica Acta (BBA)-Molecular Basis of Disease***, 1762(11-12): 1025–1037.

Ramaswami, M., Taylor, J. P. & Parker, R. 2013. Altered ribostasis: RNA-protein granules in degenerative disorders. ***Cell***, 154(4): 727–736.

Ramesh, N. & Pandey, U. B. 2017. Autophagy dysregulation in ALS: when protein aggregates get out of hand. ***Frontiers in molecular neuroscience***, 10(263): 1–18.

Rapali, P., Radnai, L., Süveges, D., Harmat, V., Tölgyesi, F., Wahlgren, W. Y., et al. 2011. Directed evolution reveals the binding motif preference of the LC8/DYNLL hub protein and predicts large numbers of novel binders in the human proteome. ***PLoS One***, 6(4): 1–14.

Ratti, A. & Buratti, E. 2016. Physiological functions and pathobiology of TDP-43 and FUS/TLS proteins. ***Journal of neurochemistry***, 138: 95–111.

Ravikumar, B., Acevedo-Arozena, A., Imarisio, S., Berger, Z., Vacher, C., O'Kane, C. J., et al. 2005. Dynein mutations impair autophagic clearance of aggregate-prone proteins. ***Nature genetics***, 37(7): 771–776.

Ravikumar, B., Sarkar, S., Davies, J. E., Futter, M., Garcia-Arencibia, M., Green-Thompson, Z. W., et al. 2010. Regulation of mammalian autophagy in physiology and pathophysiology. ***Physiological reviews***, 90(4): 1383–1435.

Redemann, S., Pecreaux, J., Goehring, N. W., Khairy, K., Stelzer, E. H. K., Hyman, A. A., et al. 2010. Membrane invaginations reveal cortical sites that pull on mitotic spindles in one-cell C. elegans embryos. ***PloS one***, 5(8): 1–10.

Reed, N. A., Cai, D., Blasius, T. L., Jih, G. T., Meyhofer, E., Gaertig, J., et al. 2006. Microtubule acetylation promotes kinesin-1 binding and transport. ***Current biology : CB***, 16(21): 2166–2172.

Renton, A. E., Chiò, A. & Traynor, B. J. 2014. State of play in amyotrophic lateral sclerosis genetics. ***Nature neuroscience***, 17(1): 1–7.

Renton, A. E., Majounie, E., Waite, A., Simón-Sánchez, J., Rollinson, S., Gibbs, J. R., et al. 2011. A hexanucleotide repeat expansion in C9ORF72 is the cause of chromosome 9p21-linked ALS-FTD. ***Neuron***, 72(2): 257–268.

Ritch, R., Darbro, B., Menon, G., Khanna, C. L., Solivan-Timpe, F., Roos, B. R., et al. 2014. TBK1 gene duplication and normal-tension glaucoma. ***JAMA ophthalmology***, 132(5): 544–552.

Roberts, A. J. 2018. Emerging mechanisms of dynein transport in the cytoplasm versus the cilium. ***Biochemical Society Transactions***, 46(4): 967–982.

Roberts, A. J., Kon, T., Knight, P. J., Sutoh, K. & Burgess, S. A. 2013. Functions and mechanics of dynein motor proteins. ***Nature reviews Molecular cell biology***, 14(11):

713–726.

Rohn, T. T. 2008. Caspase-cleaved TAR DNA-binding protein-43 is a major pathological finding in Alzheimer's disease. ***Brain research***, 1228: 189–198.

Roossien, D., Miller, K. & Gallo, G. 2015. Ciliobrevins as tools for studying dynein motor function. ***Frontiers in cellular neuroscience***, 9(252): 1–10.

Rosen, D. R., Siddique, T., Patterson, D., Figlewicz, D. A., Sapp, P., Hentati, A., et al. 1993. Mutations in Cu/Zn superoxide dismutase gene are associated with familial amyotrophic lateral sclerosis. ***Nature***, 362(6415): 59–62.

Rui, Y.-N., Xu, Z., Patel, B., Chen, Z., Chen, D., Tito, A., et al. 2015. Huntingtin functions as a scaffold for selective macroautophagy. ***Nature cell biology***, 17(3): 1–28.

Russell, R. C., Tian, Y., Yuan, H., Park, H. W., Chang, Y.-Y., Kim, J., et al. 2013. ULK1 induces autophagy by phosphorylating Beclin-1 and activating VPS34 lipid kinase. ***Nature cell biology***, 15(7): 741–750.

Russo, A., Scardigli, R., La Regina, F., Murray, M. E., Romano, N., Dickson, D. W., et al. 2017. Increased cytoplasmic TDP-43 reduces global protein synthesis by interacting with RACK1 on polyribosomes. ***Human molecular genetics***, 26(8): 1407–1418.

Rutherford, N. J., Zhang, Y.-J., Baker, M., Gass, J. M., Finch, N. A., Xu, Y.-F., et al. 2008. Novel mutations in TARDBP (TDP-43) in patients with familial amyotrophic lateral sclerosis. ***PLoS genetics***, 4(9): 1–8.

Ryu, H.-H., Jun, M.-H., Min, K.-J., Jang, D.-J., Lee, Y.-S., Kim, H. K., et al. 2014. Autophagy regulates amyotrophic lateral sclerosis-linked fused in sarcoma-positive stress granules in neurons. ***Neurobiology of aging***, 35(12): 2822–2831.

Sadoul, K. & Khochbin, S. 2016. The growing landscape of tubulin acetylation: lysine 40 and many more. ***Biochemical Journal***, 473(13): 1859–1868.

Sahu, R., Kaushik, S., Clement, C. C., Cannizzo, E. S., Scharf, B., Follenzi, A., et al. 2011. Microautophagy of cytosolic proteins by late endosomes. ***Developmental cell***, 20(1): 131–147.

Sainath, R. & Gallo, G. 2015. The dynein inhibitor C iliobrevin D inhibits the bidirectional transport of organelles along sensory axons and impairs NGF-mediated regulation of growth cones and axon branches. ***Developmental neurobiology***, 75(7): 757–777.

Sakai, Y., Koller, A., Rangell, L. K., Keller, G. A. & Subramani, S. 1998. Peroxisome degradation by microautophagy in Pichia pastoris: identification of specific steps and morphological intermediates. ***The Journal of cell biology***, 141(3): 625–636.

Saleeb, R. S., Kavanagh, D. M., Dun, A. R., Dalgarno, P. A. & Duncan, R. R. 2019. A VPS33A-binding motif on syntaxin 17 controls autophagy completion in mammalian cells. ***Journal of Biological Chemistry***, 294(11): 4188–4201.

Salemi, L. M., Almawi, A. W., Lefebvre, K. J. & Schild-Poulter, C. 2014. Aggresome formation is regulated by RanBPM through an interaction with HDAC6. ***Biology open***, 3: 1–13.

Sánchez-Martin, P. & Komatsu, M. 2018. p62/SQSTM1-steering the cell through health and disease. ***Journal of cell science***, 131(21): 1–13.

Sardiello, M., Palmieri, M., di Ronza, A., Medina, D. L., Valenza, M., Gennarino, V. A., et al. 2009. A gene network regulating lysosomal biogenesis and function. ***Science***, 325(5939): 473–477.

Sasaki, S., Shionoya, A., Ishida, M., Gambello, M. J., Yingling, J., Wynshaw-Boris, A., et al. 2000. A LIS1/NUDEL/cytoplasmic dynein heavy chain complex in the developing and adult nervous system. ***Neuron***, 28(3): 681–696.

Sasayama, H., Shimamura, M., Tokuda, T., Azuma, Y., Yoshida, T., Mizuno, T., et al. 2012. Knockdown of the Drosophila fused in sarcoma (FUS) homologue causes deficient locomotive behavior and shortening of motoneuron terminal branches. ***PLoS One***, 7(6): 1–13.

Sato, M., Seki, T., Konno, A., Hirai, H., Kurauchi, Y., Hisatsune, A., et al. 2019. Rapamycin activates mammalian microautophagy. ***Journal of pharmacological sciences***, 140(2): 201–204.

Scaravilli, F. & Duchen, L. 1980. The development of sensory ganglion cells in normal and Sprawling mutant mice. ***Journal of neurocytology***, 9(3): 363–371.

Scherer, J., Yi, J. & Vallee, R. B. 2014. PKA-dependent dynein switching from lysosomes to adenovirus: a novel form of host-virus competition. ***Journal of Cell Biology***, 205(2): 163–177.

Schiavo, G., Greensmith, L., Hafezparast, M. & Fisher, E. M. 2013. Cytoplasmic dynein heavy chain: the servant of many masters. ***Trends in neurosciences***, 36(11): 641–651.

Schlager, M. A., Hoang, H. T., Urnavicius, L., Bullock, S. L. & Carter, A. P. 2014. In vitro reconstitution of a highly processive recombinant human dynein complex. ***The EMBO journal***, 33(17): 1855–1868.

Schlager, M. A., Serra-Marques, A., Grigoriev, I., Gumy, L. F., da Silva, M. E., Wulf, P. S., et al. 2014. Bicaudal d family adaptor proteins control the velocity of Dynein-based movements. ***Cell reports***, 8(5): 1248–1256.

Schmidt, H., Gleave, E. S. & Carter, A. P. 2012. Insights into dynein motor domain function from a 3.3-Å crystal structure. ***Nature structural & molecular biology***, 19(5): 492–508.

Schroeder, C. M., Ostrem, J. M., Hertz, N. T. & Vale, R. D. 2014. A Ras-like domain in the light intermediate chain bridges the dynein motor to a cargo-binding region. ***Elife***, 3: 1–22.

Schroeder, C. M. & Vale, R. D. 2016. Assembly and activation of dynein-dynactin by the cargo adaptor protein Hook3. ***Journal of Cell Biology***, 214(3): 309–318.

Schroer, T. A. 2004. Dynactin. ***Annu. Rev. Cell Dev. Biol.***, 20: 759–779.

Schwerin, S., Dewald, J. P., Haztl, M., Jovanovich, S., Nickeas, M. & MacKinnon, C. 2008. Ipsilateral versus contralateral cortical motor projections to a shoulder adductor in chronic hemiparetic stroke: implications for the expression of arm synergies. ***Experimental brain research***, 185(3): 509–519.

Scoto, M., Rossor, A. M., Harms, M. B., Cirak, S., Calissano, M., Robb, S., et al. 2015. Novel mutations expand the clinical spectrum of DYNC1H1-associated spinal muscular atrophy. ***Neurology***, 84(7): 668–679.

Scotter, E. L., Vance, C., Nishimura, A. L., Lee, Y.-B., Chen, H.-J., Urwin, H., et al. 2014. Differential roles of the ubiquitin proteasome system and autophagy in the clearance of soluble and aggregated TDP-43 species. ***Journal of cell science***, 127(6): 1263–1278.

Seguin, S., Morelli, F. F., Vinet, J., Amore, D., De Biasi, S., Poletti, A., et al. 2014. Inhibition of autophagy, lysosome and VCP function impairs stress granule assembly. ***Cell Death & Differentiation***, 21(12): 1838–1851.

Seibenhener, M. L., Babu, J. R., Geetha, T., Wong, H. C., Krishna, N. R. & Wooten, M. W. 2004. Sequestosome 1/p62 is a polyubiquitin chain binding protein involved in ubiquitin proteasome degradation. ***Molecular and cellular biology***, 24(18): 8055–8068.

Selenica, M.-L., Benner, L., Housley, S. B., Manchec, B., Lee, D. C., Nash, K. R., et al. 2014. Histone deacetylase 6 inhibition improves memory and reduces total tau levels in a mouse model of tau deposition. ***Alzheimer's research & therapy***, 6(1): 1–12.

Sellier, C., Campanari, M.-L., Corbier, C. J., Gaucherot, A., Kolb-Cheynel, I., Oulad-Abdelghani, M., et al. 2016. Loss of C9ORF72 impairs autophagy and synergizes with polyQ Ataxin-2 to induce motor neuron dysfunction and cell death. ***The EMBO Journal***, 35(12): 1276–1297.

Sha, Z., Schnell, H. M., Ruoff, K. & Goldberg, A. 2018. Rapid induction of p62 and GABARAPL1 upon proteasome inhibition promotes survival before autophagy activation. ***J Cell Biol***, 217(5): 1757–1776.

Shah, N., Kumar, S., Zaman, N., Pan, C. C., Bloodworth, J. C., Lei, W., et al. 2018. TAK1 activation of alpha-TAT1 and microtubule hyperacetylation control AKT signaling and cell growth. ***Nature communications***, 9(1): 1696–1707.

She, Z.-Y., Pan, M.-Y., Tan, F.-Q. & Yang, W.-X. 2017. Minus end-directed kinesin-14 KIFC1 regulates the positioning and architecture of the Golgi apparatus. ***Oncotarget***, 8(22): 1–15.

Shekhar, N., Wu, J., Dickinson, R. B. & Lele, T. P. 2013. Cytoplasmic dynein: tension generation on microtubules and the nucleus. ***Cellular and molecular bioengineering***, 6(1): 74–81.

Shelkovnikova, T. A., Robinson, H. K., Connor-Robson, N. & Buchman, V. L. 2013. Recruitment into stress granules prevents irreversible aggregation of FUS protein mislocalized to the cytoplasm. ***Cell Cycle***, 12(19): 3383–3391.

Shelkovnikova, T. A., Robinson, H. K., Southcombe, J. A., Ninkina, N. & Buchman, V. L. 2014. Multistep process of FUS aggregation in the cell cytoplasm involves RNA-dependent and RNA-independent mechanisms. ***Human molecular genetics***, 23(19): 5211–5226.

Sheth, U. & Parker, R. 2003. Decapping and decay of messenger RNA occur in cytoplasmic processing bodies. ***Science***, 300(5620): 805–808.

Shi, X., Yao, Y., Wang, Y., Zhang, Y., Huang, Q., Zhou, J., et al. 2015. Cep70 regulates microtubule stability by interacting with HDAC6. ***FEBS letters***, 589(15): 1771–1777.

Shi, Y., Lin, S., Staats, K. A., Li, Y., Chang, W.-H., Hung, S.-T., et al. 2018. Haploinsufficiency leads to neurodegeneration in C9ORF72 ALS/FTD human induced motor neurons. ***Nature medicine***, 24(3): 313–325.

Shida, T., Cueva, J. G., Xu, Z., Goodman, M. B. & Nachury, M. V. 2010. The major α-tubulin K40 acetyltransferase αTAT1 promotes rapid ciliogenesis and efficient mechanosensation. ***Proceedings of the National Academy of Sciences***, 107(50): 21517–

21522.

Shukla, S. & Parker, R. 2016. Hypo-and hyper-assembly diseases of RNA-protein complexes. ***Trends in molecular medicine***, 22(7): 615–628.

Silva, J. M., Rodrigues, S., Sampaio-Marques, B., Gomes, P., Neves-Carvalho, A., Dioli, C., et al. 2019. Dysregulation of autophagy and stress granule-related proteins in stress-driven Tau pathology. ***Cell Death & Differentiation***, 26(8): 1411–1427.

Silverman, M., Kaech, S., Ramser, E., Lu, X., Lasarev, M., Nagalla, S., et al. 2010. Expression of kinesin superfamily genes in cultured hippocampal neurons. ***Cytoskeleton***, 67(12): 784–795.

Simpson, C. L. & Al-Chalabi, A. 2006. Amyotrophic lateral sclerosis as a complex genetic disease. ***Biochimica et Biophysica Acta (BBA)-Molecular Basis of Disease***, 1762(11-12): 973–985.

Sirajuddin, M., Rice, L. M. & Vale, R. D. 2014. Regulation of microtubule motors by tubulin isotypes and post-translational modifications. ***Nature cell biology***, 16(4): 335–344.

Sivagurunathan, S., Schnittker, R. R., Razafsky, D. S., Nandini, S., Plamann, M. D. & King, S. J. 2012. Analyses of dynein heavy chain mutations reveal complex interactions between dynein motor domains and cellular dynein functions. ***Genetics***, 191(4): 1157–1179.

Skibinski, G., Parkinson, N. J., Brown, J. M., Chakrabarti, L., Lloyd, S. L., Hummerich, H., et al. 2005. Mutations in the endosomal ESCRTIII-complex subunit CHMP2B in frontotemporal dementia. ***Nature genetics***, 37(8): 806–808.

Skiniotis, G., Cochran, J. C., Müller, J., Mandelkow, E., Gilbert, S. P. & Hoenger, A. 2004. Modulation of kinesin binding by the C-termini of tubulin. ***The EMBO journal***, 23(5): 989–999.

Sleigh, J. N., Tosolini, A. P., Gordon, D., Devoy, A., Fratta, P., Fisher, E. M., et al. 2020. Mice carrying ALS mutant TDP-43, but not mutant FUS, display in vivo defects in axonal transport of signaling endosomes. ***Cell reports***, 30(11): 3655–3662.

Smith, B. N., Ticozzi, N., Fallini, C., Gkazi, A. S., Topp, S., Kenna, K. P., et al. 2014. Exome-wide rare variant analysis identifies TUBA4A mutations associated with familial ALS. ***Neuron***, 84(2): 324–331.

Solomon, D. A., Stepto, A., Au, W. H., Adachi, Y., Diaper, D. C., Hall, R., et al. 2018. A feedback loop between dipeptide-repeat protein, TDP-43 and karyopherin-α mediates C9orf72-related neurodegeneration. ***Brain***, 141(10): 2908–2924.

Song, Y. & Brady, S. T. 2015. Post-translational modifications of tubulin: pathways to functional diversity of microtubules. ***Trends in cell biology***, 25(3): 125–136.

Song, Y., Kirkpatrick, L. L., Schilling, A. B., Helseth, D. L., Chabot, N., Keillor, J. W., et al. 2013. Transglutaminase and polyamination of tubulin: posttranslational modification for stabilizing axonal microtubules. ***Neuron***, 78(1): 109–123.

Soo, K., Sultana, J., King, A., Atkinson, R., Warraich, S., Sundaramoorthy, V., et al. 2015. ALS-associated mutant FUS inhibits macroautophagy which is restored by overexpression of Rab1. ***Cell death discovery***, 1(1): 1–12.

Soppina, V., Herbstman, J. F., Skiniotis, G. & Verhey, K. J. 2012. Luminal localization of α-tubulin K40 acetylation by cryo-EM analysis of fab-labeled microtubules. ***PloS one***, 7(10): 1–9.

Sreedharan, J., Blair, I. P., Tripathi, V. B., Hu, X., Vance, C., Rogelj, B., et al. 2008. TDP-43 mutations in familial and sporadic amyotrophic lateral sclerosis. ***Science***, 319(5870): 1668–1672.

St George-Hyslop, P., Lin, J. Q., Miyashita, A., Phillips, E. C., Qamar, S., Randle, S. J., et al. 2018. The physiological and pathological biophysics of phase separation and gelation of RNA binding proteins in amyotrophic lateral sclerosis and fronto-temporal lobar degeneration. ***Brain research***, 1693: 11–23.

Steffen, W., Hodgkinson, J. L. & Wiche, G. 1996. Immunogold localisation of the intermediate chain within the protein complex of cytoplasmic dynein. ***Journal of***

structural biology, 117(3): 227–235.

Stehbens, S. & Wittmann, T. 2012. Targeting and transport: how microtubules control focal adhesion dynamics. ***Journal of Cell Biology***, 198(4): 481–489.

Stiess, M. & Bradke, F. 2011. Neuronal polarization: the cytoskeleton leads the way. ***Developmental neurobiology***, 71(6): 430–444.

Stifani, N. 2014. Motor neurons and the generation of spinal motor neurons diversity. ***Frontiers in cellular neuroscience***, 8(293): 1–22.

Stokin, G. B., Lillo, C., Falzone, T. L., Brusch, R. G., Rockenstein, E., Mount, S. L., et al. 2005. Axonopathy and transport deficits early in the pathogenesis of Alzheimer's disease. ***Science***, 307(5713): 1282–1288.

Stuchell-Brereton, M. D., Siglin, A., Li, J., Moore, J. K., Ahmed, S., Williams, J. C., et al. 2011. Functional interaction between dynein light chain and intermediate chain is required for mitotic spindle positioning. ***Molecular biology of the cell***, 22(15): 2690–2701.

Subramanian, R. & Kapoor, T. M. 2012. Building complexity: insights into self-organized assembly of microtubule-based architectures. ***Developmental cell***, 23(5): 874–885.

Suk, T. R. & Rousseaux, M. W. 2020. The role of TDP-43 mislocalization in amyotrophic lateral sclerosis. ***Molecular Neurodegeneration***, 15(1): 1–16.

Sullivan, P. M., Zhou, X., Robins, A. M., Paushter, D. H., Kim, D., Smolka, M. B., et al. 2016. The ALS/FTLD associated protein C9orf72 associates with SMCR8 and WDR41 to regulate the autophagy-lysosome pathway. ***Acta neuropathologica communications***, 4(1): 1–16.

Summers, K. E. & Gibbons, I. R. 1971. Adenosine triphosphate-induced sliding of tubules in trypsin-treated flagella of sea-urchin sperm. ***Proceedings of the National Academy of Sciences of the United States of America***, 68(12): 3092–3096.

Sun, Z., Diaz, Z., Fang, X., Hart, M. P., Chesi, A., Shorter, J., et al. 2011. Molecular determinants and genetic modifiers of aggregation and toxicity for the ALS disease protein FUS/TLS. ***PLoS biology***, 9(4): 1–25.

Sundaramoorthy, V., Sultana, J. M. & Atkin, J. D. 2015. Golgi fragmentation in amyotrophic lateral sclerosis, an overview of possible triggers and consequences. ***Frontiers in neuroscience***, 9(400): 1–11.

Susalka, S. J., Nikulina, K., Salata, M. W., Vaughan, P. S., King, S. M., Vaughan, K. T., et al. 2002. The roadblock light chain binds a novel region of the cytoplasmic dynein intermediate chain. ***Journal of Biological Chemistry***, 277(36): 32939–32946.

Swinnen, B. & Robberecht, W. 2014. The phenotypic variability of amyotrophic lateral sclerosis. ***Nature Reviews Neurology***, 10(11): 661–670.

Szyk, A., Deaconescu, A. M., Spector, J., Goodman, B., Valenstein, M. L., Ziolkowska, N. E., et al. 2014. Molecular basis for age-dependent microtubule acetylation by tubulin acetyltransferase. ***Cell***, 157(6): 1405–1415.

Taes, I., Timmers, M., Hersmus, N., Bento-Abreu, A., Van Den Bosch, L., Van Damme, P., et al. 2013. Hdac6 deletion delays disease progression in the SOD1G93A mouse model of ALS. ***Human molecular genetics***, 22(9): 1783–1790.

Tai, H.-C. & Schuman, E. M. 2008. Ubiquitin, the proteasome and protein degradation in neuronal function and dysfunction. ***Nature Reviews Neuroscience***, 9(11): 826–838.

Takeda, T., Kitagawa, K. & Arai, K. 2020. Phenotypic variability and its pathological basis in amyotrophic lateral sclerosis. ***Neuropathology***, 40(1): 40–56.

Tan, C.-F., Eguchi, H., Tagawa, A., Onodera, O., Iwasaki, T., Tsujino, A., et al. 2007. TDP-43 immunoreactivity in neuronal inclusions in familial amyotrophic lateral sclerosis with or without SOD1 gene mutation. ***Acta neuropathologica***, 113(5): 535–542.

Tashiro, Y., Urushitani, M., Inoue, H., Koike, M., Uchiyama, Y., Komatsu, M., et al. 2012. Motor neuron-specific disruption of proteasomes, but not autophagy, replicates

amyotrophic lateral sclerosis. ***Journal of Biological Chemistry***, 287(51): 42984–42994.

Tateishi, T., Hokonohara, T., Yamasaki, R., Miura, S., Kikuchi, H., Iwaki, A., et al. 2010. Multiple system degeneration with basophilic inclusions in Japanese ALS patients with FUS mutation. ***Acta neuropathologica***, 119(3): 355–364.

Taylor, J. P., Brown Jr, R. H. & Cleveland, D. W. 2016. Decoding ALS: from genes to mechanism. ***Nature***, 539(7628): 197–206.

Taylor, J. P., Hardy, J. & Fischbeck, K. H. 2002. Toxic proteins in neurodegenerative disease. ***Science***, 296(5575): 1991–1995.

Terenzio, M., Di Pizio, A., Rishal, I., Marvaldi, L., Di Matteo, P., Kawaguchi, R., et al. 2020. DYNLRB1 is essential for dynein mediated transport and neuronal survival. ***Neurobiology of Disease***, 140: 1–13.

Teuling, E., van Dis, V., Wulf, P. S., Haasdijk, E. D., Akhmanova, A., Hoogenraad, C. C., et al. 2008. A novel mouse model with impaired dynein/dynactin function develops amyotrophic lateral sclerosis (ALS)-like features in motor neurons and improves lifespan in SOD1-ALS mice. ***Human molecular genetics***, 17(18): 2849–2862.

Teyssou, E., Takeda, T., Lebon, V., Boillée, S., Doukouré, B., Bataillon, G., et al. 2013. Mutations in SQSTM1 encoding p62 in amyotrophic lateral sclerosis: genetics and neuropathology. ***Acta neuropathologica***, 125(4): 511–522.

THokési, N., Lehotzky, A., Horváth, I., Szabó, B., Oláh, J., Lau, P., et al. 2010. TPPP/p25 promotes tubulin acetylation by inhibiting histone deacetylase 6. ***Journal of Biological Chemistry***, 285(23): 17896–17906.

Tian, Y., Li, Z., Hu, W., Ren, H., Tian, E., Zhao, Y., et al. 2010. C. elegans screen identifies autophagy genes specific to multicellular organisms. ***Cell***, 141(6): 1042–1055.

Titus, M. A. 2018. Myosin-driven intracellular transport. ***Cold Spring Harbor perspectives in biology***, 10(3): 1–15.

Torii, S., Yamaguchi, H., Nakanishi, A., Arakawa, S., Honda, S., Moriwaki, K., et al. 2020. Identification of a phosphorylation site on Ulk1 required for genotoxic stress-induced alternative autophagy. ***Nature communications***, 11(1): 1–19.

Torisawa, T., Ichikawa, M., Furuta, A., Saito, K., Oiwa, K., Kojima, H., et al. 2014. Autoinhibition and cooperative activation mechanisms of cytoplasmic dynein. ***Nature cell biology***, 16(11): 1118–1124.

Torisawa, T., Nakayama, A., Furuta, K., Yamada, M., Hirotsune, S. & Toyoshima, Y. Y. 2011. Functional dissection of LIS1 and NDEL1 towards understanding the molecular mechanisms of cytoplasmic dynein regulation. ***Journal of Biological Chemistry***, 286(3): 1959–1965.

Toropova, K., Mladenov, M. & Roberts, A. J. 2017. Intraflagellar transport dynein is autoinhibited by trapping of its mechanical and track-binding elements. ***Nature structural \& molecular biology***, 24(5): 1–10.

Trokter, M., Mücke, N. & Surrey, T. 2012. Reconstitution of the human cytoplasmic dynein complex. ***Proceedings of the National Academy of Sciences***, 109(51): 20895–20900.

Tsai, N.-P., Tsui, Y.-C. & Wei, L.-N. 2009. Dynein motor contributes to stress granule dynamics in primary neurons. ***Neuroscience***, 159(2): 647–656.

Tsurusaki, Y., Saitoh, S., Tomizawa, K., Sudo, A., Asahina, N., Shiraishi, H., et al. 2012. A DYNC1H1 mutation causes a dominant spinal muscular atrophy with lower extremity predominance. ***Neurogenetics***, 13(4): 327–332.

Tu, D., Zhu, Z., Zhou, A. Y., Yun, C., Lee, K.-E., Toms, A. V., et al. 2013. Structure and ubiquitination-dependent activation of TANK-binding kinase 1. ***Cell reports***, 3(3): 747–758.

Tummala, H., Jung, C., Tiwari, A., Higgins, C. M. J., Hayward, L. J. & Xu, Z. 2005. Inhibition of chaperone activity is a shared property of several Cu,Zn-superoxide dismutase mutants that cause amyotrophic lateral sclerosis. ***The Journal of biological chemistry***,

280(18): 17725–1731.

Tuszynski, J., Brown, J. & Sept, D. 2003. Models of the collective behavior of proteins in cells: tubulin, actin and motor proteins. ***Journal of biological physics***, 29(4): 401–428.

Twelvetrees, A. E., Pernigo, S., Sanger, A., Guedes-Dias, P., Schiavo, G., Steiner, R. A., et al. 2016. The dynamic localization of cytoplasmic dynein in neurons is driven by kinesin-1. ***Neuron***, 90(5): 1000–1015.

Tynan, S. H., Gee, M. A. & Vallee, R. B. 2000. Distinct but overlapping sites within the cytoplasmic dynein heavy chain for dimerization and for intermediate chain and light intermediate chain binding. ***Journal of Biological Chemistry***, 275(42): 32769–32774.

Tyzack, G. E., Luisier, R., Taha, D. M., Neeves, J., Modic, M., Mitchell, J. S., et al. 2019. Widespread FUS mislocalization is a molecular hallmark of amyotrophic lateral sclerosis. ***Brain***, 142(9): 2572–2580.

Uhlén, M., Fagerberg, L., Hallström, B. M., Lindskog, C., Oksvold, P., Mardinoglu, A., et al. 2015. Tissue-based map of the human proteome. ***Science***, 347(6220): 1–11.

Urnavicius, L., Lau, C. K., Elshenawy, M. M., Morales-Rios, E., Motz, C., Yildiz, A., et al. 2018. Cryo-EM shows how dynactin recruits two dyneins for faster movement. ***Nature***, 554(7691): 202–206.

Urnavicius, L., Zhang, K., Diamant, A. G., Motz, C., Schlager, M. A., Yu, M., et al. 2015. The structure of the dynactin complex and its interaction with dynein. ***Science***, 347(6229): 1441–1446.

Ustinova, K., Novakova, Z., Saito, M., Meleshin, M., Mikesova, J., Kutil, Z., et al. 2020. The disordered N-terminus of HDAC6 is a microtubule-binding domain critical for efficient tubulin deacetylation. ***Journal of Biological Chemistry***, 295(9): 2614–2628.

Uytterhoeven, V., Lauwers, E., Maes, I., Miskiewicz, K., Melo, M. N., Swerts, J., et al. 2015. Hsc70-4 deforms membranes to promote synaptic protein turnover by endosomal microautophagy. ***Neuron***, 88(4): 735–748.

Vahsen, B. F., Ribas, V. T., Sundermeyer, J., Boecker, A., Dambeck, V., Lenz, C., et al. 2020. Inhibition of the autophagic protein ULK1 attenuates axonal degeneration in vitro and in vivo, enhances translation, and modulates splicing. ***Cell Death & Differentiation***, 27: 1–18.

Valenzuela-Fernandez, A., Cabrero, J. R., Serrador, J. M. & Sánchez-Madrid, F. 2008. HDAC6: a key regulator of cytoskeleton, cell migration and cell-cell interactions. ***Trends in cell biology***, 18(6): 291–297.

Vallee, R. B., McKenney, R. J. & Ori-McKenney, K. M. 2012. Multiple modes of cytoplasmic dynein regulation. ***Nature cell biology***, 14(3): 224–230.

Van der Vaart, B., van Riel, W. E., Doodhi, H., Kevenaar, J. T., Katrukha, E. A., Gumy, L., et al. 2013. CFEOM1-associated kinesin KIF21A is a cortical microtubule growth inhibitor. ***Developmental cell***, 27(2): 145–160.

Van Dis, V., Kuijpers, M., Haasdijk, E. D., Teuling, E., Oakes, S. A., Hoogenraad, C. C., et al. 2014. Golgi fragmentation precedes neuromuscular denervation and is associated with endosome abnormalities in SOD1-ALS mouse motor neurons. ***Acta neuropathologica communications***, 2(1): 1–15.

Van Eersel, J., Ke, Y. D., Gladbach, A., Bi, M., Götz, J., Kril, J. J., et al. 2011. Cytoplasmic accumulation and aggregation of TDP-43 upon proteasome inhibition in cultured neurons., 6(7): 1–13.

Van Mossevelde, S., Van der Zee, J., Gijselinck, I., Engelborghs, S., Sieben, A., Van Langenhove, T., et al. 2016. Clinical features of TBK1 carriers compared with C9orf72, GRN and non-mutation carriers in a Belgian cohort. ***Brain***, 139(2): 452–467.

Vance, C., Rogelj, B., Hortobágyi, T., De Vos, K. J., Nishimura, A. L., Sreedharan, J., et al. 2009. Mutations in FUS, an RNA processing protein, cause familial amyotrophic lateral sclerosis type 6. ***Science***, 323(5918): 1208–1211.

Vance, C., Scotter, E. L., Nishimura, A. L., Troakes, C., Mitchell, J. C., Kathe, C., et al. 2013. ALS mutant FUS disrupts nuclear localization and sequesters wild-type FUS within cytoplasmic stress granules. ***Human molecular genetics***, 22(13): 2676–2688.

Vedula, P. & Kashina, A. 2018. The makings of the “actin code”: regulation of actin’s biological function at the amino acid and nucleotide level. ***Journal of cell science***, 131(9): jcs215509.

Verdel, A., Curtet, S., Brocard, M.-P., Rousseaux, S., Lemercier, C., Yoshida, M., et al. 2000. Active maintenance of mHDA2/mHDAC6 histone-deacetylase in the cytoplasm. ***Current Biology***, 10(12): 747–749.

Verschueren, A. 2017. Motor neuropathies and lower motor neuron syndromes. ***Revue Neurologique***, 173(5): 320–325.

Vicencio, E., Beltrán, S., Labrador, L., Manque, P., Nassif, M. & Woehlbier, U. 2020. Implications of Selective Autophagy Dysfunction for ALS Pathology. ***Cells***, 9(2): 381–401.

Voigt, A., Herholz, D., Fiesel, F. C., Kaur, K., Müller, D., Karsten, P., et al. 2010. TDP-43-mediated neuron loss in vivo requires RNA-binding activity. ***PloS one***, 5(8): 12247–12258.

Volk, A. E., Weishaupt, J. H., Andersen, P. M., Ludolph, A. C. & Kubisch, C. 2018. Current knowledge and recent insights into the genetic basis of amyotrophic lateral sclerosis. ***medizinische genetik***, 30(2): 252–258.

Vu, H. T., Akatsu, H., Hashizume, Y., Setou, M. & Ikegami, K. 2017. Increase in α-tubulin modifications in the neuronal processes of hippocampal neurons in both kainic acid-induced epileptic seizure and Alzheimer’s disease. ***Scientific reports***, 7(1): 1–14.

Waibel, S., Neumann, M., Rosenbohm, A., Birve, A., Volk, A., Weishaupt, J., et al. 2013. Truncating mutations in FUS/TLS give rise to a more aggressive ALS-phenotype than missense mutations: a clinico-genetic study in G ermany. ***European journal of neurology***, 20(3): 540–546.

Walker, A. K., Tripathy, K., Restrepo, C. R., Ge, G., Xu, Y., Kwong, L. K., et al. 2015. An insoluble frontotemporal lobar degeneration-associated TDP-43 C-terminal fragment causes neurodegeneration and hippocampus pathology in transgenic mice. ***Human molecular genetics***, 24(25): 7241–7254.

Walters, R. W., Muhlrad, D., Garcia, J. & Parker, R. 2015. Differential effects of Ydj1 and Sis1 on Hsp70-mediated clearance of stress granules in Saccharomyces cerevisiae. ***Rna***, 21(9): 1660–1671.

Wang, B., Abraham, N., Gao, G. & Yang, Q. 2016. Dysregulation of autophagy and mitochondrial function in Parkinson's disease. ***Translational Neurodegeneration***, 5(1): 1–9.

Wang, C., Telpoukhovskaia, M. A., Bahr, B. A., Chen, X. & Gan, L. 2018. Endo-lysosomal dysfunction: a converging mechanism in neurodegenerative diseases. ***Current opinion in neurobiology***, 48: 52–58.

Wang, D., Xu, Q., Yuan, Q., Jia, M., Niu, H., Liu, X., et al. 2019. Proteasome inhibition boosts autophagic degradation of ubiquitinated-AGR2 and enhances the antitumor efficiency of bevacizumab. ***Oncogene***, 38(18): 3458–3474.

Wang, H., Ling, L., Ai, L. & Bai, L. 2019. HDAC6 inhibition induces the failure of mouse early embryonic development. ***Journal of cellular physiology***, 234(6): 8752–8759.

Wang, I.-F., Wu, L.-S. & Shen, C. J. 2008. TDP-43: an emerging new player in neurodegenerative diseases. ***Trends in molecular medicine***, 14(11): 479–485.

Wang, X., Fan, H., Ying, Z., Li, B., Wang, H. & Wang, G. 2010. Degradation of TDP-43 and its pathogenic form by autophagy and the ubiquitin-proteasome system. ***Neuroscience letters***, 469(1): 112–116.

Wang, Y. & Qin, Z. 2013. Coordination of autophagy with other cellular activities. ***Acta Pharmacologica Sinica***, 34(5): 585–594.

Wang, Z., Miao, G., Xue, X., Guo, X., Yuan, C., Wang, Z., et al. 2016. The Vici syndrome protein EPG5 is a Rab7 effector that determines the fusion specificity of autophagosomes with late endosomes/lysosomes. ***Molecular cell***, 63(5): 781–795.

Webster, C. P., Smith, E. F., Bauer, C. S., Moller, A., Hautbergue, G. M., Ferraiuolo, L., et al. 2016. The C9orf72 protein interacts with Rab1a and the ULK1 complex to regulate initiation of autophagy. ***The EMBO journal***, 35(15): 1656–1676.

Weedon, M. N., Hastings, R., Caswell, R., Xie, W., Paszkiewicz, K., Antoniadi, T., et al. 2011. Exome sequencing identifies a DYNC1H1 mutation in a large pedigree with dominant axonal Charcot-Marie-Tooth disease. ***The American Journal of Human Genetics***, 89(2): 308–312.

Wei, D., Gao, N., Li, L., Zhu, J.-X., Diao, L., Huang, J., et al. 2017. α-Tubulin acetylation restricts axon overbranching by dampening microtubule plus-end dynamics in neurons. ***Cerebral Cortex***, 28(9): 3332–3346.

Wen-You, Y. W. & Noboru, M. 2020. Lysosome biology in autophagy. ***Cell Discovery***, 6(1): 1–12.

Weskamp, K., Tank, E. M., Miguez, R., McBride, J. P., Gómez, N. B., White, M., et al. 2020. Shortened TDP43 isoforms upregulated by neuronal hyperactivity drive TDP43 pathology in ALS. ***The Journal of clinical investigation***, 130(3): 1–18.

Wheeler, J. R., Matheny, T., Jain, S., Abrisch, R. & Parker, R. 2016. Distinct stages in stress granule assembly and disassembly. ***Elife***, 5: 18413–18437.

Willemsen, M. H., Vissers, L. E., Willemsen, M. A., van Bon, B. W., Kroes, T., de Ligt, J., et al. 2012. Mutations in DYNC1H1 cause severe intellectual disability with neuronal migration defects. ***Journal of medical genetics***, 49(3): 179–183.

Williams, D., Hicks, S. W., Machamer, C. E. & Pessin, J. E. 2006. Golgin-160 is required for the Golgi membrane sorting of the insulin-responsive glucose transporter GLUT4 in adipocytes. ***Molecular biology of the cell***, 17(12): 5346–5355.

Williams, J. C., Roulhac, P. L., Roy, A. G., Vallee, R. B., Fitzgerald, M. C. & Hendrickson, W. A. 2007. Structural and thermodynamic characterization of a cytoplasmic dynein light chain-intermediate chain complex. ***Proceedings of the National Academy of Sciences of the United States of America***, 104(24): 10028–10033.

Winton, M. J., Igaz, L. M., Wong, M. M., Kwong, L. K., Trojanowski, J. Q. & Lee, V. M.-Y. 2008. Disturbance of nuclear and cytoplasmic TAR DNA-binding protein (TDP-43) induces disease-like redistribution, sequestration, and aggregate formation. ***Journal of Biological Chemistry***, 283(19): 13302–13309.

Winton, M. J., Van Deerlin, V. M., Kwong, L. K., Yuan, W., Wood, E. M., Yu, C.-E., et al. 2008. A90V TDP-43 variant results in the aberrant localization of TDP-43 in vitro. ***FEBS letters***, 582(15): 2252–2256.

Wolozin, B. 2014. Physiological protein aggregation run amuck: stress granules and the genesis of neurodegenerative disease. ***Discovery medicine***, 17(91): 47–52.

Wong, V. S., Picci, C., Swift, M., Levinson, M., Willis, D. & Langley, B. 2018. α-Tubulin Acetyltransferase Is a Novel Target Mediating Neurite Growth Inhibitory Effects of Chondroitin Sulfate Proteoglycans and Myelin-Associated Glycoprotein. ***eneuro***, 5(1): 1–13.

Wong, Y. C. & Holzbaur, E. L. 2014. The regulation of autophagosome dynamics by huntingtin and HAP1 is disrupted by expression of mutant huntingtin, leading to defective cargo degradation. ***Journal of Neuroscience***, 34(4): 1293–1305.

Wrobel, L., Topf, U., Bragoszewski, P., Wiese, S., Sztolsztener, M. E., Oeljeklaus, S., et al. 2015. Mistargeted mitochondrial proteins activate a proteostatic response in the cytosol. ***Nature***, 524(7566): 485–488.

Wu, H., Chen, S., Ammar, A.-B., Xu, J., Wu, Q., Pan, K., et al. 2015. Crosstalk between macroautophagy and chaperone-mediated autophagy: implications for the treatment of neurological diseases. ***Molecular neurobiology***, 52(3): 1284–1296.

Wu, L.-S., Cheng, W.-C., Hou, S.-C., Yan, Y.-T., Jiang, S.-T. & Shen, C.-K. J. 2010. TDP-43, a neuro-pathosignature factor, is essential for early mouse embryogenesis. ***Genesis (New***

York, N.Y. : 2000), 48(1): 56–62.

Wu, Y., Ding, Y., Zheng, X. & Liao, K. 2019. The molecular chaperone Hsp90 maintains Golgi organization and vesicular trafficking by regulating microtubule stability. ***Journal of Molecular Cell Biology***, 12(6): 448–461.

Xia, Q., Wang, H., Hao, Z., Fu, C., Hu, Q., Gao, F., et al. 2015. TDP-43 loss of function increases TFEB activity and blocks autophagosome-lysosome fusion. ***The EMBO journal***, 23(2): 1–22.

Xiang, Y., Zhang, X., Nix, D. B., Katoh, T., Aoki, K., Tiemeyer, M., et al. 2013. Regulation of protein glycosylation and sorting by the Golgi matrix proteins GRASP55/65. ***Nature communications***, 4(1659): 1–25.

Xie, R., Nguyen, S., McKeehan, K., Wang, F., McKeehan, W. L. & Liu, L. 2011. Microtubule-associated protein 1S (MAP1S) bridges autophagic components with microtubules and mitochondria to affect autophagosomal biogenesis and degradation. ***Journal of Biological Chemistry***, 286(12): 10367–10377.

Xie, R., Nguyen, S., McKeehan, W. L. & Liu, L. 2010. Acetylated microtubules are required for fusion of autophagosomes with lysosomes. ***BMC cell biology***, 11(1): 1–12.

Xu, M., Li, X.-X., Chen, Y., Pitzer, A. L., Zhang, Y. & Li, P.-L. 2014. Enhancement of dynein-mediated autophagosome trafficking and autophagy maturation by ROS in mouse coronary arterial myocytes. ***Journal of cellular and molecular medicine***, 18(11): 2165–2175.

Xu, Z., Schaedel, L., Portran, D., Aguilar, A., Gaillard, J., Marinkovich, M. P., et al. 2017. Microtubules acquire resistance from mechanical breakage through intralumenal acetylation. ***Science***, 356(6335): 328–332.

Yadav, S. & Linstedt, A. D. 2011. Golgi positioning. ***Cold Spring Harbor perspectives in biology***, 3(5): 1–17.

Yadav, S., Puri, S. & Linstedt, A. D. 2009. A primary role for Golgi positioning in directed secretion, cell polarity, and wound healing. ***Molecular biology of the cell***, 20(6): 1728–1736.

Yadav, S., Puthenveedu, M. A. & Linstedt, A. D. 2012. Golgin160 recruits the dynein motor to position the Golgi apparatus. ***Developmental cell***, 23(1): 153–165.

Yamamoto, M., Suzuki, S. O. & Himeno, M. 2010. The effects of dynein inhibition on the autophagic pathway in glioma cells. ***Neuropathology : official journal of the Japanese Society of Neuropathology***, 30(1): 1–6.

Yan, J. 2014. Interplay between HDAC6 and its interacting partners: essential roles in the aggresome-autophagy pathway and neurodegenerative diseases. ***DNA and cell biology***, 33(9): 567–580.

Yan, J., Seibenhener, M. L., Calderilla-Barbosa, L., Diaz-Meco, M.-T., Moscat, J., Jiang, J., et al. 2013. SQSTM1/p62 interacts with HDAC6 and regulates deacetylase activity. ***PloS one***, 8(9): 1–10.

Yang, P., Zhang, L., Zhang, Y., Zhang, J. & Xu, W. 2013. HDAC6: physiological function and its selective inhibitors for cancer treatment. ***Drug discoveries & therapeutics***, 7(6): 233–242.

Yao, L.-L., Cao, Q.-J., Zhang, H.-M., Zhang, J., Cao, Y. & Li, X. 2015. Melanophilin stimulates myosin-5a motor function by allosterically inhibiting the interaction between the head and tail of myosin-5a. ***Scientific reports***, 5(1): 1–10.

Ye, J., Cheung, J., Gerbino, V., Ahlsén, G., Zimanyi, C., Hirsh, D., et al. 2019. Effects of ALS-associated TANK binding kinase 1 mutations on protein-protein interactions and kinase activity. ***Proceedings of the National Academy of Sciences***, 116(49): 24517–24526.

Yi, J. Y., Ori-McKenney, K. M., McKenney, R. J., Vershinin, M., Gross, S. P. & Vallee, R. B. 2011. High-resolution imaging reveals indirect coordination of opposite motors and a role for LIS1 in high-load axonal transport. ***Journal of Cell Biology***, 195(2): 193–201.

Yogev, S., Cooper, R., Fetter, R., Horowitz, M. & Shen, K. 2016. Microtubule Organization Determines Axonal Transport Dynamics. ***Neuron***, 92(2): 449–460.

Yogev, S., Maeder, C. I., Cooper, R., Horowitz, M., Hendricks, A. G. & Shen, K. 2017. Local inhibition of microtubule dynamics by dynein is required for neuronal cargo distribution. ***Nature communications***, 8(1): 1–14.

You, Z., Jiang, W.-X., Qin, L.-Y., Gong, Z., Wan, W., Li, J., et al. 2019. Requirement for p62 acetylation in the aggregation of ubiquitylated proteins under nutrient stress. ***Nature Communications***, 10(1): 1–14.

Yu, T., Yi, Y.-S., Yang, Y., Oh, J., Jeong, D. & Cho, J. Y. 2012. The pivotal role of TBK1 in inflammatory responses mediated by macrophages. ***Mediators of Inflammation***, 2012: 1–8.

Zarei, S., Carr, K., Reiley, L., Diaz, K., Guerra, O., Altamirano, P. F., et al. 2015. A comprehensive review of amyotrophic lateral sclerosis. ***Surgical neurology international***, 6(171): 1–23.

Zhang, H.-G., Chen, L., Tang, L., Zhang, N. & Fan, D.-S. 2017. Clinical features of isolated bulbar palsy of amyotrophic lateral sclerosis in Chinese population. ***Chinese Medical Journal***, 130(15): 1768–1772.

Zhang, K., Foster, H. E., Rondelet, A., Lacey, S. E., Bahi-Buisson, N., Bird, A. W., et al. 2017. Cryo-EM reveals how human cytoplasmic dynein is auto-inhibited and activated. ***Cell***, 169(7): 1303–1314.

Zhang, L., Li, J., Ouyang, L., Liu, B. & Cheng, Y. 2016. Unraveling the roles of Atg4 proteases from autophagy modulation to targeted cancer therapy. ***Cancer letters***, 373(1): 19–26.

Zhang, Y., Mun, S. R., Linares, J. F., Ahn, J., Towers, C. G., Ji, C. H., et al. 2018. ZZ-dependent regulation of p62/SQSTM1 in autophagy. ***Nature communications***, 9(1): 1–11.

Zhao, J., Wang, Y., Xu, H., Fu, Y., Qian, T., Bo, D., et al. 2016. Dync1h1 mutation causes proprioceptive sensory neuron loss and impaired retrograde axonal transport of dorsal root ganglion neurons. ***CNS Neuroscience & Therapeutics***, 22(7): 593–601.

Zheng, Q., Huang, T., Zhang, L., Zhou, Y., Luo, H., Xu, H., et al. 2016. Dysregulation of ubiquitin-proteasome system in neurodegenerative diseases. ***Frontiers in aging neuroscience***, 8(303): 1–10.

Zheng, Y., Zhu, G., Tang, Y., Yan, J., Han, S., Yin, J., et al. 2020. HDAC6, A Novel Cargo for Autophagic Clearance of Stress Granules, Mediates the Repression of the Type I Interferon Response During Coxsackievirus A16 Infection. ***Frontiers in Microbiology***, 11(78): 1–19.

Zhu, Q., Jiang, J., Gendron, T. F., McAlonis-Downes, M., Jiang, L., Taylor, A., et al. 2020. Reduced C9ORF72 function exacerbates gain of toxicity from ALS/FTD-causing repeat expansion in C9orf72. ***Nature Neuroscience***, 23: 1–10.

Zhuang, L., Zhang, J. & Xiang, X. 2007. Point mutations in the stem region and the fourth AAA domain of cytoplasmic dynein heavy chain partially suppress the phenotype of NUDF/LIS1 loss in Aspergillus nidulans. ***Genetics***, 175(3): 1185–1196.